Artificial Radionuclides in the Environment

2015

環境における人工放射能の研究 2015

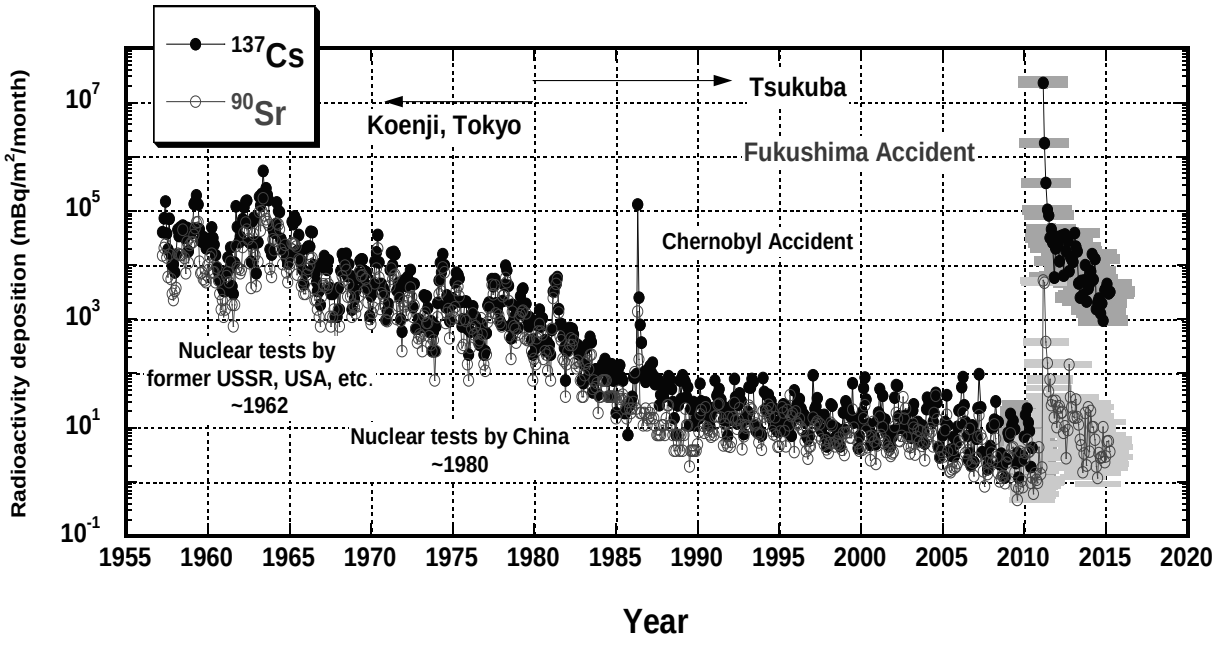

Atmospheric Environment and Applied Meteorology Research Department

&

Forecast Research Department, Meteorological Research Institute

JAPAN

August 2016

気象研究所　環境・応用気象研究部

予報研究部

最終ページに図の詳しい説明があります。

See figure caption at the end page of this publication.

「環境における人工放射能の研究 2015」について

気象研究所では、1954 年以来、大気及び海洋の環境放射能の研究を実施してきました。特に人工放射性核種の降下量を 60 年余りの長期にわたり、東京・つくばで精密測定してきました。この観測は、世界でも最長の定点観測です。このモニタリング観測の期間では、1950 年代から 1960 年代にかけては、旧ソ連や米国等による核実験が行われ、また、その後も 1986 年には旧ソ連のチェルノブイリ原子力発電所の事故が発生するなどがありましたが、この観測によって、それらの影響を含めたバックグラウンドの人工放射性核種の長期的変動を明らかにし、国民の安全・安心に寄与してきました。2011 年には不幸にして東日本大震災に伴う福島第一原子力発電所事故が発生し、それによって放出された放射性核種の推移を調査するという課題も担うこととなりました。今後も長期的視点で、人工放射性核種の変動を監視する必要があります。

この研究によるこれまでの観測や解析から、核実験や事故などによる一次放出に加え、長期的変動に対しては、一旦地面などに沈着した人工放射性核種が、風送、燃焼、植物などの働きにより空気中へ再飛散する過程が重要であることが明らかになりつつあります。このような変動メカニズムを正しく理解するためには、長期的観測に加えて、数値計算モデルを用いた解析が必要です。気象研究所では、気候変動や降水予測の研究のため、大気中の微粒子の動きを表現する数値モデルを開発してきましたが、そのような数値モデルを利用して、バックグラウンド放射能の変動メカニズムを解析する研究にも着手しています。

本論文集「環境における人工放射能の研究 2015」 は、その研究成果を、関係省庁の担当者の方々及び大学や試験研究機関の研究者の方々に広く周知するために、福島原発事故後二年から現在までの期間に出版された論文（主に英語論文）を、過去から現在までの成果と最近のトピックスに関するテーマ毎に分類し、各テーマの冒頭に簡単な日本語の解説を加えて、一冊にまとめたものです。

なお、この研究は原子力規制庁放射能調査研究費により実施されています。

平成 28 年 8 月

気象研究所 研究総務官　齊藤　和雄

序

気象研究所（現在は環境・応用気象研究部および予報研究部）では、1954 年以来、環境放射能の観測・測定法の開発、放射能汚染の実態の把握、大気や海洋における物質輸送解明のトレーサーとしての利用を目的として、60 年余にわたって環境放射能の研究を実施してきた。1957 年以降、各省庁がそれぞれの所掌で実施してきた環境放射能調査研究関連業務は、まず旧科学技術庁、その後文部科学省が所管してきた。さらに原子力規制委員会と原子力規制庁の発足に伴って 2013 年からは、原子力規制庁が所管することとなった。このような長期にわたり多数の研究者が係わり、観測・研究を継続してきた結果、環境放射能について世界的にも他に類を見ない貴重な時系列データが内外に提供され、また様々な気象学・海洋学的発見をもたらしてきた。この間の研究成果は 200 編以上の原著論文や解説資料として内外の雑誌や成書で公表されている。

1954 年 3 月 1 日に米国によりビキニ環礁で行われた水爆実験により、危険水域外で操業していた第五福竜丸乗組員が放射性物質を含む降灰（いわゆる死の灰）による被ばくを受けた事件を契機にして、日本における環境放射能研究が本格的に始まった。当時の気象研究所地球化学研究室は環境の放射能の分析・研究において日本で有数の研究室であり、海洋及び大気中の放射能汚染の調査・研究に精力的に取り組んだ。その結果、当時予想されていなかった海洋の放射能汚染、さらに大気を経由した日本への影響など放射能汚染の拡大の実態を明らかにすることができた。1958 年には、放射能調査研究費による特定研究課題の一つである「放射化学分析（落下塵・降水・海水中の放射性物質の研究）」を開始し、以降、地点の変動はあるが、札幌、仙台、東京、大阪、福岡の五つの管区気象台、秋田、稚内、釧路、石垣島の 4 地方気象台、輪島、米子の 2 測候所の全国 11 気象官署及び観測船で採取した海水中の人工放射性核種（^{90}Sr、^{137}Cs、^{3}H 及びプルトニウム）の分析を実施してきた。

東京・つくばにおける大気中の人工放射性核種の降下量は 1961 年から 1962 年に行われた大規模な大気圏核実験の翌年である 1963 年に最大値を観測した。その後、「部分的核実験禁止条約」の締結により米ソの大気圏核実験が中止された結果、降下量はおよそ 1 年の半減時間で減少した。この放射性核種の降下量の減少率は成層圏にまきあげられた物質の滞留時間を反映している。その後も、中国及びフランスにより大気圏核実験は続けられ、人工放射性核種の降下量は増減を繰り返した。1980 年の中国による最後の大気圏核実験の後、放射性フォールアウトは再度 1 年の半減期間で減少し、1985 年には 1957 年の観測開始以降最も低いレベルになった。しかし、1986 年の旧ソ連のチェルノブイリ原子力発電所事故により、大気中の人工放射性核種濃度（特に揮発性の高い ^{131}I、^{134}Cs、^{137}Cs など）は日本でも 1963 年に近いレベルに達するほど著しく増加した。大部分の放射性核種は対流圏の滞留時間（25 日）で減少したが一部 ^{137}Cs は成層圏にも輸送されていることが分かった。1988 年以降は低いレベルで推移しているが、明瞭な減少の傾向は見られなかった。この原因は一度地上に降下した放射性核種の再浮遊に由来すると考えている。さらに、再浮遊がどこで起るかについて研究を進め、東アジアの砂漠域で発生する黄砂が有力な候補であることを明らかにした。黄砂の発生は大陸域の環境変化と関連しており、降下物中の人工放射性核種は、砂漠化や関連する植生変化など大陸域の環境変化の指標となりうることが分かった。

大気フォールアウトの研究と共に、海洋における放射性核種の挙動も長期に調査研究を実施し

てきた。日本周辺海域ばかりでなく、太平洋の広域に亘って海水試料の採取を実施し、放射能汚染の実態を明らかにした。1960 年代後半から 1970 年代の調査で、海洋表面水中の放射能が北半球の中緯度で高いことを明らかにし、フォールアウトの緯度分布を反映していることが分かった。その後、海洋表面水中の放射性核種は海洋の物質循環に支配されていることを明らかにした。さらに、海水中の人工放射性核種の分析法の高度化を実現し少量の試料で分析可能にし、海洋の ^{137}Cs 濃度の精密鉛直断面を描き、核実験由来の ^{137}Cs の主な部分は北太平洋の亜熱帯中層に存在していることを明らかにした。フォールアウトによる人工放射性核種の海洋への主な降下以来数 10 年以上経過し、その広がりは北太平洋から、インド洋など他の海盆に及んでいる。これに関連して 2003－4 年に実施された BEAGLE2003 の航海で採取された海水について人工放射性核種の分析を行って、その広がりについて知見が得られた。1993 年旧ソ連/ロシアによる放射性廃棄物の日本海等への海洋投棄の実態が明らかにされ、それに伴う日本海の放射能調査の実施に参加した。放射性廃棄物による影響は検出されなかったが、調査の結果を踏まえ、日本海における固有水の生成過程及び生成場所（ウラジオストック沖）についての知見を得ることができた。これらは、海洋放射能のデータベースとして公開されている。

1990 年以降の環境放射能汚染として、1997 年の旧動力炉核燃料開発事業団「アスファルト固化処理施設」の火災爆発事故や 1999 年の JCO ウラン燃料工場の臨界事故があるが、いずれも環境中に放出された放射能は極めて低いレベルで、その影響は殆どなかった。しかしながら、2011 年 3 月に起きた東日本大震災にともなう東京電力福島第一原子力発電所事故により、^{137}Cs の総量だけで 10 PBq（ペタベクレル）以上という過去日本では経験したことのない大量の人工放射性核種が環境中に放出され、その 2 割程度が日本の国土に降下し、残りの 8 割は北太平洋に降下したと考えられている。これらの影響評価やその後の環境中での拡散状況の把握のためにも、環境放射能調査・研究は今後とも重要である。

2006 年 4 月より 2011 年 3 月まで、気象研究所では放射能調査研究費による特定研究課題として「放射性降下物の長期変動と再浮遊に関する研究」及び「海洋環境における放射性核種の長期挙動に関する研究」の二課題で環境放射能研究に取り組んできた。また、2011 年 8 月からは、「大気を通じた人工放射性核種の陸圏・水圏への沈着およびその後の移行過程の解明研究」の課題のもと、過去の知見を十分に活用しながら、同年 3 月 11 日に発生した東日本大震災にともなう福島第一原子力発電所の事故以降の新たな事態に対応し、放出された大量の人工放射性核種の挙動を解明する研究に着手した。目の前の大気に加えて、北太平洋におけるこれらの核種による汚染実態の把握やその動態の解明に取り組んだわけである。

過去 60 年余にわたり実施されてきたこうした研究成果を踏まえ、2015 年 4 月からは「人工放射性核種のバックグラウンド大気監視と数値解析に関する研究」を新たに開始した。本報告書では、この研究課題で得られた成果を含め、最新の成果やトピックスをテーマ毎に記述した。関係各位の今後の研究や業務に役立つ資料とすべく、編集作業を行った。我が国における環境放射能研究や大気科学研究に多少なりとも寄与できたとすれば、著者一同の望外の喜びである。

2016 年 8 月

気象研究所　環境・応用気象研究部
予報研究部

Contents

目次

1. 大気中放射能濃度の推移

1）はじめに

気象研究所では、大気圏内核実験が盛んに実施された 1950 年代後期から 60 年近くの期間にわたり、大気圏での人工放射性核種の濃度水準の実態とその変動要因を明らかにすべく、環境影響の大きい重要な核種について観測を継続してきた。特に、^{90}Sr（半減期 28.8 年）および ^{137}Cs（半減期 30.2 年）の月間降下量（大気降下物）の長期観測結果は、2016 年 4 月で満 59 年を迎える。また、2011 年 3 月の東京電力福島第一原子力発電所事故（福島第一原発事故）前後では、大気エアロゾル試料の採取及び放射能分析を継続し、その結果をいち早く学会で報告するとともに、研究所のホームページにも掲載してきた。ここでは前報に続き蓄積したデータ、すなわち Igarashi et al. (2015) に掲載した茨城県つくば市での約三年間にわたる福島第一原発事故による大気環境影響に関する観測結果（時系列データ）の概略を紹介し、事故直後における放射性物質の再浮遊（二次飛散）などに関する考察について解説する。

2）研究方法

月間大気降下物の捕集は、茨城県つくば市長峰にある気象研究所の露場観測実験棟屋上に設置した大気降下物捕集用のプラスチック製水盤（面積 4m^2）で 1980 年代以降実施してきた。福島第一原発事故以降（2011 年 4 月以降）は、放射能水準の上昇を考慮し、1 m^2 水盤２基での捕集を実施している。得られた試料はポリ製保管容器で保存しつつ、ロータリーエバポレーターや蒸発皿等を使用して全量を蒸発濃縮・固化し、まず Ge 半導体検出器により γ 線放出核種（放射性 Cs 等）を測定した。次いで試料の一部を分取して濃硝酸、過酸化水素を添加し加熱酸分解操作によって溶液化した。その後放射化学分離により ^{90}Sr を精製し、最終的に炭酸 Sr として固定した。数週間放置して ^{90}Sr と ^{90}Y とが放射平衡に達した後に、低バックグラウンド 2π ガスフロー検出器で β 放射能を測定した。福島第一原発事故後の試料については、事故により放出された ^{89}Sr の影響があるため、生成固定した炭酸 Sr 線源の β 放射能を繰り返し測定することで、^{90}Y の放射平衡達成と ^{89}Sr 放射能の減衰の様子とを確認しつつ評価し、必要な場合は計算で ^{89}Sr の影響を除去した。

3）結果・議論

3.1) ^{90}Sr および ^{137}Cs 大気降下量の変動と推移

Fig.1 に気象研究所における月間降下量の変動を 1950 年代後半より福島第一原発事故以降、2014 年末までのデータを含めて描画した。単位は毎月当たりの降下量（mBq/m^2）とした。福島第一原発事故が発生した 2011 年 3 月の ^{137}Cs 月間降下量は 23±0.9 kBq/m^2 であり、震災前の水準よりも 6〜7 桁大きかった。ここで示した福島第一原発事故後のデータの絶対値については、発生源が近いためその空間代表性は小さくなっていることに注意いただきたい。しかし、2012 年以降は（二次的な放出）が主な過程となりつつあることから、時系列変動の傾向は関東地方全体でほぼ同様となり、それなりの空間代表性を持つと考えている。2011 年全体では、気象研究所における ^{137}Cs 降下量は 25.5 kBq/m^2/年であった。
Fig. 1 に示すように 1957 年から福島原発事故以前についての単純な ^{137}Cs 降下量積算は、およそ 7 kBq/m^2 である。福島第一原発事故は単一事象としてこの数倍をもたらした。また、^{137}Cs の放射壊変を考慮した現存量（およそ 2 kBq/m^2）と比較したときには 10 倍強の量をもたらした。これに加え ^{134}Cs（半減期 2.1 年）がほぼ同量降下し、両核種併せての地表面汚染はおよそ 50 kBq/m^2 を超えた。この値は、文部科学省が実施した航空機マッピングによるつくば市周辺の値とほぼ整合する。その後の降下量は急速に低下してきたが、2005－2010 年における ^{137}Cs 降下量は 1.2－97 mBq/m^2/月の範囲で、2013 年における降下量は 2－39 Bq/m^2/月の範囲であり、依然として 3〜4 桁の差がある。2011 年 3 月の ^{90}Sr 降下量は 4.4±0.1 Bq/m^2

であり、同月の ^{137}Cs 降下量の約 1/5,000 だった。この降下量水準は、震災前の水準からすると 2～3 桁大きい。2011 年全体では ^{90}Sr 降下量は 10.6 Bq/m^2/年であり、^{137}Cs 降下量の約 1/2,500 であった。これに対し、1957 年からの ^{90}Sr の放射壊変を考慮した蓄積量はおよそ 0.9 kBq/m^2 である。したがって、^{90}Sr による関東地方の汚染はかなり軽微であった。また、事故前の 2005－2011 年における ^{90}Sr 月間降下量は、0.5－19 mBq/m^2/月であったのに対し、2013 年での降下量は 1－33 mBq/m^2/月となった。すなわち、^{90}Sr については福島第一原発事故以前の降下量水準に戻りつつあるが、^{137}Cs については 1970 年代～1980 年代前半の水準に依然として匹敵する。降下量水準の低下は事故直後とは異なり、全体に 2012 年以降緩やかなものとなっている。

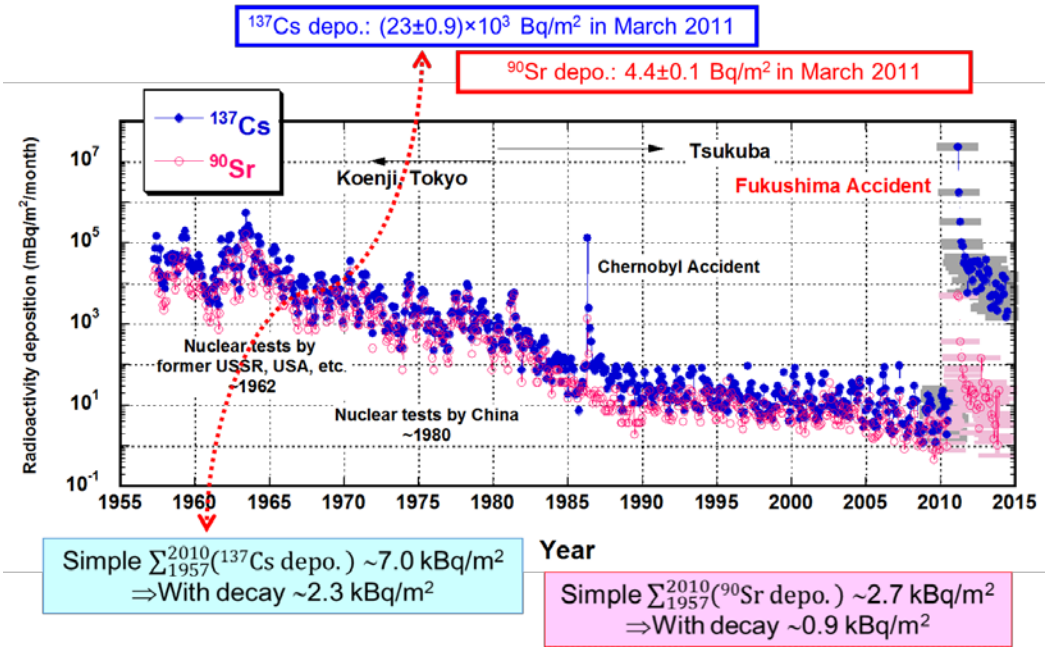

Fig. 1 Monthly deposition is expressed in mBq/m^2 on a logarithmic scale. Sr-90 and ^{137}Cs analyses from deposition samples taken 6 and 8 months before the accident, respectively, are ongoing to avoid possible sample contamination at the MRI because of the accident. Thus, these data are missing not only in Figure 1. The measurement uncertainty (1σ) is shown only for the data obtained after the Fukushima Dai-ichi Nuclear Power Plant (FDNPP) accident, and is reasonably small compared to the analytical data. For comparison, uncertainty for the monthly data in 2010 is also given. The effects of atmospheric nuclear bomb tests have been recorded since 1957. Until the Partial Test Ban Treaty (PTBT) became effective in 1963, the USA, Soviet Union, and UK conducted atmospheric tests. France and China continued atmospheric testing until 1974 and 1980, respectively. Since 1981, all the nuclear bomb tests have shifted underground, so additional radioSr and Cs contamination should be negligible. However, the Chernobyl accident in 1986 also affected the time series. The simple summation of the deposition from 1957 to the time before the FDNPP accident (mid-2010) and decay-corrected summations for ^{90}Sr and ^{137}Cs can be compared to the FDNPP-derived deposition. From Igarashi et al. (2015)

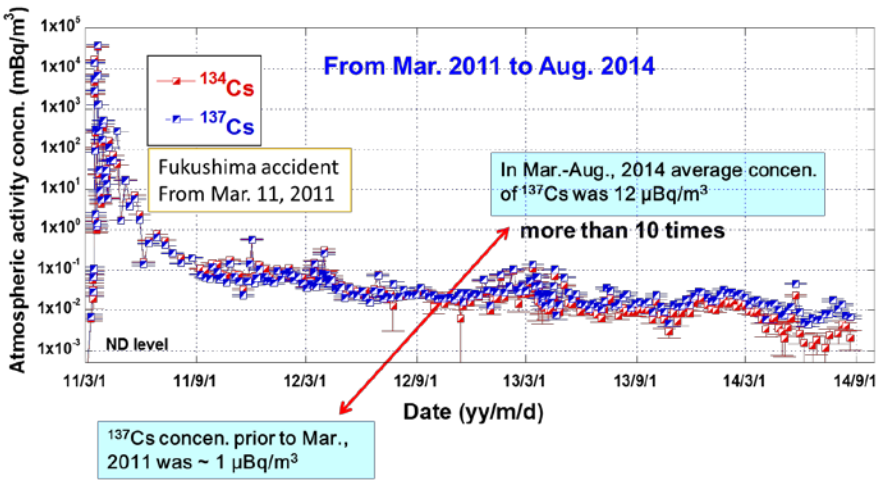

Fig. 2 Activity concentration is expressed in Bq/m^3 on a logarithmic scale. The measurement uncertainty (1σ) is shown. The maximum concentration of 38 Bq/m^3 of ^{137}Cs was observed during March 20–21, 2011. After that, the radioCs concentrations rapidly decreased until fall 2011, when the decrease slowed. The levels before (approximately 1 μBq/m^3) and three years after the FDNPP accident (12 μBq/m^3 from March to August 2014) are also compared. A difference of at least one order of magnitude is observed between the concentration level from March to August 2014 and the level before the FDNPP accident. From Igarashi et al. (2015)

3.2) ^{137}Cs 大気中濃度の変動と推移

大気中 ^{137}Cs 濃度は、2011 年 3 月 20～21 日の期間、最高値として 38 Bq/m^3 を記録した。その後、濃度は 2011 年秋までは速やかに減少し、それ以降は減少が鈍くなった。福島第一原発事故以前の ^{137}Cs 濃度水準は高くとも約 1 μBq/m^3 であったが、事故の 3 年後、2014 年での ^{137}Cs の平均濃度水準は約 12 μBq/m^3 で、事故前の水準には戻っていない。この原因は大気中に放射性 Cs を供給する過程として、汚染した環境からの再浮遊（二次的な放出）があるためと考えられる。時折、濃度上昇が観測され、グラフではスパイク状に見える。これらは事故サイトからの空気の流れがあった際に発生していた。

事故以来数年間の大気データは、放射性 Cs 濃度がどのような減少傾向を示したか、その時間変動を表し、再浮遊過程について検討・考察するための重要な根拠となる。

これらに加えて、Igarashi et al. (2015)では、福島第一原発事故発生直後からのモニタリング即応活動の結果（^{90}Sr の大気中濃度を他のγ線放出核種と併せて示した）や、大気放射能汚染に対するモデリング、モデルを利用したデータ解析アプローチなど、関連した情報が付属資料で提供されている。

3.3) 事故直後の ^{137}Cs 大気中濃度の変動とエアロゾルモデルによる解析－事故直後の再浮遊

Fig. 3 に a) 放射性核種の福島第一原発事故直後の大気中濃度の時間変動、b) そのエアロゾルモデルによる再現計算の結果の比較を示した。b)では実測値とモデル計算値は全体によく一致するが、モデル値ではプルームが通過すると濃度値はほぼゼロにまで低下し、たとえば 3 月 16－20 日の期間は実測値とまったく一致しない。この不一致の原因はモデルでは再浮遊をまったく計算していないことにあると考えた。そこで、観測値とモデル計算値を組み合わせて、放射性物質が沈着した直後にどの程度の再浮遊が生じているのか、求めてみた（Igarashi et al., 2015）。

放射性物質、^{137}Cs の大気中濃度の時間変動（$\partial C/\partial t$）は、連続の式を考えたとき、

$$\partial C/\partial t = \nabla(\boldsymbol{K}_{dif}\nabla C) - \nabla(\boldsymbol{U}C) - \lambda C + \Phi$$ と表される。

ここで、$\boldsymbol{K}_{dif}$ は 3 次元の拡散係数、$\boldsymbol{U}$ は風の場、λは壊変定数、そして Φ が放射性核種の再浮遊となる。他方 ボックスモデルにおいて ^{137}Cs の濃度変動を考えると、以下のように表される。

$$\Delta C/\Delta t = \Phi = ki \cdot Di \cdot (\Delta x \Delta y/\Delta x \Delta y \Delta z)$$

ここで *ki* と *Di* はそれぞれ、核種 *i* の再浮遊係数（毎秒 s^{-1}）、および地表面汚染（Bq/m^2）である。つまり、地表面汚染 *Di* に比例して、比例定数 *ki* で、常時大気へ ^{137}Cs が供給されていると考える。Δx、Δy および Δz はモデルのボックスの縦・横および高さである。放射性壊変、水平拡散を無視し、積雲による急速な対流がなかったとして、流入と流出の収支をとったとき、最終的に次式が得られる。

$$(ki \cdot Di)/(\Delta z) = (\Delta Kz/\Delta z) \cdot (\Delta Ci/\Delta z) + (\Delta u/\Delta x + \Delta v/\Delta y) \cdot Ci$$

ここで *i* は核種を、*Di* はモデル計算（ガス+エアロゾル）で得られた 3 月 17 日 9 時までの累積沈着量（Bq/m^2）を、*ki* は地表面汚染がどの程度の割合で再浮遊するかを表す比率（再浮遊係数；s^{-1}）であり、*u*、*v* と *Kz* はそれぞれモデルによる平均水平風速(m/s)、鉛直の乱流拡散係数（m^2/s）である。*Ci* は ^{137}Cs の平均実測濃度で（9.75×10^{-4} Bq/m^3）、Δx、Δy、を 3 km、9 km または 15km とし、Δz を 100、200 または 400 m と変化させた。上式で流入濃度がゼロとおいて *ki* を求めると、最小で 1.6×10^{-6}~1.5×10^{-5} 毎秒（平均 6.1×10^{-6} 毎秒）となり、放射性 Cs が沈着した直後には 1 時間当たり沈着量の 2%程度が大気へ再浮遊していたと考えられた。この値は過去のチェルノブイリ事故によるデータとも整合していた。事故直後の再浮遊はかなり大きな値を取るが、時間経過とともに急速に小さくなっていくらしい。

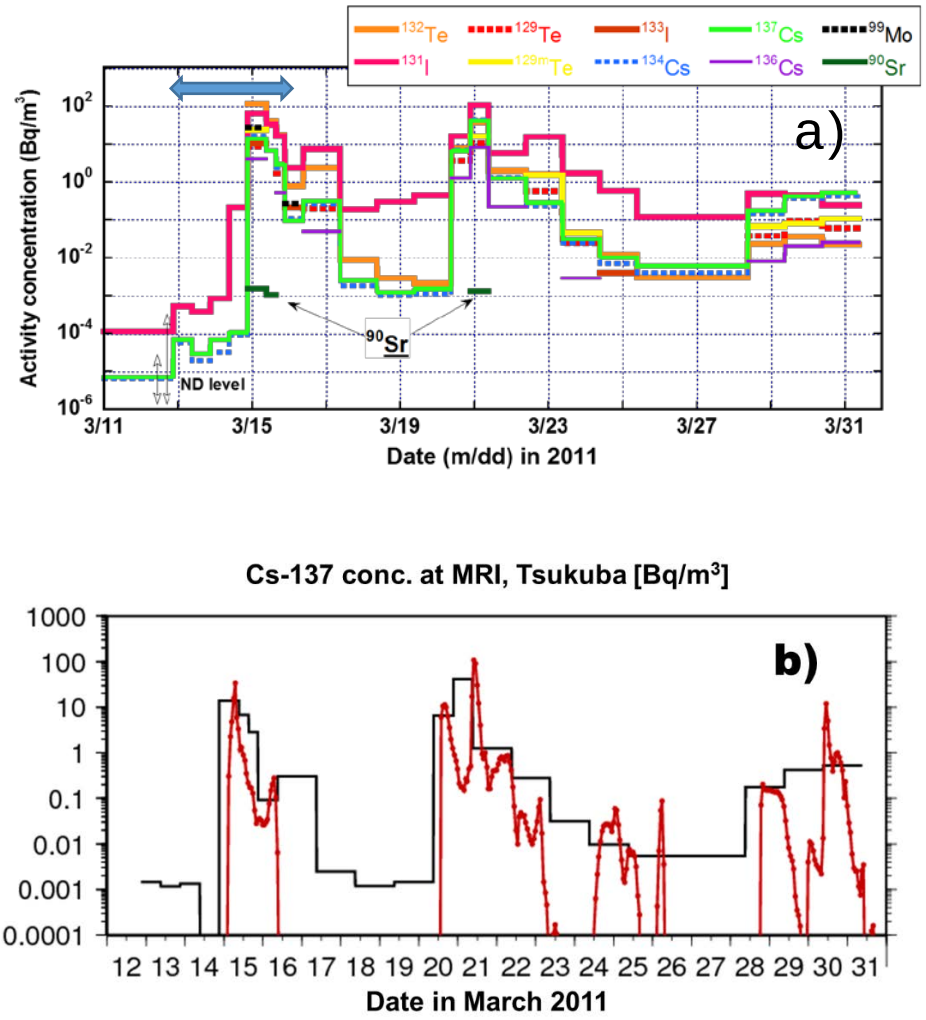

Fig. 3 Atmospheric activity concentrations of radionuclides from the FDNPP accident in March 2011 a) Observed data from filter samples collected at the MRI, Tsukuba, Japan; b) comparison of observed (black) and simulated results (red) for ^{137}Cs The abscissa is expressed in dates in March 2011 and is labeled at the start of the day in a) and the middle of the day in b). Contamination of the filter samples cannot be totally ruled out for the period before March 14 in a), which is depicted by the left-right pointing double arrow. From Igarashi et al. (2015)

4）まとめと今後に向けて

福島第一原発事故後、茨城県つくば市の気象研究所における ^{90}Sr および ^{137}Cs の月間降下量（大気降下物）観測の結果について報告した。2014 年末の時点では、福島第一原発事故直後と比較すると降下量は数桁も低下し、甚大な汚染というべき水準ではない。^{90}Sr については、事故以前の降下量とほぼ同じ水準に戻りつつある。しかし、^{137}Cs については依然として 3〜4 桁より大きな値となっている。水準低下にはまだ時間がかかるであろう。ただし、福島第一原発事故サイトからの放出はあっても、現状の大気中の濃度水準を説明できるほどの量にはないと考えられる（Igarashi et al., 2015）。

一次放出に替わり、大気へのこれらの核種の供給を続けている過程は、いわゆる再浮遊（二次放出）である。沈着直後の二次放出はかなり大きな値を取ることがわかった。二次放出は周辺の環境から由来すると考えられるから、周辺の汚染度がつくばに比し数桁高い地域においては、降下量もそれに比例し数桁高い。従って、二次放出過程の解明は必須な科学的課題である。二次放出源には、従来、汚染した地表面からの表土ダスト、汚染植生からの再浮遊、または汚染したゴミの燃焼、野焼き等による放射性物質の大気への揮散などが想定されてきた。最近、夏季における発生源として森林生態系からのバイオエアロゾル発生が寄与するのではないかとの仮説が急浮上してきている。今後は、その解明に努めねばならない。

上記に加えて、こうした長期の観測においては分析やデータの品質管理が必ず問題となる。このような点についても常に留意しながら、観測の継続を図っていくことが肝要である。（木村ほか、2015）

参考文献

Igarashi, Y., Kajino, M., Zaizen, Y., Adachi, K., and Mikami, M., Atmospheric radioactivity over Tsukuba, Japan: a summary of three years of observations after the FDNPP accident, Progress in Earth and Planetary Science 2:44, 2015. doi: 10.1186/s40645-015-0066-1

木村徹，五十嵐康人，「大気降下物試料の放射能分析の品質管理」Proceedings of the 16th Workshop Environmental Radioactivity. KEK Proceedings 2015-4, 23-27, 2015

2. 大気中の放射性物質の物理・化学性状

1）はじめに

大気中で観測される放射性物質は、ガスや粒子（エアロゾル）として大気中に漂い、やがて地上や海水面に降下する。その大気拡散や環境動態、また発生メカニズムを理解するには、放射性物質がどのような物理化学性状を持ち、またどのようなエアロゾルを担体としているかを解明する必要がある。本章では、一例として東日本大震災で発生した福島第一原子力発電所事故によって直接放出された放射性物質の物理化学特性の理解を目指した研究成果を報告する。

2011 年 3 月に発生した事故によって様々な放射性物質が大気・海洋に放出されたが、放出された放射性物質は重量としては非常に微量であるので、放射能測定以外の分析手法で環境試料から検出することは困難であった。しかしながら、放射性物質の環境動態は、それ自体の性質だけで決まるものではなく、その運び手となる粒子の化学組成、イオン状態、粒径、表面状態といった物理化学特性に支配されるため、担体を含めた物理特性や化学特性の分析は重要である。微量化学物質の有効な分析手法として、電子顕微鏡や放射光分析などの微小領域化学分析がある。本研究においては、それらの手法を用いて 2011 年 3 月 14-15 日につくば市で採取されたフィルター試料中の放射性粒子の特定を行った（Adachi et al., 2013）。またそれらの粒子の組成、化学状態、結晶状態をマイクロビーム放射光によって分析し（Abe et al., 2014）、さらに放射性粒子の断面を透過型電子顕微鏡により詳細に解析した（Yamaguchi et al., 2016）。なお、Adachi et al. (2013)と Abe et al., (2014)は総説として日本語の論文にまとめた（足立, 2015）。

2）主な研究成果

一連の研究の中で、最初の研究（Adachi et al., 2013）では、走査型電子顕微鏡（SEM-EDS）を用いて 2011 年 3 月 14－15 日にかけて関東に飛来した放射性粒子を分析し、セシウム、鉄、亜鉛や多くの核燃料由来と考えられる元素を含み、水に溶けにくい２マイクロメートル前後の球状ガラス様粒子であることを示した。そして、これらの詳細な物理特性は、事故時における粒子の拡散モデルの精度向上に重要であることを示唆した。

続いて行った研究（Abe et al., 2014）では、大型放射光施設 SPring8 において、感度の高い極微量元素分析を行い、SEM-EDS 分析で得られた元素（鉄、亜鉛、セシウム）に加え、ルビジウム、ジルコニウム、モリブデン、スズ、アンチモン、テルル、バリウムが全ての放射性粒子から検出されることを示した。加えて、マンガン、クロム、銀、ウラン、鉛などの元素も 1 個もしくは 2 個の粒子から検出された。また、化学状態や結晶状態を X 線吸収端近傍構造分析（XANES）や X 線回折法（XRD）を用いて分析し、大気中に放出された放射性粒子が非晶質のガラス状であることを示した。これらの研究成果は、炉内での粒子発生メカニズムの解明へ貢献することが期待される。

さらに、Yamaguchi et al. (2016) は、事故によって放出された放射性粒子を、収束イオンビーム装置を用いて薄片化し、透過型電子顕微鏡（TEM）による分析に供した。その結果、表面分析ではわからなかった内部の構造、すなわちセシウムが粒子表面に濃集していることを示した。また、銀やテルルなどのナノ粒子が放射性粒子に内在していることも明らかにした。これらの発見は、放射性粒子の長期的環境動態の予測や粒子生成メカニズムの解明において重要な知見である。

3）まとめ

このように、気象研究所で行った研究により、福島第一原子力発電所事故において放出された放射性物質の大気中の物理化学特性の一部が明らかとなった。これらの研究はケーススタディであるが、今後様々な発生源から放出される放射性物質の発生源メカニズムの解明や環境動態の予測への貢献が期待される。

参考文献

Abe, Y., Iizawa, Y., Terada, Y., Adachi, K., Igarashi, Y., and Nakai, I., Detection of uranium and chemical state analysis of individual radioactive microparticles emitted from the Fukushima nuclear accident using multiple synchrotron radiation X-ray analyses, Analytical Chemistry, 86, 8521-8525, 2014.

Adachi, K., Kajino, M., Zaizen, Y., and Igarashi, Y., Emission of spherical cesium-bearing particles from an early stage of the Fukushima nuclear accident, Scientific Reports, 3, 2554, 2013.

Yamaguchi, N., Mitome, M., Kotone, A. H., Asano, M., Adachi, K., and Kogure, T., Internal structure of cesium-bearing radioactive microparticles released from Fukushima nuclear power plant. Scientific Reports, 6, 20548, 2016.

足立光司, 電子顕微鏡がとらえた放射性粒子, 地球化学, 49, 185–193, 2015.

3. 大気中の放射性物質のモデルによる評価

1）放射性物質移流拡散沈着モデル

本研究を進めるにあたり、Kajino et al.（2012）によって開発された領域大気質モデル（Regional Air Quality Model 2; RAQM2）を放射性物質移流拡散モデルとして使用できるよう改変した（Adachi et al., 2013）。このモデル（RAQM2）はエアロゾルの粒径分布を対数正規分布関数で仮定して、核生成・凝結・凝集・乾性沈着・グリッドスケールの雲凝結／氷晶核活性化といったエアロゾル力学過程をトリプルモーメント法で記述する独自のエアロゾルモジュールを実装している。また、エアロゾル力学過程とそれに続く雲微物理過程（雲内部での降水除去過程）と雲底下での降水除去過程に関する方程式系がすべてモデル（RAQM2）内で記述されている。

RAQM2 はオフラインモデルであり、気象場（気象物理量の格子点解析値）は外部から与えられる。標準的なシミュレーション計算では、気象庁非静力学気象モデル（JMA-NHM; Saito et al., 2007）を水平解像度 3km（東日本を 215×259 グリッドに分割）で実行することによって気象場を作成し、同じ解像度とドメインで RAQM2 の計算も行った。この際、JMA-NHM の鉛直解像度 50 層（最上層は 50hPa＝高度 20km 程度）を RAQM2 では 20 層（最上層は高度 10km）に変換した。JMA-NHM の初期値および境界値（スペクトルナッジング）には気象庁メソ客観解析値（水平解像度 5km ; 時間解像度 3 時間）を用いた。また、異なる気象場の計算法として、JMA-NHM を局所アンサンブル変換カルマンフィルタ（LETKF）データ同化システムに組み込み、気象観測値（アメダス、ラジオゾンデ、海上風等）をデータ同化することによって独自に格子点解析値を作成することも試みた（Sekiyama et al., 2015）。

福島第一原子力発電所事故による大気汚染シミュレーションをモデル計算のテストケースとして実施する場合には、原子力発電所から放出された ^{137}Cs の量として Katata et al.（2011）の時系列インベントリーを利用した。^{137}Cs は全量が硫酸エアロゾルと有機炭素エアロゾルの内部混合粒子に含まれていると仮定し、その ^{137}Cs 含有粒子は数等価幾何平均の乾燥直径を 0.5μm、標準偏差を 1.6、粒子密度を 1.83 g/cm^3、吸湿性を 0.4 としてモデル内の方程式系を計算した。^{137}Cs 含有粒子の放出高度は Katata et al.（2011）の推定シナリオに合わせて高度 20m から 150m の間で時間変化させた。

2）エアロゾルの物理・化学特性に関するモデル感度実験

Kajino（2015）では、1）節で解説したモデルを用いて、2011 年 3 月における原発事故由来の ^{137}Cs の放出、輸送、沈着過程の再現実験を行った。そして、2 章で解説した放射性セシウムを含むエアロゾルの物理・化学特性の違いや、複数の異なる気象モデルの計算結果を用いた比較・感度実験を実施した。放射性セシウムを運ぶエアロゾルは 2 種類考慮した : 1）節で述べた水溶性のサブミクロン粒子、および 2 章で述べた Adachi et al.（2013）で発見された非水溶性の粗大粒子である。

同じエアロゾル特性や沈着モジュールを用いた計算であっても、用いた気象モデルの違いにより ^{137}Cs の沈着量は 3 倍程度変化した。またエアロゾル特性の違いによる沈着量の変化は、気象モデルによる違いよりは小さいが、最大で 2.1 倍程度の変化をもたらした。したがって、気象モデルの違い（すなわち力学コアや物理スキームの違い）やエアロゾル微物理特性の違いもまた放射性セシウムの動態モデリングにとって重要なパラメータであることが判明した。

参考文献

Adachi, K., Kajino, M., Zaizen, Y., and Igarashi, Y., Emission of spherical cesium-bearing particles from an early stage of the Fukushima nuclear accident, Sci. Rep., 3, 2554, 2013.

Kajino, M., Inomata, Y., Sato, K., Ueda, H., Han, Z., An, J., Katata, G., Deushi, M., Maki, T., Oshima, N., Kurokawa, J., Ohara, T., Tamami, A., and Hatakeyama, S., Development of the RAQM2 aerosol chemical transport model and prediction of the Northeast Asian aerosol mass, size, chemistry, and mixing type, Atmos, Chem. Phys., 12, 11833–11856, 2012.

Kajino, M ., G-3. NHM-Chem: Sensitivity of Cs deposition to the size and hygroscopicity of Cs-bearing aerosols, Technical Reports of the Meteorological Research Institute, 76, 132–142, 2015.

Katata, G., Ota, M., Terada, H., Chino, M., and Nagai, H., Atmospheric discharge and dispersion of radionuclides during the Fukushima Dai-ichi Nuclear Power Plant accident. Part I: Source term estimation and local-scale atmospheric dispersion in early phase of the accident, J. Environ. Radioactivity, 109, 103–113, 2011.

Saito, K., Ishida, J., Aranami, K., Hara, T., Segawa, T., Narita, M., and Honda, Y., Nonhydrostatic atmospheric models and operational development at JMA, J. Meteorol. Soc. Jpn., 85B, 271–304, 2007.

Sekiyama, T. T., Kunii, M., Kajino, M., and Shinbori, T., Horizontal Resolution Dependence of Atmospheric Simulations of the Fukushima Nuclear Accident Using 15-km, 3-km, and 500-m Grid Models, J. Meteorol. Soc. Jpn., 93B, 49–64, 2015.

4. 福島第一原発事故前に採取されデータ未報告だった試料の分析・測定結果について

1）はじめに

福島第一原発事故前に採取された試料で、事故当時分析や前処理の途上にあった試料はつくば市の研究所の実験や測定環境が著しく汚染されたために、その汚染を極力避け、濃縮操作・測定自体を汚染度の低い関西の大阪大学や㈱環境総合テクノス及び㈱アトックスにおいて実施した。そのデータの分析結果をここでは報告する。

2）主な研究成果

2.1) ^{137}Cs のデータ

Table 1 に福島第一原発事故前につくばと榛名山で観測された ^{137}Cs の月間降下量を示す。^{137}Cs の降下量は、福島第一原発事故によって ^{134}Cs がほぼ 1:1 の放射能比で放出されたということに基づき、試料に含まれる ^{137}Cs 放射能はグローバルフォールアウトと原発事故の両者から由来するが、^{134}Cs は原発事故からのみ由来したと考え、差分放射能を求めた。この差分放射能を減衰補正することで、グローバルフォールアウト由来の ^{137}Cs 放射能を得る。しかし、差分放射能の値はほとんどの試料において僅かな数値であり、不確実なデータとなったことから ND（検出限界値以下）と判断せざるを得なかった。一部、差分放射能値が有為となった試料がある（榛名山 1010、同 1011、同 1012）。しかしながら、榛名山 1010 の値は 1 Bq/m^2/月を超えており、事故以前の水準を超えている。試料の保管、輸送、その後の操作では細心の注意を払って、厳重に汚染管理に努めたものの、汚染を受けている可能性も否定できない。榛名山 1011、同 1012 については、汚染を受けなかったと判断される。

2.1) ^{90}Sr のデータ

つくば市での ^{90}Sr の月間降下量については、Table 2 に掲げるとおりである。^{90}Sr の汚染水準は放射性 Cs に比べ何桁も小さいことから、細心の注意を払った汚染管理によって充分に事故の影響を避けることができた。しかし、残念ながら、2011 年 1 月の降下量は ND となって定量化できていない。引き続き値を出せないか、再測定を行っていく。

3）まとめ

以上のように、大変残念ではあるが、福島第一原発事故による実験・測定環境の汚染により、気象研究所の月間降下量時系列データに欠測が発生したことを報告する。

試料の前処理・化学分析・放射能測定に協力いただいた大阪大学、(株)環境総合テクノス、(株)アトックスと関係者各位に感謝する。

Table 1　Monthly ^{137}Cs deposition at the MRI, Tsukuba and Mt. Haruna

試料名	分析番号	採取地点	採取月（期間）	放射能(2011/3/11に減衰補正)				差分放射能 (^{137}Cs-^{134}Cs)		差分放射能 (^{137}Cs-^{134}Cs)(採取日に減衰補正)		
				^{134}Cs (mBq/㎡)	誤差 (mBq/㎡)	^{137}Cs (mBq/㎡)	誤差 (mBq/㎡)	^{137}Cs (mBq/㎡)	誤差 (mBq/㎡)	^{137}Cs (mBq/㎡)	誤差 (mBq/㎡)	
MRI 1009 4㎡	–	MRI	2010年9月	42.2	3.6	41.5	2.6	−0.7	4.4	ND	–	
MRI 1010 4㎡	1	MRI	2010年10月	1452	73.0	1492	74.8	41	105	ND	–	
MRI 1011 4㎡	–	MRI	2010年11月	36.2	3.3	37.3	2.3	1.1	4.0	ND	–	
MRI 1012 4㎡	2	MRI	2010年12月	44.6	3.6	57.8	3.2	13.2	4.8	ND	–	
MRI 1101 4㎡	3	MRI	2011年1月	0.4	2.0	5.1	1.1	4.6	2.3	ND	–	
MRI 1102 4㎡	4	MRI	2011年2月	51.0	3.9	48.4	2.8	−2.5	4.8	ND	–	
榛名山 1008 4㎡	5	榛名山	2010年8月					144	117	ND	–	
				32.6	6.9	60.3	3.9	27.7	7.9			注1
				1521	81.3	1637	83	117	116			注2
榛名山 1009 4㎡	6	榛名山	2010年9月	57.4	8.4	85.2	4.9	27.8	9.7	ND	–	
榛名山 1010 4㎡	7	榛名山	2010年10月					1387	172	1398	173	
				26.0	15.4	1310	67.0	1283	69			注1
				2139	110	2242	113	103	158			注2
榛名山 1011 4㎡	8	榛名山	2010年11月	11.9	2.8	54.9	3.2	43.0	4.2	43.3	4.2	
榛名山 1012 4㎡	9	榛名山	2010年12月	71.7	6.6	104.0	5.6	32.3	8.7	32.4	8.7	
榛名山 1101 4㎡	10	榛名山	2011年1月	5.7	3.6	14.1	1.5	8.4	3.9	ND	–	
榛名山 1102 4㎡	11	榛名山	2011年2月	33.3	5.5	38.8	2.6	5.5	6.1	ND	–	

*^{134}Csの標準が無いため、標準に同形の土壌試料を使用した

*差分放射能については、^{137}Csがマイナス（統計的誤差）となっているものもあるがそのまま表記した

*減衰補正後の差分放射能については、誤差の3倍を超えないものについては、NDとして放射能を算出した

注1　保管容器、ロンテナに収納した試料のみを濃縮乾燥し測定した値

注2　濃縮途中試料のみを濃縮乾燥し測定した値

Table 2 Monthly deposition of ^{90}Sr and ^{137}Cs at the MRI, Tsukuba during the years of 2010 and 2011
Regarding some of the samples, we could not obtain the correct data due to the heavy contaminations of the sample itself, experimental environment, measurement environment as well as detectors themselves.

年	月	^{90}Sr			^{137}Cs			$^{137}Cs/^{90}Sr$	降水量	残渣重量
		mBq/m^2			mBq/m^2			放射能比	mm	g/m^2
2010	1月	2.55	±	0.89	6.76	±	1.27	2.7	9.5	1.26
	2月	3.36	±	0.72	17.1	±	3.05	5.1	96.5	2.84
	3月	5.98	±	0.80	22.5	±	3.40	3.8	101.0	2.92
	4月	3.56	±	0.67	12.3	±	2.14	3.4	169.0	2.48
	5月	3.67	±	0.35	8.69	±	1.69	2.4	132.0	1.72
	6月	0.97	±	0.19	1.87	±	0.35	1.9	95.0	0.94
	7月	1.19	±	0.73	4.23	±	0.62	3.6	69.5	1.39
	8月	0.60	±	0.05	ND	±		-	5.0	0.81
	9月	1.44	±	0.62	ND	±		-	379.5	1.34
	10月	1.09	±	0.49	ND	±		-	157.5	0.70
	11月	0.97	±	0.14	ND	±		-	81.5	0.30
	12月	4.31	±	0.77	ND	±		-	102.0	1.11
合計		29.7			73.4			2.5	1398.0	17.81
2011	1月	ND	±		ND	±		-	0.0	0.74
	2月	1.84	±	0.86	ND	±		-	104.5	1.03
	3月	5160	±	46.6	23100000	±	924000	4480	74.0	4.65
	4月	4660	±	40.7	1780000	±	1300	382	74.5	5.97
	5月	376	±	14.9	330000	±	273	878	210.0	3.90
	6月	152	±	10.9	104000	±	142	683	138.5	2.09
	7月	46.0	±	7.13	82000	±	125	1780	184.0	2.53
	8月	76.8	±	6.18	32000	±	99.1	417	142.5	1.17
	9月	25.7	±	6.65	45900	±	88.8	1780	186.0	2.76
	10月	31.3	±	4.98	25800	±	103	824	160.5	1.29
	11月	15.2	±	1.38	5850	±	47.4	385	79.0	0.73
	12月	31.0	±	4.84	20300	±	83.8	654	41.0	1.79
合計		10580			25530000			2410	1394.5	28.65

Activity unit: mBq/m^2/month

ND: We could not obtain the significant data.

5. Publications 2013-2015

出版論文 2013-2015

Igarashi et al. Progress in Earth and Planetary Science (2015) 2:44
DOI 10.1186/s40645-015-0066-1

Progress in Earth and Planetary Science
a SpringerOpen Journal

RESEARCH ARTICLE Open Access

Atmospheric radioactivity over Tsukuba, Japan: a summary of three years of observations after the FDNPP accident

Yasuhito Igarashi[1*], Mizuo Kajino[1], Yuji Zaizen[1], Kouji Adachi[1] and Masao Mikami[1,2]

Abstract

A severe accident occurred in March 2011 at the Fukushima Dai-ichi nuclear power plant (FDNPP) operated by the Tokyo Electric Power Company (TEPCO), causing serious environmental pollution over a wide range covering eastern Japan and the northwestern Pacific. This accident created a large mark in the atmospheric radionuclide chronological record at the Meteorological Research Institute (MRI). This paper reports the impacts from the FDNPP accident over approximately 3 years in Tsukuba, Ibaraki (approximately 170 km southwest from the accident site), as a typical example of the atmospheric pollution from the accident. The monthly atmospheric ^{90}Sr and ^{137}Cs depositional fluxes in March 2011 reached approximately 5 Bq/m^2/month and 23 kBq/m^2/month, respectively. They are 3–4 and 6–7 orders of magnitude higher, respectively, than before the accident. Sr-90 pollution was relatively insignificant compared to that of ^{137}Cs. The ^{137}Cs atmospheric concentration reached a maximum of 38 Bq/m^3 during March 20–21, 2011. After that, the concentrations quickly decreased until fall 2011 when the decrease slowed. The pre-FDNPP accident ^{137}Cs concentration levels were, at most, approximately 1 μBq/m^3. The average level 3 years after the accident was approximately 12 μBq/m^3 during 2014. The atmospheric data for the 3 years since the accident form a basis for considering temporal changes in the decreasing trends and re-suspension (secondary emission), supporting our understanding of radioCs' atmospheric concentration and deposition. Information regarding our immediate monitoring, modeling, and data analysis approaches for pollution from the FDNPP accident is provided in the Appendices.

Keywords: Temporal change, ^{90}Sr, ^{137}Cs, Atmospheric deposition, Atmospheric concentration, FDNPP accident

Background

We have conducted observational research on radionuclides in the environment for almost 60 years at the Meteorological Research Institute (MRI) in Japan, ever since the 1950s when the USA, Soviet Union, and others performed vigorous nuclear tests in the atmosphere. The atmosphere is the major medium into which radioactive materials were directly injected by the nuclear tests and accidents, and within it, transport, diffusion, and wet and dry removal of these materials occur. During the nuclear testing era, the major purpose of our research was to clarify the radioactive pollution situation and its major controlling factors in the atmosphere (Hirose et al. 1986; Katsuragi 1983; Miyake 1954; Miyake et al. 1963, 1975) and hydrosphere (Miyake et al. 1955, 1962, 1988). After the Chernobyl accident, the purpose of the research gradually shifted to obtaining more data about various processes in the atmosphere (Aoyama 1988; Aoyama et al. 1986, 1987, 1991, 2006; Hirose et al. 1993, 2001; Igarashi et al. 1996, 2003, 2009) and hydrosphere (Aoyama 1995, Aoyama and Hirose 2004; Hirose et al. 1999, Hirose and Aoyama 2003; Miyao et al. 2000). Of particular interest in this study, observation of monthly radionuclide deposition (atmospheric total deposition/radioactive fallout) for ^{90}Sr (half-life, 28.8 years) and ^{137}Cs (half-life, 30.2 years) had continued for 57 years as of April 2014, although the location of the observations moved from Koenji, Tokyo, to Tsukuba in 1980 when the science city was built (Katsuragi 1983). Both radionuclides are

* Correspondence: yigarash@mri-jma.go.jp
[1]Meteorological Research Institute, 1-1 Nagamine, Tsukuba, Ibaraki 305-0052, Japan
Full list of author information is available at the end of the article

scientifically important because of their health and environmental impacts (e.g., see U.S. Department of Health and Human Services, Public Health Service, Agency for Toxic Substances and Disease Registry ATSDR2004Cs 2004; U.S. Department of Health and Human Services, Public Health Service, Agency for Toxic Substances and Disease Registry ATSDR2004Sr 2004). We continued collecting and analyzing atmospheric samples after the accident at Tokyo Electric Power Company's (TEPCO) Fukushima Dai-ichi Nuclear Power Plant (FDNPP) in Ohkuma-machi and Futaba-machi, Fukushima prefecture (37.42 °N, 140.97 °E) in March 2011.

Many authors have attempted to determine the environmental impacts of the FDNPP accident, which have gradually come to light (e.g., Aoyama et al. 2012, 2013; Hirose 2012; Kusakabe et al. 2013; Masson et al. 2011; Masumoto et al. 2012; MEXT 2011a ; MEXT and USDOE 2011; Povinec et al. 2013a, b; Tsumune et al. 2013; Yamamoto et al. 2012; Yoshida and Kanda 2012; Yoshida and Takahashi 2012). We still need to study the following issues from an atmospheric science point of view (Igarashi 2009): (1) primary source terms including emissions inventory and temporal changes (e.g., Chino et al. 2011; Katata et al. 2012, b, 2014; Maki et al. 2013; Stohl et al. 2012; Terada et al. 2012; Winiarek et al. 2012), (2) transport and diffusion (e.g., Masson et al. 2011; Morino et al. 2011; Sekiyama et al. 2015; Stohl et al. 2012; Takemura et al. 2011; Tanaka 2013; Terada et al. 2012), and (3) dry and wet removal (e.g., Adachi et al. 2013; Hirose et al. 1993; Kristiansen et al. 2012), which governed radioactive surface contamination during the early phase of the accident. In addition, the physical and chemical properties of the radioactive materials (e.g., Adachi et al. 2013; Kaneyasu et al. 2012) are important factors that influence the second and third subjects to be investigated. Here, we summarize the observations, present a time series of the atmospheric impacts of the TEPCO FDNPP accident over approximately 3 years in Tsukuba, Ibaraki, Japan, and compare the levels to the situation before the accident as very basic scientific information (Igarashi, 2009). In addition, secondary emissions from contaminated surfaces to the atmosphere (re-suspension; Igarashi 2009) have become important during the later phases. Resuspension comes from contaminated surfaces, terrestrial ecosystems, and open-field burning. These sources have undoubtedly supported atmospheric radionuclides but are not yet well understood and are thus considered briefly. Other information about the accident, related to our immediate monitoring and modeling endeavors and data analysis approaches to short-lived γ-emitters and ^{89}Sr, is summarized in the Appendices.

Methods

Atmospheric deposition samples

The monthly atmospheric total deposition/atmospheric fallout has been sampled using a weathering-resistant plastic tray (area = 4 m^2) installed on a cottage roof in an open field of the MRI in Tsukuba, Ibaraki (36.1 °N, 140.1 °E; approximately 170 km southwest of the FDNPP) since the 1980s. After April 2011, the sample size was reduced to two trays, each 1 m^2, which we considered sufficient for the levels present after the FDNPP accident. The collected samples were evaporated and concentrated into a gross quantity with a rotary evaporator (Eyela NE-12) or an evaporating dish, and the samples were saved in a polyethylene safekeeping container. Each evaporated sample, packed in a cylindrical plastic container, was measured for γ-ray emitting radionuclides (^{134}Cs and ^{137}Cs) using a Ge semiconductor detector (coaxial-type from ORTEC EG&G or Eurisys) coupled with a computed spectrometric analyzer (Oxford-Tennelec Multiport or Seiko EG&G 92x). The precision, accuracy, and quality control of the measurements are described elsewhere (Otsuji-Hatori et al. 1996).

Part of the sample was then stored for future reanalysis. The remaining sample was added to concentrated nitric acid along with H_2O_2 and digested in a heating operation. Sr-90 was radiochemically recovered from the obtained sample solution, purified and finally fixed as Sr carbonate precipitate, an activity measurement source. After the source was left for several weeks to achieve ^{90}Sr and ^{90}Y radioequilibrium, its β-activity was measured using a low-background 2π gas-flow detector (Tennelec LB5100) with P10 gas (Otsuji-Hatori et al. 1996). Within several months after the FDNPP accident, ^{89}Sr (half-life, 50.5 days) from the accident coexisted with ^{90}Sr and affected the β-activity measurement. To remove the ^{89}Sr influence, we occasionally repeated the Sr source measurement and evaluated the radioequilibrium between ^{90}Sr and ^{90}Y, as well as the decrease in ^{89}Sr activity (see Appendix 2). When required, the influence of the ^{89}Sr activity was subtracted from the β-activity counts to obtain the ^{90}Sr activity. The activity was always decay-corrected mid-sampling. The detection limit for ^{90}Sr was approximately 7.0 mBq/sample, approximately 3.5 mBq/m^2 using a total of 30,000 s of measurement. For ^{137}Cs, the limit was approximately 16.0 mBq/sample, approximately 8.0 mBq/m^2 for an average of 120,000 s of measurement.

Atmospheric radioactive aerosols

Aerosol samples were collected weekly using a high-volume air sampler (HV; Sibata Scientific Technology Ltd., HV-1000 F) on a quartz fiber filter (Advantech QR100; 203 mm × 254 mm) (Igarashi et al. 1999a). During March 2011, the sampling frequency was intensified.

The flow rate was set at 0.7 m^3/min, and the daily sucked air volume was approximately 1000 m^3. After collection, the filters were compressed into pellets using a hydraulic press device. They then underwent conventional γ-ray spectrometry with Ge detectors as described above. Current detection limits for ^{134}Cs and ^{137}Cs are approximately 9.0 mBq/sample (1.3 μBq/m^3) and 10 mBq/sample (1.5 μBq/m^3) for approximately 1,000,000 s measurements, respectively.

The filter samples collected before the radioactive plume arrived at Tsukuba were measured at the Kyoto University Research Reactor Institute to achieve lower detection limits and avoid contamination from the FDNPP accident. This was necessary because the Ge detectors, measurement environment, and experimental materials at the MRI were somehow contaminated by the radioactive plume's passage on March 14–15 and 20–23, 2011 (see Appendix 1). To date, radioSr analysis has been performed on only a limited number of aerosol samples collected during March 2011. The results are presented in Appendix 2.

Results and discussion

Figures 1 and 2 depict the results of the atmospheric ^{90}Sr and ^{137}Cs deposition observations at the MRI for different durations. The temporal changes in monthly radionuclide depositions shown in Fig. 1 include those from the late 1950s to more recently available data, i.e., after the FDNPP accident. Figure 2 compares the amounts of atmospheric deposition after the FDNPP accident and from the late 2000s. Analyses of ^{90}Sr and ^{137}Cs deposition samples taken 6 and 8 months before the accident are ongoing to control for possible sample contamination at the MRI caused by the accident. Thus, these data are missing in Figs. 1 and 2.

Figure 3 depicts the temporal change in atmospheric activity concentrations of radioCs since March 2011. Before the FDNPP accident, it was difficult to detect ^{137}Cs below about 1 μBq/m^3 in the air (the global fallout background level).

Although there were small-scale Japanese nuclear accidents in the 1990s (Igarashi et al. 1999a, 2000; Komura et al. 2000), they did not cause significant marks in the present time series of monthly ^{90}Sr and ^{137}Cs depositions. The effects of the Chernobyl accident that occurred in 1986 were more evident for ^{137}Cs than ^{90}Sr (e.g., Aoyama et al. 1991) as illustrated in Fig. 1. However, the previous maximum ^{137}Cs deposition was two orders of magnitude lower than those caused by the FDNPP accident. Thus, the impact of the FDNPP

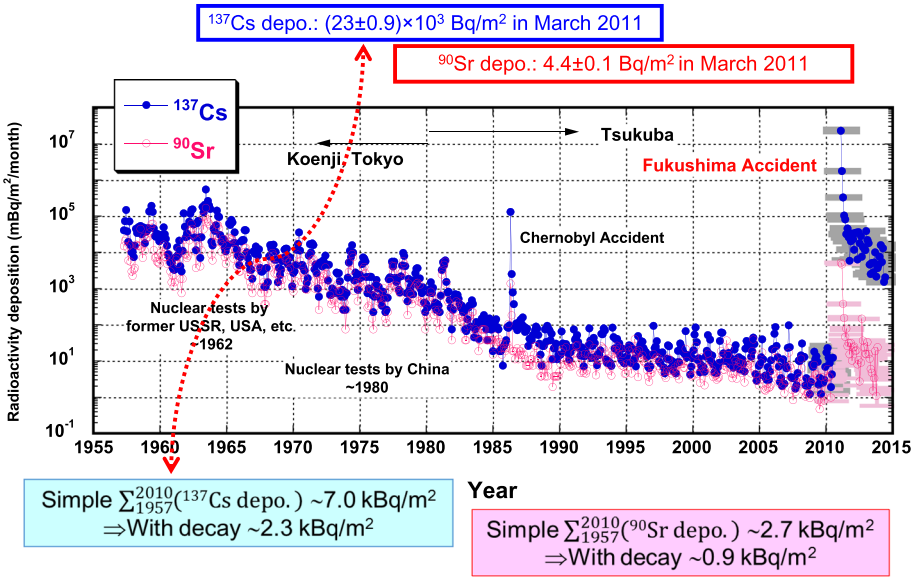

Fig. 1 Sr-90 and ^{137}Cs monthly deposition observed at the Meteorological Research Institute (MRI) from 1957 to 2014. Monthly deposition is expressed in millibecquerel per square meter on a logarithmic scale. Sr-90 and ^{137}Cs analyses from deposition samples taken 6 and 8 months before the accident, respectively, are ongoing to avoid possible sample contamination at the MRI because of the accident. Thus, these data are missing not only in Fig. 1 but also in Fig. 2. The measurement uncertainty (1σ) is shown only for the data obtained after the FDNPP accident and is reasonably small compared to the analytical data. For comparison, uncertainty for the monthly data in 2010 is also given. The effects of atmospheric nuclear bomb tests have been recorded since 1957. Until the Partial Test Ban Treaty (PTBT) became effective in 1963, the USA, Soviet Union, and UK conducted atmospheric tests. France and China continued atmospheric testing until 1974 and 1980, respectively. Since 1981, all the nuclear bomb tests have shifted underground, so additional radioSr and Cs contamination should be negligible. However, the Chernobyl accident in 1986 also affected the time series. The simple summation of the deposition from 1957 to the time before the FDNPP accident (mid-2010) and decay-corrected summations for ^{90}Sr and ^{137}Cs can be compared to the FDNPP-derived deposition

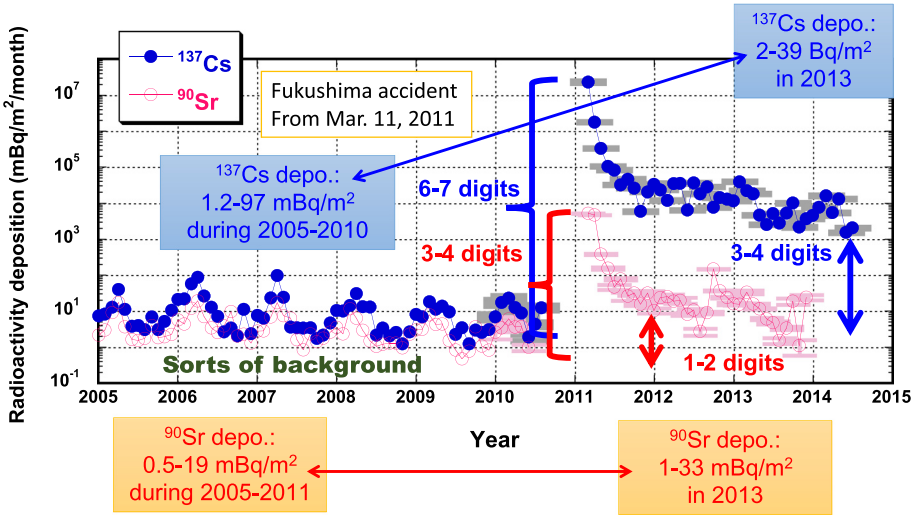

Fig. 2 Monthly ^{90}Sr and ^{137}Cs deposition levels in pre- and post-accident periods. Partial enlargement of Fig. 1. The monthly deposition is expressed in millibecquerel per square meter on a logarithmic scale. The atmospheric depositions of ^{90}Sr and ^{137}Cs in 2013 observed at the MRI were a few orders of magnitude higher than those from 2005 to 2011 before the FDNPP accident. For ^{90}Sr and ^{137}Cs, monthly depositions during 2005 to 2010 were 0.5–19 mBq/m^2/month and 1.2–97 mBq/m^2/month, whereas they were 1–33 mBq/m^2/month and 2–39 Bq/m^2/month in 2013, respectively

accident was more remarkable than any previous incident in our time series.

Temporal changes in monthly ^{137}Cs atmospheric deposition

The monthly ^{137}Cs deposition in March 2011, when the FDNPP accident occurred, was 23 ± 0.9 kBq/m^2/month, which is six to seven orders of magnitude higher than the level before the Fukushima disaster (Figs. 1 and 2). Because the pollution source of the FDNPP accident is closer to the observation site (170 km) than it is to the weapons testing sites and Chernobyl (several thousand kilometers), the spatial representativeness of the MRI data (as an absolute value) is lower.

The cumulative ^{137}Cs deposition at the MRI was 25.5 kBq/m^2/year for the year 2011. The sum of the

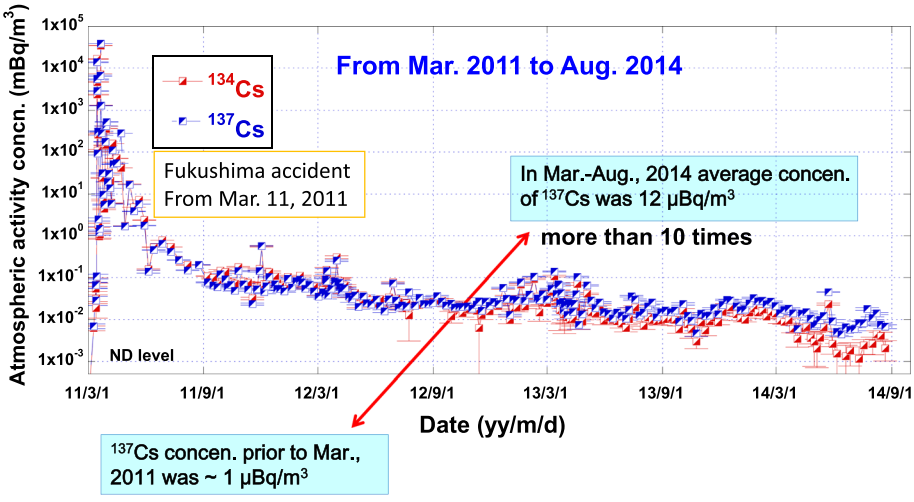

Fig. 3 Temporal change in atmospheric radioCs concentrations at the MRI before and after the FDNPP accident ("Mar.-Aug. 2014"). Activity concentration is expressed in milli becquerel per cubic meter on a logarithmic scale. The measurement uncertainty (1σ) is shown. The maximum concentration of 38 Bq/m^3 of ^{137}Cs was observed during March 20–21, 2011. After that, the radioCs concentrations rapidly decreased until fall 2011 when the decrease slowed. The levels before (approximately 1 μBq/m^3) and 3 years after the FDNPP accident (12 μBq/m^3 from March to August 2014) are also compared. A difference of at least one order of magnitude is observed between the concentration level from March to August 2014 and the level before the FDNPP accident

simple monthly ^{137}Cs depositions from 1957 to mid-2010, the time before the Fukushima disaster, is approximately 7.0 kBq/m^2 (this figure is thought to contain some error since the pre-1970s data did show individual undefined errors), as shown in Fig. 1. Considering the radioactive decay of the individual monthly ^{137}Cs depositions, this past total contribution represents 2.3 kBq/m^2. The FDNPP accident's influence was over ten times larger than that of any past event. Almost the same amount of ^{134}Cs (half-life, 2.1 years) was simultaneously deposited with the ^{137}Cs; thus, the total cesium deposition came to more than 50 kBq/m^2. This value agrees quite well with figures for the area around Tsukuba in observation mapping provided by the Ministry of Education, Culture, Sports, Science and Technology (MEXT 2011a).

Later, the deposition decreased rapidly, but the monthly ^{137}Cs deposition in 2012 and 2013 ranged from 8–36 and 2–39 Bq/m^2/month, respectively, where deposition during 2005–2010 had been in the range of 1.2–97 mBq/m^2/month, i.e., three to four orders of magnitude higher. The deposition level at the end of 2013 was still as high as values registered when atmospheric nuclear tests were conducted by China in the 1970s to the early 1980s. The deposition rate slowly decreased in the following years.

Atmospheric concentrations of radioCs

Figure 3 displays the temporal change in the atmospheric radioCs activity concentrations at the MRI in Tsukuba since the FDNPP accident. The temporal trend shows an abrupt increase (peak) of several orders of magnitude, followed by a rather rapid concentration decrease over a short period (3 to 4 months after the FDNPP accident), with a smaller decreasing rate after. The highest ^{137}Cs atmospheric concentrations (38 Bq/m^3 in a 12 h sampling period) were registered on March 20–21, 2011, which slightly exceeded the limit stipulated by Japanese regulations and ordinances (30 Bq/m^3). Although the pre-accident activity concentration level was not measured, it had been observed for a short period, from February to April 1997, which includes the time when the Power Reactor and Nuclear Fuel Development Corporation Tokai accident occurred (Igarashi et al. 1999a). The background level was approximately 1 μBq/m^3 and did not decrease far below half that value (approximately 0.5 μBq/m^3) until 2011. The decrease in monthly ^{137}Cs deposition was small during the same period (Igarashi et al. 2003, 2009). Thus, the ^{137}Cs activity concentration level registered during summer 2014 appears at least 10 times higher than that before the accident. During 2011 and 2012, small spikes were recorded from time to time (Fig. 4). In these cases, daily forward trajectory analysis suggested that the polluted air masses were transported from the accident site during the corresponding observation period as shown in the figure. In addition, relatively high concentrations were registered in the winter (Fig. 3). This phenomenon was noted at other places in northern and eastern Japan (Hirose 2013), so there is most likely a common explanation, as described in the literature.

Temporal change in monthly ^{90}Sr atmospheric deposition

In contrast to ^{137}Cs, the monthly ^{90}Sr deposition in March 2011 was 5.2 ± 0.1 Bq/m^2/month. This was approximately 1/5000 the amount of ^{137}Cs deposited in the same month. This deposition was 2–3 orders of magnitude larger than the level before the FDNPP disaster. The annual ^{90}Sr deposition was 10.6 Bq/m^2/year during 2011, approximately 1/2500 of the quantity of ^{137}Cs deposited. The simple sum of the monthly ^{90}Sr depositions from 1957 to mid-2010, before the Fukushima disaster, was approximately 2.7 kBq/m^2, as shown in Fig. 1. Taking the radioactive decay of the individual monthly ^{90}Sr depositions into account, the sum represents approximately 0.9 kBq/m^2. The FDNPP accident's impact on ^{90}Sr was very small. The most extreme monthly ^{90}Sr deposition, recorded during the global fallout era of May 1963 in Tokyo, was 170 Bq/m^2/month. The FDNPP accident's impact on the monthly ^{90}Sr deposition was less than one-thirtieth of this maximum. Therefore, it is probable that ^{90}Sr pollution over the Kanto Plain from the accident was relatively insignificant; the environmental and health impacts of ^{90}Sr are relatively minor.

In addition, the ^{137}Cs/^{90}Sr activity ratio fluctuated between approximately 400 and 5000 (Fig. 5), except for some abnormal cases described below. This confirms that the degree of radioSr pollution is relatively insignificant compared to that of radioCs. However, it is still unknown why the ^{137}Cs/^{90}Sr activity ratio varied so widely despite the radionuclides having a common accident emission source, namely, the FDNPP accident. More discussion on the ^{137}Cs/^{90}Sr activity ratio is given in Appendix 2. The reason for the variability is worth studying in the future. The monthly ^{90}Sr deposition recorded in 2012 was 10–31 mBq/m^2/month, whereas during 2005–2010, it was 0.5–19 mBq/m^2/month, a difference of up to two orders of magnitude.

A ^{90}Sr deposition anomaly in October 2012

In October 2012, the monthly ^{90}Sr deposition showed a peak of 145 ± 2 mBq/m^2/month (see the arrow in Figs. 5 and 6), which is 1–2 orders of magnitude higher than any monthly ^{90}Sr deposition registered that year, and its influence lasted a few months (Fig. 6). This small ^{90}Sr event remains puzzling. By applying forward trajectory analysis and closely examining the precipitation over Tsukuba, we believe that the ^{90}Sr may have come from

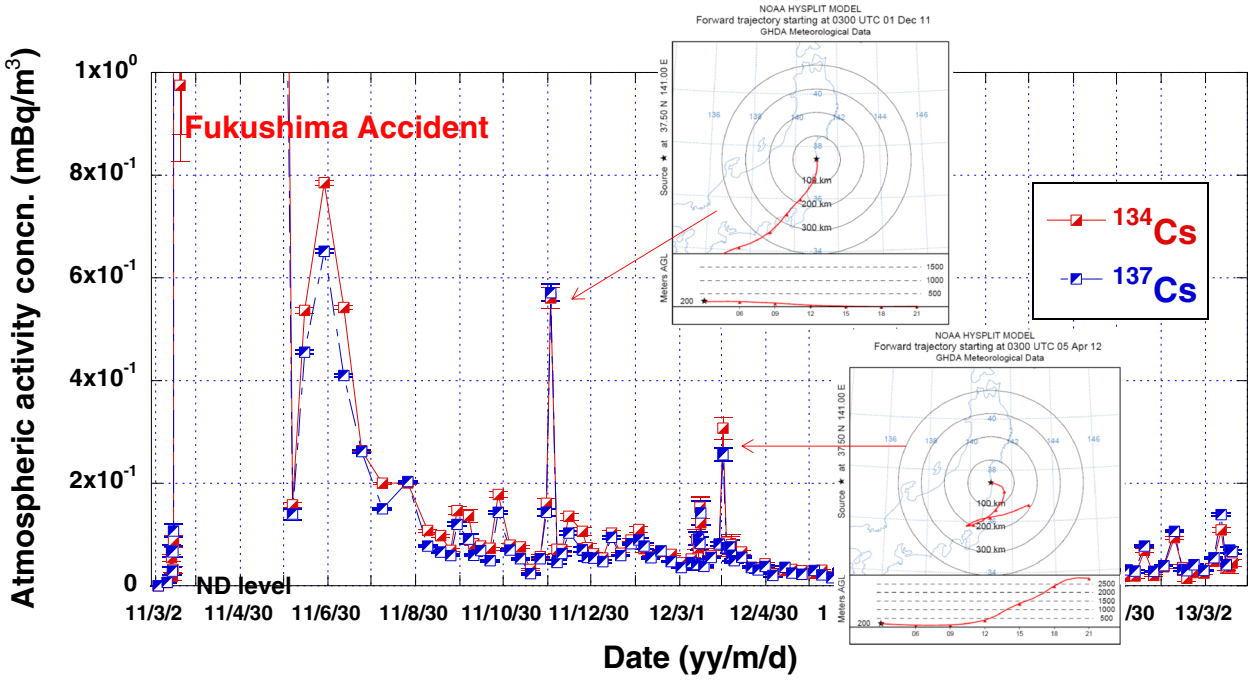

Fig. 4 Atmospheric concentration increases observed during 2011 and 2012 and their air mass trajectories. Note that the activity concentration scale is linear. The forward air mass trajectory calculated by the NOAA's HYSPLIT model is depicted for the radioCs activity concentration peaks, suggesting that the plume from the FDNPP site passed over the Tsukuba region. The shown trajectory cases are December 1, 2011 and April 5, 2012. The increases seem to be attributable to the transport of primary radioCs from the accident site

the FDNPP and encountered precipitation on October 7 and 18–19, 2012. However, this increase was not accompanied by a radioCs deposition peak, and the major radionuclide emitted by the FDNPP accident is radioCs, which is inconsistent with FDNPP accident being the source of the October anomaly.

The Japanese Radioactivity Survey data on the Internet were checked, but no consistent data were evident for the corresponding period. In addition, no such anomaly was reported in Europe (Masson 2014, personal communication). Based on the timescale of this contamination, however, the source should be neither very local nor very small. This episode shows some similarities to the case in fall 1995 in Tsukuba (Igarashi et al. 1999b). We also assume unidentified, unreported incidents of burning and/or melting of industrial ^{90}Sr sources in the Far East region as a possible explanation, such as the Algeciras (Spain) incident in 1998 with its ^{137}Cs source of

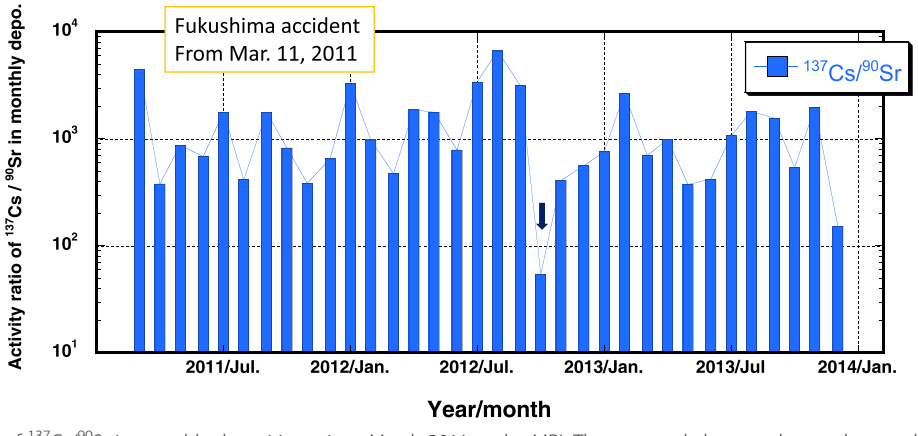

Fig. 5 Activity ratio of ^{137}Cs/^{90}Sr in monthly depositions since March 2011 at the MRI. The temporal changes do not show a clear decreasing or increasing trend. The *arrow* shows the month during which an anomalous deposition of ^{90}Sr was observed. Except for the anomaly, the ^{137}Cs/^{90}Sr activity ratio fluctuated from approximately 150 to 6700

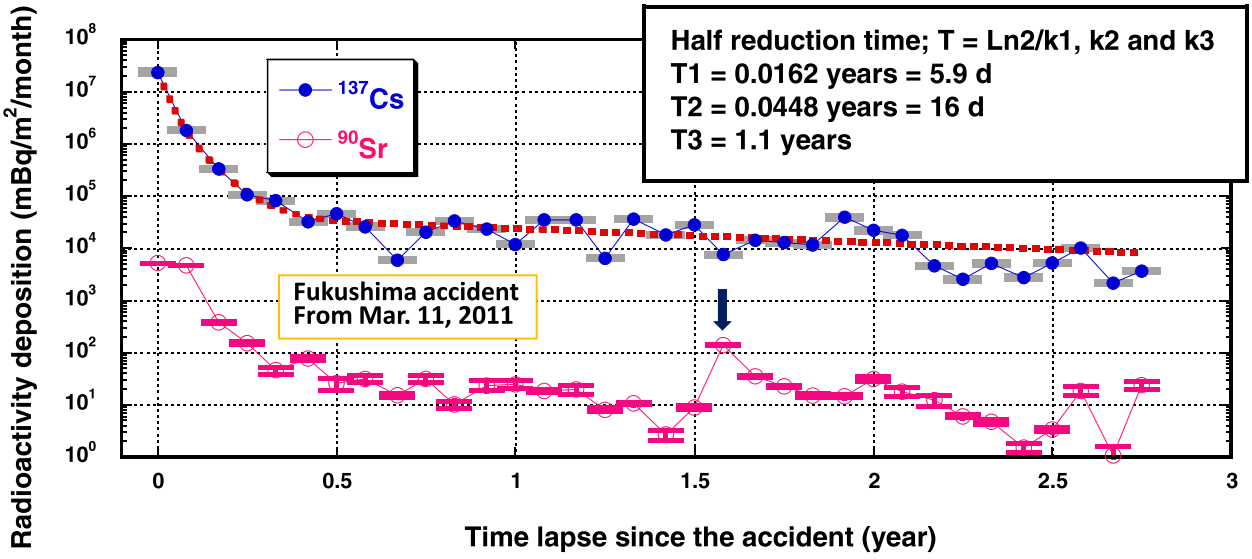

Fig. 6 Exponential fitting of the decreasing monthly ^{137}Cs deposition trend since March 2011 at the MRI. The curve is composed of three exponential functions. These are attributable to the decreasing intensity of primary emission, tropospheric aerosol residence and re-suspension. The *arrow* shows the month during which an anomalous ^{90}Sr deposition was observed. Possible causes are mentioned in the text

3.7 TBq (Estevan 2003). Sr-90 is widely used in industrial applications, such as in thickness gauges, and its activity size ranges from 740 MBq to 3.7 GBq in Japan. Because ^{90}Sr is a pure β-emitter, it is more difficult to determine the sources of its environmental pollution than it is for ^{137}Cs.

Decrease in monthly ^{137}Cs deposition after the FDNPP accident

Although researchers do not agree precisely on the FDNPP radioactivity emission inventory (Chino et al. 2011; Katata et al. 2012, 2012b, 2014; Maki et al. 2013; Stohl et al. 2012; Terada et al. 2012; Winiarek et al. 2012), if the ^{137}Cs emission in March 2011 is assumed to be 10 PBq/month, the deposition/emission ratio (the monthly deposition at the MRI divided by the monthly emissions from TEPCO (2012)) would be approximately 10^{-12}. If the MRI is included in the so-called "hot spot" area, the deposition could be approximately 100 kBq/m^2 (five times larger). This would give a deposition/emission ratio of approximately 10^{-11}. After March 2011, the ratio is calculated to be in the range of 10^{-10} to 10^{-9}, which appears to be large, if the emission-deposition relation above is correct. We can presume that this excess deposition at the MRI, Tsukuba came from secondary emissions. Thus, Tsukuba can be regarded as representative of a typical suburban area in the Kanto Plain, and the relative trend of temporal changes there can be considered comparable to surface contamination levels for similar geographical domains. The temporal trends (holding time constant) may also be spatially representative, although this potential is limited.

To study the decreasing trend in monthly ^{137}Cs atmospheric deposition caused by the FDNPP accident and to make future projections, a curve was fitted on the temporal trends using multiple components. A drawing software was employed, and the fitting operation was put through 100 iterations, each time changing the initial value so that the calculation results would converge, as shown in Fig. 6. A trinomial exponential function of the form $a \times (e^{-k \times t})$ was applied to fit the data (where a is a constant and k is an inverted time scale; $Ln2/T_{1/2}$), and the individual half-times (T1, T2, and T3 in Fig. 6) were approximately 5.9 (±11 %) days, 16 (±18 %) days, and 1.1 (±32 %) years, respectively. The relative uncertainty is shown in parentheses. These appear to correspond to the time scale of (1) the reduction in the original FDNPP accident surge (primary emission source), (2) the tropospheric transportation and diffusion of the radioactive plume (equivalent to the removal of radioactive aerosols from the atmosphere), and (3) the emission intensity of re-suspension (secondary emission sources). We posit that some primary radiological release to the atmosphere continues because the FDNPP is not isolated from the neighboring environment (Hirose 2013; TEPCO 2012). The results, then, cannot be assumed to be completely free of primary release. However, the first and second terms can be reasonable estimates corresponding to the primary emission and tropospheric aerosol residence, respectively.

The second term is almost identical to figures obtained by other recent studies (e.g., Hirose 2012, 2013; Kristiansen et al. 2012). Hirose (2013) analyzed radioCs deposition data obtained during 2011–2012 from several places over the Kanto Plain and Fukushima prefecture, Japan. According to his report, "The apparent half-lives at Ichihara, Tokyo, Utsunomiya, Hitachinaka and Maebashi were 11.9, 10.6, 13.5, 11.5 and 12 d, respectively." Hirose (2012) states that "the residence times of aerosols in the troposphere, which are in the range of 5–30 d, have been determined by natural and anthropogenic radionuclides, which depend on particle size and altitude (Ehhalt, 1973)." Hirose (2012) also argues "the temporal change of the Fukushima-derived ^{137}Cs revealed that the apparent atmospheric residence time of the Fukushima-derived ^{137}Cs in sites within 300 km from the Fukushima Dai-ichi NPP is about 10 d." This long residence time might reflect the Fukushima radioactive plume's circulation over the Northern Hemisphere, which takes about 20 days (Hernández-Ceballos et al. 2012). As shown in Fig. 8a in the Appendix 1, the third Fukushima plume's arrival over the Kanto Plain was observed from March 28–31, 2011. It was well reconstructed by the aerosol transport model. Other observations over the Kanto Plain also revealed this transport event (e.g., Amano et al. 2012; Haba et al. 2012). However, we cannot clearly determine whether this concentration peak is due to delayed primary emission (e.g., Terada et al. 2012), hemispheric circulation, or a combination of both. This is because the current model simulation uses the emission inventory, which is also based on atmospheric monitoring results (e.g., Terada et al. 2012). Regarding this connection, Kristiansen et al. (2012) investigated the ^{131}I and ^{137}Cs removal times from the atmosphere using global-scale monitoring data. Their estimated ^{137}Cs removal times were in the range of 10.0–13.9 days, which is closer to our present result. They also noted the difference from the typical values of 3–7 days obtained by aerosol model simulations, suggesting that the aerosol transportation models need improvement. We would like to add that the deposition results should be interpreted to reflect not only the surface air but also the air column up to at least the mixed layer. Therefore, the deposition may be affected by large-scale transportation, in contrast to indications obtained from the surface concentration only. For further reference, based on the monthly emission of radioCs until the end of 2011 estimated by TEPCO 2012, the primary emission decrease can be fitted using two exponential laws with half-time constants of 2.3 days (±2 %) and 48 days (±23 %).

The third term's half-time of 1.1 years for the MRI data, despite its relatively large associated uncertainty, appears to reveal the total re-suspension of radioCs from contaminated surfaces. This value is too large to correspond to any primary releases from the FDNPP in the early phases. In addition, it agrees with the value for the re-suspension "descending trend" due to the Chernobyl accident reported by Garger et al. (2012), which was 300 days. It was possible to fit a two-term exponential curve to the present ^{137}Cs data by fixing the 1.1-year half-time, obtaining a value of 7.8 days for the first term. When compared with the triple exponential (three-term) model, the fitting distance (defined by the ratio of the calculation to the observation) for the double exponential (two-term) model was larger for elapsed times of 2–12 months, although there were exceptions. The mean and standard deviation for the two- and three-term fit distances are 2.50 ± 2.02 and 1.54 ± 1.14, respectively. The medians are 1.82 and 1.09, respectively, suggesting that the three-term model fits better. Although we do not provide an illustration here, we found that fitting with three-term functions for the decrease in monthly ^{90}Sr deposition after the disaster was also possible. Therefore, we preferred fitting with a trinomial exponential function to reproduce the deposition flux of radionuclides from the FDNPP accident. Again, the primary emissions of radioCs to the atmosphere are anticipated to continue at a non-negligible level (less than 7.2 GBq/month is assumed in TEPCO's latest press release (in Japanese) at http://www.tepco.co.jp/life/custom/faq/images/d150129-j.pdf) because the FDNPP is not isolated from the surrounding environment (Hirose 2013). These delayed primary emissions of approximately 7 GBq are 6–7 orders of magnitude lower than the emissions in March 2011 (e.g., 15 PBq for ^{137}Cs; NISA 2011). If the primary emission deposits were delayed in a fashion similar to those from March 2011, recent MRI records after the FDNPP accident would correspondingly be 6–7 orders of magnitude lower than the peak value caused by the accident (see Fig. 2). Therefore, we consider that the present decrease in the third term reflects secondary emission (re-suspension) trends over the Kanto Plain moderately well. In future, we plan to confirm this by applying different evaluation methods such as transport simulations or others.

Consideration of re-suspension and its persistence

Currently, there may be interest and concern about how long it will take for the atmospheric radionuclide deposition fluxes to return to pre-FDNPP accident levels (cf. Garger et al. 2012; Hatano and Hatano 2003). Although it seems slightly arbitrary, the monthly ^{137}Cs depositions can be estimated if the fitted curve described above is extrapolated. The result of this extrapolation is illustrated in Fig. 7. This simple estimation shows that more than a decade will likely be required for the activity levels to return to pre-accident levels. Thus, re-suspension (secondary emission to the atmosphere;

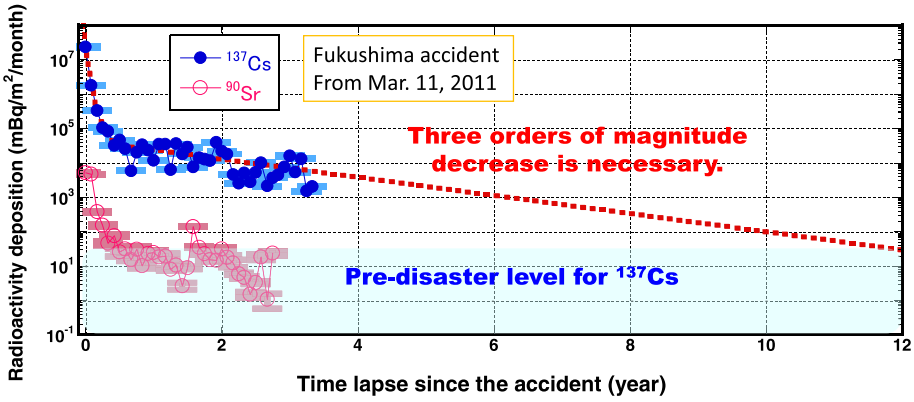

Fig. 7 Future projection for monthly ^{137}Cs deposition level using a trinomial exponential function. The present simple estimation shows that more than a decade would be necessary for the ^{137}Cs atmospheric deposition level to return to pre-accident levels

e.g., Igarashi 2009) must be scrutinized with long-term monitoring. Because it seems natural that radionuclide emission flux would be proportional to surface pollution density, there could be radioCs fluxes several orders of magnitude higher than those measured in Tsukuba in areas nearer the FDNPP site whose Cs surface pollution is several orders of magnitude higher than in Tsukuba. Therefore, elucidating the secondary emission processes of the FDNPP radionuclides remains an imminent scientific challenge, especially for heavily polluted areas. Secondary sources can include soil dust suspension from polluted earth surfaces, emissions from polluted vegetation and forests, and volatilization and release from combustion of polluted garbage and open field burning (e.g., Igarashi 2009). Although the main emission sources are not yet well understood, this elucidation must be performed as soon as possible.

Conclusions

The authors conducted atmospheric monitoring of airborne radioSr and Cs and their deposition at the MRI in Tsukuba, Japan. The monitoring period encompasses the FDNPP accident and the subsequent few years. The monthly ^{137}Cs deposition at the MRI was $(23 \pm 0.9) \times 10^3$ Bq/m^2/month in March 2011, which is 6–7 orders of magnitude higher than pre-accident levels. Almost equal amounts of ^{134}Cs and ^{137}Cs were deposited, causing surface pollution of more than 50 kBq/m^2 in Tsukuba in 2011, in close agreement with the Ministry of Education, Culture, Sports, Science and Technology, Japan (MEXT)'s airborne mapping. Deposition of ^{90}Sr was 5.2 ± 0.1 Bq/m^2/month in March 2011, which is less than 0.02 % of the total ^{137}Cs deposition in that month. The level of ^{90}Sr deposition was 3–4 orders of magnitude higher than pre-accident levels and did not reach the level registered during the 1960s after nuclear tests; the effects from ^{90}Sr will not be as large as from radioCs. During 2013, the Fukushima fallout decreased by 3–4 orders from its magnitude at the time of the accident, yet some becquerel per square meter of monthly deposition continues. This corresponds to the level in the 1970s and early 1980s when China performed atmospheric nuclear tests. During 2013, the ^{137}Cs concentration remained at a level of tens of micro becquerel per cubic meter. Because re-suspension (secondary emission) will continue over a long time, it is necessary to monitor its future trends and variability. An apparent decrease in atmospheric radioCs deposition was fitted by trinomial exponentials, giving information regarding the reducing trend of airborne radionuclide persistence through re-suspension into the atmosphere. Extrapolation of the decreasing rate suggests that it would take at least a decade for the activity to return to pre-disaster period levels. Further monitoring efforts are essential.

Appendix

Appendix 1 Temporal changes in radioactive aerosol concentrations and plume transport from the FDNPP accident over Tsukuba in March 2011

Introduction

The heat and blast at the FDNPP accident resulted in the leakage of a huge amount of anthropogenic radionuclides, near the levels of the Chernobyl accident in 1986, into the environment (IAEA 2006; Janžekovič and Križman 2011; NISA 2011), as seen on both the domestic and Northern Hemispheric scale (Hernández-Ceballos et al. 2012; Masson et al. 2011; Takemura et al. 2011; Tanaka 2013). The transport of the radioactive plume and its deposition over the Pacific Ocean (Aoyama et al. 2013; Honda et al. 2012), North America (e.g., Schwantes et al. 2012; Zhang et al. 2011), and Europe (e.g., Masson et al. 2011) as well as within the Japanese

territories (Hirose 2012; Kinoshita et al. 2011; Morino et al. 2011; Terada et al. 2012; Tsuruta et al. 2014) has been well depicted by many researchers. The pattern of domestic pollution of the land by local fallout was made fairly clear by the creation of a contamination map based on many university investigations (Kinoshita et al. 2011; Tanihata 2013) and airborne surveys by Japan's MEXT and the USA's NASA/DOE (MEXT and USDOE 2011; Sanada et al. 2014; Torii et al. 2013; USDOE 2013). The transport of the radioactive plume and its subsequent deposition over the capital area (the Kanto Plain; Amano et al. 2012; Haba et al. 2012; Tsuruta et al. 2014) has been reported and monitored in Tsukuba (Doi et al. 2013; Kanai 2012). The MRI in Tsukuba suffered almost no electricity outage soon after the earthquake. Thus, aerosol sampling at the observation field continued from before the FDNPP accident through its aftermath. Here, we add our independent observations of the temporal changes in atmospheric radionuclide concentrations over Tsukuba covering all of March 2011, with our specific transport model simulation for reference.

Experiment

Intensified aerosol sampling

Aerosol samples were collected onto quartz fiber filters using a high-volume sampler, as described in the body of the paper; the only change was the duration of sampling, from 1 day to 6 h—which was altered as soon as the accident was made public. The total sucked air volume was thus between 250 and 1000 m^3.

Activity measurement

After collection, the filters were treated in the same manner as usual and measured with Ge detectors, as described previously. The filter samples collected before the radioactive plume's arrival at Tsukuba were measured at the Kyoto University Research Reactor Institute (KURRI) to lower the detection limits. This was necessary because the Ge detector and the laboratory environment at the MRI building were contaminated by the radioactive plume on March 14–15 and 20–22, increasing the background levels. Before the compression procedure, portions of the filter were punched out (33 mmϕ × 4 pieces), of which one piece was selected for radioSr analysis, as noted in Appendix 2.

Transport modeling

The Eulerian chemical transport model RAQM2 (Kajino et al. 2012; Adachi et al. 2013; Sekiyama et al. 2015) was used to simulate radioactive plume transport from the FDNPP accident over the Kanto Plain. The JMA/MRI non-hydrostatic meteorological model (NHM; Saito et al. 2007) was used to simulate the meteorological field to calculate the transport and deposition processes of radionuclides using RAQM2. The horizontal domain and its grid resolution (3 km) were common to both NHM and RAQM2, with 50 vertical layers from the surface up to 22 km for NHM and 20 layers to 10 km for RAQM2. The JMA's Meso-Regional Objective Analysis (MANAL), which has a horizontal resolution of 5 km, was used to define the boundary conditions for NHM. The calculated domains cover southern Tohoku and the central part of Honshu. Details of the transport (advection, diffusion, and convective transport) and deposition schemes (dry and wet (in cloud and below cloud, grid-scale and subgrid-scale)) are described in Kajino et al. (2012) and Sekiyama et al. (2015).

We simulated five species of particulate radionuclides (volatile and reactive ^{131}I (I_2), volatile and non-reactive ^{131}I (CH_3I), non-volatile ^{131}I, ^{134}Cs, and ^{137}Cs). We conducted dispersion and deposition simulation of radioCs in two very different forms—hygroscopic submicrons vs. hydrophobic supermicrons—in a previous study (Adachi et al. 2013) and showed that the deposition regions were significantly different. However, because the proportions of hygroscopic and hydrophobic radioCs in emissions have never been estimated, we assumed the hygroscopic submicron aerosols to be the carriers of radionuclides and used dimensions equivalent to the geometric mean of the dry diameter $D_{g,n,\mathrm{dry}} = 102$ nm, geometric standard deviation $\sigma_g = 1.6$, particle density $\rho_p = 1.83$ g/cm^3, and hygroscopicity $\kappa = 0.4$ (Petters and Kreidenweis 2007; Adachi et al. 2013). The emission inventories of ^{131}I and ^{137}Cs were taken from Katata et al. (2014). RAQM2 incorporates aerosol dynamic processes, such as nucleation, condensation/volatilization, and coagulation, within and among different aerosol categories, but the size distribution of the aerosols was assumed to remain unchanged in this simulation.

Results and discussion

Particulate fission products and radioCs

The detected γ-emitting radionuclides were ^{99}Mo-^{99m}Tc (half-life, 65.9–6 hours), ^{129m}Te (33.6 days), ^{131}I (8.02 days), ^{132}Te-^{132}I (3.20 days–2.3 hours), ^{133}I (20.8 hours), ^{134}Cs (2.07 years), ^{136}Cs (13.2 days), and ^{137}Cs (30.0 years) as shown in Fig. 8a in the Appendix 1. Note that gaseous iodine was not captured by the present sampling. The ^{90}Sr results are also plotted in the figure (for analytical details, please refer to Appendix 2). There were two significant transport events that brought the radioactive plume toward the Kanto Plain in March 2011. One was during March 14–15 and the other occurred during March 20–22. Plume transport is determined by temporal changes in emission

intensity and the wind field near the ground surface, which have been addressed by many authors (e.g., Katata et al. 2012, 2014; Morino et al. 2011; Terada et al. 2012). The releasing sources are attributed to a venting operation at an individual reactor vessel, reactor core damage, buildings damaged by a hydrogen explosion, and continuous release through a reactor building (see, e.g., TEPCO 2012; Katata et al. 2014). The activity concentrations of these radionuclides were consistent with those described in previous reports regarding Tsukuba (e.g., Doi et al. 2013; Kanai 2012). The March 7–12, 12–13, 13, and 13–14 samples exhibited detectable levels of radioCs and ^{131}I, for which we cannot totally rule out the possibility of sample contamination despite their measurement at KURRI. The two events exhibited different radionuclide compositions, reflecting different source at the accident site. Although the ^{134}Cs/^{137}Cs ratio was unity for both transport events, the activity ratios were ^{131}I/^{137}Cs ≈ 5 and ^{132}Te/^{137}Cs ≈ 8 during the first event and ^{131}I/^{137}Cs ≈ 2.5 and ^{132}Te/^{137}Cs ≈ 1 during the second event. Te-132 was significant during the first transport event. Because the melting point of metallic Te is 450 °C, whereas that of Cs is only 28 °C, the finding may suggest a higher temperature for the source in the earlier phase. For comparison, ^{90}Sr data are included in Fig. 8a in the Appendix 1; the details of the measurements are given in Appendix 2.

After the FDNPP accident, unlike in Chernobyl, no radioRu was found (Aoyama et al. 1986, 1987). This may be because of the different accident scenarios; the melting temperature of metallic Ru is very high (approximately 2500 °C).

Another notable point is the magnitude of the concentration drop between the first and second plume events. RadioCs and ^{132}Te concentrations were 4–5 orders of magnitude lower for the second plume than the concentration peaks, and those for ^{131}I were 2–3 orders of magnitude lower. This difference appeared to be caused by either the re-suspension of radioI or the contamination of our materials and instruments. The latter seems unlikely, however, because the filter samples were treated identically and the maximum contamination levels would be those found for the March 7–14 samples (measured at the KURRI). We gave sufficient attention to reducing contamination during sampling and sample handling. Nevertheless, the entire environment was contaminated, and therefore, it was difficult to avoid entirely. In any case, the volatile nature of iodine (the boiling point of CH_3I is 42 °C, while the melting point of I_2 is 113 °C) is likely part of the cause. Therefore, immediate re-suspension of radioI should be given more attention. This is briefly addressed below.

Transport model simulation

The aerosol simulation model captures the events that transported the radioactive plume to the Kanto Plain very well (see Fig. 8b and 9 in the Appendix 1). The transport of the plume from the southern Tohoku district is not considered very exceptional (the MRI is approximately 170 km southwest from the accident site). Aoyama et al. (1999) and Igarashi et al. (1999a) analyzed the radioactive plume over the Kanto Plain from the earlier PNC accident in Tokai, Ibaraki, in 1997. Igarashi et al. (2000a,b) conducted continuous observations at the MRI of ^{85}Kr, of which the local source was the Tokai nuclear fuel reprocessing plant approximately 60 km northeast of Tsukuba. They noted the incidence of plume transport from a point source in northern Ibaraki over the Kanto Plain with a northeasterly wind, a prevalent weekly wind pattern occurring during the spring in Japan. Similar meteorological situations appeared to occur on March 14–15 and March 20–22, 2011 over the Kanto Plain. Notably, the drop in activity concentration between the plume advections is evident in the simulation results (Fig. 8b and c in the Appendix 1) despite only primary emissions coming from the FDNPP accident. The reality of the observations differed from the simulations (Fig. 8a in the Appendix 1). As described above, contamination in the observation procedures cannot be totally ruled out, but by coupling the model and observations, it is possible to evaluate the immediate re-suspension of the atmospheric Fukushima radionuclides (see section below).

Finally, we argue that aerosol transport modeling is an indispensable tool for the assessment of accident effects. However, many uncertainties remain, especially concerning the emission inventory, wet and dry deposition, and cloud processes. Data and information are collected to improve the transport model schemes, and comparison of different models has been performed to contribute to an accurate evaluation of the source term and transport and deposition processes (SCJ 2014).

Estimation of immediate re-suspension factor

The quantity of the deposited radionuclides that could return again to the air (re-suspension) is notable. Maximum re-suspension is known to occur just after radioactive plume passage (hereafter, we call this immediate re-suspension). Thus, as a primary approach, immediate re-suspension factors were roughly estimated with modeled amounts deposited in the Kanto Plain by the first plume and the observed minimum activity concentration between the two plume events, i.e., March 17 09JST to March 20 09JST. We assumed mass closure between re-suspension from the contaminated surface and outflow by horizontal advection and turbulence vertical mixing as below.

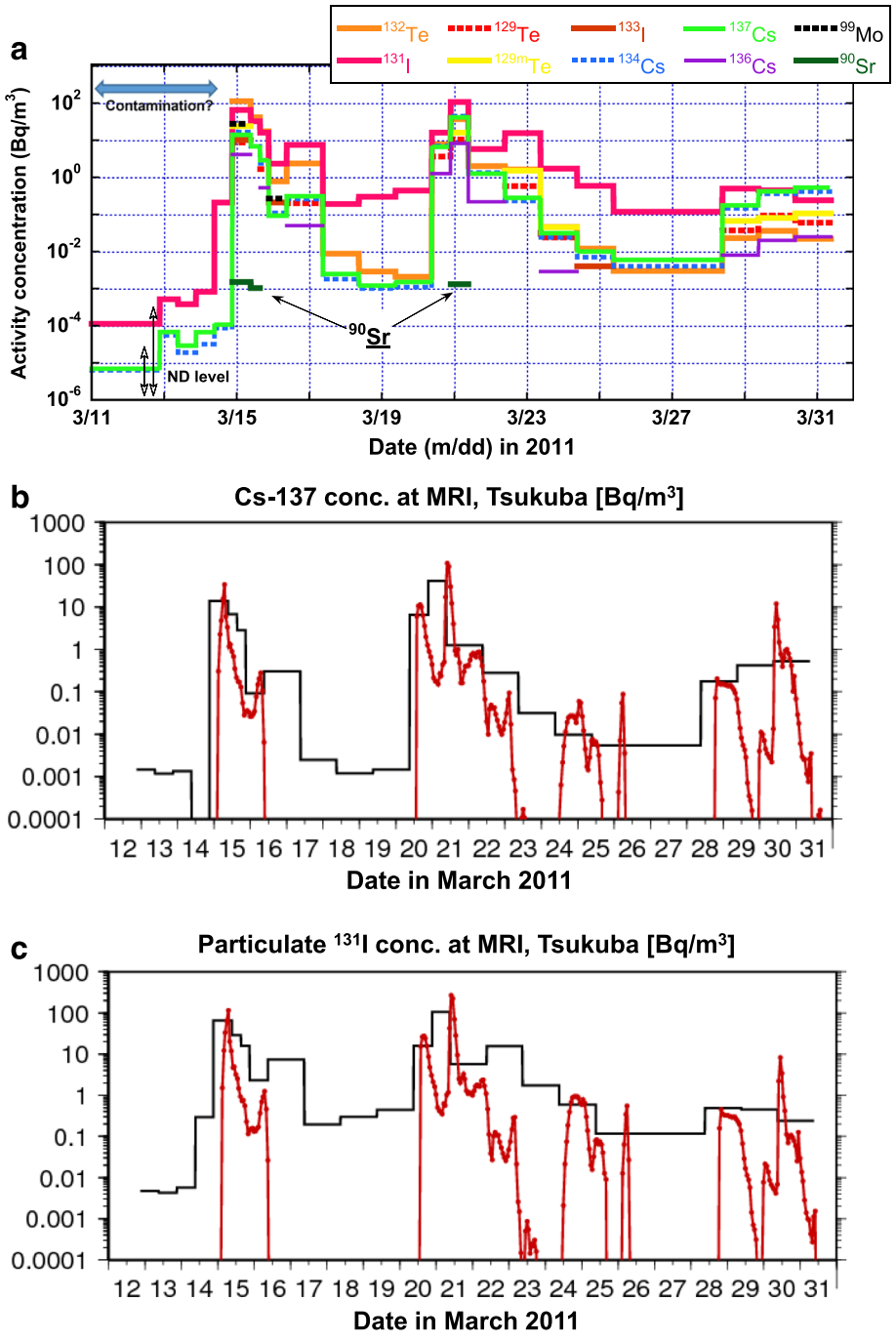

Fig. 8 Atmospheric activity concentrations of radionuclides from the FDNPP accident in March 2011. **a** Observed data from filter samples collected at the MRI, Tsukuba, Japan; **b** comparison of observed (*black*) and simulated results (*red*) for ^{137}Cs; and **c** similar to **b** but for particulate ^{131}I. The abscissa is expressed in dates in March 2011 and is labeled at the start of the day in **a** and the middle of the day in **b** and **c**. Contamination of the filter samples cannot be totally ruled out for the period before March 14 in **a**, which is depicted by the *left-right pointing double arrow*

The continuity equation is expressed as

$$\partial C/\partial t = \nabla(\boldsymbol{K}_{\mathrm{dif}}\nabla C) - \nabla(\boldsymbol{U}C) - \lambda C + \Phi,$$

in which C is concentration, $\boldsymbol{K}_{\mathrm{dif}}$ indicates three-dimensional diffusion terms, $\boldsymbol{U}$ denotes the wind field, λ is the decay constant, and Φ is a re-suspension term for individual radionuclides. On the other hand, the concentration increase in one unit of time from re-suspension is expressed as

$$\Delta C/\Delta t = \Phi = k_i \times D_i \times (\Delta x \Delta y/\Delta x \Delta y \Delta z),$$

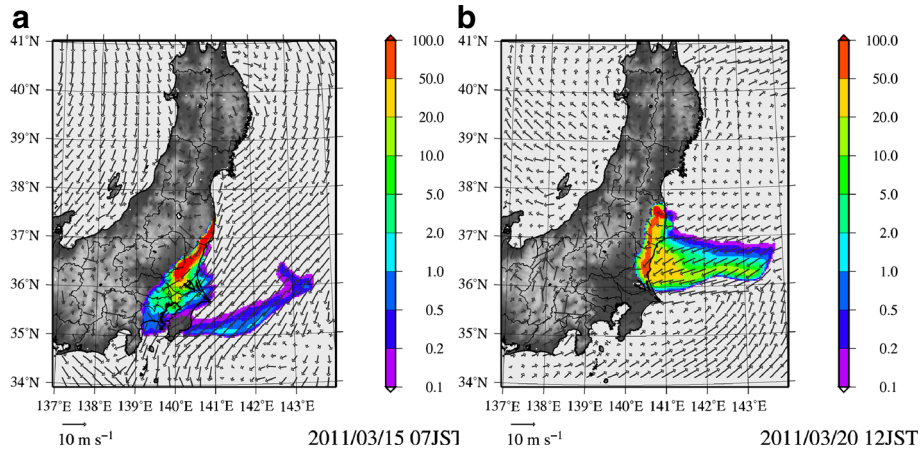

Fig. 9 Radioactive plume transport from the FDNPP accident in the Kanto Plain in March 2011. **a** On March 15 07JST and **b** on March 20 12JST. The figures show the simulated surface ^{137}Cs concentration in *shaded colors* with the model topography in *grayscale*

in which k_i and D_i are a re-suspension factor (/s) and surface contamination (Bq/m^2) for individual radionuclides, respectively. Also, Δx, Δy, and Δz are the horizontal and vertical lengths of the space where the mass closure is obtained.

We can disregard radioactive decay, horizontal diffusion, and convective wind. Balancing the mass between inflow and outflow, we finally obtain the following relationship:

$$(k_i \cdot D_i)/(\Delta z) = (\Delta K_z/\Delta z) \times (\Delta C/\Delta z) + (\Delta u/\Delta x + \Delta v/\Delta y) \times C_i,$$

in which i indicates the radionuclides, namely, ^{137}Cs and ^{131}I; D_i indicates the modeled total (gas + aerosol) cumulative deposition (Bq/m^2) by March 17 09JST; k_i is the re-suspension factor (s^{-1}); $\boldsymbol{U}$ and K_z are the modeled space- and time-averaged horizontal wind speed (m/s) and vertical turbulent diffusivity (m^2/s), respectively; C_i indicates the time-averaged observed concentrations of the radionuclides (9.75×10^{-4} and 3.14×10^{-1} Bq/m^3 for ^{137}Cs and ^{131}I, respectively); and Δx, Δy, and Δz are the horizontal and vertical distances in space over which the above mass closure is obtained. To obtain the horizontal and vertical gradient terms on the right-hand side of the equation, the concentrations outside the space are assumed to be zero (no inflow into the space).

The re-suspension factors for ^{137}Cs and ^{131}I are 7.0×10^{-6} /s and 5.3×10^{-4} /s, respectively, for the smallest volume of the RAQM2 model grid (Δx = 3 km, Δy = 3 km, and Δz = 100 m). Those for ^{137}Cs and ^{131}I varied from 1.6×10^{-6} /s to 1.5×10^{-5} /s (6.1×10^{-6} /s on average) and from 5.3×10^{-4} /s to 1.3×10^{-3} /s (4.6×10^{-4} /s on average), respectively, for the various horizontal spaces plus neighboring zero, one, or two RAQM2 grids from the grid where the MRI is located (i.e., Δx, Δy = 3, 9, or 15 km) and vertical spaces plus zero, one, or two RAQM2 grids from the bottom (Δz = 100, 200, or 400 m).

In summary, the immediate re-suspension factors k_i of ^{137}Cs and ^{131}I are estimated to be on the order of 10^{-6}–10^{-5} /s and 10^{-4}–10^{-3} /s, respectively, and that of ^{131}I is approximately two orders of magnitude larger than that of ^{137}Cs. These values are converted correspondingly, often quoting the concentration ratio over the contaminated surface as follows: 5.8×10^{-6} – $1.7 \times 10^{-5}$and 4.4×10^{-4} – 1.3×10^{-3} /m) for ^{137}Cs and ^{131}I, respectively. The present data do not display the large deviation hitherto reported (e.g., 10^{-6}–10^{-4} /m; Maxwell and Anspaugh 2011). Because those values are based on rough assumptions, further studies based on surface flux measurements need to be conducted to more accurately estimate the re-suspension factors.

Appendix 2 RadioSr in the aerosol samples collected during March 2011

Introduction

There are several reports containing estimates of the radioactive contamination from the FDNPP accident, presented in the form of mapped images produced from the results of investigations of radionuclides in the soil (e.g., MEXT 2011a ; Sanada et al. 2014; Torii et al. 2013) and in the form of air dose rate figures produced from aircraft observations. Among the radionuclides, radioSr is an important indicator of contamination. The former Nuclear and Industrial Safety Agency (NISA) in Japan reported the following emission estimates within the atmosphere: ^{89}Sr (half-life, 50.5 days) as 2.0×10^{15} Bq and ^{90}Sr (half-life, 28.8 years) as 1.4×10^{14} Bq (NISA 2011). Nevertheless, there have been no reports on ^{89}Sr and ^{90}Sr in air samples because of analytical difficulty. The detection of nine different γ-emitting radionuclides, including ^{99}Mo, is described in Appendix 1. However, ^{89}Sr

and ^{90}Sr emit no γ-rays with their radioactive decay, making it impossible to determine their presence by γ-spectrometry. To evaluate their radioactive pollution levels, the aerosol components were radiochemically extracted from the HV filter sample to analyze the radioSr and assess the emission ratios of ^{137}Cs, ^{89}Sr, and ^{90}Sr.

Experiment

Sub-HV filter sample for Sr analysis

HV filter samples from the γ-spectrometry measurements noted earlier were used for the radioSr analysis. Approximately 2 % of the filter area was punched out (as circles) and provided for this analysis, which was performed on sub-filter samples collected during March 2011 (Table 1 in the Appendix 2).

Analysis of radioSr

To dissolve the aerosols on the filter, 100–200 ml of concentrated nitric acid was added and heated on a 200 °C hotplate, then 1–5 ml of hydrogen peroxide solution was added to accelerate the decomposition of any organic matter. This was followed by further thermolysis for more than an hour. The obtained solution was subjected to separation, which was conducted through radiochemical analysis comprising several precipitation separations, such as oxalate, fuming nitric acid, hydroxide, carbonate, and barium chromate precipitations. The last separation was repeated twice, which allowed the Sr fraction to be freed from radioBa and Ra isotopes. The final strontium carbonate deposit was β-counted with the low-background 2π gas-flow counter described earlier (Tennelec LB5100).

Estimating the activity ratio of ^{89}Sr and ^{90}Sr

The atmospheric aerosol sample contained ^{89}Sr and ^{90}Sr, indicating that the total β-activity must be deconvoluted. The measurement sensitivity of the gas-flow counter was confirmed for possible energy independence; therefore, the temporal change in the β-counting rate of a purified ^{90}Sr (maximum β-ray energy 0.546 MeV) source and ^{90}Y (maximum β-ray energy 2.24 MeV) growth from the parent nuclide was observed in five specimens of the MRI reference fallout samples (Otsuji-Hatori et al. 1996) that contained no ^{89}Sr. The following equation was then applied to find the counting efficiency of ^{90}Sr and ^{90}Y:

$$N_{\text{total}} = A_{\text{Sr-90}} \times m_1 + A_{Y\text{-}90} \times (1 - e^{-\lambda t}) \times m_2.$$

N_{total} is the total counting rate (cpm); A stands for each nuclide's β-activity (dpm); λ is the decay constant of ^{90}Y; t is the elapsed time; and m_1 and m_2 are the counting efficiencies of ^{90}Sr and ^{90}Y, respectively. The β-ray energy emitted by ^{90}Y is approximately 4 times that of ^{90}Sr, and the average values of m_1 and m_2 from the five specimens were 27.3 ± 1.8 % and 24.8 ± 3.7 %, respectively.

Table 1 Temporal variation of ^{90}Sr activity concentration in the air over Tsukuba

Sampling start date and time (JST)	End date and time (JST)	^{90}Sr activity concentration (mBq/m^3)
March 12 21 pm	March 13 9 am	nd
March 13 21 pm	March 14 9 am	nd
March 14 9 am	March 14 21 pm	nd
March 14 21 pm	March 15 9 am	1.50 ± 0.13
March 15 9 am	March 15 15 pm	1.04 ± 0.095
March 15 15 pm	March 15 21 pm	nd
March 15 21 pm	March 16 9 am	nd
March 16 9 am	March 17 8 am	nd
March 17 9 am	March 18 8 am	nd
March 18 8 am	March 19 9 am	nd
March 19 9 am	March 20 8 am	nd
March 20 9 am	March 20 21 pm	nd
March 20 21 pm	March 21 9 am	1.32 ± 0.13
March 21 9 am	March 22 9 am	nd
March 22 9 am	March 23 8 am	nd
March 23 9 am	March 24 9 am	nd
March 24 9 am	March 25 9 am	nd
March 25 9 am	March 28 9 am	nd
March 28 9 am	March 29 9 am	nd
March 29 9 am	March 30 9 am	nd

Although the "nd" measurements change, depending mainly on the sample volume, the average level was approximately 0.2 mBq/m^3
nd not detected

There were no statistically significant differences. Thus, the β-activities of radioSr were interpreted to have the same counting efficiency regardless of the β-energy. The activity ratio of ^{89}Sr and ^{90}Sr was elucidated from the value traced back to the date of sample collection as well as the fixed date when the strontium carbonate precipitated. The activity was always decay corrected in the middle of the sampling time. The current detection limit for radioSr in air at that time was approximately 230 μBq/m^3.

Results and discussion

Estimation of ^{90}Sr in the aerosol sample

We will now quantify and describe the radioSr found in the air over Tsukuba. The radioactivity in Tsukuba indicated a two-fold concentration increase in March 2011, as shown in Fig. 8 in the Appendix 1. The amount of radioSr in the sample was smaller than what was anticipated based on past experience (e.g., Aoyama et al. 1991). ^{90}Sr was unable to be detected except when plume transport occurred. From March 14 9 pm (JST) to March 15 9 am, from March 15 9 am to 3 pm, and March 20 9 pm to March 21 9 am, the results were 1.5 ± 0.13, 1.0 ± 0.10, and 1.3 ± 0.13 mBq/m^3, respectively. For the other samples, the radioSr was

lower than the detection limits (Table 1 in the Appendix 2). The ^{90}Sr activity results shown here were calculated based on β-counts made long enough after the events that the contribution of ^{89}Sr could be negligible (less than 5 % of ^{90}Sr activity). For example, we waited at least 200 days after chemical separation (separation was performed after December 2011). The accompanying uncertainty was estimated from the average of the relative β-count uncertainties in the five latest individual measurements.

The activity ratio of ^{137}Cs/^{90}Sr in the aerosol samples, which was in the range of 4700–23,000, is very large compared with the activity ratio of radioactive fallout, which was 1.63 during the 1960–1970s; this indicates a clear difference in the data before and after the FDNPP accident. Furthermore, the MRI's estimated ^{137}Cs/^{90}Sr ratio for the Chernobyl radionuclides in May 1986 in Japan was 96 (Aoyama et al. 1991), which indicates that the Fukushima radionuclide composition was dominated by radioCs. In the activity peak on March 14–15, the ratio was 4700–6000, and the peak on March 20–21 was 23,000 times higher with ^{137}Cs, which also shows that the composition of the radioactive plume differed between the earlier and later dates during the course of the FDNPP accident.

The measured ^{137}Cs/^{90}Sr activity ratio in Tsukuba was more than 40 times higher than the emission assessment by NISA 2011 for the FDNPP accident (^{137}Cs: ^{90}Sr = 15: 0.14). The IAEA (2006) had estimated that the amount of ^{90}Sr emitted (approximately 10 PBq) for the Chernobyl accident was only 12 % that of ^{137}Cs (approximately 85 PBq), yet in reality, the atmosphere/precipitation observations in Japan showed approximately the amount of ^{90}Sr to be only 1/100 that of ^{137}Cs (Aoyama et al. 1991), indicating that less than 1/10 of the emitted ^{90}Sr was transported. Thus, the 8000 km long-range transportation from Chernobyl produced the radionuclide separation. With that in mind, it could be possible that fractionation caused by particle size deviation (Hirose et al. 1993) occurred in the FDNPP plume. The plume was transported less than a few hundred kilometers in the present case, but fractionation could be very effective.

Table 2 Curve fitting results with assumed ^{89}Sr over ^{90}Sr activity ratio

March 14–15, 2011		March 20–21, 2011	
^{89}Sr:^{90}Sr	σ	^{89}Sr:^{90}Sr	σ
9:0.14	0.3356	8:0.14	0.4550
10:0.14	0.3340	9:0.14	0.4165
11:0.14	0.3493	10:0.14	0.5432
12:0.14.	0.3795	11:0.14	0.5869

The results for two air filter samples collected in March 2011. The minimum standard deviation σ suggests the best estimate

^{89}Sr/^{90}Sr activity ratio

The emissions estimated by NISA 2011 showed that the ^{89}Sr proportion was 14 times higher than that of ^{90}Sr after the nuclear accident, which indicated that the radioactivity estimate would be 1/3 that of ^{90}Sr after a year. The results from the aerosol sample observations suggest the presence of ^{89}Sr; therefore, the temporal change in the β-counts was fitted based on emission estimates by the former NISA (^{89}Sr:^{90}Sr = 2:0.14). Figure 10 in the Appendix 2 shows the fitted results of the aerosol sample measurements for March 14–15. As shown in the figure, the sample counting values exhibited a large decay after 40 days of fixation as strontium carbonate, which indicates that the amount of coexisting ^{89}Sr was relatively large. Therefore, appropriately different ratios were examined instead of the 2:0.14 ratio, which could not be fitted. Therefore, the emitted ratio for the sample collected on March 14–15 was 10:0.14 for ^{89}Sr:^{90}Sr. The peak data for March 20–21 indicated that a ratio of 9:0.14 fit perfectly. Table 2 in

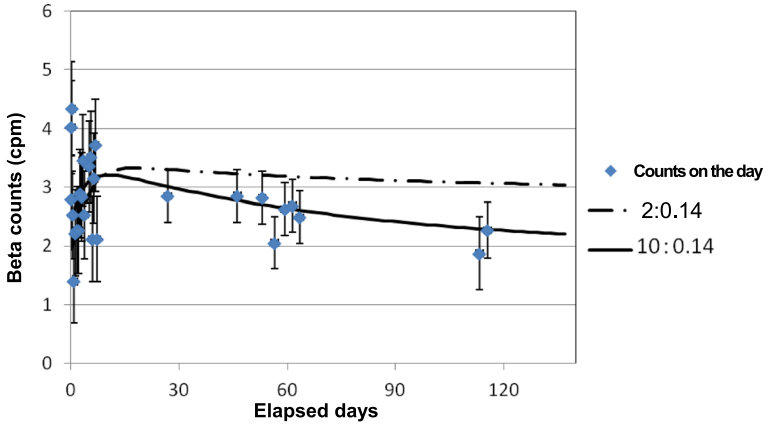

Fig. 10 Deconvolution of the ^{89}Sr, ^{90}Sr and ^{90}Y activities. It is possible to deconvolute radionuclides by measuring the temporal change in the total β-activity (cpm) of the purified radioSr source (March 14–15, 2011 sample). Elapsed days means the time after the radiochemical separation. An initial activity ratio of ^{89}Sr/^{90}Sr was assumed and applied to the curve fit as 2/0.14 and 10/0.14.

Table 3 Efficiency of ^{137}Cs extracted from air filter samples by heated concentrated nitric acid

Sampling date and time (JST)	Before ext. ^{137}Cs (Bq)	After ext. ^{137}Cs (Bq)	Extraction efficiency (%)
March 14 21 pm–March15 9 am	243 ± 0.7	72 ± 0.4	70.4
March 15 9 am–March 15 15 pm	41 ± 0.3	7.4 ± 0.12	82.0
March 15 15 pm–March 15 21 pm	20 ± 0.2	6.1 ± 0.11	69.5
March 15 21 pm–March 16 9 am	19 ± 0.2	0.51 ± 0.04	97.3
March 16 9 am–March 17 9 am	9.2 ± 0.19	0.52 ± 0.04	94.3
March 19 9 am–March 20 21 pm	94.2 ± 0.6	0.20 ± 0.03	99.8
March 20 21 pm–March 21 9 am	423 ± 0.9	1.2 ± 0.05	99.7
March 21 9 am–March 22 9 pm	30.8 ± 0.24	0.15 ± 0.03	99.5

Air filter samples were subjected to heated conc. nitric acid extraction for Sr analysis. Cs-137 was measured to confirm the extraction efficiency. Samples shown as "nd" before extraction were excluded from the table. Some samples exhibited significantly lower extraction efficiencies of 70–80 %. Insoluble and refractory radioactive particles must have been incorporated in these samples

the Appendix 2 shows these fitting results. Therefore, the emission ratio of ^{89}Sr/^{90}Sr for both March 14–15 and 20–21 was approximately 70 (10:0.14), which was five times bigger than what NISA 2011 had estimated.

The MEXT has reported ^{89,90}Sr in approximately 50 soil samples within 80 km of the FDNPP (MEXT 2011b). The decay data are corrected as of June 2011, and the activity ratio was reported to be in the range of 1.9–6.5 (average: 4). Another decay correction as of March 11, 2011 gives ^{89}Sr/^{90}Sr ratios of 7–24 with an average of 15. The ratio is not consistent with our results, and the fluctuation was large. The cause of the discrepancy and fluctuation is still unknown. The most likely explanation is that stable Sr, already present in reactor materials or seawater components, absorbed neutrons and formed ^{89}Sr. The extent of and fluctuation in mixing (inhomogeneity) might produce the discrepancy.

Efficiency of acid extraction of ^{137}Cs from filter specimens

The rates at which ^{137}Cs could be extracted from the filter and aerosol samples using acid are shown in Table 3 in the Appendix 2. The samples collected on March 14–15 and 20–21 have different extraction rates, indicating that the ^{137}Cs in the sample from the March 14–15 was refractory to some extent (20–30 %), even in a heated solution of nitric acid. This is possibly because of the difference in the physical and chemical nature of the radioactive aerosol. Thus, it is possible that the current radioSr concentration has been slightly underestimated (20–30 %) because of the low water dissolution rate of the radioactive material, especially for the March 14–15 sample.

As shown here, observations of the radioactive plume over Tsukuba at different times demonstrated that the ^{89}Sr/^{90}Sr ratio was almost constant, but the ^{137}Cs/^{90}Sr ratio and the extraction efficiency of ^{137}Cs with nitric acid differed. Moreover, it was shown earlier that the activity ratios among other γ-emitters differed (see Appendix 1). These findings confirm that the characteristics of the aerosol particles that carried major radionuclides from the first plume differed from later advected radioactive plumes. Adachi et al. (2013) addressed this sort of contrast in the characteristics of the two plumes' radioactive aerosols in detail, and Abe et al. (2014) added more information. They documented the discovery of insoluble, glassy spherules containing radioCs and assumed that the major fraction came from the first event. Indeed, no such particles were detected in the later event. This should also affect the ratio of ^{137}Cs/^{90}Sr in the air, and evidence regarding this will be obtained in future work. In conclusion, the present results support the previous findings of less ^{90}Sr contamination than radioCs contamination from the FDNPP accident and indicate the necessity of further investigations of radioSr in the atmospheric environment.

Abbreviations

ATSDR: US Department of Health and Human Services, Public Health Service, Agency for Toxic Substances and Disease Registry; DOE: US Department of Energy; FDNPP: Fukushima Dai-ichi nuclear power plant; HYSPLIT: Hybrid Single Particle Lagrangian Integrated Trajectory Model; IAEA: International Atomic Energy Agency; JMA: Japan Meteorological Agency; KURRI: Kyoto University Research Reactor Institute; MANAL: Meso-regional objective analysis; MEXT: Ministry of Education, Culture, Sports, Science and Technology, Japan; MRI: Meteorological Research Institute, Japan; NASA: National Aeronautics and Space Administration, USA; NHM: The JMA/MRI non-hydrostatic meteorological model; NISA: The former Nuclear and Industrial Safety Agency, Japan Carriage Return; RAQM2: Regional Air Quality Model 2; SCJ: Science Council of Japan Carriage Return; TEPCO: Tokyo Electric Power Company.

Competing interests

The authors declare that they have no competing interests.

Authors' contributions

YI designed and supervised the study and summarized the manuscript. MK conducted the transport simulation and wrote that part of the manuscript. Both YI and MK analyzed the data and helped in their interpretation. YZ helped conduct the sampling. KA and MM provided important suggestions for summarizing the work. They collaborated with the corresponding author in the preparation of the manuscript. All the authors read and approved the final manuscript.

Authors' information

YI received his PhD degree in chemistry from the University of Tsukuba in 1987. From 1987 to 1991, he was at the National Institute of Radiological Sciences and studied radiochemical analysis and radioecology. He moved to the MRI in 1991 because of his scientific ambition to be involved in more global issues. His current interests are atmospheric aerosols and their precursors, including Asian dust and $PM_{2.5}$, and their possible influences on climate, general environmental change, and other phenomena. He is working enthusiastically and is a member of several organizations, including the Japan Association of Aerosol Science and Technology, the Geochemical Society of Japan, the Japan Society of Nuclear and Radiochemical Sciences, the Meteorological Society of Japan, the Japan Radioisotope Association, the Japan Society of Analytical Chemistry, and the Japan Geoscience Union. He considers collaboration between observational researchers and modelers as a basic requisite in pursuing the geo- and environmental sciences.
MK received his PhD from the Graduate School of Science at Kyoto University in 2005. Since then, he has been engaged in the development of chemical transport models coupled with regional-scale meteorological models at the Disaster Prevention Research Institute, Kyoto University, Research Center for Advanced Science and Technology, University of Tokyo, and currently, the MRI. His main research interest is elemental processes of chemistry and microphysics of airborne particles and its impacts on air quality, ecosystem, and climate.
YZ graduated Meteorological College in 1984 and worked at the Nagasaki Marine Observatory, Japan Meteorological Agency from 1984 to 1989. He has been studying atmospheric aerosols at the MRI since 1989 and received his PhD from Nagoya University in 2005.
KA received his PhD from Kobe University in 2005, worked at Arizona State University between 2005 and 2011 as a postdoctoral/faculty research associate, and is currently studying atmospheric aerosols at the MRI.
MM received his PhD from Tohoku University in 1996, has worked at the MRI from 1985 to 2015, and finally holds the position of Senior Researcher for Research Affairs at the institute. Currently, he is working at Japan Meteorological Business Support Center.

Acknowledgements

The authors are deeply indebted to the following part-time and temporary staff members at the MRI: Chitsuko Takeda, Tokyo Nuclear Service Co. Ltd., and Kazue Inukai and Keiko Kamioka, currently at ATOX Co. Ltd. for the difficult work of analyzing samples and preparing samples measurements under an unusually severe accident situation; Hiroshi Sakou, Toru Kimura, and Sakae Mayama, ATOX Co. Ltd. for sampling, sample preparation, and general analysis; Wakari Iwai and Kazuma Nabeshima for radiochemical analysis of Sr isotopes and sample preparation, respectively; and Yuriko Kamiya, Kayo Yanagida, and Rina Mori for sampling, logistical support, figure preparation, and manuscript editing. Takeshi Ito helped with the trajectory analysis in the revised manuscript. The authors are also grateful to the following MRI academic colleagues: Hiroaki Naoe, Michio Aoyama (currently at Fukushima University), and Hiroshi Takahashi (currently at the Japan Meteorological Agency) for their help with sampling. Additionally, they acknowledge the assistance of Naoyuki Osada (currently at Okayama University) and Yuichi Oki (Kyoto University Research Reactor Institute) with low-background γ-ray measurements. The authors benefitted from discussions with Kazuyuki Kita (Ibaraki University) and Yuko Hatano (University of Tsukuba) regarding the re-suspension issue. Olivier Masson, IRSN, France, kindly gave critical comments on an early version of the manuscript, for which the authors are grateful. This study was financially supported by the former MEXT and current Nuclear Regulation Authority "Japanese Radioactivity Survey" fund and partially by the MEXT "Kakenhi" (a Grant-in-Aid for Scientific Research on Innovative Areas under the A01-1 and A01-2 research teams in the "Interdisciplinary Study on Environmental Transfer of Radionuclides from the Fukushima Daiichi NPP Accident (ISET-R; leader: Professor Yuichi Onda, University of Tsukuba)"; grant nos. 24110002 and 24110003) and the JSPS "Kakenhi" (leader Dr. Tsuyoshi T Sekiyama, MRI; grant no. 24340115). We gratefully acknowledge NOAA's ARL for providing the HYSPLIT transport and dispersion model and the READY website used in this study. The present paper was written and organized based on previous proceedings (Iwai et al. 2012; Igarashi et al. 2013a) and presentations at the ICAS, AMS, EGU, domestic meetings, and other settings (Igarashi et al. 2011, 2013b , 2013c) and the MRI home page (MRI 2011).

Author details

[1]Meteorological Research Institute, 1-1 Nagamine, Tsukuba, Ibaraki 305-0052, Japan. [2]Present address: Japan Meteorological Business Support Center, Chiyoda-ku, Tokyo 101-0054, Japan.

Received: 16 March 2015 Accepted: 22 October 2015
Published online: 09 December 2015

References

Abe Y, Iizawa Y, Terada Y, Adachi K, Igarashi Y, Nakai I. Detection of uranium and chemical state analysis of individual radioactive microparticles emitted from the Fukushima nuclear accident using multiple synchrotron radiation X-ray analyses. Anal Chem. 2014;86:8521–5. doi:10.1021/ac501998d.

Adachi K, Kajino M, Zaizen Y, Igarashi Y. Emission of spherical cesium-bearing particles from an early stage of the Fukushima nuclear accident. Sci Rep. 2013;3:2554. doi:10.1038/srep02554.

Amano H, Akiyama M, Chunlei B, Kawamura T, Kishimoto T, Kuroda T, et al. Radiation measurements in the Chiba Metropolitan Area and radiological aspects of fallout from the Fukushima Dai-ichi Nuclear Power Plants accident. J Environ Radioact. 2012;111:42–52. doi:10.1016/j.jenvrad.2011.10.019.

Aoyama M. Evidence of stratospheric fallout of caesium isotopes from Chernobyl accident. Geophys Res Lett. 1988;15:327–30. doi:10.1029/GL015i004p00327.

Aoyama M, Hirose K. The temporal and spatial variation of ^{137}Cs concentration in the Western North Pacific and its marginal seas during the period from 1979 to 1988. J Environ Radioact. 1995;29:57–74. doi:10.1016/0265-931X(94)00050-7.

Aoyama M, Hirose K. Artificial radionuclides database in the Pacific Ocean: HAM database. Sci World J. 2004;4:200–15. doi:10.1100/tsw.2004.15.

Aoyama M, Hirose K, Suzuki Y, Inoue H, Sugimura Y. High level radioactive nuclides in Japan in May. Nature. 1986;321:819–20. doi:10.1038/321819a0.

Aoyama M, Hirose K, Sugimura Y. Deposition of gamma-emitting nuclides in Japan after the reactor-IV accident at Chernobyl. J Radioanal Nucl Chem. 1987;116:291–306. doi:10.1007/BF02035773.

Aoyama M, Hirose K, Sugimura Y. The temporal variation of stratospheric fallout derived from the Chernobyl accident. J Environ Radioact. 1991;13:103–15. doi:10.1016/0265-931X(91)90053-I.

Aoyama M, Ohara T, Komura K. Donen Tokai jiko niyoru houshasei sesiumu no Kanto heiya heno hirogari (Transport and diffusion of radioactive caesium to the Kanto plain by the PNC Tokai accident). Kagaku. 1999;69(1):16–21 (in Japanese).

Aoyama M, Hirose K, Igarashi Y. Re-construction and updating our understanding on the global weapons tests ^{137}Cs fallout. J Environ Monitor. 2006;8:431–8. doi:10.1039/B512601K.

Aoyama M, Tsumune D, Hamajima Y. Distribution of ^{137}Cs and ^{134}Cs in the North Pacific Ocean: impacts of the TEPCO Fukushima-Daiichi NPP accident. J Radioanal Nucl Chem. 2012;296(1):535–9. doi:10.1007/s10967-012-2033-2.

Aoyama M, Uematsu M, Tsumune D, Hamajima Y. Surface pathway of radioactive plume of TEPCO Fukushima NPP1 released ^{134}Cs and ^{137}Cs. Biogeosciences. 2013;10:3067–78. doi:10.5194/bg-10-3067-2013.

Chino M, Nakayama H, Nagai H, Terada H, Katata G, Yamazawa H. Preliminary estimation of release amounts of ^{131}I and ^{137}Cs accidentally discharged from the Fukushima Daiichi Nuclear Power Plant into atmosphere. J Nucl Sci Technol. 2011;48:1129–34. doi:10.1080/18811248.2011.9711799.

Doi T, Masumoto K, Toyoda A, Tanaka A, Shibata Y, Hirose K. Anthropogenic radionuclides in the atmosphere observed at Tsukuba: characteristics of the radionuclides derived from Fukushima. J Environ Radioact. 2013;122:55–62. doi:10.1016/j.jenvrad.2013.02.001.

Ehhalt DH. Turnover times of ^{137}Cs and HTO in the troposphere and removal rates of natural particles and vapor. J Geophys Res. 1973;78:7076–86.

Estevan MT. Consequences of the Algeciras accident, and the Spanish system for the radiological surveillance and control of scrap and the products of its processing. In: Security of radioactive sources, proceedings of an international conference. Vienna Austria: IAEA; 2003. p. 357–62. 10–13 March 2003.

Garger EK, Kuzmenko YI, Sickinger S, Tschiersch J. Prediction of the ^{137}Cs activity concentration in the atmospheric surface layer of the Chernobyl exclusion zone. J Environ Radioact. 2012;110:53–8. doi:10.1016/j.jenvrad.2012.01.017.

Haba H, Kanaya J, Mukai H, Kambara T, Kase M. One-year monitoring of air-borne radionuclides in Wako, Japan, after the Fukushima Dai-ichi nuclear power plant accident in 2011. Geochem J. 2012;46(4):271–8. Special Issue: Fukushima Review.

Hatano Y, Hatano N. Formula for the resuspension factor and estimation of the date of surface contamination. Atmos Environ. 2003;37:3475–80. doi:10.1016/S1352-2310(03)00410-2.

Hernández-Ceballos MA, Hong GH, Lozano RL, Kim YI, Lee HM, Kim SH, et al. Tracking the complete revolution of surface westerlies over Northern Hemisphere using radionuclides emitted from Fukushima. Sci Total Environ. 2012;438:80–5.

Hirose K. Fukushima Dai-ichi nuclear power plant accident: summary of regional radioactive deposition monitoring results. J Environ Radioact. 2012;111:13–7. doi:10.1016/j.jenvrad.2011.09.003.

Hirose K. Temporal variation of monthly ^{137}Cs deposition observed in Japan: effects of the Fukushima Daiichi nuclear power plant accident. Appl Radiat Isot. 2013;81:325–9. doi:10.1016/j.apradiso.2013.03.076.

Hirose K, Aoyama M. Present background levels of surface ^{137}Cs and ^{239,240}Pu concentrations in the Pacific. J Environ Radioact. 2003;69(1–2):53–60. doi:10.1016/S0265-931X(03)00086-9.

Hirose K, Sugimura Y, Katsuragi Y. ^{90}Sr and $^{239+240}$Pu in the surface air in Japan: their concentrations and size distributions. Pap Met Geophys. 1986;37(4):255–69.

Hirose K, Takatani S, Aoyama M. Wet deposition of radionuclides derived from the Chernobyl accident. J Atmos Chem. 1993;17:61–71. doi:10.1007/BF00699114.

Hirose K, Amano H, Baxter MS, Chaykovskaya E, Chumichev VB, Hong GH, et al. Anthropogenic radionuclides in seawater in the East Sea/Japan Sea: results of the first-stage Japanese-Korean-Russian expedition. J Environ Radioact. 1999;43:1–13.

Hirose K, Igarashi Y, Aoyama M, Miyao T. Long-term trends of plutonium fallout observed in Japan. In: Kudo A (ed) Radioactivity in the environment Vol 1. pp 251–266. Plutonium in the environment proceedings of the second international symposium, Osaka, Japan, November 9–12, 1999. Amsterdam: Elsevier; 2001. doi:10.1016/S1569-4860(01)80018-8.

Honda MC, Aono T, Aoyama M, Hamajima Y, Kawakami H, Kitamura M, et al. Dispersion of artificial caesium-134 and −137 in the western North Pacific one month after the Fukushima accident. Geochem J. 2012;46:e1–9.

Igarashi Y. Anthropogenic radioactivity in aerosol: a review focusing on studies during the 2000s. Jpn J Health Phys. 2009;44(3):313–23.

Igarashi Y, Otsuji–Hatori M, Hirose K. Recent deposition of ^{90}Sr and ^{137}Cs observed in Tsukuba. J Environ Radioact. 1996;31:157–69. doi:10.1016/0265-931X(96)88491-8.

Igarashi Y, Aoyama M, Miyao T, Hirose K, Komura K, Yamamoto M. Air concentration of radiocaesium in Tsukuba, Japan following the release from the Tokai waste treatment plant: comparisons of observations with predictions. Appl Radiat Isotopes. 1999a;50:1063–73. doi:10.1016/S0969-8043(98)00129-8.

Igarashi Y, Aoyama M, Miyao T, Hirose K, Tomita M. Anomalous ^{90}Sr deposition during the fall, 1995 at MRI, Tsukuba, Japan. J Radioanal Nucl Chem. 1999b;239:539–42. doi:10.1007/BF02349065.

Igarashi Y, Miyao T, Aoyama M, Hirose K, Sartorius H, Weiss W. Radioactive noble gases in the surface air monitored at MRI, Tsukuba, before and after the JCO accident. J Environ Radioact. 2000a;50:107–18.

Igarashi Y, Sartorius H, Miyao T, Weiss W, Fushimi K, Aoyama M, et al. ^{85}Kr and ^{133}Xe monitoring at MRI, Tsukuba and its importance. J Envrion Radioactiv. 2000b;48:191–202. doi:10.1016/S0265-931X(99)00076-4.

Igarashi Y, Aoyama M, Hirose K, Miyao T, Nemoto K, Tomita M, et al. Resuspension: decadal monitoring time series of the anthropogenic radioactivity deposition in Japan. J Radiat Res. 2003;44:319–28.

Igarashi Y, Inomata Y, Aoyama M, Hirose K, Takahashi H, Shinoda Y, et al. Possible change in Asian dust source suggested by atmospheric anthropogenic radionuclides during the 2000s. Atmos Environ. 2009;43:2971–80.

Igarashi Y, Kajino M, Osada N, Oki Y, Takeda C. Aerosol radioactivity observed in Tsukuba during March 2011. Kyoto: ICAS2011 (IUPAC International Congress on Analytical Sciences); 2011.

Igarashi Y, Zaizen Y, Adachi K, Kajino M. Mikami M. Atmospheric pollution by the Fukushima accident: two years observations in Tsukuba. In: Bessho K, Tagami K, Takamiya K, Miura T, editors. Proceedings the 14th workshop on environmental radioactivity, pp 35–39 (in Japanese with English abstract). Tsukuba: High Energy Accelerator Research Organization; 2013a.

Igarashi Y, Kajino M, Zaizen Y, Mikami M. Observations of atmospheric radionuclides from the Fukushima nuclear accident in Tsukuba, Japan, American Meteorological Society 93rd annual meeting, Austin, Texas, Jan 2013. 2013b.

Igarashi Y, Kajino M, Zaizen Y, Adachi K, Mikami M, Kita K, et al. Atmospheric radionuclides from the Fukushima nuclear accident: two years observations in Tsukuba, Japan, the EGU general assembly 2013, Vienna, Austria, Apr 2013. 2013c.

International Atomic Energy Agency. Environmental consequences of the Chernobyl accident and their remediation: twenty years of experience report of the Chernobyl Forum Expert Group "Environment". Vienna, Austria: 2006. ISBN 92–0–114705–8, ISSN 1020–6566

Iwai W, Igarashi Y, Nabeshima K. Observation of radioactivity of the atmospheric aerosol (radioactive Sr). In: Bessho K, Tagami K, Takamiya K, Miura T, editors. Proceedings the 13th workshop on environmental radioactivity. Tsukuba: High Energy Accelerator Research Organization; 2012. p. 102–7 (in Japanese with English abstract).

Janžekovič H, Križman MJ. Comparison of discharges of the nuclear accidents in Japan 2011 and Chernobyl 1986. In: Proceedings of the international conference nuclear energy for New Europe, Bovec, Slovenia, Sept 12–15, 2011. 2011.

Kajino M, Inomata Y, Sato K, Ueda H, Han Z, An J, et al. Development of the RAQM2 aerosol chemical transport model and predictions of the Northeast Asian aerosol mass, size, chemistry, and mixing type. Atmos Chem Phys. 2012;12:11833–56. doi:10.5194/acp-12-11833-2012.

Kanai Y. Monitoring of aerosols in Tsukuba after Fukushima Nuclear Power Plant incident in 2011. J Environ Radioact. 2012;111:33–7. doi:10.1016/j.jenvrad.2011.10.011.

Kaneyasu N, Ohashi H, Suzuki F, Okuda T, Ikemori F. Sulfate aerosol as a potential transport medium of radiocesium from the Fukushima nuclear accident. Environ Sci Technol. 2012;46:5720–6.

Katata G, Ota M, Terada H, Chino M, Nagai H. Atmospheric discharge and dispersion of radionuclides during the Fukushima Dai-ichi Nuclear Power Plant accident. Part I: source term estimation and local-scale atmospheric dispersion in early phase of the accident. J Environ Radioact. 2012a;109:103–13.

Katata G, Terada H, Nagai H, Chino M. Numerical reconstruction of high dose rate zones due to the Fukushima Dai-ichi Nuclear Power Plant accident. J Environ Radioact. 2012b;111:2–12.

Katata G, Chino M, Kobayashi T, Terada H, Ota M, Nagai H, et al. Detailed source term estimation of the atmospheric release for the Fukushima Daiichi Nuclear Power Station accident by coupling simulations of atmospheric dispersion model with improved deposition scheme and oceanic dispersion model. Atmos Chem Phys Discuss. 2014;14:14725–832. doi:10.5194/acpd-14-14725-2014.

Katsuragi Y. A study of ^{90}Sr fallout in Japan. Pap Met Geophys. 1983;33(4):277–91.

Kinoshita N, Sueki K, Sasa K, Kitagawa J, Ikarashi S, Nishimura T, et al. Assessment of individual radionuclide distributions from the Fukushima nuclear accident covering central-east Japan. Proc Natl Acad Sci U S A. 2011;108(49):19526–9. doi:10.1073/pnas.1111724108.

Komura K, Yamamoto M, Muroyama T, Murata Y, Nakanishi T, Hoshi M, et al. The JCO criticality accident at Tokai-mura, Japan: an overview of the sampling campaign and preliminary results. J Environ Radioactiv. 2000;50:3–14.

Kristiansen NI, Stohl A, Wotawa G. Atmospheric removal times of the aerosol-bound radionuclides ^{137}Cs and ^{131}I measured after the Fukushima Dai-ichi nuclear accident: a constraint for air quality and climate models. Atmos Chem Phys. 2012;12:10759–69.

Kusakabe M, Oikawa S, Takata H, Misonoo J. Spatiotemporal distributions of Fukushima-derived radionuclides in nearby marine surface sediments. Biogeosciences. 2013;10:5019–30. doi:10.5194/bg-10-5019-2013.

Maki T, Tanaka TY, Kajino M, Sekiyama TT, Igaraashi Y, Mikami M. Radioactive nuclei emission analysis from Fukushima Daiichi Nuclear Power Plant by inverse model, Manuscript for 93rd American Meteorological Society annual meeting, Austin Texas U.S. 2013. (https://ams.confex.com/ams/93Annual/webprogram/Paper216873.html Accessed date: October 14, 2015)

Masson O. Private communication, Radioprotection Division, Environmental Radioactivity Study and Monitoring Department, Institute for Radiological Protection and Nuclear Safety, France. 2014.

Masson O, Baeza A, Bieringer J, Brudecki K, Bucci S, Cappai M, et al. Tracking of air-borne radionuclides from the damaged Fukushima Dai-ichi nuclear reactors by European networks. Environ Sci Technol. 2011;45:7670–7.

Masumoto Y, Miyazawa Y, Tsumune D, Kobayashi T, Estournel C, Marsaleix P, et al. Oceanic dispersion simulation of Cesium-137 from Fukushima Dai-ichi Nuclear Power Plant. Elements. 2012;8:207–12.

Maxwell RM, Anspaugh LR. An improved model for prediction of resuspension. Health Phys. 2011;101:722–30. doi:10.1097/HP.0b013e31821ddb07.

Meteorological Research Institute (MRI). Tokyo Denryoku Fukushima Dai-ichi Genshiryoku Hatsudensho Jiko nitomonau houshaseibusshitsu no iryuukakusan nitsuite (On the transport and diffusion of radioactive materials by the Fukushima Dai-ichi Nuclear Power Station accident)" (in Japanese). 2011. http://www.mri-jma.go.jp/Topics/H23/H23_tohoku-taiheiyo-oki-eq/1107fukushima.html.

Ministry of Education, Culture, Sports, Science and Technology (MEXT). Monbu Kagaku-sho oyobi Ibaraki-ken niyoru kokuki monitaringu no sokutei kekka no shuusei nitsuite (On the correction of the aerial monitoring results conducted by MEXT and Ibaraki prefecture) dated August 31, 2011 (in Japanese). 2011a. http://radioactivity.nsr.go.jp/ja/contents/5000/4933/24/1940_0831.pdf.

Ministry of Education, Culture, Sports, Science and Technology (MEXT). Monbu Kagaku-sho ni yoru, purutoniumu, sutoronchiumu no kakushu bunseki no kekka nitsuite (On the analytical results for Pu and Sr by MEXT) dated September 30, 2011 (in Japanese). 2011b. http://radioactivity.nsr.go.jp/ja/contents/6000/5048/24/5600_110930_rev130701.pdf.

Ministry of Education, Culture, Sports, Science and Technology, Results of Air-borne Monitoring by the Ministry of Education, Culture, Sports, Science and Technology and the U.S. Department of Energy (MEXT & USDOE). 2011. dated May 6, 2011.

Miyake Y. The artificial radioactivity in rain water observed in Japan, from autumn 1954 to spring 1955. Pap Met Geophys. 1954;6(1):26–31.

Miyake Y, Sugiura Y, Kameda K. On the distribution of radioactivity in the sea: around Bikini Atoll in June, 1954. Pap Met Geophys. 1955;5:253–62.

Miyake Y, Saruhashi K, Katsuragi Y, Kanazawa T. Penetration of ^{90}Sr and ^{137}Cs in deep layers of the Pacific and vertical diffusion rate of deep water. J Radiat Res. 1962;3(3):141–7.

Miyake Y, Samhashi K, Katsuragi Y, Kanazawa T, Tsunogai S. Deposition of Sr-90 and Cs-137 in Tokyo through the end of July 1963. Pap Met Geophys. 1963;14:58–65.

Miyake Y, Katsuragi Y, Sugimura Y. Plutonium fallout in Tokyo. Pap Met Geophys. 1975;26(1):1–8.

Miyake Y, Saruhashi K, Sugimura Y, Kanazawa T, Hirose K. Contents of ^{137}Cs, plutonium and americium isotopes in the Southern Ocean waters. Pap Met Geophys. 1988;39:95–113.

Miyao T, Hirose K, Aoyama M, Igarashi Y. Trace of the recent deep water formation in the Japan Sea deduced from historical ^{137}Cs data. Geophys Res Lett. 2000;27(22):3731–4.

Morino Y, Ohara T, Nishizawa M. Atmospheric behavior, deposition, and budget of radioactive materials from the Fukushima Daiichi nuclear power plant in March 2011. Geophys Res Lett. 2011;38:L00G11. doi:10.1029/2011GL048689.

Nuclear and Industrial Safety Agency (NISA). Houshasei bussitsu houshutsuryo deta no ichibu ayamari nitsuite (On a partial mistake in emission inventory estimate of radioactive materials) dated October 20, 2011 (in Japanese). 2011. http://warp.ndl.go.jp/info:ndljp/pid/6086248/www.meti.go.jp/press/2011/10/20111020001/20111020001.pdf.

Otsuji-Hatori M, Igarashi Y, Hirose K. Preparation of a reference fallout material for activity measurements. J Environ Radioact. 1996;31:143–55.

Petters MD, Kreidenweis SM. A single parameter representation of hygroscopic growth and cloud condensation nucleus activity. Atmos Chem Phys. 2007;7:1961–71. doi:10.5194/acp-7-1961-2007.

Povinec PP, Gera M, Holý K, Hirose K, Lujanienė G, Nakano M, et al. Dispersion of Fukushima radionuclides in the global atmosphere and the ocean. Appl Radiat Isot. 2013a;81:383–92.

Povinec PP, Aoyama M, Biddulph D, Breier R, Buesseler K, Chang CC, et al. Cesium, iodine and tritium in NW Pacific waters: a comparison of the Fukushima impact with global fallout. Biogeosciences. 2013b;10:5481–96. doi:10.5194/bg-10-5481-2013.

Saito K, Ishida J, Aranami K, Hara T, Segawa T, Narita M, et al. Nonhydrostatic atmospheric models and operational development at JMA. J Meteorol Soc Jpn. 2007;85B:271–304. doi:10.2151/jmsj.85B.271.

Sanada Y, Sugita T, Nishizawa Y, Kondo A, Torii T. The aerial radiation monitoring in Japan after the Fukushima Daiichi nuclear power plant accident. Progress in Nuclear Science and Technology. 2014;4:76–80.

Schwantes JM, Orton CR, Clark RA. Analysis of a nuclear accident: fission and activation product releases from the Fukushima Daiichi Nuclear Facility as remote indicators of source identification, extent of release, and state of damaged spent nuclear fuel. Environ Sci Technol. 2012;46(16):8621–7. doi:10.1021/es300556m.

Sectional Committee on Nuclear Accident Committee on Comprehensive Synthetic Engineering, Science Council of Japan (SCJ). Report "A review of the model comparison of transportation and deposition of radioactive materials released to the environment as a result of the Tokyo Electric Power Company's Fukushima Daiichi Nuclear Power Plant Accident" dated September 2, 2014. 2014. http://www.scj.go.jp/en/report/index.html.

Sekiyama TT, Kunii M, Kajino M, Shimbori T. Horizontal resolution dependence of atmospheric simulations of the Fukushima nuclear accident using 15-km, 3-km, and 500 m grid models. J Meteor Soc Japan. 2015;93(1):49–64. doi:10.2151/jmsj.2015-002.

Stohl A, Seibert P, Wotawa G, Arnold D, Burkhart JF, Eckhardt S, et al. Xenon-133 and caesium-137 releases into the atmosphere from the Fukushima Dai-ichi Nuclear Power Plant: determination of the source term, atmospheric dispersion, and deposition. Atmos Chem Phys. 2012;12:2313–43. doi:10.5194/acp-12-2313-2012.

Takemura T, Nakamura H, Takigawa M, Kondo H, Satonuma T, Miyasaka T, et al. A numerical simulation of global transport of atmospheric particles emitted from the Fukushima Daiichi Nuclear Power Plant. Scientific Online Letters on the Atmosphere (SOLA). 2011;7:101–4.

Tanaka TY. Numerical simulation of global dispersion of radionuclides. Wind Engineers JAWE. 2013;38(4):388–95 (in Japanese).

Tanihata I. Sampling and mapping of soil contamination and what we have learn from it. Radioisotopes. 2013;62:724–40 (in Japanese).

Terada H, Katata G, Chino M, Nagai H. Atmospheric discharge and dispersion of radionuclides during the Fukushima Dai-ichi Nuclear Power Plant accident. Part II: verification of the source term and analysis of regional-scale atmospheric dispersion. J Environ Radioact. 2012;112:141–54. doi:10.1016/j.jenvrad.2012.05.023.

Tokyo Electric Power Company (TEPCO). Estimation of radioactive material released to the atmosphere during the Fukushima Daiichi NPS Accident dated May 2012. 2012. http://www.tepco.co.jp/en/press/corp-com/release/betu12_e/images/120524e0205.pdf.

Torii T, Sugita T, Okada CE, Reed MS, Blumenthal DJ. Enhanced analysis methods to derive the spatial distribution of ^{131}I deposition on the ground by air-borne surveys at an early stage after the Fukushima Daiichi Nuclear Power Plant accident. Health Phys. 2013;105(2):192–200.

Tsumune D, Tsubono T, Aoyama M, Uematsu M, Misumi K, Maeda Y, et al. One-year, regional-scale simulation of ^{137}Cs radioactivity in the ocean following the Fukushima Dai-ichi Nuclear Power Plant accident. Biogeosciences. 2013;10:5601–17. doi:10.5194/bg-10-5601-2013.

Tsuruta H, Oura Y, Ebihara M, Ohara T, Nakajima T. First retrieval of hourly atmospheric radionuclides just after the Fukushima accident by analyzing filter-tapes of operational air pollution monitoring stations. Sci Rep. 2014;4:6717. doi:10.1038/srep06717.

U.S. Department of Energy (USDOE). 2013. http://energy.gov/situation-japan-updated-12513

U.S. Department of Health and Human Services, Public Health Service, Agency for Toxic Substances and Disease Registry (ATSDR2004Cs). Toxicological Profile for Cesium. 2004. http://www.atsdr.cdc.gov/ToxProfiles/tp157.pdf.

U.S. Department of Health and Human Services, Public Health Service, Agency for Toxic Substances and Disease Registry (ATSDR2004Sr). Toxicological Profile for Strontium. 2004. http://www.atsdr.cdc.gov/ToxProfiles/tp159.pdf.

Winiarek V, Bocquet M, Saunier O, Mathieu A. Estimation of errors in the inverse modeling of accidental release of atmospheric pollutant: Application to the reconstruction of the cesium-137 and iodine-131 source terms from the Fukushima Daiichi Power Plant. J Geophys Res. 2012;117, D05122. doi:10.1029/2011JD016932.

Yamamoto M, Takada T, Nagao S, Koike T, Shimada K, Hoshi M, et al. An early survey of the radioactive contamination of soil due to the Fukushima Dai-ichi Nuclear Power Plant accident, with emphasis on plutonium analysis. Geochem J. 2012;46:341–53.

Yoshida N, Kanda J. Tracking the Fukushima radionuclides. Science. 2012;336:1115–6. doi:10.1126/science.1219493.

Yoshida N, Takahashi Y. Land-surface contamination by radionuclides from the Fukushima Daiichi Nuclear Power Plant accident. Elements. 2012;8:201–6. doi:10.2113/gselements.8.3.201.

Zhang W, Bean M, Benotto M, Cheung J, Ungar K, BAhier B. Development of a new aerosol monitoring system and its application in Fukushima nuclear accident related aerosol radioactivity measurement at the CTBT radionuclide station in Sidney of Canada. J Environ Radioactiv. 2011;102:1065–9. doi:10.1016/j.jenvrad.2011.08.007.

KEK Proceedings 2015-4
November 2015 R

Proceedings of the 16th Workshop on Environmental Radioactivity
KEK, Tsukuba, Japan March 9-11, 2015
High Energy Accelerator Research Organization

Quality control of radioactivity analysis in atomospheric fallout sample

Toru Kimura[1],Yasuhito Igarashi[2]
[1]ATOX Co.,Ltd.,[2]Meteorological Research Institute

In the Meteorological Research Institute, observations of ^{90}Sr and ^{137}Cs in atmospheric deposition have been carried out for more than 50 years from the late 1950s. And a part of this observation, especially of radioactivity analysis, was undertaken by ATOX Co. from a few years ago. In this report analytical results (^{90}Sr, ^{137}Cs) that have been obtained in the past are compared with our recent values and reference values, indicating the current status of quality control have been made with a good accuracy. ^{137}Cs analysis was made by measuring the reference fallout samples by using a Ge detector. For ^{90}Sr analysis, after decomposition of organic substances, Sr fraction was radiochemically-separated and finally purified strontium carbonate was measured with a low background 2π gas flow counter. Comparing the reference value with the analytical ones, ^{90}Sr and ^{137}Cs analysis results were generally within the favorable range. The average values were also in good agreement with the past analytical values. However, distribution normality for the ^{90}Sr analytical values was not confirmed clearly due to small total sample analysis. Also, the difference between the average analytical values for ^{90}Sr and ^{137}Cs and the reference values was subjected to t-test at the 5% significance level, significant difference was not observed. Therefore, it is concluded that quality control of the whole analytical procedures has been done properly.

大気降下物試料の放射能分析の品質管理

木村徹*1，五十嵐康人*2
*1 ㈱アトックス、*2 気象研究所 環境・応用気象研究部

1．はじめに

気象研究所では、1950 年代後半から 50 年以上の期間にわたり大気降下物中の ^{90}Sr と ^{137}Cs について観測を行っている。アトックスでは数年前からこの観測の一部を請負い、放射能分析を実施してきた。その中で定期的に技術水準を確認することは、適正な品質を確保する観点から重要な事である。今回はこれまでの結果（^{90}Sr，^{137}Cs）をまとめ、過去に実施された分析結果や参照値と比較し、良好な精度で品質管理がなされている現状を報告する。

2．分析試料

技術水準の確認に用いた試料は、気象研究所から供された標準試料(Fig.1)である。この標準試料は 1963 年～1979 年にかけて日本全国 14 地点で採取された降下物試料を、気象研究所において混合・調製したものである。なおこの試料は、調整後に他の分析機関においても分析が行われ、参照値が与えられている[1,2]。

Fig.1 Reference fallout materials

Fig.2 A Ge semiconductor detector with a sample auto-changer

3．分析方法

^{137}Cs については、標準試料約 4g～60g をそれぞれ外径 6cm のプラスチック容器（丸型 V 式容器 V-1 又は V-7)に詰め、高さを測定後、Ge 半導体検出器(Fig.2)で測定した。^{90}Sr については、約 4g の標準試料をテフロン容器内に入れ、濃硝酸と過酸化水素を加えて 200℃に加熱し有機物を分解後、不溶残渣をろ過で除去する。担体として Sr 50mg 相当を加えたろ液に水酸化ナトリウムを加えアルカリにして、炭酸塩沈殿(Fig.3a)、つづいてシュウ酸塩沈殿(Fig.3b)、発煙硝酸法によるカルシウム除去(Fig.3c)、重クロム酸バリウム共沈によるバリウム・ラジウム除去、鉄共沈による Y 除去により化学分離し、最終的に炭酸ストロンチウムとしてろ紙ばさみに固定した。二週間以上放置し、^{90}Sr と ^{90}Y とが放射平衡に達した後に、低バックグラウンド 2π ガスフロー検出器(Tennelec LB-5100)(Fig.4)で測定した[2]。

Sr の回収率については、以下の計算式による。

$$Y = \frac{W_2}{W_1} * 100$$

Y：Sr yield(%)、W_1 ： The quantity of added strontium as a carrier (mg)、
W_2 ： The quantity of recovered strontium (mg)

Fig.3a Radiochemical separation (carbonate)

Fig.3b Radiochemical separation (oxalate)

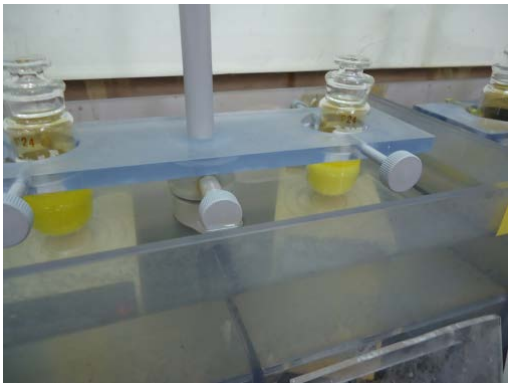

Fig.3c Radiochemical separation (calcium removal)

Fig.4 A 2π gas-flow detector

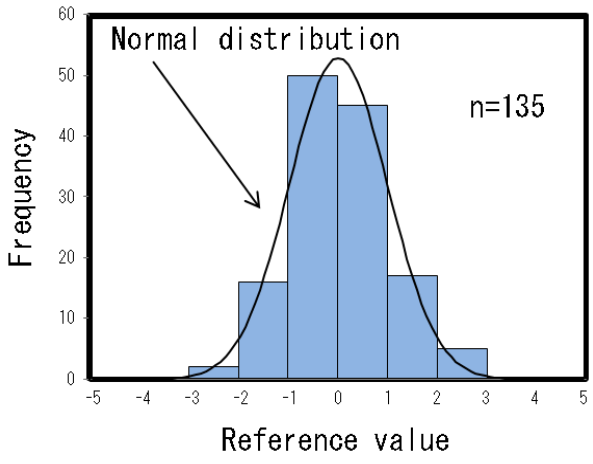

Fig.5 The ratio between the standard deviation deviation and the ^{137}Cs analysis value

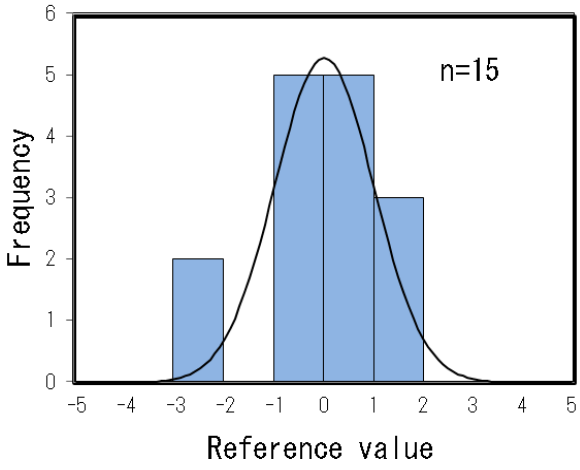

Fig.6 The ratio between the standard and the ^{90}Sr analysis value

Table-1 Comparison of ^{90}Sr and ^{137}Cs between analysis value and reference value (Bq/g)

	Past analysis value	QC analysis value	Reference value
^{137}Cs	307±9 (n=699)	315±10 (n=135)	312±16
^{90}Sr	208±8 (n=95)	206±10 (n=15)	211±33

Table-2 t-test for ^{137}Cs data

	QC analysis value	Reference value	QC analysis value	Past analysis value	Past analysis value	Reference value
Average	315	312	315	307	307	312
Variance	109	246	109	88	88	246
Observation number	135	9	135	699	699	9
Degrees of freedom	142		832		706	
t	0.92		9.22		-1.53	
P(T<=t) one-sided test	0.18		1.2E-19		0.06	
P(T<=t) two-sided test	**0.36**		**2.4E-19**		**0.13**	

Table-3 t-test for ^{90}Sr data

	QC analysis value	Reference value	QC analysis value	Past analysis value	Past analysis value	Reference value
Average	206	211	206	208	208	211
Variance	109	1081	109	63	63	1081
Observation number	15	3	15	95	95	3
Degrees of freedom	16		108		96	
t	-0.46		-0.91		-0.43	
P(T<=t) one-sided test	0.33		0.18		0.33	
P(T<=t) two-sided test	**0.65**		**0.37**		**0.67**	

４．データ解析

これまでにアトックスが実施した標準試料の分析結果を QC 分析値（^{137}Cs については、9 試料×Ge 5 台/半年の直近 135 試料、^{90}Sr については 5 試料/年、2012～2014 年の 15 試料の分析値）とし、核種毎にその値から標準偏差を求め、標準偏差との差を 1σ 毎基準化した度数分布からヒストグラムを作成し、正規分布と比較した（Fig.5 および Fig.6）。

また、過去の分析値（弊社以前に分析業務を請負っていた他社の標準試料分析値。^{137}Cs については 1996～2007 年、^{90}Sr については 1992～2007 年の分析値）・QC 分析値・参照値[2]の平均値を比較(Table-1）し、平均値の差が統計的に有意かを確かめるために、有意水準 5%で両側検定の t 検定を行った(Table-2 および Table-3)。

５．結果と考察

^{90}Sr および ^{137}Cs の分析結果は概ね良好なばらつきの範囲内であったが、^{90}Sr については分析試料総数が少ないため正規性の確認は確実ではない。しかし、平均値は参照値とよく一致している。また、t 検定結果から ^{137}Cs については過去の分析値と QC 分析値の間で平均値は統計的に有意であったものの、その平均値の差は 2.5%であり、環境放射能分析においては許容範囲内であると判断できる。その他の ^{90}Sr 分析値や ^{137}Cs 分析値の t 検定結果は、P（両側検定）>0.05 であることから平均値の差に有意差は見られない。従って、分析の品質管理が適正に行われていると判断している。結果として、アトックスが分析を請負って以降も分析の質におい

て変化はなく、気象研究所の分析データの信頼性について、大きく変わることは無かった。
今後もこのような分析データの品質管理を継続し、安全・安心の確保に貢献していきたい。

[参考文献]

[1] 五十嵐康人,広瀬勝己,「放射性降下物標準試料の調整を通じた ^{90}Sr、^{137}Cs、プルトニウムなどの人工放射性核種分析の相互比較と参照値の決定」、放射化分析研究会,17,39-42 (2004)

[2] M. Otsuji-Hatori, Y. Igarashi & K. Hirose, Preparation of Reference Fallout Material for Activity Measurements, J. Environ. Radioactivity, 31, 143-155 (1996)

analytical chemistry

Letter

pubs.acs.org/ac

Detection of Uranium and Chemical State Analysis of Individual Radioactive Microparticles Emitted from the Fukushima Nuclear Accident Using Multiple Synchrotron Radiation X-ray Analyses

Yoshinari Abe,*[,†] Yushin Iizawa,[†] Yasuko Terada,[‡] Kouji Adachi,[§] Yasuhito Igarashi,[§] and Izumi Nakai*[,†]

[†]Department of Applied Chemistry, Faculty of Science, Tokyo University of Science, 1-3 Kagurazaka, Shinjuku, Tokyo 162-8601, Japan

[‡]Japan Synchrotron Radiation Research Institute (JASRI), SPring-8, 1-1-1 Kouto, Sayo-cho, Sayo-gun, Hyogo 679-5148, Japan

[§]Meteorological Research Institute, 1-1 Nagamine, Tsukuba, Ibaraki 305-0052, Japan

Supporting Information

ABSTRACT: Synchrotron radiation (SR) X-ray microbeam analyses revealed the detailed chemical nature of radioactive aerosol microparticles emitted during the Fukushima Daiichi Nuclear Power Plant (FDNPP) accident, resulting in better understanding of what occurred in the plant during the early stages of the accident. Three spherical microparticles (~2 μm, diameter) containing radioactive Cs were found in aerosol samples collected on March 14th and 15th, 2011, in Tsukuba, 172 km southwest of the FDNPP. SR-μ-X-ray fluorescence analysis detected the following 10 heavy elements in all three particles: Fe, Zn, Rb, Zr, Mo, Sn, Sb, Te, Cs, and Ba. In addition, U was found for the first time in two of the particles, further confirmed by U L−edge X-ray absorption near-edge structure (XANES) spectra, implying that U fuel and its fission products were contained in these particles along with radioactive Cs. These results strongly suggest that the FDNPP was damaged sufficiently to emit U fuel and fission products outside the containment vessel as aerosol particles. SR-μ-XANES spectra of Fe, Zn, Mo, and Sn K−edges for the individual particles revealed that they were present at high oxidation states, i.e., Fe^{3+}, Zn^{2+}, Mo^{6+}, and Sn^{4+} in the glass matrix, confirmed by SR-μ-X-ray diffraction analysis. These radioactive materials in a glassy state may remain in the environment longer than those emitted as water-soluble radioactive Cs aerosol particles.

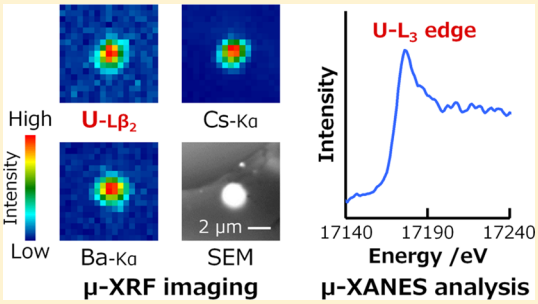

The Fukushima Daiichi Nuclear Power Plant (FDNPP) accident is the largest nuclear incident since the 1986 Chernobyl disaster and has been rated at the maximum level of 7 on the International Nuclear Event Scale.[1] Large amounts of radioactive materials were released into the environment during the accident.[2−4] Although more than 3 years have passed since the accident, the radioactive materials emitted from the FDNPP have been detectable in the environment. However, little is known about the physical and chemical natures of radioactive materials released during the early stages of the accident.[5−7]

Adachi et al.[5] found spherical microparticles containing radioactive Cs in aerosol samples collected on March 14th and 15th, 2011, in Tsukuba, 172 km southwest of the FDNPP and about 60 km northeast of central Tokyo. They revealed that these microparticles consisted of Fe, Zn, and Cs and were insoluble in water. Additionally, they calculated deposition area of these particles based on the size and hygroscopicity of the particles and concluded that these particles mainly fell to the ground through dry deposition. Such knowledge of the radioactive materials from the accident is important to understand potential environmental and human health impacts, an assessment of the accident sequence, and methods for decontamination of the radioactive pollution.

In this study, we conducted a more detailed study of the nature of the Cs-bearing radioactive aerosol microparticles by means of advanced analytical techniques using a synchrotron radiation (SR)-X-ray microbeam. In the previous study,[5] a scanning electron microscope (SEM) with an energy dispersive X-ray spectrometer (EDS) was used for chemical characterization of the particles. In this study, X-ray fluorescence (XRF) analysis using a high-energy SR-X-ray microbeam, which is much more sensitive to heavy elements than SEM-EDS analysis, was introduced to carry out nondestructive identification and qualitative detection of trace amounts of heavy elements in individual microparticles. Although chemical analyses such as a laser ablation-inductively coupled plasma mass spectrometry (LA-ICPMS) may have a better sensitivity than SR-XRF, it is difficult to analyze single microparticle sample. Moreover, chemical state and crystal structure information could not be obtained with LA-ICPMS.

To evaluate the conditions under which these particles were formed, chemical state analysis of the transition elements in the

Received: May 17, 2014
Accepted: August 1, 2014
Published: August 1, 2014

dx.doi.org/10.1021/ac501998d | Anal. Chem. 2014, 86, 8521−8525

particles was carried out by applying X-ray absorption near-edge structure (XANES) analysis. X-ray diffraction (XRD) analysis was also conducted to reveal the crystal structures of the particles. Brilliant X-rays from an advanced SR light source at SPring-8 enabled us to use a combination of these three analytical techniques. The SR-X-ray microbeam was particularly suitable to obtain detailed information from individual microparticles.[8,9] This study aims to apply these analytical techniques to the Cs-bearing microparticles from the FDNPP accident and to reveal their nature to further understand the accident as well as their effects on the environment and human health.

EXPERIMENTAL SECTION

Sample Collection. From March 14th at 21:10 to March 15th at 9:10 (JST), aerosol particles containing radioactive materials were collected at the Meteorological Research Institute (Tsukuba, Japan; 36.05° N, 140.13° E) using a high-volume aerosol sampler (HV-1000F, 1000 m^3/24 h; Sibata Scientific Technology Ltd.) on a quartz fiber filter (QR100; Advantec). The detailed sampling procedures were described elsewhere.[5] An imaging plate (IP; GE Measurement and Control, CR×25P computed radiography scanner) and micromanipulator (AP-xy-01; Micro Support Corp.) were used to detect and separate the radioactive particles from the filter. Approximately 100 small dots, each of which suggests the presence of radioactive material, appeared on the IP image of the filter (Figure 1a). In the previous study,[5] the particle number concentration was estimated to be around 10 radioactive particles/m^3. Three radioactive particles, designated particles A, B, and C, were sampled from the filter and placed on glass substrates. Particles A and C in this study are the same as the particle nos. 3 and 2, respectively, in the previous study.[5] They were subjected to the SEM-EDS analysis and gamma-ray spectrometry (see details of the measurements in the Supporting Information). After these analyses, the radioactive particles on the carbon tape fragment were removed and placed on a flat Kapton tape with a plastic holder for the SR X-ray analyses.

Synchrotron Radiation X-ray Analyses. The SR experiments were carried out at the BL37XU,[8,9] a hard X-ray undulator beamline at SPring-8, at Japan Synchrotron Radiation Research Institute (JASRI). We used two beamtimes: beamtime A for measurements with a high-energy X-ray beam (17.1−37.5 keV) and beamtime B for those with a low-energy X-ray beam (7.0−15.0 keV). The sample was placed on an automatic *XY* stage. Monochromatic X-rays were obtained with a Si(111) double crystal monochromator, and the X-ray microbeam was produced by focusing Kirkpatrick−Baez mirrors. The area of the X-ray microbeam in beamtime A was 1.0 μm (V) × 1.2 μm (H), while that of beamtime B was 0.6 μm (V) × 0.8 μm (H). Using these X-ray microbeams, we applied three X-ray analytical techniques, SR-μ-XRF, SR-μ-XANES, and SR-μ-XRD. The intensity of the incident X-ray (I_0 intensity) was continuously monitored using an ionization chamber located before the focusing mirror. The SR-μ-XRF analysis, including two-dimensional imaging analysis, was carried out using 37.5 keV X-rays and a Si (Li) detector in beamtime A. The SR-μ-XRF spectrum was measured for 1 000 s in live time per sample. The intensity of each spectrum was normalized to that of the Thomson scattering peak. To visualize the distributions of the elements in each particle, SR-μ-XRF imaging analysis of the particle was conducted with a step size of 0.5 μm (V) × 0.5 μm (H) with an integration time of 4.0 s/point. The XRF intensities for each measured point were normalized to the I_0 intensity.

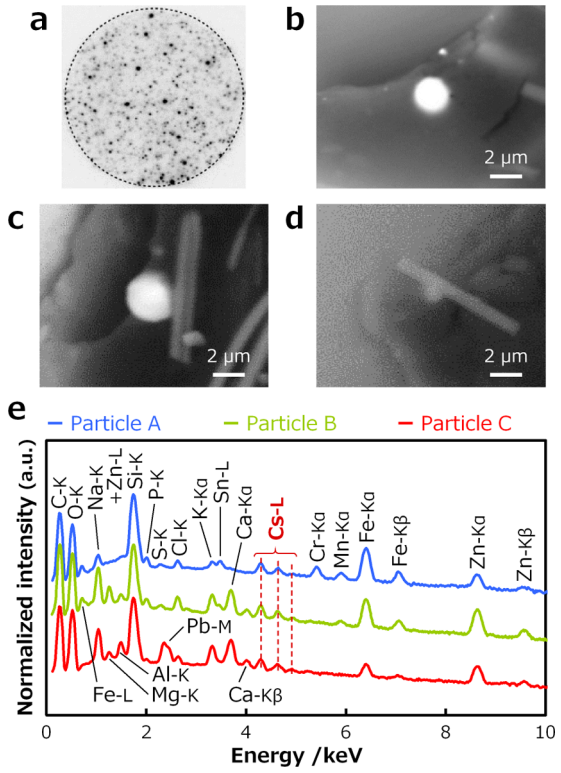

Figure 1. Characterization of radioactive aerosol particles prior to SR experiments. (a) IP autoradiography of the aerosol filter collected in Tsukuba after the FDNPP accident.[5] Black dots indicate the presence of radioactive materials. (b−d) SEM images of (b) particle A (2.0 μm diameter), (c) particle B (2.8 μm diameter), and (d) particle C (1.4 μm diameter). (e) Comparison of the EDS spectra of the three particles. The intensity of each spectrum is displayed on a logarithmic scale and shifted in a longitudinal direction. A rodlike extraneous fouling over particle C (d) is a fragment of quartz fiber filter attached to the carbon tape.

The SR-μ-XANES spectra of the particles and the reference samples were measured in fluorescence mode for the following absorption edges: the Fe−K edge (7 111 eV), Zn−K edge (9 661 eV), U−L_3 edge (17 171 eV), Mo−K edge (20 000 eV), and Sn−K edge (29 200 eV). The absorption edge energies used were based on experimental values in Deslattes et al.[10]

In the SR-μ-XRD analysis, the X-ray diffraction patterns of the samples were measured with a Debye−Scherrer optical system using a two-dimensional detector (CMOS flat panel) placed 200 mm behind the sample in beamtime B. Si powder (NIST SRM640c) was also measured as a reference material. The energy of the incident X-ray was set to 15.0 keV with an exposure time of 440 ms and an integration of 100 times/sample. Details of the SR measurements are given in the Supporting Information.

RESULTS AND DISCUSSION

Scanning Electron Microscope and Gamma-Ray Spectra Analyses of Radioactive Aerosol Microparticles. Figure 1b−d shows SEM images of the three microparticles analyzed in the SR experiments. They are spherical with diameters of ∼2 μm. EDS spectra of the three particles are shown in Figure 1e. There were no apparent differences among

dx.doi.org/10.1021/ac501998d | Anal. Chem. 2014, 86, 8521−8525

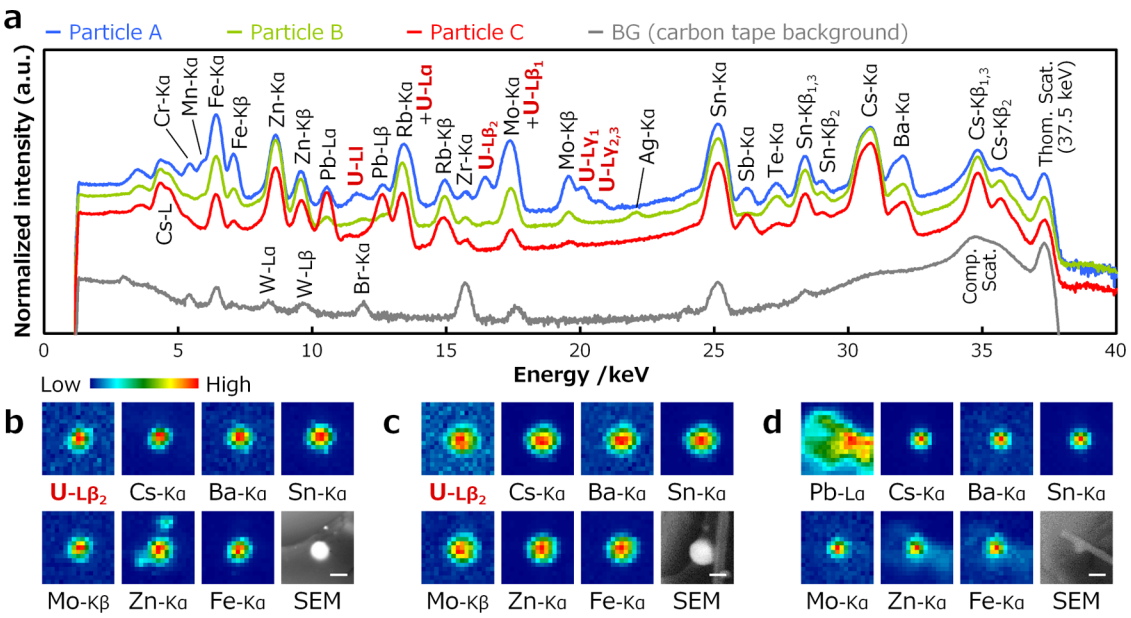

Figure 2. Results of SR-μ-XRF analyses. (a) Comparison of the SR-μ-XRF spectra obtained for particles A, B, and C and the carbon tape background. The intensity of each spectrum was displayed on a logarithmic scale and shifted in a longitudinal direction. (b–d) Distributions of representative elements extracted from the SR-μ-XRF images of (b) particle A, (c) particle B, and (d) particle C with enlarged SEM image corresponding to the imaging area (scale bar: 2 μm).

the three spectra, consistent with the previous results[5] indicating that their major components were Fe, Zn, and Cs. Some of the peaks for light elements (e.g., Si and Ca) may have originated from both the glass substrate and the particle itself. Gamma-ray spectra of the three particles detected both ^{134}Cs and ^{137}Cs in each particle with activity ratios of ~1 (decay corrected as of March 2011). The decay-corrected activities for ^{134}Cs and ^{137}Cs were 1.20 (±0.05) Bq and 1.29 (±0.02) Bq for particle A, 1.49 (±0.06) Bq and 1.49 (±0.03) Bq for particle B, and 1.07 (±0.05) Bq and 1.10 (±0.02) Bq for particle C, respectively. In the previous study,[5] it is pointed out that the activity ratios between ^{134}Cs and ^{137}Cs of the radioactive materials released by the FDNPP accident were ~1. It is thus confirmed that these three particles are radioactive ones derived from the FDNPP accident.[5]

Detailed Chemical Composition Analysis. The SR-μ-XRF spectra of the three particles and the carbon tape background are shown in Figure 2a. In addition to Fe, Zn, and Cs, all of which were previously reported,[5] the following eight heavy elements were detected in all three particles: Rb, Zr, Mo, Sn, Sb, Te, Ba, and Pb. Several unique elements were also detected from specific particles, i.e., Mn and Cr in particle A and Ag in particle B.

In addition to these elements, U–L lines in the SR-μ-XRF spectra appeared in particles A and B. To address potential interferences from elemental contamination such as W, which could be due to contamination from the micromanipulator needles during the particle separation procedure, we used SR-μ-XRF imaging analysis and visualized the elemental distributions within each particle. Figure 2b–d shows the distributions of selected elements from the SR-μ-XRF imaging of the three particles with enlarged SEM images corresponding to the imaging area (additional SR-μ-XRF images are shown in Figure S1 in Supporting Information). In particles A and B, the two-dimensional distributions of characteristic elements, including U corresponded well to the particle shapes in the SEM images and the Cs distributions identified by the SEM-EDS analysis.

In these images, we found homogeneous distributions of most elements in the particles except that of Pb in particle C (Figure 2d). Although strong peaks for Pb–L lines were detected in the spectrum of particle C, the Pb distribution was distinctly different from those of the other elements and the SEM image of the particle, indicating that the Pb did not originate from the particle components.

Verification of the Presence of Uranium. In order to obtain additional evidence for the presence of U in the microparticles, we conducted U–L_3 edge SR-μ-XANES analysis (Figure 3a). While no absorption edge for U was observed for particle C, clear edge jumps were observed for both particles A and B at the energy of the U–L_3 edge, confirming the presence of U within the aerosol microparticles in the environment. This result implies that elements other than radioactive Cs were emitted along with Cs from the reactor into the atmosphere.

Chemical State and Crystal Structure. SR-μ-XANES spectra of the Fe, Mo, and Sn K–edges for these three particles are shown in Figure 3b–d (see Figure S2 in Supporting Information for Zn K–edge). Peak positions and the shapes of the pre-edges between the particles and the reference materials agreed well, indicating that these elements occurred as Fe^{3+}, Mo^{6+}, Sn^{4+}, and Zn^{2+}. In addition, features of the SR-μ-XANES spectra of the three particles corresponded to those of the glass references.

SR-μ-XRD patterns of the three particles and Si powder as a reference material (see Figure S3 in Supporting Information) showed that the particles had no diffraction peak while the Si powder showed clear Debye–Scherrer rings. This result suggests that the particles are amorphous, glassy materials. These observations together with their spherule shapes implied that they experienced melting at a high temperature and rapid cooling as aerosol under oxidative conditions.

Relevant Element Sources around the Reactors. We explored the possible sources of the 14 elements (Cr, Mn, Fe, Zn, Rb, Zr, Mo, Ag, Sn, Sb, Te, Cs, Ba, and U) found within the microparticles by the SR-μ-XRF analysis. The reactors of the

dx.doi.org/10.1021/ac501998d | Anal. Chem. 2014, 86, 8521–8525

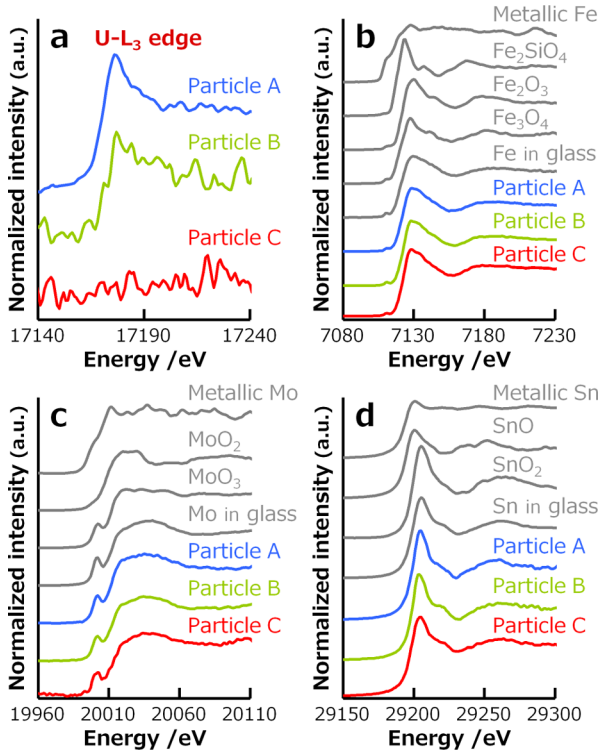

Figure 3. Results of SR-μ-XANES analyses. (a) Comparison of the U−L_3 edge SR-μ-XANES spectra of the three radioactive particles demonstrating the presence of U in particles A and B. (b−d) Comparisons of the (b) Fe−K edge, (c) Mo−K edge, and (d) Sn−K edge SR-μ-XANES spectra of the three particles and the reference materials.

FDNPP (see Figure S4 in Supporting Information) were boiling-water reactors (BWR),[11] and the fission fuels composed of U (only no. 3 reactor used mixed oxide fuel[11]). As a result of the nuclear fission reaction of U, the fission products (FPs) could yield 9 elements (Rb, Zr, Mo, Ag, Sn, Sb, Te, Cs, and Ba)[11−13] found in the particles. Zr−Sn alloy was used for fuel cladding within the reactors.[14] Stainless steel, which commonly consists of Fe, Cr, and Mn, was used in the structure of the vessel. Zn had been added to the primary cooling water in the FDNPP[15] for corrosion control to reduce ^{60}Co. On the other hand, given the possibility of a molten core as a result of the nuclear meltdown may react with a concrete base as suggested by the presence of Si in the particles, it should be noted that a percentage of some elements (e.g., Rb and Zn) may be originated from components of the concrete. Because of the lack of the access to the damaged reactors, we do not have direct evidence to identify the source of these elements. However, we conclude that U fuel, FPs, and components of the reactors are very likely the sources of the elements identified within the three radioactive microparticles, although further investigation will be needed to confirm their sources. We assume that, because these elements could have originated from multiple sources, they were melted together during the accident and eventually formed spherical microparticles.

Environmental Impacts of the Microparticles. If our hypothesis that some heavy elements in the particles were produced by nuclear fission reactions is correct, these particles likely contained additional short-lived radionuclides when they were released during the accident.[11,12] Thus, the specific activity of these particles at the time of release may have been several times higher than that presently associated with the radioactive Cs. In addition to the previous report that these particles are insoluble in water,[5] our study revealed that they are glassy materials with highly oxidized states. These characteristics suggest that they could have a relatively long-term impact on the environment, i.e., continued release of soluble radioactive Cs into the environment as these insoluble glassy particles degrade. Similar radioactive particles have been detected in soils, plants, and mushrooms collected from the area surrounding the FDNPP as shown by IP autoradiography.[7] Although there is no chemical and size information for the particles reported in other studies, it is probable that some radioactive particles found in these previous studies are the same as the microparticles characterized in our study.

CONCLUSIONS

The present study has provided better understanding the accident based on chemical information recorded in individual 2-μm radioactive Cs-bearing particles emitted from the FDNPP accident using an SR-X-ray microbeam. The SR-μ-XRF analyses directly identified U and heavy elements, that may originate from the fuel, FPs and materials used in the FDNPP, contained in the aerosol particles together with radioactive Cs, although isotope ratios should be identified to conclude their exact sources. The SR-μ-XANES and XRD analyses showed that these particles were highly oxidized glassy materials. Clarifying the nature of these microparticles assists in understanding what occurred in the reactors during the early stages of the accident. Simulation of distribution and deposition of the radioactive materials depends on physical and chemical natures of materials of interest, and our results could improve models simulating how radioactive materials were formed and were distributed from the reactors into the environment during the accident. Further quantitative investigations of the chemical nature of the radioactive particles including quantification and chemical state analysis of U and FPs in the particles will be important to understand further mechanisms of particle formation and emissions, as well as their potential human health and environmental impacts.

ASSOCIATED CONTENT

Supporting Information

Additional material as described in the text. This material is available free of charge via the Internet at http://pubs.acs.org.

AUTHOR INFORMATION

Corresponding Authors

*E-mail: y.abe@rs.tus.ac.jp.
*E-mail: inakai@rs.kagu.tus.ac.jp.

Notes

The authors declare no competing financial interest.

ACKNOWLEDGMENTS

This work was supported by MEXT/JSPS KAKENHI Grants (Grant-in-Aid for Scientific Research on Innovative Areas under the A01-02 research teams and publicly offered research on the Interdisciplinary Study on Environmental Transfer of Radionuclides from the Fukushima Daiichi NPP Accident; Grant Numbers 24110003 and 25110510, respectively). The synchrotron radiation experiments were performed with the approval of the SPring-8 Program Advisory Committee (Proposal Numbers 2013A1392 and 2013B1309).

REFERENCES

(1) INES. *The International Nuclear and Radiological Event Scale User's Manual*; International Atomic Energy Agency: Vienna, Austria, 2008.
(2) Yoshida, N.; Kanda, J. *Science* **2012**, *336* (6085), 1115−1116.
(3) MEXT. Japanese Ministry of Education, Culture, Sports, Science and Technology. http://www.mext.go.jp/english, accessed on May 16, 2014.
(4) Anzai, K.; Ban, N.; Ozawa, T.; Tokonami, S. *J. Clin. Biochem. Nutr.* **2012**, *50* (1), 2−8.
(5) Adachi, K.; Kajino, M.; Zaizen, Y.; Igarashi, Y. *Sci. Rep.* **2013**, *3*, No. 2554.
(6) Shinonaga, T.; Steier, P.; Lagos, M.; Ohkura, T. *Environ. Sci. Technol.* **2014**, *48*, 3808−3814.
(7) Niimura, N.; Kikuchi, K.; Tuyen, N. D.; Komatsuzaki, M.; Motohashi, Y. *J. Environ. Radioact.* **2014**, DOI: 10.1016/j.jenvrad.2013.12.020.
(8) Terada, Y.; Goto, S.; Takimoto, N.; Takeshita, K.; Yamazaki, H.; Shimizu, Y.; Takahashi, S.; Ohashi, H.; Furukawa, Y.; Matsushita, T.; Ohata, T.; Ishizawa, Y.; Uruga, T.; Kitamura, H.; Ishikawa, T.; Hayakawa, S. *AIP Conf. Proc.* **2004**, *705*, 376−379.
(9) Terada, Y.; Yumoto, H.; Takeuchi, A.; Suzuki, Y.; Yamauchi, K.; Uruga, T. *Nucl. Instrum. Meth. Phys. Res. A* **2010**, *616* (2−3), 270−272.
(10) Deslattes, R. D.; Kessler, E. G., Jr.; Indelicato, P.; de Billy, L.; Lindroth, E.; Anton, J. *Rev. Mod. Phys.* **2003**, *75* (1), 35−99.
(11) Burns, P. T.; Ewing, R. C.; Navrotsky, A. *Science* **2012**, *335* (6073), 1184−1188.
(12) Yamamoto, T. *J. Nucl. Sci. Technol.* **2012**, *49* (12), 1116−1133.
(13) Crouch, E. A. C. *At. Data Nucl. Data Tables* **1977**, *19* (5), 417−532.
(14) Zinkle, S. J.; Was, G. S. *Acta Mater.* **2013**, *61* (3), 735−758.
(15) Hori, S.; Suzuki, A. TEPCO's Challenges for Occupational Exposure Reduction—installation of Additional CF in Fukushima Daiichi NPP. Presented at the *ISOE International ALARA Symposium*, Aomori, Japan, September 8−9, 2009.

SCIENTIFIC REPORTS

OPEN

SUBJECT AREAS:
ENVIRONMENTAL SCIENCES
ENVIRONMENTAL MONITORING
ATMOSPHERIC CHEMISTRY
GEOCHEMISTRY

Received
12 June 2013

Accepted
15 August 2013

Published
30 August 2013

Correspondence and requests for materials should be addressed to K.A. (adachik@mri-jma.go.jp)

Emission of spherical cesium-bearing particles from an early stage of the Fukushima nuclear accident

Kouji Adachi, Mizuo Kajino, Yuji Zaizen & Yasuhito Igarashi

Meteorological Research Institute, 1-1 Nagamine, Tsukuba, Ibaraki, Japan 305-0052.

The Fukushima nuclear accident released radioactive materials into the environment over the entire Northern Hemisphere in March 2011, and the Japanese government is spending large amounts of money to clean up the contaminated residential areas and agricultural fields. However, we still do not know the exact physical and chemical properties of the radioactive materials. This study directly observed spherical Cs-bearing particles emitted during a relatively early stage (March 14–15) of the accident. In contrast to the Cs-bearing radioactive materials that are currently assumed, these particles are larger, contain Fe, Zn, and Cs, and are water insoluble. Our simulation indicates that the spherical Cs-bearing particles mainly fell onto the ground by dry deposition. The finding of the spherical Cs particles will be a key to understand the processes of the accident and to accurately evaluate the health impacts and the residence time in the environment.

An earthquake with a magnitude of 9.0 occurred in Japan on March 11, 2011. In addition to the earthquake itself, a tsunami struck along the east coast of Honshu and damaged the Fukushima Daiichi nuclear power plant (FNPP). The FNPP eventually lost its ability to cool the nuclear fuel, which caused hydrogen explosions and released radioactive materials into the environment[1,2]. Because of the local contamination, many people still cannot return home. Currently, the Japanese government is spending considerable amounts of money to clean up the contaminated residential environment and agricultural fields.

The radioactive materials released to the atmosphere traveled over the entire Northern Hemisphere[3–7]. In Europe, for example, Masson et al.[3] measured increases in radioactive cesium and iodine in the air from March 19, 2011 and showed that the maximum levels occurred between March 28 and 30. Although the accident has global impacts, we still do not know exactly what happened in the reactors during the accident, and the estimates of the radioactive Cs releases vary largely from 9 to 36 PBq[6,8–10].

The chemical and physical properties (i.e., chemical forms, particle sizes, shape, phases (gas or aerosol), water solubility, and residence time) of the radioactive materials released into the environment are not well known[11]. Such knowledge is necessary to improve the numerical models to estimate the geographical distributions and evaluate the human exposures during and after the accident. Because the mass of released radioactive material was small, i.e., the release of ^{137}Cs from the accident was $<$20 kg, and the material spread globally, it is extremely difficult to chemically detect it other than by radioactivity detectors. In this study, we chemically detected Cs within single particles for the first time by using electron microscopy and report the shape, composition, water solubility, and sizes of the particles to evaluate the implications of their formation process, occurrences in the environment, and potential health effects. This knowledge is still important for preventing further accidents, finding effective ways to remove the radioactive materials from the environment, and preventing further resuspension of the materials.

Results

Two plume events. The major radioactive material release events occurred during March 12 and 23, 2011 at the FNPP[5]. We collected aerosol samples on quartz fiber filters (25 cm $\times$ 20 cm) at the Meteorological Research Institute, Tsukuba, Japan, which is located 170 km southwest of FNPP (see the Method section). In these samples, we found two significant peaks in the radioactivity concentrations between March 14 and 15 (Plume 1) and between March 20 and 22 (Plume 2) (Fig. 1). These significant plumes in the air were also reported in eastern Japan and polluted the water and soil[2,12–15]. Meteorological conditions, such as rain and the wind direction, and the releases of radioactive materials were the main causes of the high surface deposition events[14]. We used the

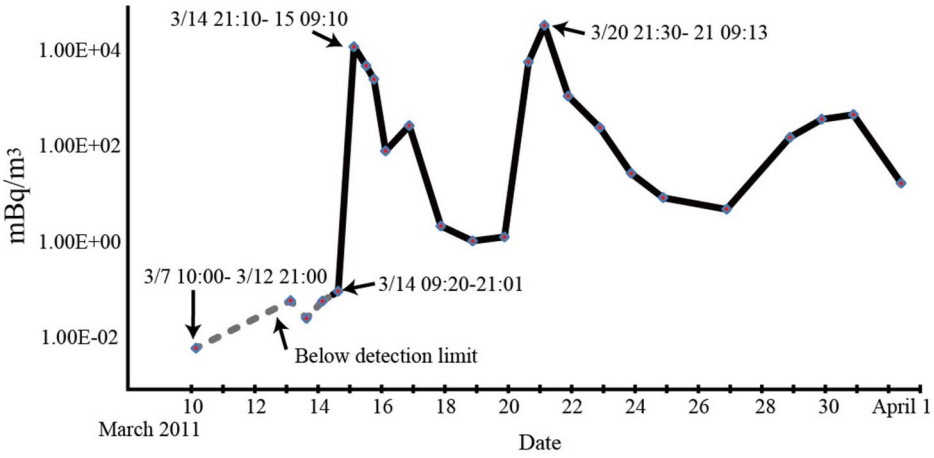

Figure 1 | The radioactivity of the aerosol particles after the Fukushima Daiichi nuclear power plant accident in Tsukuba, Japan. Red dots indicate the midpoints of each sampling period.

filters that had the maximum radioactivity levels from each plume (from March 14, 21:10 (local time) to March 15, 09:10 and from March 20, 21:30 to March 21, 09:13) and analyzed portions of these filters (~10 cm^2 per filter) using an imaging plate (IP) and a scanning electron microscope (SEM) to directly observe the radioactive materials. In addition, we measured the aerosol particle size distributions within the plumes (Figs. S1 and S2).

First plume (March 14–15). We measured the radioactive materials that were collected in the filter at ground level on March 14–15 using the IP (Fig. 2). The radioactive materials were distributed spotty, suggesting that the number of radioactive particles was relatively small but that their activity levels were relatively strong. Within this filter sample, we counted approximately 100 spots caused by radioactive materials, suggesting a concentration of approximately 10 radioactive particles per m^3. For reference, the average particle number concentration was 4.1×10^7 per m^3 for particles larger than 0.5 μm from March 15 (Fig. S1). The spotty distribution in the IP image was also observed in the rooftop filter sample from March 15 (Fig. S3).

To detect radioactive particles using SEM, it is necessary to reduce the number of non-radioactive particles on the filter. Therefore, we cut the filter into many small parts to include the radioactive spots features (Fig. S4). We then measured the radioactivity of each segment using IP and/or a Ge detector to chase the radioactive particle. After reducing the particle numbers in the segments from the three radioactive spots, we used the SEM and found three radioactive Cs-bearing particles.

In Figure 3, we show a particle containing Cs (Cs Particle 1). The particle is spherical with a diameter of 2.6 μm. The energy dispersive X-ray spectrometer (EDS) spectrum shows Cs peaks. The Cs distribution in the elemental mapping image indicates that the spherical particles consist of Cs along with substantial amounts of Fe and Zn and minor amounts of Cl, Mn, and O. The decay-corrected activity (as of March 2011) of Cs Particle 1 is 3.27 ± 0.04 and 3.31 ± 0.06 Bq for ^{137}Cs and ^{134}Cs, respectively

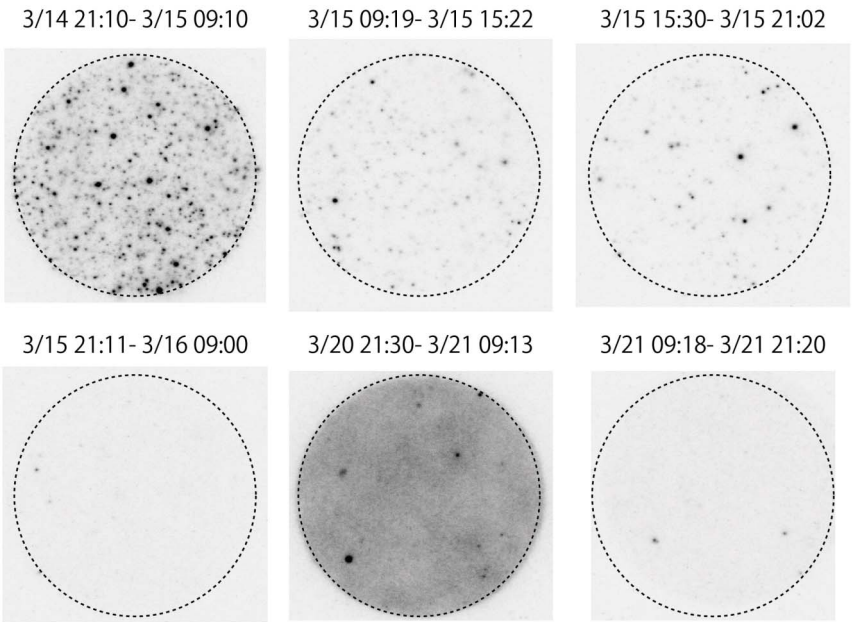

Figure 2 | The distribution of radioactive materials on the filter samples measured with the IP. Black dots indicate the presence of radioactive materials. The outer rims (dotted line) of the filters were added artificially. This study focused on the filter samples from March 14, 21:10 to March 15, 09:10 (upper left), and from March 20, 21:30 to March 21, 09:13 (bottom center).

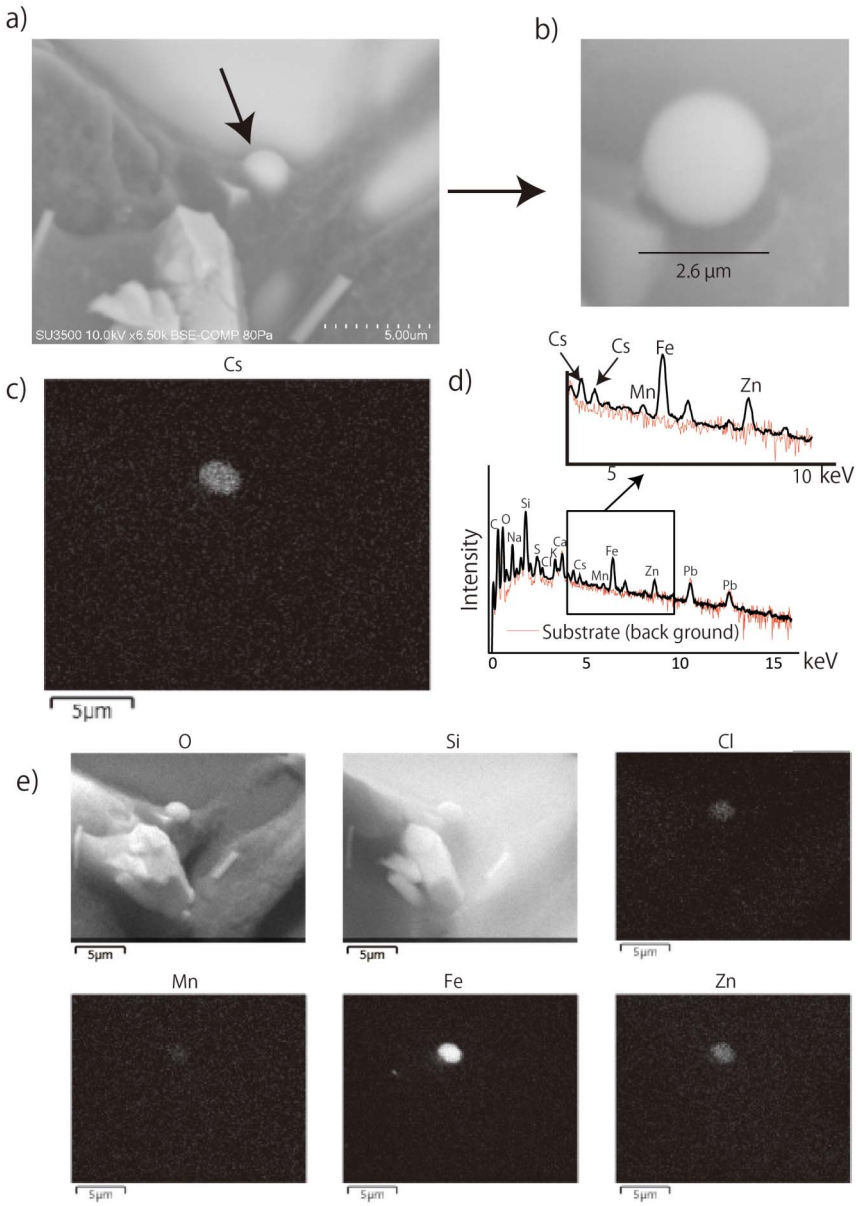

Figure 3 | SEM and EDS mapping images of a radioactive Cs-bearing particle from the sample collected during March 14, 21:10 and March 15, 09:10. (a) A Cs-bearing particle partially embedded within a carbon paste. (b) The same Cs-bearing particle as a) but measured the next day. The particle shows a spherical shape. (c) An elemental mapping (Cs) of the particle (a). (d) The EDS spectrum of the particle a) (black line). The red line shows the spectrum from the glass substrate. The Cs in the particle shows multiple peaks. (e) An elemental mapping of the other elements within the area. O, Si, Cl, Mn, Fe, and Zn are possibly coexistent with Cs within the particle.

(Fig. S5). Assuming a particle density of 2.0 g/cm^3, the Cs mass percentage within the particle is estimated from its activity (Bq) to be 5.5. Another Cs-bearing particles (Cs particles 2 and 3) from the same filter but different spots are similar to Cs Particle 1, although they have weaker activity (Fig. S6). The particles consist of Fe, Zn, and Cs and are approximately 2.0 μm in diameter. The radioactivity for Cs particle 2 is 0.66 ± 0.02 and 0.78 ± 0.04 Bq for ^{137}Cs and ^{134}Cs, respectively. The Cs mass percentage within Particle 2 is estimated from its activity to be 2.5. Assuming that the entire the radioactivity in the Plume 1 was from the Cs-bearing spherical particles gives an average of 1.4 Bq per particle, which is comparable to that of Particle 2.

We analyzed the water solubility of Cs Particle 1 by comparing the particle's shape before and after exposure to water (Fig. S7). The results show that there was no change in shape, suggesting that the particle was insoluble to water at least during atmospheric transportation.

Second plume (March 20–21). The IP image of the filter collected on March 20–21 indicates that the radioactive materials are evenly distributed within the filter with approximately 10 diffused spots (Fig. 2). We cut the filter including a diffused spot, formed several layers, and captured the IP image (Fig. S8). The radioactivity is distributed along the filter segments, a result which differs from that of Plume 1. We interpret that small amounts of the radioactive Cs attach to other dominant aerosol particles and that the occurrence is consistent with the results of Kaneyasu et al.[16] about the role of sulfate aerosols as carriers of ^{137}Cs. An SEM analysis with EDS elemental mapping shows numerous sulfate and mineral dust, as is commonly found in aerosol samples (Fig. S8). The aerosol filter

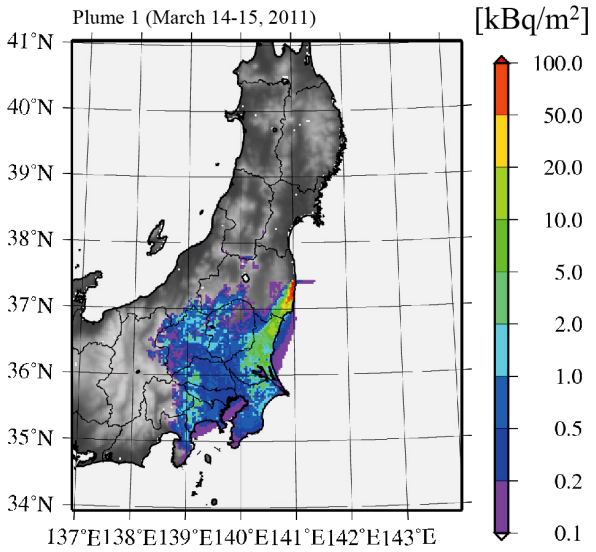

Figure 4 | The model simulation of the total deposition of the ^{137}Cs released from the FNPP in Plume 1 (between March 14, 17:00 and March 15, 02:00 (JST)). We assumed that all Cs consists of relatively large, water-insoluble particles. The Regional Air Quality Model 2 (RAQM2[17]) was used for the model calculation. We used the Generic Mapping Tools (GMT) developed at University of Hawaii to draw the figure. The model elevation in the figures was generated based on a 1 km resolution Global 30 Arc-Second Elevation (GTOPO30) of U.S. Geological Survey (USGS).

sample from the rooftop site also indicates a similar distribution of radioactive materials (Fig. S3).

Model. We simulated the depositions of the radioactive particles from Plumes 1 and 2 using a tagged chemical transport model. Unlike other simulation models (e.g.[4,6,9,12]), we considered the aerosol dynamical processes explicitly and used the measured values and assumptions of the particle physical and chemical properties from our observations, i.e., on March 14–15, radioactive Cs consisted of 2.3 μm hydrophobic particles, whereas on March 20–21, the Cs was carried by hydrophilic submicron particles (e.g., sulfate).

The tagged simulation result indicates that the aerosol particles on the filter sample from Plume 1 were mainly emitted during March 14, 17:00 to March 15, 02:00 (JST) from the FNPP. On the other hand, the aerosol particles on the filter sample from Plume 2 were mainly emitted during March 19, 20:00 and March 20, 07:00.

In Figure 4, we show simulation of the total (dry + wet) ^{137}Cs deposition. Within Plume 1, 17% and 5.1 × 10^{-3}% of the ^{137}Cs released from the FNPP fell onto the ground by dry and wet deposition processes, respectively, and the rest (83%) was deposited into the ocean or was transported out of the model domain. In contrast, the deposition ratios onto the ground for the particles within Plume 2 were 1.9% and 3.8% by dry and wet deposition, respectively.

Discussion

This study reports for the first time the presence of spherical radioactive Cs-bearing particles emitted from the FNPP during a relatively early stage (March 14–15) of the accident. The particles coexist with Fe, Zn, and possibly other elements, and their diameters are approximately 2 μm. Because these elements were evenly distributed within the particle, we conclude that they are internally mixed and form an alloy. This result differs from that reported by Kaneyasu et al.[16], who showed that the Cs measured on samples collected during April and May 2011 was carried by sulfate aerosol particles approximately 0.5 μm in size. Due to its spherical shape and composition, the particle is likely solid and is largely insoluble in water. Spherical aerosol particles, such as fly ash, commonly form from liquidized materials or during the condensation of vaporized materials depending on their sizes[17].

The spherical Cs-bearing particles were larger and less water soluble than sulfate particles, resulting in more dry deposition and less deposition in the region northwest of the FNPP (Figs. 4 and S9). If we assume that all of the Cs had been carried by the sulfate aerosol particles in Plume 1, 5.6% and 9.3% of the released ^{137}Cs should have been deposited through dry and wet deposition processes, respectively. Accordingly, the geographical distribution of Cs deposition differs depending on the physical and chemical properties (Fig. S9), although the quantitative radioactivity levels for the total deposition in the model depend on assumptions such as cloud microphysics and the total amount of emissions from the FNPP, which is still under debate. Our model results suggest that because the dry and wet deposition processes are sensitive to the chemical form and sizes of the Cs carriers, multiple numerical simulation models based on the accurate chemical and physical properties of Cs-bearing particles will be needed to reevaluate how the Cs from the early stages of the accident was deposited.

It is probable that the emission processes had changed between the emissions of Plumes 1 and 2 as the accident and water injection progressed; however, further studies will be needed to reveal the emission process during the accident.

This study aims to show the presence of spherical radioactive Cs-bearing particles to stimulate and facilitate further studies across multidisciplinary fields that will enable the proper understanding and evaluation of particle effects. We believe the finding of the Cs-bearing particles will have implications to the following studies.

1) The composition and the spherical shape of the Cs-bearing particles emitted by the FNPP accident will be a key to understand what happened in the nuclear reactors during the accident.
2) The spherical Cs-bearing particles likely have longer retention times on the land surface than those of the water-soluble Cs particles. The retention time of the particles in the soil or other environments needs to be reconsidered.
3) The health effects of the particles should be evaluated based on the particle sizes and insolubility in water.

Methods

Sampling. The samples were collected at the Meteorological Research Institute (Tsukuba, 36.05N, 140.13E) using both a high-volume aerosol sampler (Sibata Scientific Technology ltd., HV-1000F; 1000 m^3/24 h) placed on the ground and a PM2.5 aerosol sampler (24 m^3/24 h) placed on the roof of the 6-floor building (approximately 25 m from ground level). Quartz fiber filters were used in both samplers. The sampling times were 6, 12, or 24 h for the high volume air sampler and 24 h for the PM2.5 aerosol sampler. The particle size distributions were monitored using an aerosol particle sizer (APS; TSI-3321) and a scanning mobility particle sizer (SMPS; TSI-3080 and TSI-3775) on the rooftop site for particle sizes >0.5 μm and between 7 and 289 nm in diameter, respectively, with a 2.5 μm cutoff size.

Analyses. An imaging plate (IP; GE CRx25P) was used to detect the radioactivity on the filters with a pixel spatial resolution of 50 μm. An intrinsic Ge detector (SEIKO EG&G) coupled with a multi-channel analyzer was used to obtain the gamma spectra of each Cs-bearing particle and filters. A scanning electron microscope (SEM; Hitachi high-Technologies SU 3500) and an energy dispersive X-ray spectrometer (EDS; Horiba ltd. X-max 50 mm) were used to observe and analyze the shapes and compositions of the particles. The particles attached to the filter fibers were mounted within a carbon tape (Fig. S4). A manipulator (Micro Support Corp., AP-xy-01) was used to cut the carbon tape into as small segments as possible (<0.1 mm).

Model. We used the Regional Air Quality Model 2 (RAQM2[18]), which implements a triple-moment modal aerosol dynamics module assuming a log-normal size distribution of the aerosol populations. This model describes the nature of the aerosol dynamical processes, such as nucleation, condensation, coagulation, dry deposition, grid-scale cloud condensation and ice nuclei activation, and the subsequent cloud microphysical processes (rainout) and the washout processes. A non-hydrostatic meteorological model (NHM)[19] was used to produce the meteorological field. There were 215 × 259 grids with a 3 km horizontal grid resolution in both the NHM and RAQM2. There were 50 vertical layers to 50 hPa in the NHM, and 20 layers to 10 km in the RAQM2. The Japan Meteorological Agency (JMA) Meso-Regional Objective

Analysis data sets (3 h, 5 km × 5 km) were used for the initial and boundary conditions for the NHM and for the spectral nudging method. The ^{137}Cs released from the FNPP was tagged with a temporal resolution of 1 hour. We assumed 0.43 PBq (Plume 1) and 0.39 PBq (Plume 2) for the total amounts of ^{137}Cs activity released from the FNPP by using the inventory of Katata et al.[20]. We used a number equivalent geometric mean dry diameter $D_{g,n,dry} = 2.3$ μm (an averaged value of the Cs-bearing particles 1 and 2), geometric standard deviation $\sigma_g = 1.3$, particle density $\rho_p = 2.0$ g/cm^3, and hygroscopicity $\kappa = 0$ for Plume 1. For Plume 2, we used $D_{g,n,dry} = 102$ nm (measured by SMPS), $\sigma_g = 1.6$, $\rho_p = 1.83$ g/cm^3, and $\kappa = 0.4$. The calculated dry deposition velocities of the particles in Plume 1 are approximately 4–5 times greater than those of the particles in Plume 2. For the particles in Plume 2, both the rainout and washout processes were considered, whereas for particles in Plume 1, only washout was considered because no cloud condensation nuclei activity is assumed (i.e., $\kappa = 0$).

1. Yoshida, N. & Kanda, J. Tracking the Fukushima radionuclides. *Science* **336**, 1115–1116 (2012).
2. MEXT: Japanese Ministry of Education, Culture, Sports, Science and Technology, http://www.mext.go.jp/english, accessed on May, 07, 2013.
3. Masson, O. *et al.* Tracking of airborne radionuclides from the damaged Fukushima Dai-ichi nuclear reactors by European networks. *Environ Sci. Technol.* **45**, 7670–7677 (2011).
4. Takemura, T. *et al.* A numerical simulation of global transport of atmospheric particles emitted from the Fukushima Daiichi Nuclear Power Plant. *Sola* **7**, 101–104 (2011).
5. Achim, P. *et al.* Analysis of radionuclide releases from Fukushima Dai-Ichi Nuclear Power Plant accident Part II. *Pure Appl. Geophys.* 10.1007/s00024-012-0578-1 (2012).
6. Stohl, A. *et al.* Xenon-133 and caesium-137 releases into the atmosphere from the Fukushima Dai-ichi nuclear power plant: determination of the source term, atmospheric dispersion, and deposition. *Atmos. Chem. Phys.* **12**, 2313–2343 (2012).
7. Christoudias, T. & Lelieveld, J. Modelling the global atmospheric transport and deposition of radionuclides from the Fukushima Dai-ichi nuclear accident. *Atmos. Chem. Phys.* **13**, 1425–1438 (2013).
8. Chino, M. *et al.* Preliminary estimation of release amounts of ^{131}I and ^{137}Cs accidentally discharged from the Fukushima Daiichi nuclear power plant into the atmosphere. *J. Nucl. Sci. Technol.* **48**, 1129–1134 (2011).
9. Katata, G., Ota, M., Terada, H., Chino, M. & Nagai, H. Atmospheric discharge and dispersion of radionuclides during the Fukushima Dai-ichi Nuclear Power Plant accident. Part I: Source term estimation and local-scale atmospheric dispersion in early phase of the accident. *J. Environ Radioactivity* **109**, 103–113 (2011).
10. Winiarek, V., Bocquet, M., Saunier, O. & Mathieu, A. Estimation of errors in the inverse modeling of accidental release of atmospheric pollutant: Application to the reconstruction of the cesium-137 and iodine-131 source terms from the Fukushima Daiichi power plant. *J. Geophys. Res.* **117**, D05122, doi: 10.1029/2011JD016932 (2012).
11. Burns, P. C., Ewing, R. C. & Navrotsky, A. nuclear fuel in a reactor accident. *Science* **335**, 1184–1188 (2012).
12. Morino, Y., Ohara, T. & Nishizawa, M. Atmospheric behavior, deposition, and budget of radioactive materials from the Fukushima Daiichi nuclear power plant in March 2011. *Geophys. Res. Lett.* **38**, GL048689 (2011).
13. Yasunari, T. J. *et al.* Cesium-137 deposition and contamination of Japanese soils due to the Fukushima nuclear accident. *Proc. Natl. Acad. Sci. USA* **108**, 19447–19448 (2011).
14. Kinoshita, N. *et al.* Assessment of individual radionuclide distributions from the Fukushima nuclear accident covering central-east Japan. *Proc. Natl. Acad. Sci. USA* **108**, 19526–19529 (2011).
15. Doi, T. *et al.* Anthropogenic radionuclides in the atmosphere observed at Tsukuba: characteristics of the radionuclides derived from Fukushima. *J. Environ Radioactivity* **122**, 55–62 (2013).
16. Kaneyasu, N., Ohashi, H., Suzuki, F., Okuda, T. & Ikemori, F. Sulfate aerosol as a potential transport medium of radiocesium from the Fukushima nuclear accident. *Environ. Sci. Technol.* **46**, 5720–5726 (2012).
17. Damle, A. S., Ensor, D. S. & Ranade, M. B. Coal combustion aerosol formation mechanisms: A review. *Aerosol Sci. Technol.* **1**, 119–133(1981).
18. Kajino, M. *et al.* Development of the RAQM2 aerosol chemical transport model and prediction of the Northeast Asian aerosol mass, size, chemistry, and mixing type. *Atmos. Chem. Phys.* **12**, 11833–11856 (2012).
19. Saito, K. *et al.* Nonhydrostatic atmospheric models and operational development at JMA. *J. Meteorol. Soc. Jpn.* **85B**, 271–304 (2007).
20. Katata, G., Ota, M., Terada, H., Chino, M. & Nagai, H. Atmospheric discharge and dispersion of radionuclides during the Fukushima Dai-ichi Nuclear Power Plant accident. Part I: Source term estimation and local-scale atmospheric dispersion in early phase of the accident. *J. Environ Radioactivity* **109**, 103–113 (2011).

Acknowledgements

This study was supported by MEXT KAKENHI (a Grant-in-Aid for Scientific Research on Innovative Areas under the A01-01 and A01-02 research teams in the "Interdisciplinary Study on Environmental Transfer of Radionuclides from the Fukushima Daiichi NPP Accident"; grant numbers 24110002 and 24110003, respectively) and the MEXT Japanese Radioactivity Survey. We acknowledge Mr. H. Sako and Mr. T. Kimura (Atox Co. ltd.) for their help with the IP and gamma spectrometry, Ms. C. Takeda (Tokyo Nuclear Services co. ltd.), Ms. K. Inukai, and Ms. K. Kamioka for their help with the HV sampling, and Mr. Y. Iizawa (Tokyo University of Science) for his help with finding the Cs-bearing particle 3. The PM2.5 filters sampled by Mr. K. Kuchiki and Dr. T. Aoki (MRI) were courteously provided for the present analyses.

Author contributions

K.A. found the Cs-bearing particles, performed the IP and SEM analyses, and was the primary author of the manuscript; M.K. performed numerical model calculations; Y.Z. performed the SMPS and APS analyses; Y.I. performed the filter sampling and supervised the study; all authors contributed to the manuscript.

Additional information

Supplementary information accompanies this paper at http://www.nature.com/scientificreports

Competing financial interests: The authors declare no competing financial interests.

How to cite this article: Adachi, K., Kajino, M., Zaizen, Y. & Igarashi, Y. Emission of spherical cesium-bearing particles from an early stage of the Fukushima nuclear accident. *Sci. Rep.* **3**, 2554; DOI:10.1038/srep02554 (2013).

SUPPORTING INFORMATION FOR

Emission of spherical cesium-bearing particles from an early stage of the Fukushima nuclear accident

Kouji Adachi[1]*, Mizuo Kajino[1], Yuji Zaizen[1], and Yasuhito Igarashi[1]

1: Meteorological Research Institute, 1-1 Nagamine, Tsukuba, Ibaraki, Japan 305-0052

*Corresponding author: Kouji Adachi, Meteorological Research Institute, 1-1 Nagamine, Tsukuba, Ibaraki, Japan 305-0052, tel: +81-29-853-8570, adachik@mri-jma.go.jp

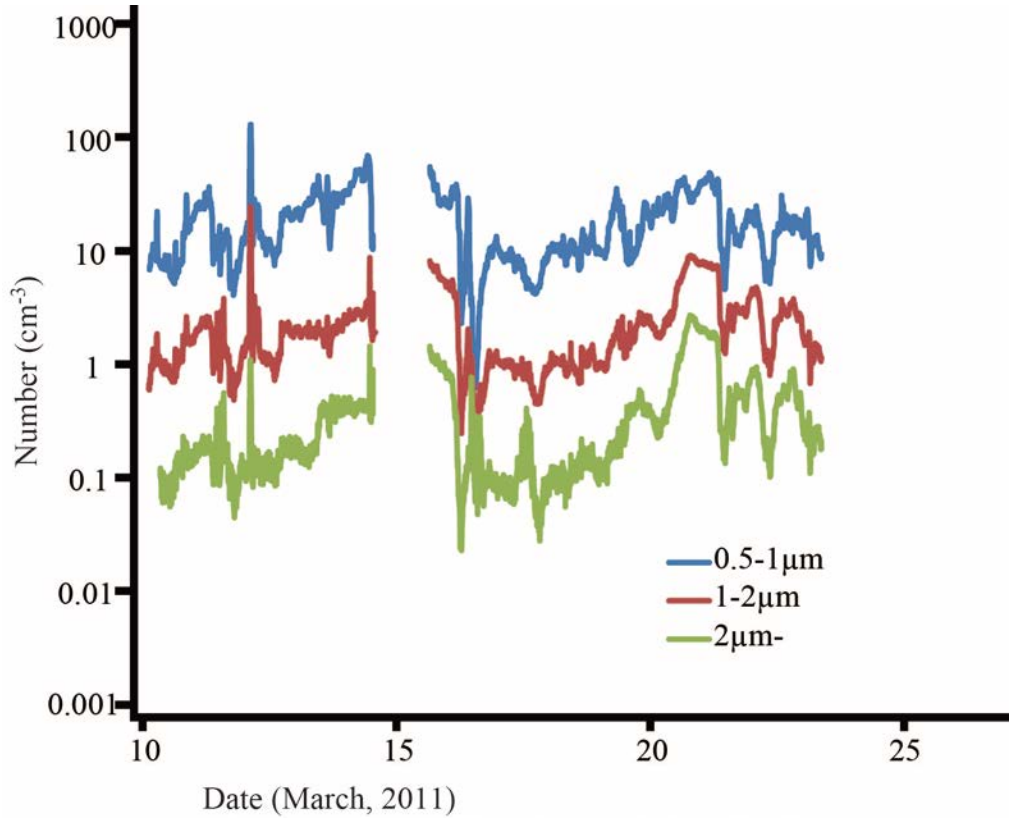

SI 1. Particle number concentrations for particles of 0.5-1.0, 1.0-2.0, and >2.0 μm. These data were measured using an aerosol particle sizer (APS). The data around March 15 were missing because of a regional unstable power supply caused by the earthquake. The APS was located on the rooftop site.

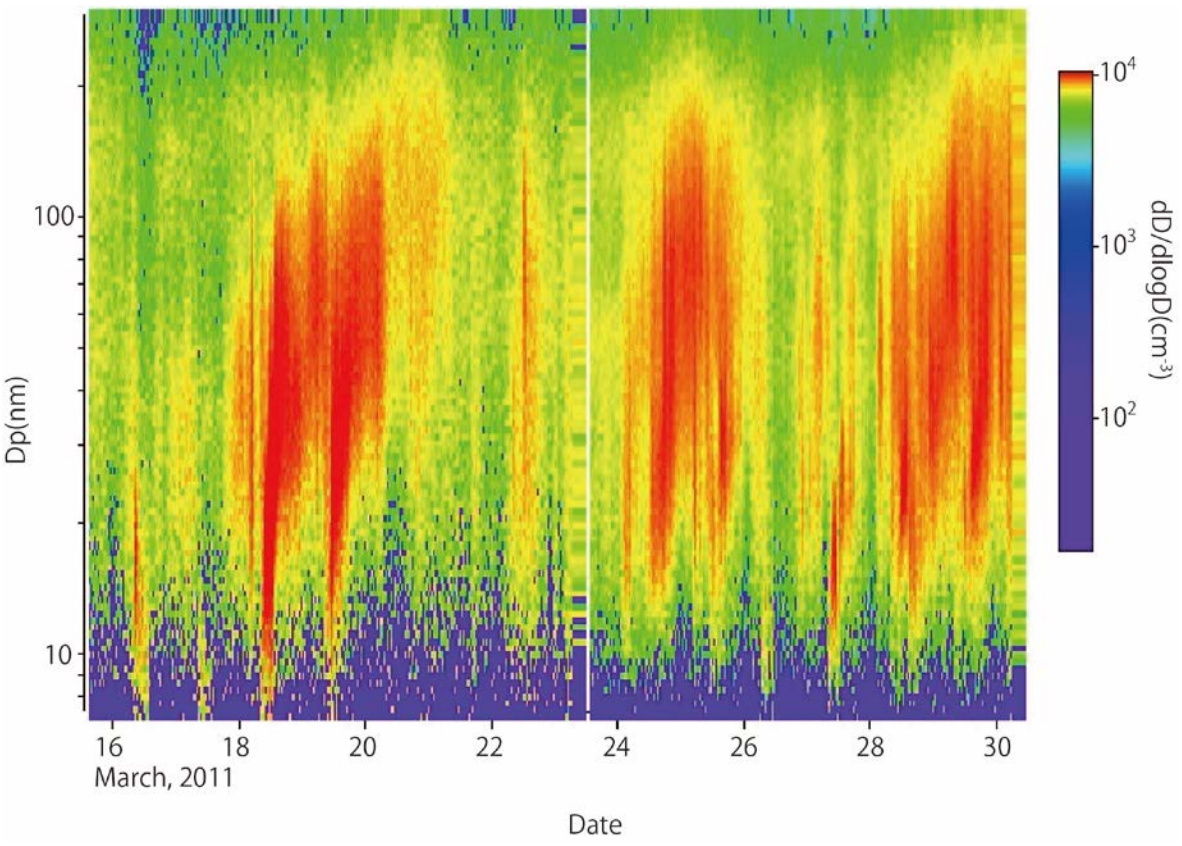

SI 2. The size distribution of aerosol particles between 7 and 289 nm using a scanning mobility particle sizer (SMPS). The averaged particle number concentration was 1.9×10^9 per m^3 during the second plume (March 20-21). The data prior to March 15, 17:18 (local time) were missing because of the emergency stop caused by the earthquake. The SMPS was located on the rooftop site.

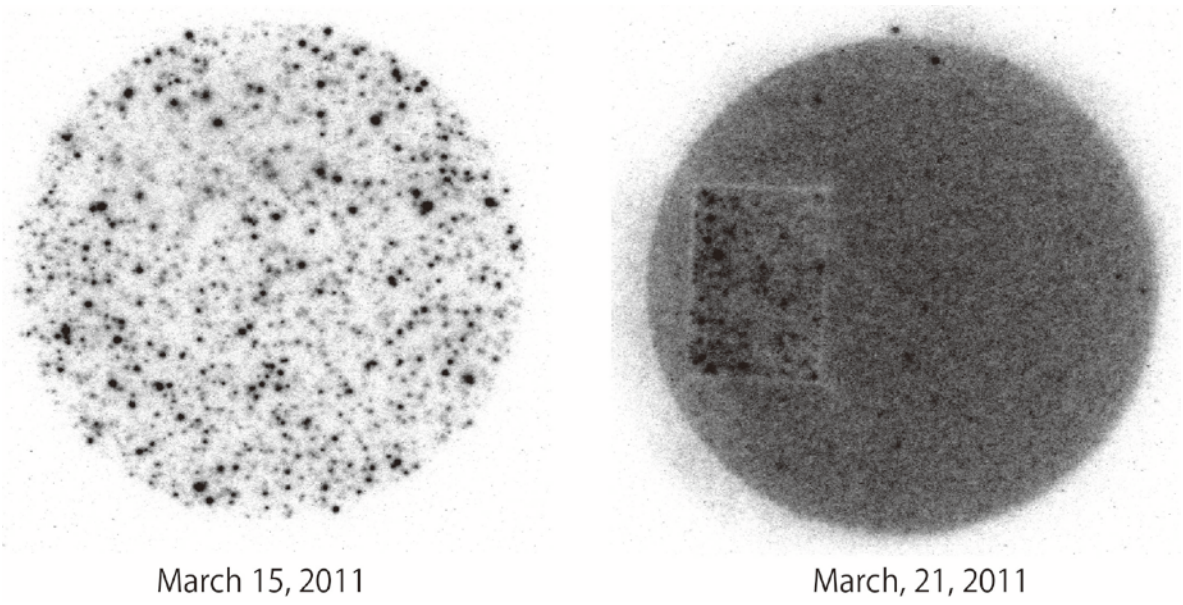

SI 3. The IP images of the PM2.5 filter samples collected on March 15 (left) and March 21 (right) on the rooftop site. The left filter includes many spots whereas the right filter appears dark all over. The features are similar to those in the Figure 2, which were collected at the ground level of the site. A part of each filter was cut for carbonaceous measurements and replaced (the trace is apparent in the right filter). A two hour exposure time was used for the IP analysis.

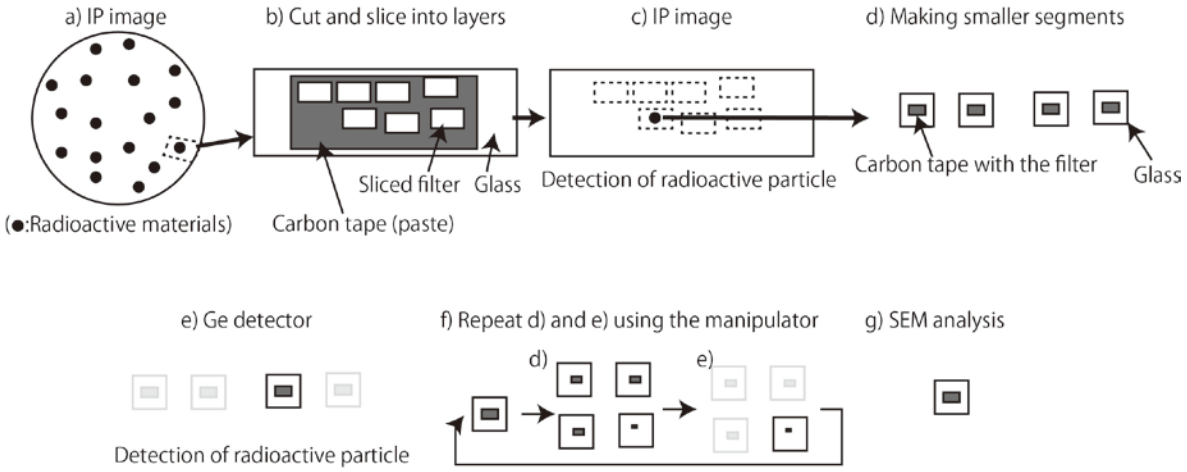

SI 4. The selection of radioactive particles for the SEM analysis. a) The IP image of the filter was captured, and a part of the filter that includes radioactive material was cut off (dotted line). b) The segment of the filter was separated into approximately 10 layers and put onto a carbon tape attached to a glass substrate. c) The IP image was taken to identify the position of the radioactive material. d) The carbon tape including the radioactive material was cut into small pieces. e) The radioactive material was detected using a Ge detector from the filter segments. f) The processes d) and e) were repeated to make the filter and the number of particles as small as possible. g) The radioactive particle embedded within carbon paste was analyzed using the SEM.

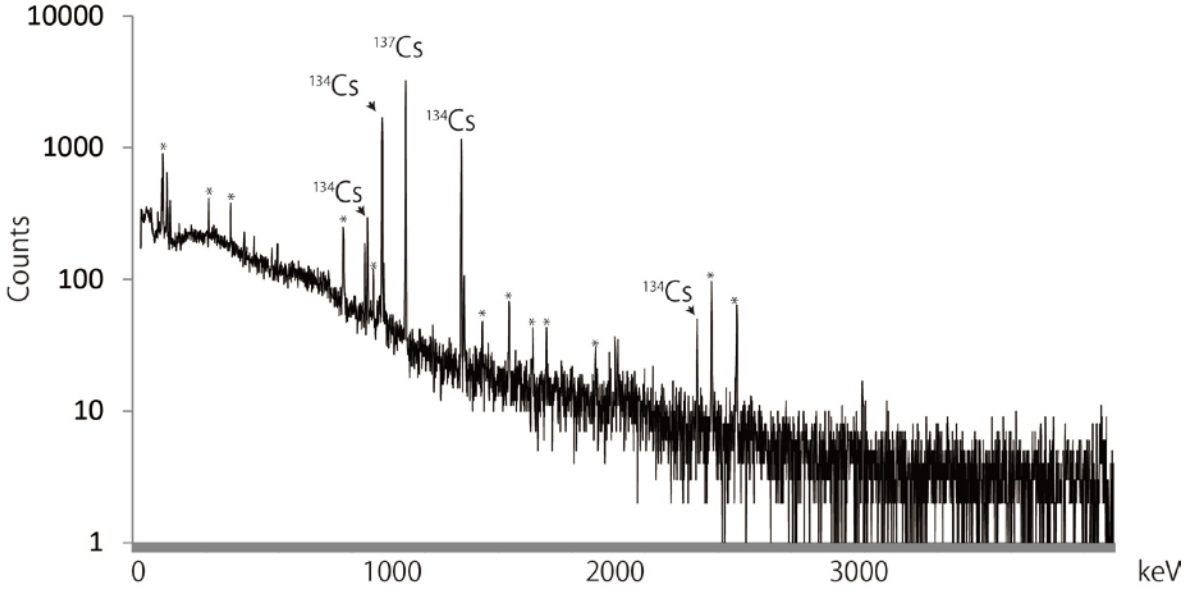

SI 5. The gamma spectrum of radioactive Cs particle 1. A 50,000 sec detection time was used. Peaks marked with * were from the background or the glass substrate. The sample was analyzed two years after the accident, and short-lived radionuclides would not have been detected even if they had been present when emitted.

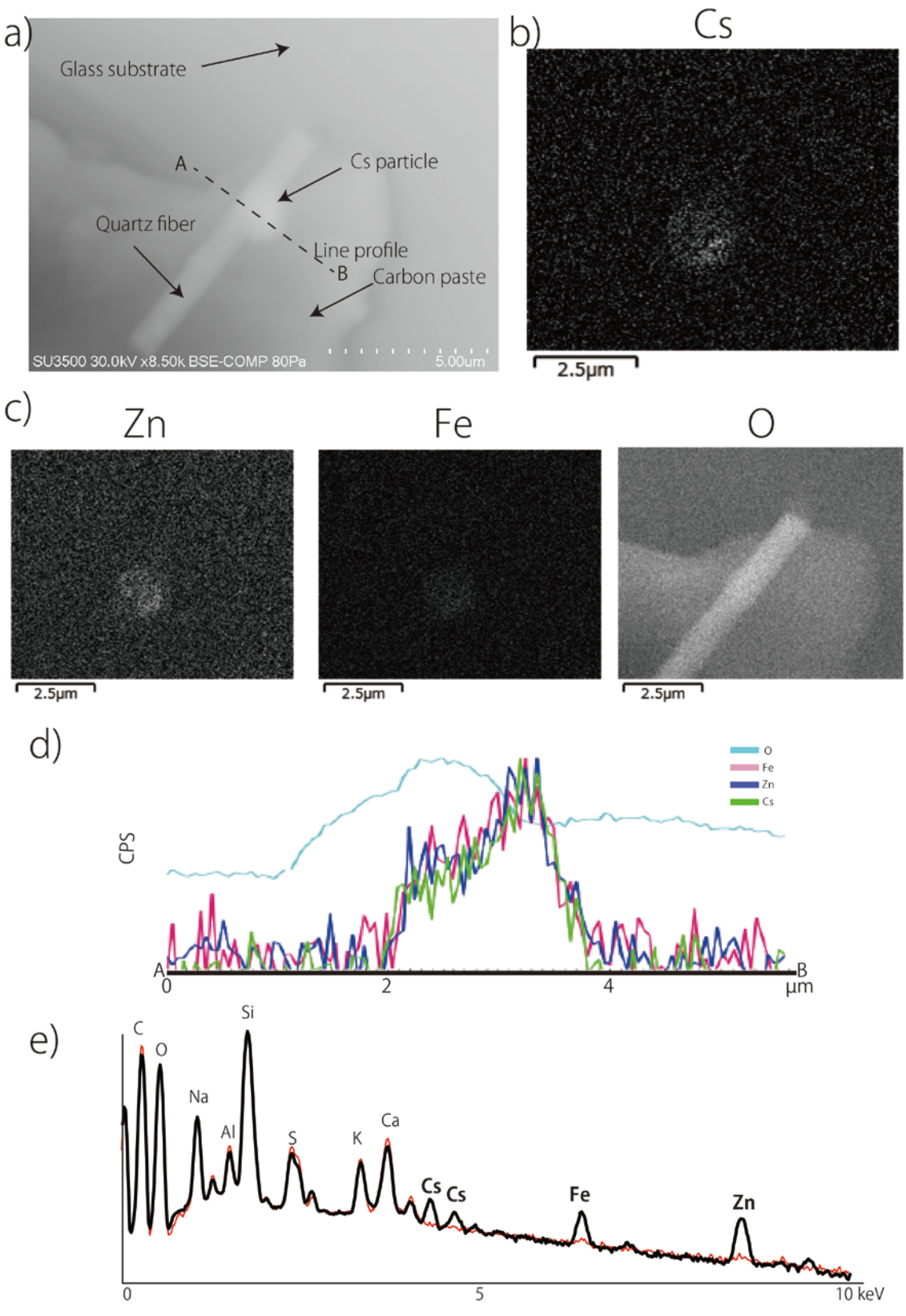
a)
Glass substrate
A
Cs particle
Quartz fiber
Line profile
B
Carbon paste
SU3500 30.0kV x8.50k BSE-COMP 80Pa
5.00um
b)
Cs
2.5µm
c)
Zn
Fe
O
2.5µm
2.5µm
2.5µm
d)
O
Fe
Zn
Cs
CPS
A
B
0
2
4
µm
e)
C
O
Na
Al
Si
S
K
Ca
Cs
Cs
Fe
Zn
0
5
10 keV

SI 6. The SEM analyses of radioactive Cs particle 2 from the March 14-15 sample. 1) An SEM image of the Cs-bearing particle. The particle was embedded within a carbon paste and was partially covered with a quartz fiber. b) The elemental mapping of Cs in the particle. c) The elemental mapping for Zn, Fe, and O in the particle. Unlike in particle 1, oxygen is not apparent. d) The line profile of the selected elements over the particle. The analyzed line is shown in a). e) The EDS spectra of the particle (black line) and glass substrate (red line).

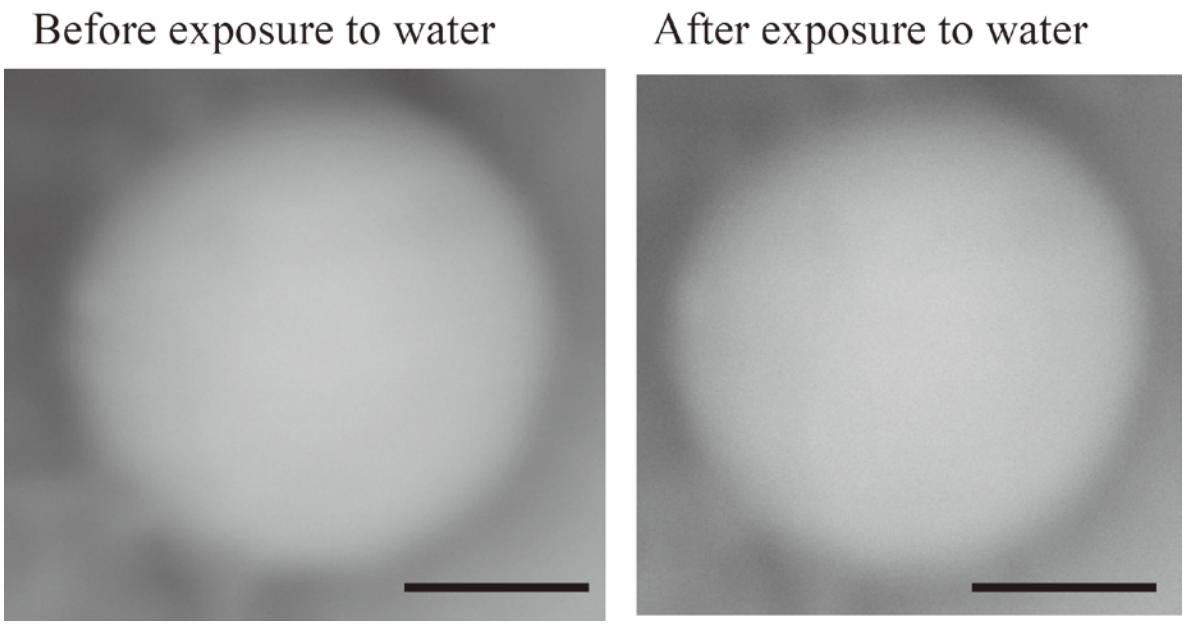

SI 7. SEM images of the Cs particle 1 before and after exposure to water. There is no change between the images, suggesting that the particle is largely insoluble to water. Scale bars: 1 µm.

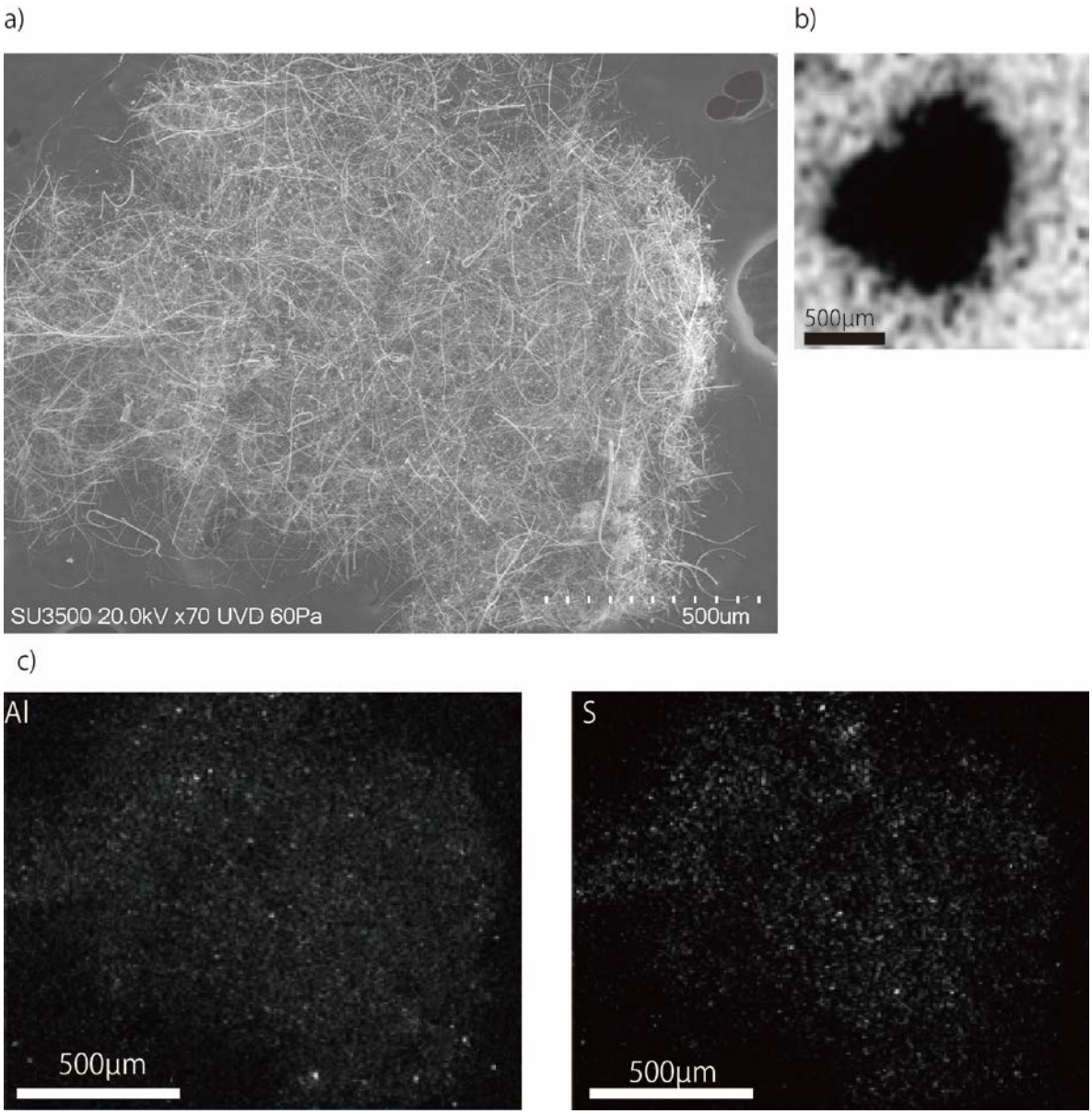

SI 8. The SEM analyses of the filter sample from March 20-21. a) An SEM image of a filter segment containing a diffused spot (Fig. 2). The filter was divided into several layers (SI 4-b), and this image corresponds to one of those layers. b) An IP image of the filter. Radioactive materials are distributed all over the filter. c) Elemental mapping images for Al and S, which represent aluminosilicate minerals and sulfate particles, respectively. These particles are distributed all over the filter.

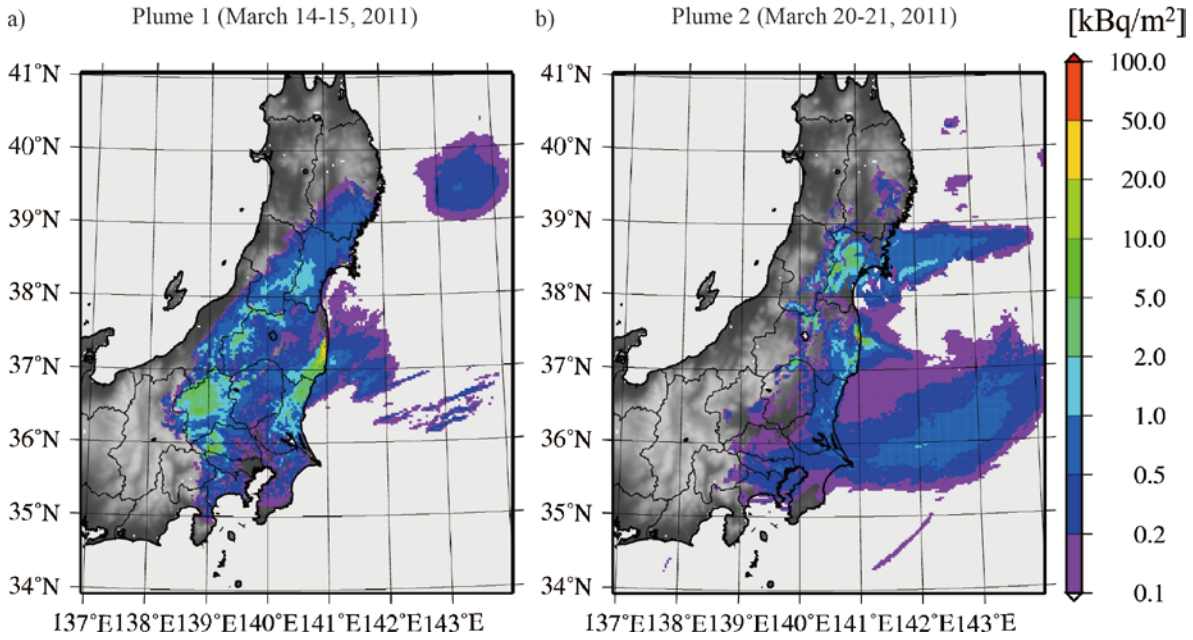

SI 9. The total (dry + wet) deposition of ^{137}Cs released from the FNPP between (a) March 14, 17:00 and March 15, 02:00 (JST) and (b) March 19, 20:00 and March 20, 07:00. The Cs carriers are assumed to be water-soluble submicron particles, such as sulfates, in both plume. The Regional Air Quality Model 2 (RAQM2) was used for the model calculation. We used the Generic Mapping Tools (GMT) developed at University of Hawaii to draw the figure. The model elevation in the figures was generated based on a 1km resolution Global 30 Arc-Second Elevation (GTOPO30) of U.S. Geological Survey (USGS).

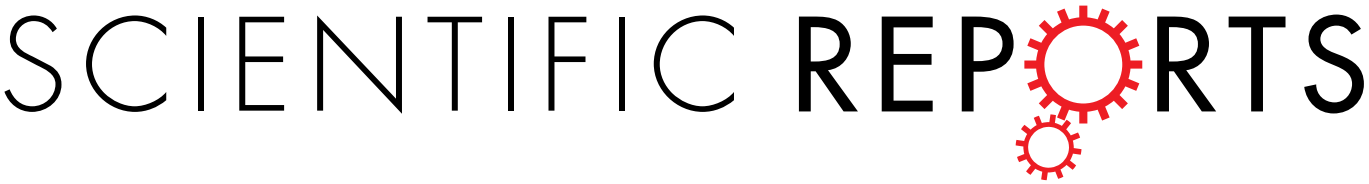

OPEN

Internal structure of cesium-bearing radioactive microparticles released from Fukushima nuclear power plant

Received: 03 June 2015
Accepted: 06 January 2016
Published: 03 February 2016

Noriko Yamaguchi[1,*], Masanori Mitome[2], Akiyama-Hasegawa Kotone[2], Maki Asano[1,3], Kouji Adachi[4] & Toshihiro Kogure[5,*]

Microparticles containing substantial amounts of radiocesium collected from the ground in Fukushima were investigated mainly by transmission electron microscopy (TEM) and X-ray microanalysis with scanning TEM (STEM). Particles of around 2 μm in diameter are basically silicate glass containing Fe and Zn as transition metals, Cs, Rb and K as alkali ions, and Sn as substantial elements. These elements are homogeneously distributed in the glass except Cs which has a concentration gradient, increasing from center to surface. Nano-sized crystallites such as copper- zinc- and molybdenum sulfide, and silver telluride were found inside the microparticles, which probably resulted from the segregation of the silicate and sulfide (telluride) during molten-stage. An alkali-depleted layer of ca. 0.2 μm thick exists at the outer side of the particle collected from cedar leaves 8 months after the nuclear accident, suggesting gradual leaching of radiocesium from the microparticles in the natural environment.

Although almost five years have passed since the accident of Fukushima Daiichi Nuclear Power Plant (FDNPP), radioactive contamination in the surrounding area is still a serious problem in Japan. The largest radionuclide deposition event occurred on March 15–16 and the second largest on 21–23, 2011. Wet deposition was a major source of radiocesium contamination of terrestrial environment[1], while contribution of dry deposition was larger near the FDNPP[2]. In order to understand and predict the fate of radioactive materials contaminating the terrestrial environment, it is important to clarify the physicochemical properties of the deposited materials. From previous cases of radionuclide release, it is known that the chemical species of released radiocesium is monovalent cation (Cs^+) which is soluble[3]. Deposition of radiocesium as insoluble particles has also been pointed out. Autoradiography analyses using imaging plate (IP) showed spots of particulate materials on plant tissues collected from Fukushima[4–6]. On the aerosol filter collected from March 14–15, 2011 in Tsukuba, 170 km south-southwest of FDNPP, Adachi *et al.*[7] discovered spherical particulate radiocesium of 2.0–2.6 μm in diameter, with particles insoluble in water having a glass-like structure[8]. These microparticles contain several fission products of U-235 other than radiocesium, and Fe and Zn which are also used in nuclear reactors[8]. Hence, they were considered to be released directly from nuclear reactors.

Kaneyasu *et al.*[9] suggested that vaporized radiocesium was transported with sulfate aerosol in the air, dissolved to cloud droplets and fell as rain. On the aerosol filter collected on March 20–21, 2011, rainy days in Tsukuba, the majority of radiocesium was in water-soluble form[7]. Such water-soluble radiocesium that reached the ground surface as a solute was fixed to soils, especially to clay minerals[10]. In the terrestrial environment, the majority of radiocesium is present in solid form regardless of the initial form of deposition. However, compared to clay minerals originally contaminated by soluble radiocesium in soil, the solid radiocesium, which was initially deposited as radioactive microparticles, had stronger radioactivity. Although the contribution or percentage of such radioactive microparticles in the contamination level of Fukushima has not been evaluated, its influence on human

[1]National Institute for Agro-Environmental Sciences, Kannondai, Tsukuba 305-0864, Japan. [2]National Institute for Materials Science, Namiki, Tsukuba 305-0044, Japan. [3]Graduate School of Life and Environmental Sciences, University of Tsukuba, Tennodai, Tsukuba, 305-8572, Japan. [4]Meteorological Research Institute, Nagamine, Tsukuba, 305-0052, Japan. [5]Graduate School of Sciences, The University of Tokyo, Bunkyo, Tokyo 113-0033, Japan. *These authors contributed equally to this work. Correspondence and requests for materials should be addressed to N.Y. (email: nyamag@affrc.go.jp) or T.K. (email: kogure@eps.s.u-tokyo.ac.jp)

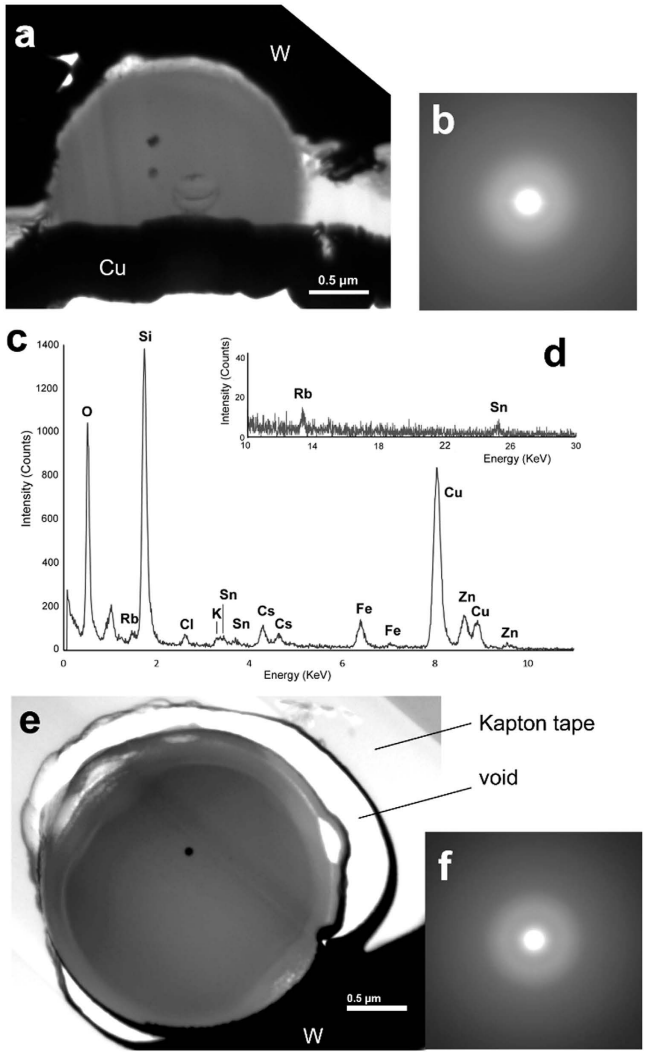

Figure 1. (**a**) Bright-field (BF) image of NWC-1. The opaque material outside the microparticle is tungsten (W) and copper (Cu) deposited in the FIB process. (**b**) Electron diffraction (ED) pattern from the particle. (**c,d**) EDS spectrum acquired from almost the whole area of the particle for the energy range of (**c**) 0–11 keV and (**d**) 10–30 keV. (**e**) BF image of CB-8. The opaque material outside the sphere is W and the thin transparent material is Kapton tape. (**f**) ED pattern from the particle.

health may be serious in terms of its intense radioactivity. Moreover, the structural detail of the microparticles may give insights into the state of the broken reactor and fuel debris.

In the present study, we investigated radioactive microparticles, similar to those reported by Adachi *et al.*[7], but collected from the ground, by observing their internal structure with transmission electron microscopic (TEM) techniques.

Results

Structure and composition of Cesium-bearing radioactive microparticles. Cesium-bearing radioactive microparticles that had been deposited on non-woven fabric cloth (NWC-1) and on a needle of Japanese cedar (*Cryptomeria japonica*) (CB-8) were investigated. They were in the field for five and eight months, respectively, until sampling. Scanning electron microscope (SEM) images of NWC-1 of the whole microparticle before preparing thin sections for TEM analyses; and elemental composition of the whole particle determined by synchrotron radiation microbeam X-ray fluorescence (SXRF) are shown in Supplementary Figs S1 and S2 online, respectively. The activities of ^{137}Cs for the NWC-1 and CB-8 were 5.04 ± 0.472 and 3.14 ± 0.178 Bq, respectively.

Bright-field (BF) images and selected-area electron diffraction (SAED) patterns recorded in TEM from the whole area of NWC-1 and CB-8 are shown in Fig. 1, along with the energy-dispersive X-ray spectrum (EDS) acquired in TEM from NWC-1. Preparation of thin specimens from NWC-1 microparticle by focused-ion-beam (FIB) process was successful only for the upper half of the sphere. The BF contrast of NWC-1 (Fig. 1a) was almost uniform except for two dark nanoparticles inside the sphere. These nanoparticles will be described in a later subsection. The SAED pattern from the whole particle consists of only a halo (Fig. 1b) and the EDS from the whole

particle (Fig. 1c,d) mainly consist of peaks of Si and O (Cu is from the supporting mesh), indicating that the particle was basically silicate glass. Additionally, Cl, K, Cs, Fe, Zn, Rb, and Sn were definitely identified. The presence of Na was not confirmed since its peak overlapped with the L-peak of Zn. These elements were previously reported[7,8] except for K. EDS Semi-quantitative analysis for almost the entire area of the TEM specimen, without considering the absorption effect estimated the glass composition (wt.%) to be SiO_2; 69.3, K_2O; 1.9, Fe_2O_3; 8.6, ZnO; 11.0, Rb_2O; 1.3, SnO_2; 1.4, Cs_2O; 3.4 with a small amount of Cl (1.4 wt.%). The valence states of cations were assumed to be in line with results in an X-ray absorption spectroscopic study[8]. Rubidium, Cs and Sn are the fission products of U-235. Tin is also used for fuel cladding[11]. Iron is used as steel for reactor pressure vessels, and Si and O are main components of concrete at the bottom of the containment vessel, where the melt-down fuel or core debris is thought to exist. Zinc had been added to the primary cooling water[12]. Potassium and Cl may originate from concrete and/or seawater, which was used to cool down the reactor.

The BF TEM image of CB-8 showed a two-layer structure having an inner core with darker contrast, an outer crust with a lighter one, and a small dark nanoparticle near the center (Fig. 1e). The thickness of the crust was around 0.2 μm. SAED pattern indicated that both are amorphous (Fig. 1f). Locally, a bubble-like structure was observed at a certain radius in the crust, or the outside part was peeled off at the radius (Fig. 1e). The chemical composition of the entire area of the specimen was SiO_2; 73.3, K_2O; 1.4, Fe_2O_3; 7.2, ZnO; 11.4, Rb_2O; 1.2, SnO_2; 1.5, Cs_2O; 3.3 and Cl; 0.7, which is similar to that of NWC-1.

Distributions of elements in microparticles. Elemental maps from NWC-1 using STEM-EDS are shown in Fig. 2a. Brighter color indicates higher concentration of the elements. All elements were almost uniformly distributed in the particle with Cs the only exception. Cesium concentration was lower near the center than the outside of the particle. The ratio of the amounts between the center and outside is around two. It is possible that vapor-phase cesium in the reactor was absorbed to the molten silicate microparticles, from their surface. The low diffusion velocity of cesium in the glass may have left the concentration gradient. On the contrary, elemental mapping for CB-8 (Fig. 2b) indicates that K, Rb and Cs were distinctively depleted in the crust but concentrated in the vicinity of the surface. Although the reason for the high concentration at the surface is not certain, it might be an artifact by diffusion of alkali cations caused by electron-beam radiation in the analysis. Chlorine was concentrated in the crust.

Crystalline nanoparticles in the glass. Two nanoparticles with dark contrast were observed in the TEM image of NWC-1 (Fig. 1a). Although EDS spectrum only from the particles cannot be obtained since they are still buried in the glass in spite of the thinning by FIB, S was distinctively identified from the particles (Fig. 3a). Elemental mapping by STEM-EDS indicated enrichment of Cu, Zn and Mo at the nanoparticles along with S, indicating that they are sulfide. The possibility of sulfate was excluded because oxygen is deficient in the nanoparticles in the oxygen map (Fig. 3a). Moreover, the locations of Cu, Zn and Mo do not overlap within the nanoparticles, suggesting that these metal elements form different sulfide phases in the nanoparticle (Fig. 3a). SAED from the left particle showed a single-crystal diffraction pattern (Fig. 3b), which can be explained by the crystallographic parameters for a high-temperature polymorph of digenite ($Cu_{2-x}S$). The origin of Cu and S may be minor elements in the concrete. On the other hand, Ag and Te were distinctively detected by EDS in TEM from the nanoparticle in CB-8 (Supplementary Fig. S3 online), indicating the particle to be silver telluride. Both elements can be fission products of U. Diffraction spots were observed in the SAED pattern from the particle, indicating that it is crystalline but the phase could not be identified. These sulfide and telluride were probably segregated and crystallized in the microparticles at the molten state.

Discussion

Our most significant finding is that the matrix of the Cs-bearing microparticles is silicate glass, based on the TEM-EDS analysis with FIB sample preparation. Previous studies suggested that Fe, Mo, Sn and Zn in the Cs-bearing microparticles had a similar X-ray absorption near-edge structure to those composed of glass[8], however the presence of Si in the microparticles has not been verified[7,8]. It is probable that the high-temperature melt-down fuel from the reactor came into contact with and melted the concrete, and then splashed microparticles of silicate melt, which were solidified by cooling to form silicate glass in the atmosphere. However, there are several questions with respect to the selection of the constituting elements in the glass from various ones in the reactor. For instance, Ca which is one of the major elements in concrete, was almost absent in the microparticles of NWC-1. Since TEM observed only a small portion of the microparticles, by making them thin using FIB, there may have been other elements in the microparticles, for instance, as a form of chalcogenide nanoparticle.

The next important finding is the alkali-depleted crust in CB-8 microparticle. This is probably the result of elution of alkali ions by contact with acidic solution in the field, commonly observed in silicate glass[13]. On the other hand, such alkali-depleted crust was not observed in NWC-1. This may be attributed to the different environments of the two microparticles after release from the nuclear plant. NWC-1 was on non-woven cloth and CB-8 on a cedar leaf before it was collected. It is well-known that silicate glass elutes alkali components from their surface by ion-exchange with proton or hydronium ions to form an alkali-leaching layer on the surface if pH of reacting solution is low, whereas the silicate framework of the glass itself is dissolved with high-pH solution[13,14]. Coniferous forest canopy induces acidic condition due to ammonia uptake, nitrification and leaching of plant-derived acid[15]. It was likely that CB-8 deposited on the cedar leaf had been in acidic conditions, which derives alkali depletion in the crust, for eight months. The finding of the alkali-depleting crust on the surface of the Cs-bearing radioactive microparticle indicates that radiocesium in the particles can be released by "weathering" of the glass in natural environments, and considering its small size, duration for the total release of the radioactive cesium from the particles is probably not long, from several years to a few decades, though it will strongly depends on the environment.

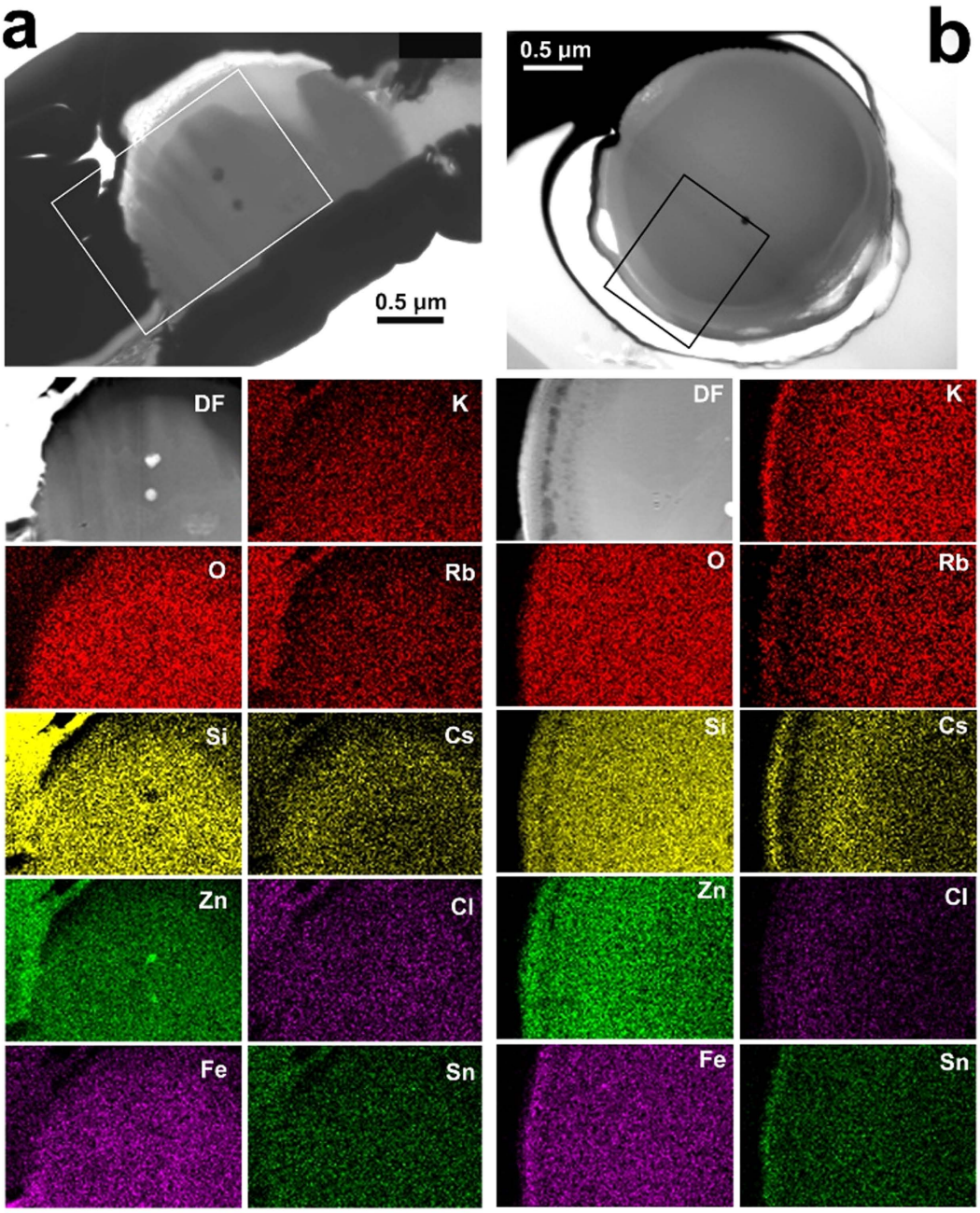

Figure 2. (**a**) Element maps of NWC-1 acquired by STEM-EDS with a STEM Dark-field (DF) image at the same area, and (top) TEM Bright-field image in which the rectangle indicates the area analyzed by STEM-EDS. The thin area around the top of the particle which was not observed in Fig. 1a was formed by a further thinning process by FIB. (**b**) Element maps and images of CB-8 with the same framing as in (**a**).

In order to investigate the dissolution rate and detailed Cs-leaching properties of the Cs-bearing radioactive microparticles, a leaching experiment should be conducted as a function of temperature and pH. However, collecting and isolating the Cs-bearing microparticles is time-consuming and it is difficult to obtain a large enough number of Cs-bearing microparticles to investigate dissolution properties. Alternatively, synthesized silicate glass with the same composition as the microparticles presented in this study may help to obtain information on the fate of Cs-bearing radioactive microparticles. However, in our preliminary experiment, we were unable to make uniform glass with the same composition at present. This is probably due to the liquid immiscibility at the composition. A solution to this problem is now being considered.

There are mainly two types of solid-phase radiocesium in the terrestrial environment affected by FDNPP accident; that fixed to clay minerals in the soil via wet deposition and that contained in the microparticles of silicate glass flown directly from the nuclear reactors. The radioactivity of the former is rather in low-density but distributed widely, therefore it is a major source of external radiation from ground. Part of the radiocesium adsorbed on

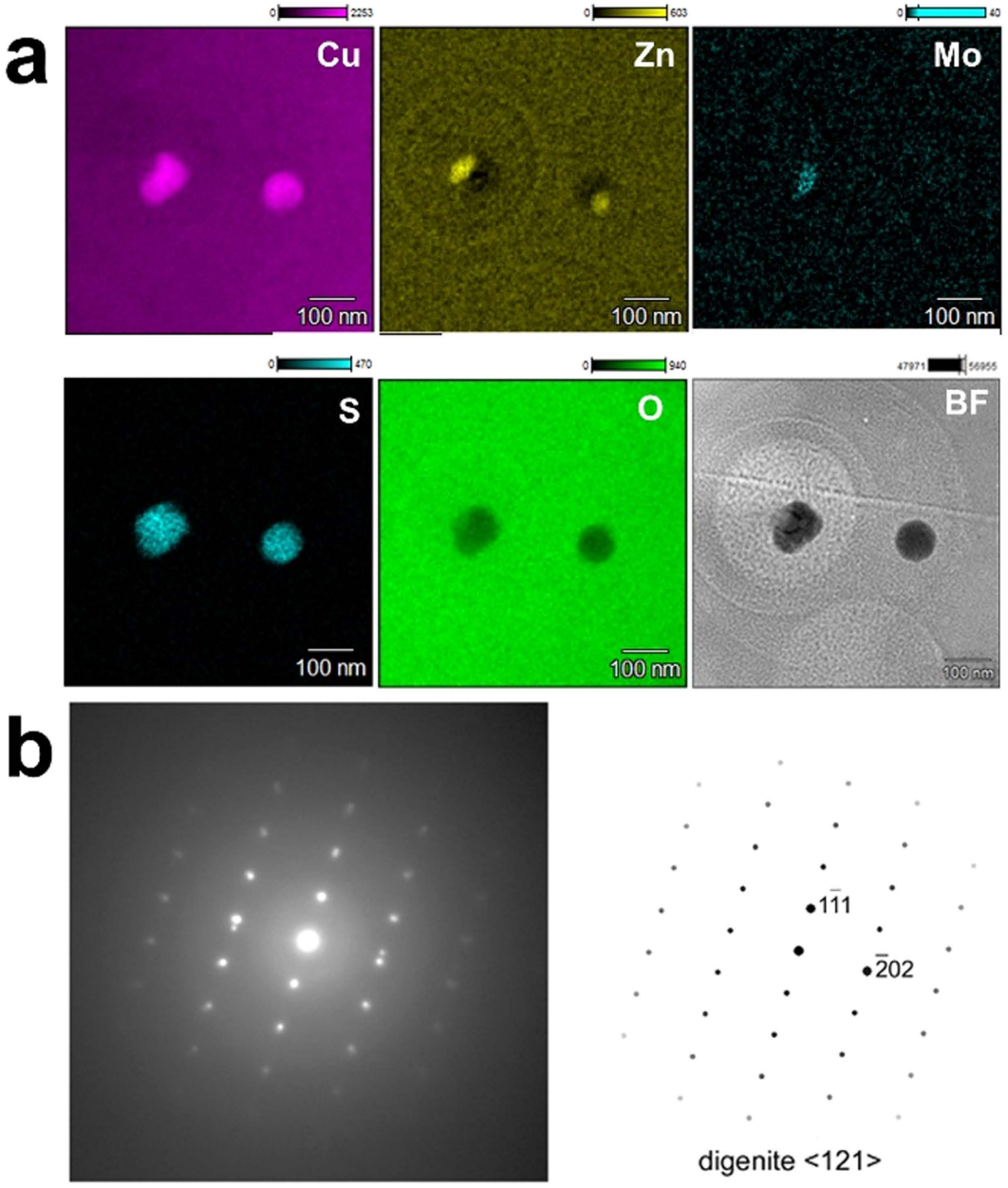

Figure 3. (**a**) Element maps and STEM bright-field (BF) image of the two nanoparticles inside NWC-1. The circular contrasts outside the nanoparticles in the BF image are radiation damage in glass formed by the electron probe for chemical analyses. (**b**) (Left) ED pattern from the left nanoparticle. (Right) Drawing of ED pattern for the high-temperature polymorph of digenite ($Cu_{2-x}S$) along <121>.

the soil clay is desorbed and transferred to crops thereby causing internal radiation. On the other hand, contribution of the microparticles to the air radiation is most likely not significant, but their radiation density is very high, which is particularly problematic for organisms including humans if the microparticles are inhaled or ingested. The plant availability of radiocesium in the microparticles should depend on its solubility. Consequently, further research on this material should be carried out as soon as possible.

Methods

Samples. Radioactive microparticles attached on non-woven fabric cloth and needles of Japanese cedar, collected from Fukushima, were identified by autoradiography followed by point-by-point analyses with scanning electron microscope (SEM; Hitachi high-Technologies SU3500) equipped with an energy dispersed X-ray spectrometer (EDS; Horiba X-max 50 mm). The identified particles were further determined by SXRF with excitation X-ray energy of 37.5 keV to ensure the detection of Cs-K line from the particle. The activities of ^{137}Cs was determined by a Ge detector (GCW2523S Canberra, USA). Detailed methods to identify the Cs-bearing microparticles are described in the supplementary information.

TEM Analyses. Cross-sectional thin TEM specimens were prepared from radioactive microparticles using a focused ion beam (FIB) instrument with micro-sampling system (Hitachi FB-2100) as described in the supplementary information. Then specimens were initially examined using a TEM (JEOL JEM-2010UHR) operated at 200 kV with an EDS analyzer system (JEOL JED-2200). Elemental mapping in the microparticles and quantitative analyses were performed using a JEOL JEM-3100FEF operated at 300 kV in the STEM mode, with an EDS analyzer system (Thermo Fisher Scientific NORAN System SIX). Finally, elemental maps for nanoparticulates inside the microparticles were acquired using a JEOL JEM-2800 operated at 200 kV with double wide-area (0.95 sr.) silicon drift detectors (SDD) for EDS analyses.

References

1. Yoshida, N. & Takahashi, Y. Land-surface contamination by radionuclides from the Fukushima Daiichi Nuclear Power Plant accident. *Elements* **8,** 201–206 (2012).
2. Katata, G., Ota, M., Terada, H., Chino, M. & Nagai, H. Atmospheric discharge and dispersion of radionuclides during the Fukushima Dai-ichi Nuclear Power Plant accident. Part I: Source term estimation and local-scale atmospheric dispersion in early phase of the accident. *J. Environ. Radioactiv.* **109,** 103–113 (2012).
3. Santschi, P. H. *et al.* Chernobyl radionuclides in the environment- tracers for the tight coupling of atmospheric, terrestrial, and aquatic geochemical processes. *Environ. Sci. Technol.* **22,** 510–516 (1988).
4. Nakanishi, T. M., Kobayashi, N. I. & Tanoi, K. Radioactive cesium deposition on rice, wheat, peach tree and soil after nuclear accident in Fukushima. *J. Radioanal. Nuclear Chem.* **296,** 985–989 (2013).
5. Nakanishi, H. *et al.* Radioactive cesium distribution in bamboo *Phyllostachys reticulata* (Rupr) K. Koch shoots after the TEPCO Fukushima Daiichi Nuclear Power Plant disaster. *Soil Sci. Plant Nutr.* **60,** 801–808 (2014).
6. Itoh, S., Eguchi, T., Kato, N. & Takahashi, S. Radioactive particles in soil, plant, and dust samples after the Fukushima nuclear accident. *Soil Sci. Plant Nutr.* **60,** 540–550 (2014).
7. Adachi, K., Kajino, M., Zaizen, Y. & Igarashi, Y. Emission of spherical cesium-bearing particles from an early stage of the Fukushima nuclear accident. *Sci. Rep.* **3,** No. 2554 (2013).
8. Abe, Y. *et al.* Detection of uranium and chemical state analysis of individual radioactive microparticles emitted from the Fukushima nuclear accident using multiple synchrotron radiation X-ray analyses. *Anal. Chem.* **86,** 8521–8525 (2014).
9. Kaneyasu, N., Ohashi, H., Suzuki, F., Okuda, T. & Ikemori, F. Sulfate aerosol as a potential transport medium of radiocesium from the Fukushima Nuclear accident. *Environ. Sci. Technol.* **46,** 5720–5726 (2012).
10. Mukai, H. *et al.* Speciation of radioactive soil particles in the Fukushima contaminated area by IP autoradiography and microanalyses. *Environ. Sci. Technol.* **48,** 13053–13059 (2014).
11. Zinkle, S. J. & Was, G. S. Materials challenges in nuclear energy. *Acta Mater.* **61,** 735–758 (2013).
12. Hori, S. & Suzuki, A. *TEPCO's challenges for occupational exposure reduction - installation of additional CF in Fukushima Daiichi NPP.*, <www.nsra.or.jp/isoe/english/…/pdf/atc2009-3-1ga.pdf> (2009). (Accessed 18th May 2015).
13. Bunker, B. C. Molecular mechanisms for corrosion of silica and silicate-glasses. *J. Non-Cryst. Solids* **179,** 300–308 (1994).
14. Gin, S. *et al.* Origin and consequences of silicate glass passivation by surface layers. *Nat. Commun.* **6,** No. 6360 (2015).
15. Cronan, C. S. & Reiners, W. A. Canopy processing of acidic precipitation by coniferous and hardwood forests in New England. *Oecologia* **59,** 216–223 (1983).

Acknowledgements

Part of this work was supported by a Grant-in-Aid for science research (15H04222 and 24110003) by JSPS, Japan. This work was also supported by 2014 JAEA contract research for Fukushima environment recovery, "Study on Cs adsorption and desorption process on clay minerals" and by MAFF contract research "Development of Decontamination technologies for radioactive substances in agricultural land". The synchrotron radiation experiment was performed under approval of the SPring-8 Program Advisory Committee (Proposal Number: 2014B1282). The authors wish to thank Dr. M. Kobayashi for providing the Japanese cedar samples, Ms. E. Fujii for preparing TEM specimens, Dr. T. Hara for providing the opportunity to use the STEM instrument, Prof. Clive Langham for English edition, and Dr. Y. Igarashi for comments on the manuscript.

Author Contributions

N.Y. and T.K. designed the research and wrote the paper; N.Y. performed the IP, SEM and SXRF analyses; M.A. performed SEM and SXRF analyses; M.M. and K.A.-H. performed TEM analyses; K.A. performed SEM analyses; T.K. performed SEM and TEM analyses and supervised the study; all authors contributed to the manuscript. N.Y and T.K. contributed equally to this work.

Additional Information

Supplementary information accompanies this paper at http://www.nature.com/srep

Competing financial interests: The authors declare no competing financial interests.

How to cite this article: Yamaguchi, N. *et al.* Internal structure of cesium-bearing radioactive microparticles released from Fukushima nuclear power plant. *Sci. Rep.* **6**, 20548; doi: 10.1038/srep20548 (2016).

地 球 化 学 49，185–193（2015）
Chikyukagaku（Geochemistry）49，185–193（2015）
doi:10.14934/chikyukagaku.49.185

総 説

電子顕微鏡がとらえた放射性粒子：福島第一原子力発電所事故初期に大気中に放出された放射性粒子の物理化学的性質

足 立 光 司*

（2015年8月13日受付，2015年10月9日受理）

Radioactive particles revealed by electron microscopy: Chemical and physical properties of radioactive particles in aerosol samples emitted during the early stage of Fukushima Dai-ichi Nuclear Power Plant accident

Kouji ADACHI*

Meteorological Research Institute
1–1 Nagamine, Tsukuba, Ibaraki 305–0052, Japan
* E-mail: adachik@mri-jma.go.jp

Water-insoluble radioactive materials emitted during an early stage of the Fukushima Dai-ichi Nuclear Power Plant accident in 2011 were identified, and their chemical and physical properties were characterized as particulate matters. In this report, studies on radioactive particles collected from filter samples in Tsukuba on March 14–15, 2011 are summarized. Their compositions, chemical states, sizes, shapes, crystallinity, and hygroscopicity were analyzed using microscopic analyses such as electron microscopy and synchrotron with a micro-beam. The results indicate that they include Cs, Fe, and Zn as well as elements from fission products and are water insoluble, spherical-glassy particles with *ca*. 2 micrometer in size. Understanding of their detailed properties is significant to improve the numerical models during the accident and to understand their occurrences in soil as well as the accident itself. In addition to the water-insoluble radioactive materials, water-soluble radioactive materials, which were likely emitted in different events during the accident, should be investigated to have comprehensive understanding of the accident and its environmental effects. More samples from various environments such as soil will be needed, and more detailed chemical and physical analyses will help to understand their formation process, influences on human health, and long term decrements in ambient conditions.

Key words: Radioactive particles, Fukushima Dai-ichi Nuclear Power Plant Accident, Electron microscopy, Synchrotron Radiation, Cesium

1. はじめに

東日本大震災時に発生した福島第一原子力発電所事故によって，さまざまな放射性物質が大気・海洋に放出された（Chino *et al.*, 2011; Tsuruta *et al.*, 2014; Katata *et al.*, 2015）。大気中にエアロゾルとして放出された放射性物質は，地面，森林，また海面などに沈着し環境汚染を引き起こしている（Masson *et al.*, 2011; Buesseler *et al.*, 2012; Kaneyasu *et al.*, 2012; 鶴田・中島，2012; Yoshida and Kanda, 2012）。その沈着プロセスは，放射性物質の運び手となるエアロゾルの大きさ・化学組成・水溶性といった物理化学特性（Adachi *et al.*, 2013）や，降水・降雪・霧などの気象の影響を大きく受ける（Hososhima and Kaneyasu, 2015）。これらの放射性物質は，植物（梅村ほか，2015），土壌（Kinoshita *et al.*, 2011; Fujii *et al.*, 2014），大気中（Igarashi *et al.*, in press）か

気象研究所
〒305–0052 茨城県つくば市長峰1–1

ら検出されており，それらがどのように環境で移行するかといった長期的な環境動態に対する理解は，汚染を受けた地域の将来にとって重要である。

事故によって放出された放射性物質は重量換算にすると非常に微量であり，放射能測定以外の化学分析手法で環境試料から放射性物質を検出することは困難である。一方，放射性物質の環境動態は，放射性物質自体の性質だけで決まるものではなく，その運び手となる粒子の化学組成，イオン状態，粒径，表面状態といった物理化学特性に大きく支配されるため，その特定および化学分析は重要である。本稿では，2013年に筆者らが報告した水に溶けにくい性質をもった放射性粒子を電子顕微鏡で直接分析した研究（Adachi *et al.*, 2013）および，その研究を発展させた放射光X線分析を用いた粒子の詳細な化学状態・組成分析の結果（Abe *et al.*, 2014）を中心にまとめる。それらの結果を踏まえ，事故初期に放出された放射性粒子の物理化学的特徴およびその研究がもたらす応用について，いくつかの提案を行う。

2. 関東に飛来した放射性物質

原発事故によって大気中に放出された放射性物質は，大気の流れによって原発周辺をはじめ東日本，関東，さらには北半球全域に拡散した（Masson *et al.*, 2011; Morino *et al.*, 2011; Christoudias and Lelieveld, 2013; de Vismes Ott *et al.*, 2013）。関東周辺では，3月15日，3月21日前後に高濃度汚染空気塊が到達したことが報告されている（例えばDoi *et al.*, 2013）。

茨城県つくば市にある気象研究所では，1957年から大気中放射性物質のモニタリングを行っている（Igarashi *et al.*, in press）。原発事故時においても敷地内で空気中に含まれる放射性物質の採取を行っており，ゲルマニウム半導体検出器を使った放射能濃度の時系列変化が測定されている（Fig. 1）。その結果，近隣のモニタリング結果と同様に（Doi *et al.*, 2013），3月14–15日，3月20–21日に採取された試料が高い放射能強度を示す結果が得られている。フィルターから検出された放射性元素のうち，短寿命核種を除き放射能強度が高かったものはセシウム134・137であり，最大で大気1 m^3中に40 Bq程度であった。

フィルター上に捕集された放射性物質の分布を可視化して分析する，イメージングプレート（IP）と呼ばれる方法がある（箕輪，2013; 田中ほか，2013; Itoh *et al.*, 2014）。このIPを使って放射能強度の高い3月14–15日と20–21日のフィルターを分析すると，Fig. 2のような結果が得られた。3月14–15日に捕集されたフィルターからは，比較的放射能強度の強いスポット状の放射性物質が見つかり，後者の3月20–21日に採取されたフィルターからは，ほぼ全面に均一な強度の放射性物質が検出された。これらの結果は，原発事故によって大気中にエアロゾルとして放出された放射性物質が，原発から直接放出された比較的高濃度に放射性物質を濃縮した粒子と，ガスや水溶性の放射性物質として放出された後大気での反応や水に溶けて他の物質と混ざり合ったものの二種類があることを示唆していた。3月14–15日に捕集された放射性物質は，その分布状態から事故によって直接放出された粒子であることが考えられ，次章に示す方法でその単離を試みた。

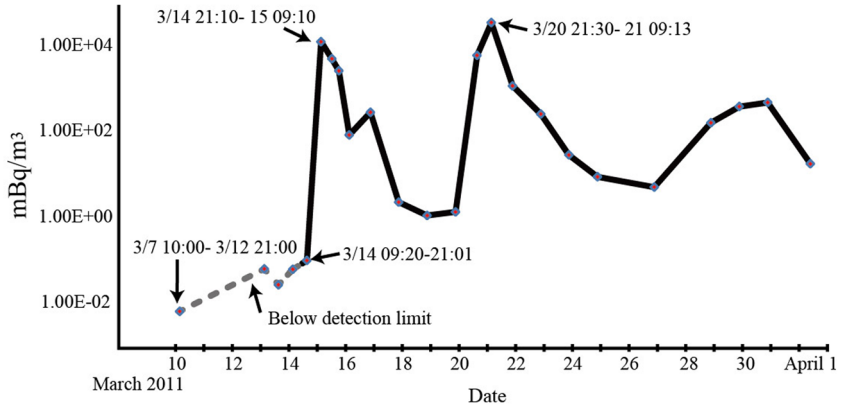

Fig. 1 (Color online) The radioactivity of the aerosol particles after the Fukushima Dai-ichi nuclear power plant accident in Tsukuba, Japan. Dots indicate the midpoints of each sampling period. Reprinted from Fig. 1 of Adachi *et al.* (2013).

3. 放射性粒子の単離

エアロゾル粒子をフィルター上に捕集した試料には，放射性粒子に加え他の発生源から生じた放射性ではない粒子が無数にある。例えばつくば市の2011年3月14日の空気中には約4×10^{7}個m^{-3}の濃度で粒子が存在した（Adachi *et al.*, 2013）。そのため，電子顕微鏡等でそのままフィルターを分析しても放射性物質を特定することはほぼ不可能であり，フィルター上の放射性物質を単離して顕微鏡分析に供する必要があ

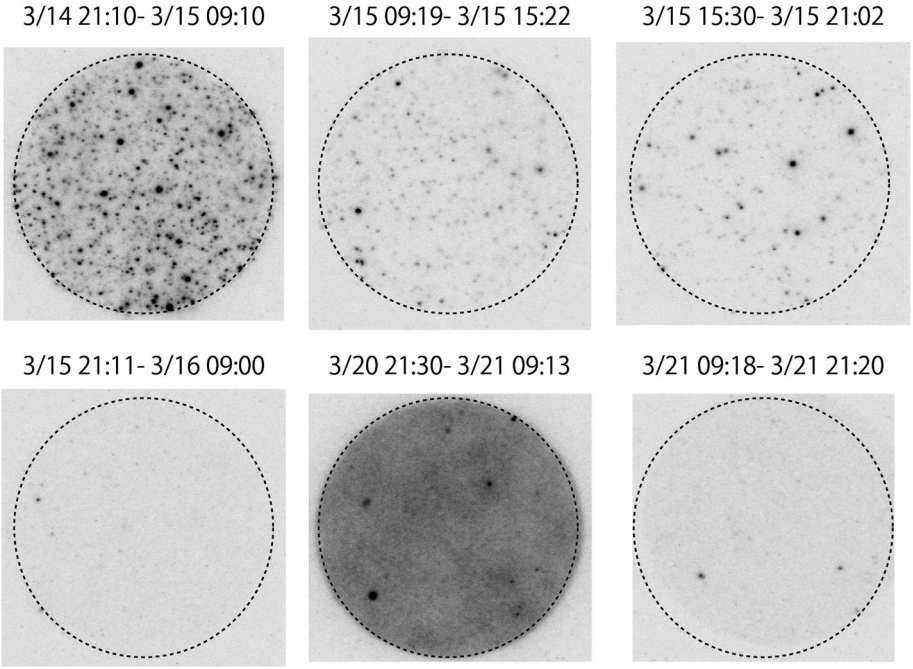

Fig. 2　The distribution of radioactive materials on the filter samples measured with the IP. Black dots indicate the presence of radioactive materials. The outer rims (dotted line) show peripheries of the filters. This study focused on the filter samples from March 14, 21 : 10 to March 15, 09 : 10 (upper left), and from March 20, 21 : 30 to March 21, 09 : 13 (bottom center). Reprinted from Fig. 2 of Adachi *et al.* (2013).

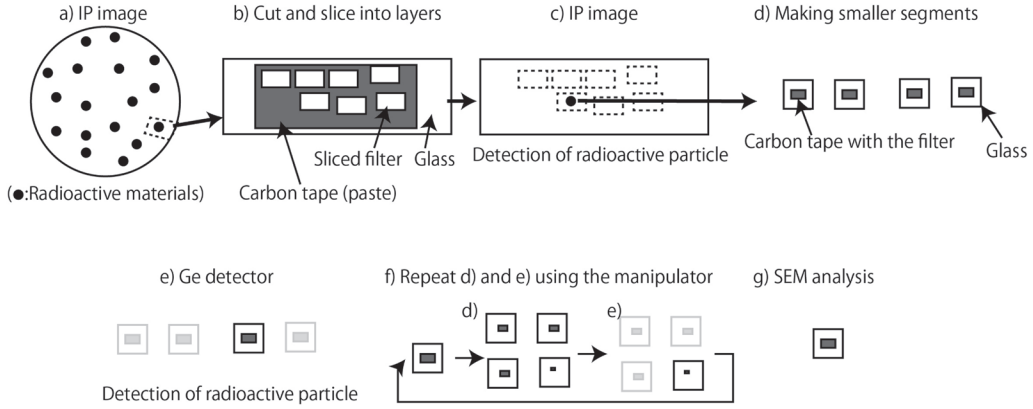

Fig. 3　The selection method of radioactive particles for the SEM analysis. a) The IP image of the filter was captured, and a part of the filter that includes radioactive material was cut off (dotted line). b) The segment of the filter was separated into approximately 10 layers and put onto a carbon tape attached to a glass substrate. c) The IP image was taken to identify the position of the radioactive material. d) The carbon tape including the radioactive material was cut into small pieces. e) The radioactive material was detected using a Ge detector from the filter segments. f) The processes d) and e) were repeated to make the filter and the number of particles as small as possible. g) The radioactive particle embedded within carbon paste was analyzed using the SEM. Reprinted from SI 4 of Adachi *et al.* (2013).

る。著者らが2013年に報告した論文では，1）フィルターをIPにかけ，黒点で示された放射性物質をフィルター繊維ごと切り取る（Fig. 3a），2）切り取ったフィルター繊維をガラスプレート上に貼られたカーボンテープ等に移す（Fig. 3b），3）マイクロマニュピレータ等を使ってカーボンテープごとできるだけ小さく分割し，IPやゲルマニウム半導体検出器を使って放射性物質が含まれた分画を特定する（Fig. 3c–e），4）3）の作業を繰り返して放射性物質を単離した状態に近くして（Fig. 3f），かつ走査型電子顕微鏡（SEM）で分析可能なように粒子を表面に露出させる（ガラスプレート上で放射性物質を含んだカーボンテープを薄く延ばす）（Fig. 3 g），という放射性物質の単離方法を提案した。そして，最後にSEMで試料の観察を行い，セシウムを含んだ球状の粒子を発見した。

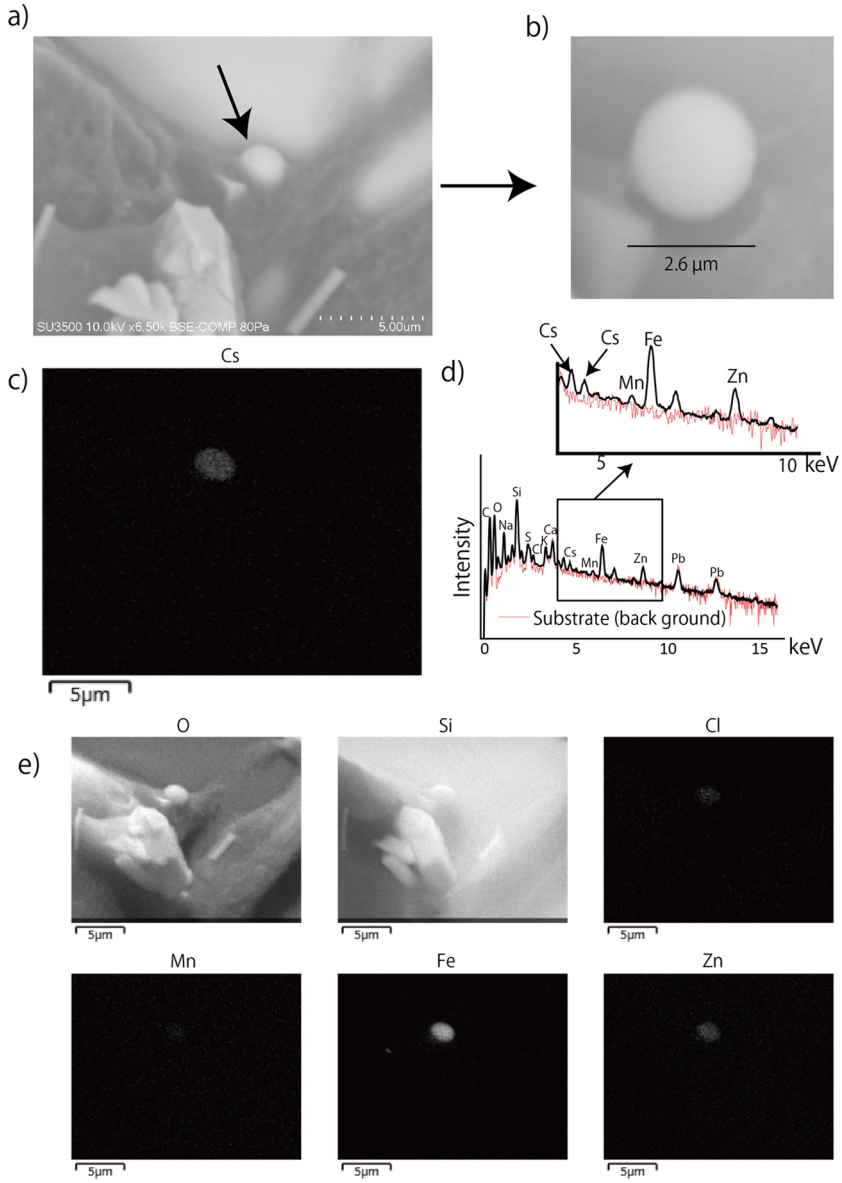

Fig. 4 (Color online) SEM and EDS mapping images of a radioactive particle from the sample collected during March 14, 21 : 10 and March 15, 09 : 10. a) A radioactive particle partially embedded within a carbon paste. b) The same radioactive particle as a) but measured the next day. The particle shows a spherical shape. c) An elemental mapping (Cs) of the particle a). d) The EDS spectrum of the particle a) (black line). The red line shows the spectrum from the glass substrate. The Cs in the particle shows multiple peaks. e) An elemental mapping of the other elements within the area. O, Si, Cl, Mn, Fe, and Zn are possibly coexistent with Cs within the particle. Reprinted from Fig. 3 of Adachi *et al.* (2013).

4. 放射性粒子の走査型電子顕微鏡分析

気象研で3月14–15日に採取されたフィルター中から最初に見つかった放射性粒子は，直径2.6マイクロメートルの球状粒子で，SEMに付属したエネルギー分散型X線分析装置（EDS）を使った分析でセシウムを含むことが確認された（Fig. 4）。ゲルマニウム半導体検出器を用いたガンマ線スペクトル分析では，事故から2年後の分析において放射性セシウム以外のガンマ線放出核種は確認されなかった（Fig. 5）。この粒子の試料採取時における（2011年3月14日）放射能強度を減衰補正して計算すると，セシウム134が3.31±0.06 Bq，セシウム137が3.27±0.04 Bqであり，セシウム137, 134比はほぼ1 : 1であった。放射能強度から換算した放射性セシウムの質量パーセントは，この粒子の密度を鉱物に近い2.0 g/cm^{3}と仮定すると5.5%となる。また，EDS分析では，この粒子はセシウムに加え，酸素，ケイ素，鉄，亜鉛を主体として，微量の塩素，マンガンなどを約0.1%以上含んでいることがわかった。同じフィルターの別の黒点から分離された放射性粒子も，放射能強度は低いながら定性的には同様の組成を有していた。また，この放射性粒子の水溶性を簡易的に調べるため，放射性粒子に水滴を垂らして約1時間自然乾燥させた前後の形態観察を行った（Fig. 6）。その結果，前後において形態に変化は見られなかったことから，この粒子は大気中を運ばれる数日以内の短時間では水に溶けない性質（非水溶性）であることが示された。

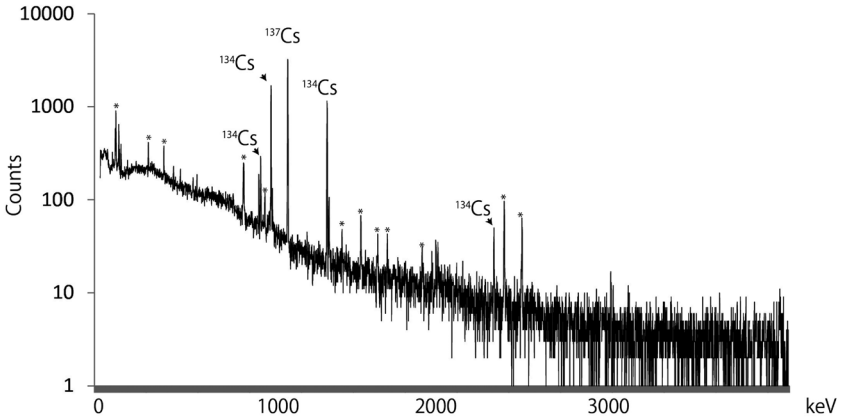

Fig. 5　The gamma spectrum of the radioactive particle. A 50,000 sec detection time was used. Peaks marked with* were from the background or the glass substrate. The sample was analyzed two years after the accident, and short-lived radionuclides would not have been detected even if they had been present when emitted. The particle was measured on March 28, 2013. Reprinted from SI 5 1 of Adachi *et al.* (2013).

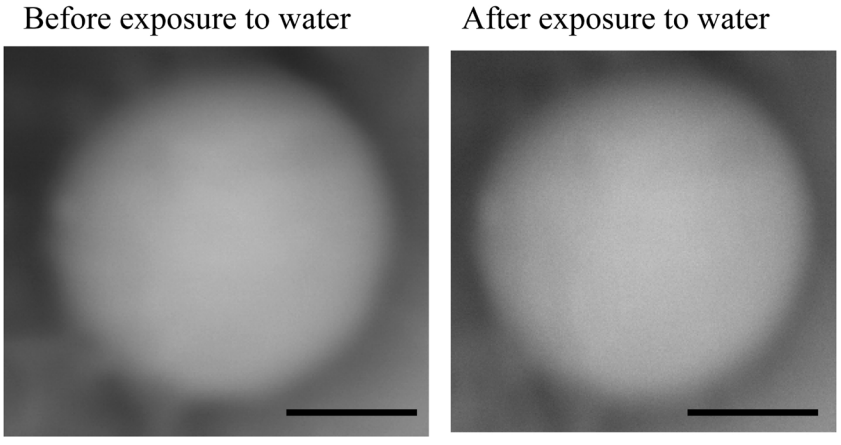

Fig. 6　SEM images of the radioactive particle 1 before and after exposure to water. There is no change between the images, suggesting that the particle is largely insoluble to water. Scale bars: 1 μm. Reprinted from SI 7 of Adachi *et al.* (2013).

5. 放射性粒子の放射光分析

2011年3月14–15日に気象研究所で採取されたフィルターから単離された放射性粒子3個に対して，大型放射光施設であるSPring8でさらに詳細な組成，化学状態，結晶性の分析が行われた（Abe *et al.*, 2014）。SPring8で行われた分析では，BL37XUにおける縦横1マイクロメートル前後に絞られた高輝度のX線ビームを用いて，1）放射光X線分析による組成分析および粒子内元素分布解析，2）X線吸収端近傍構造分析（XANES）による化学状態分析，3）X線回折法（XRD）による結晶性の分析，を行った。

SPring8での蛍光X線分析ではSEM-EDS分析で得られた元素（鉄，亜鉛，セシウム）に加え，ルビジウム，ジルコニウム，モリブデン，スズ，アンチモン，テルル，バリウムがすべての粒子から検出された（Fig. 7a）。加えて，マンガン，クロム，銀，ウラン，鉛などの元素も1もしくは2個の粒子から検出された。特にウランはL_3吸収端のXANES分析でも微量ながらその存在が確認された（Fig. 8a）。また，元素の粒子内での分布を示す図（Fig. 7b–d）では，鉛を除き球状粒子の厚さに応じた強度勾配を示しており，それぞれの元素が粒子全体に分布していることを示唆していた。図7dに見られる鉛の分布は，放射性粒子の背後にある粒子（フィルター繊維など）からの寄与が考えられる。XANESによる化学状態分析の結果は，鉄，モリブデン，スズが各粒子中に高い酸化数を持ったガラス状態で存在することを示している（Fig. 8b–d）。また各粒子について行われたXRDでは回折ピークが検出されず，これらの粒子が非晶質であることを示していた。

SPring8放射光分析とSEM-EDSの分析結果から，放射性粒子の生成に関し以下のように考えられる。1）つくばで得られた放射性粒子は，核燃料物質からの分裂生成物である元素や，核燃料以外の起源（例えば構造物）から発生した物質（ケイ素，鉄，亜鉛など）を含んだ複合的な組成をしている。2）球形の形態や，ガラス状の構造をしていることなどから，いったん溶けた溶融物が自由落下条件で急冷して粒子状になった。3）なんらかの原因（水素爆発等）により原子炉内部からこのような粒子が環境中に放出され，高濃度の放射性物質を含むプルームとして輸送された。

6. 水に溶けない放射性粒子，溶ける放射性粒子

本稿で紹介したセシウムを含む比較的放射能強度の高い放射性粒子は，事故によって直接放出されたもの

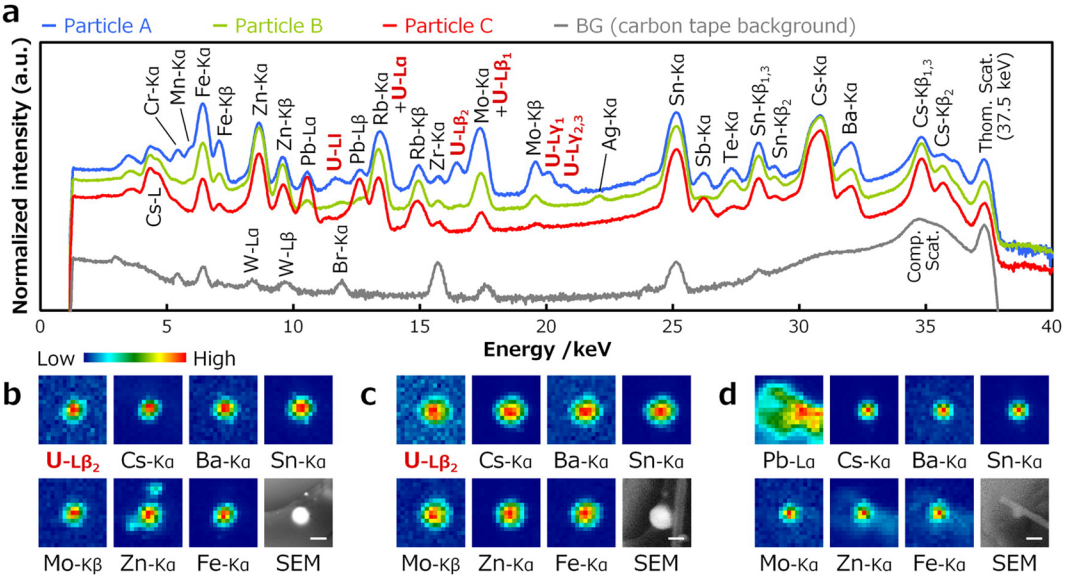

Fig. 7 (Color online) Results of Synchrotron Radiation (SR)-μ-X-Ray Fluorescence (XRF) analyses. (a) Comparison of the SR-μ-XRF spectra obtained for articles A, B, and C and the carbon tape background. The intensity of each spectrum was displayed on a logarithmic scale and shifted in a longitudinal direction. (b–d) Distributions of representative elements extracted from the SR-μ-XRF images of (b) particle A, (c) particle B, and (d) particle C with enlarged SEM image corresponding to the imaging area (scale bar: 2 μm). Reprinted with permission from Fig. 2 of Abe *et al.* (2014). Copyright 2014 American Chemical Society.

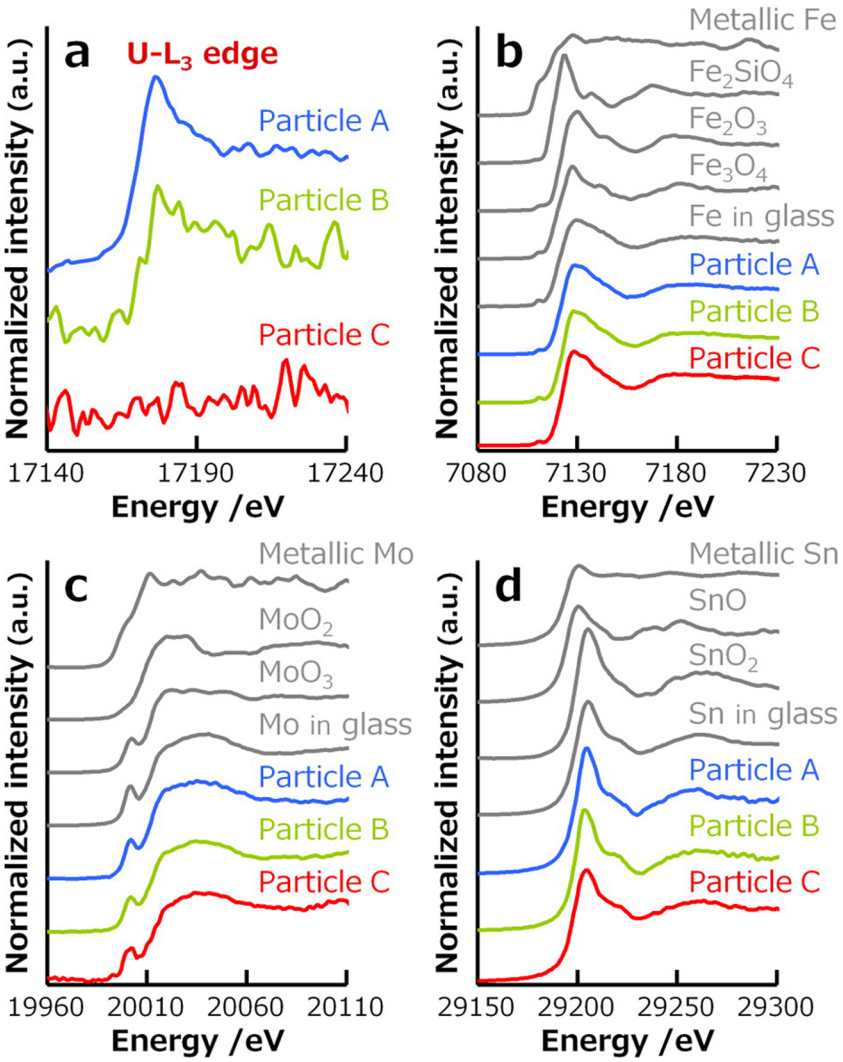

Fig. 8　(Color online) Results of SR-μ-XANES analyses. (a) Comparison of the U-L3 edge SR-μ-XANES spectra of the three radioactive particles demonstrating the presence of U in particles A and B. (b–d) Comparisons of the (b) Fe-K edge, (c) Mo-K edge, and (d) Sn-K edge SR-μ-XANES spectra of the three particles and the reference materials. Reprinted with permission from Fig. 3 of Abe *et al.* (2014). Copyright 2014 American Chemical Society.

がそのままの形態で環境中に存在すると考えられる。一方で，大気中で硫酸塩などのエアロゾルと混合したと考えられる水溶性セシウムも事故により放出され（Kaneyasu *et al.*, 2012），主に雨などによって地上に沈着したと考えられる。これらの水に溶ける放射性物質は，植物根からの吸収（梅村ほか，2015），土壌中の鉱物への吸着（Mukai *et al.*, 2014），河川や海洋へ流出（Yamashiki *et al.*, 2014），など不溶性放射性粒子とは異なった環境動態を示すことが推測される。これらの水溶性放射性物質は，極めて低い濃度で鉱物等に吸着されているため，上記に紹介した走査型電子顕微鏡での直接観察や，通常の化学分析では検出が非常に困難である。土壌や植物などの環境試料では，このような水に溶ける放射性粒子，溶けない放射性粒子の両方が混在して試料中の放射能強度や濃度を決定していると考えられる（例えばOhse *et al.*, 2015）。また，例えばつくば市に飛来した放射性粒子のうち，硝酸溶液に溶ける放射性セシウムの割合は，3月14–15日が70%程度であるのに対し，3月20–21日に飛来した試料はほぼ100%近く溶出することが知られており（Igarashi *et al.*, in press），炉からの放出タイミングの違いで異なった物理化学組成をもったと考えられる。そのため，事故時の放射性物質放出プロセスの理解と，どの日時に放出された放射性物質によって汚染された環境試料なのかを知ることが，その試料中に含まれる水溶性と非水溶性の放射性物質の割合を推定する

ために必要である。

7. 放射性粒子の物理化学特性を応用した研究の可能性

放射性粒子の物理化学特性の理解が進むことで，今後，放射性物質拡散の数値モデル，放射性物質による健康影響評価，また事故時の炉内事象推定に対する研究への応用の進展が期待される。

放射性物質の大気への飛散推定や，沈着後の環境中での中長期的に放射能が減少する時間スケールの見積もり等には，数値計算を使ったモデル予測が有効である。一方，事故当時の放射性物質の大気を通じた拡散過程にはいまだに十分理解されていない現象も多くあり，異なったシナリオをもとにした複数の数値計算結果を比較した結果にはばらつきがある（例えばKata-ta *et al.*, 2015）。そのため，観測とモデル結果を一致させることも困難である。数値モデルを使った拡散予測では，当時の気象条件や放射性物質の放出タイミングなどに加え，放射性物質の物理化学性状の理解がモデル精度向上に有効である（Adachi *et al.*, 2013）。例えば，放射性粒子の吸湿性は，それらがエアロゾルとして大気中を輸送されるとき雨によって大気から除去されるかどうかを決める重要な要素として放射性物質の大気寿命および沈着分布を決定する。また，粒子の大きさは重力沈降速度や輸送距離を決定する。

放射性物質が土壌等に沈着した後の数十年間に及ぶ中長期の挙動も，数値計算による予測が可能である。特に，土壌中での移行は，主に土壌鉱物との吸着や降水による溶脱，動植物による輸送などが考えられ，その推定には放射性物質の組成や水溶性などの情報が必要となる。

大気中に浮遊する微粒子の体内への取り込み効率や沈着部位の推定は，その粒子の大きさによって異なる（梶野ほか，2014）。例えば，10マイクロメートル前後の比較的大きな粒子は鼻やのどの粘膜に付着しやすく，それよりも小さな数十ナノメートルの粒子は肺の内部まで侵入しやすい。さらに小さな10ナノメートル以下の粒子は気管支に沈着しやすいといった特徴がある。また，粒子の水溶性は体内への取り込み効率や排出時間に大きな影響があると考えられる。これらの物理化学特性を考慮した放射性物質の健康影響については，今後も長期のモニタリングを必要とする重要な課題である。加えて，炉内から放出された放射性物質の特徴は，炉内での熱，圧力，共存する物質などの条件に応じて変化すると考えられる（Haste *et al.*, 2013）。よって，環境中に放出された放射性粒子の詳細な物理化学特性から逆に生成プロセスを推定することで，事故時に炉内がどのような状況であったかを推測する研究の進展も期待される。

8. 今後の研究課題

福島第一原子力発電所事故はその事故の詳細や放出された放射性物質の環境動態についていまだに十分理解されていない。そのため，水溶性放射物質の理解に加えて，本稿で紹介した不溶性の放射性粒子の詳細な分析を通じて，環境中に放出された放射性物質の拡散プロセス，長期的な環境からの移動速度予測などに対する理解が進むことが期待される。特に，大気エアロゾルとして放出された不溶性放射性粒子がどのように環境中に分布し，また挙動をしているかを理解するためにも，環境試料として簡易に採取可能な土壌試料中からの放射性粒子の検出，分析が求められる。今後，単離された放射性粒子に対して，地球化学分野で利用されるさまざまな機器分析を適用することで，汚染実態の理解を深めるとともに，炉内事象の理解に向けた地球化学，環境科学と原子炉工学などの複数の分野にまたがる共同研究が望まれる。また，放射性粒子の物理化学的理解を通じて，再飛散プロセスの理解，人体に取り込まれた際の健康影響に関する調査研究，効果的な除染方法の検討，除染作業で発生する汚染物質の量的軽減化等，学際的な研究課題の進展が期待される。

謝 辞

本稿は東京理科大学，阿部善也博士，気象研究所，五十嵐康人博士と議論し，貴重な意見をいただいた。また，本研究の一部は，研費新学術領域「福島原発事故により放出された放射性核種の環境動態に関する学際的研究」A01-02班（科研費番号24110003）の活動の一環として行った。ここに記して感謝いたします。

引 用 文 献

Abe, Y., Iizawa, Y., Terada, Y., Adachi, K., Igarashi, Y. and Nakai, I. (2014) Detection of uranium and chemical state analysis of individual radioactive microparticles emitted from the Fukushima nuclear accident using multiple synchrotron radiation X-ray analyses. *Analytical Chemistry*, **86**, 8521–8525.

Adachi, K., Kajino, M., Zaizen, Y. and Igarashi, Y. (2013) Emission of spherical cesium-bearing particles from an early stage of the Fukushima nuclear accident.

Scientific Reports, **3**, 2554.

Buesseler, K. O., Jayne, S. R., Fisher, N. S., Rypina, I. I., Baumann, H., Baumann, Z., Breier, C. F., Douglass, E. M., George, J., Macdonald, A. M., Miyamoto, H., Nishikawa, J., Pike, S. M. and Yoshida, S. (2012) Fukushima-derived radionuclides in the ocean and biota off Japan. *Proceedings of the National Academy of Sciences of the United States of America*, **109**, 5984–5988.

Chino, M., Nakayama, H., Nagai, H., Terada, H., Katata, G. and Yamazawa H. (2011) Preliminary estimation of release amounts of ^{131}I and ^{137}Cs accidentally discharged from the Fukushima Daiichi nuclear power plant into atmosphere. *Journal of Nuclear Science and Technology*, **48**, 1129–1134.

Christoudias, T. and Lelieveld, J. (2013) Modelling the global atmospheric transport and deposition of radionuclides from the Fukushima Dai-ichi nuclear accident. *Atmospheric Chemistry and Physics*, **13**, 1425–1438.

de Vismes Ott, A., Gurriaran, R., Cagnat, X. and Masson, O. (2013) Fission product activity ratios measured at trace level over France during the Fukushima accident. *Journal of Environmental Radioactivity*, **125**, 6–16.

Doi, T., Masumoto, K., Toyoda, A., Tanaka, A., Shibata, Y. and Hirose, K. (2013) Anthropogenic radionuclides in the atmosphere observed at Tsukuba: Characteristics of the radionuclides derived from Fukushima. *Journal of Environmental Radioactivity*, **122**, 55–62.

Fujii, K., Ikeda, S., Akama, A., Komatsu, M., Takahashi, M. and Kaneko, S. (2014) Vertical migration of radiocesium and clay mineral composition in five forest soils contaminated by the Fukushima nuclear accident. *Soil Science and Plant Nutrition*, **60**, 751–764.

Haste, T., Payot, F. and Bottomley, P. D. W. (2013) Transport and deposition in the Phébus FP circuit. *Annals of Nuclear Energy*, **61**, 102–121.

Hososhima, M. and Kaneyasu, N. (2015) Altitude-dependent distribution of ambient gamma dose rates in a mountainous area of Japan caused by the fukushima nuclear accident. *Environmental Science & Technology*, **49**, 3341–3348.

Igarashi, Y., Kajino, M., Zaizen, Y., Adachi, K. and Mikami, M., Atmospheric radioactivity over Tsukuba, Japan: A summary of three years of observations after the FDNPP accident, *Progress in Earth and Planetary Science*, doi: 10.1186/s40645-015-0066-1, *in press*.

Itoh, S., Eguchi, T., Kato, N. and Takahashi, S. (2014) Radioactive particles in soil, plant, and dust samples after the Fukushima nuclear accident. *Soil Science and Plant Nutrition*, **60**, 540–550.

梶野瑞王・五十嵐康人・藤谷雄二（2014）Fresh sootと，aged sootは，どちらが気道に沈着しやすいか：粒径分布と吸湿性の気管支・肺胞沈着率への影響．大気環境学会誌，**49**, 101–108.

Kaneyasu, N., Ohashi, H., Suzuki, F., Okuda, T. and Ikemori, F. (2012) Sulfate aerosol as a potential transport medium of radiocesium from the Fukushima nuclear accident. *Environmental Science & Technology*, **46**, 5720–5726.

Katata, G. *et al*. (2015) Detailed source term estimation of the atmospheric release for the Fukushima Daiichi Nuclear Power Station accident by coupling simulations of an atmospheric dispersion model with an improved deposition scheme and oceanic dispersion model. *Atmospheric Chemistry and Physics*, **15**, 1029–1070.

Kinoshita, N., Sueki, K., Sasa, K., Kitagawa, J., Ikarashi, S., Nishimura, T., Wong, Y. S., Satou, Y., Handa, K., Takahashi, T., Sato, M. and Yamagata, T. (2011) Assessment of individual radionuclide distributions from the Fukushima nuclear accident covering central-east Japan. *Proceedings of the National Academy of Sciences of the United States of America*, **108**, 19526–19529.

Masson, O. *et al*. (2011) Tracking of Airborne Radionuclides from the Damaged Fukushima Dai-Ichi Nuclear Reactors by European Networks. *Environmental Science & Technology*, **45**, 7670–7677.

箕輪はるか（2013）松竹梅の放射線を見る：イメージングプレートを使った解析．放射化学，**27**, 45–52.

Morino, Y., Ohara, T. and Nishizawa, M. (2011) Atmospheric behavior, deposition, and budget of radioactive materials from the Fukushima Daiichi nuclear power plant in March 2011. *Geophysical Research Letters*, **38**, L00G11, doi:10.1029/2011GL048689.

Mukai, H., Hatta, T., Kitazawa, H., Yamada, H., Yaita, T. and Kogure, T. (2014) Speciation of Radioactive Soil Particles in the Fukushima Contaminated Area by IP Autoradiography and Microanalyses. *Environmental Science & Technology*, **48**, 13053–13059.

Ohse, K., Kihou, N., Kurishima, K., Inoue, T. and Taniyama, I. (2015) Changes in concentrations of ^{131}I, ^{134}Cs and ^{137}Cs in leafy vegetables, soil and precipitation in Tsukuba city, Ibaraki, Japan, in the first 4 months after the Fukushima Daiichi nuclear power plant accident. *Soil Science and Plant Nutrition*, **61**, 225–229.

田中万也・坂口綾・岩谷北斗・高橋嘉夫（2013）福島第一原子力発電所事故由来の放射性セシウムの環境中での移行挙動とミクロスケールでの不均質性．放射化学，**27**, 12–19.

鶴田治雄・中島映至（2012）福島第一原子力発電所の事故により放出された放射性物質の大気中での動態．地球化学，**46**, 99–111.

Tsuruta, H., Oura, Y., Ebihara, M., Ohara, T. and Nakajima, T. (2014) First retrieval of hourly atmospheric radionuclides just after the Fukushima accident by analyzing filter-tapes of operational air pollution monitoring stations. *Scientific Reports*, **4**, 6717.

梅村光俊・金指努・杉浦佑樹・竹中千里（2015）福島県内のモウソウチク林における放射性セシウムの分布．日林誌，**97**, 44–50.

Yamashiki, Y., Onda, Y., Smith, H. G., Blake, W. H., Wakahara, T., Igarashi, Y., Matsuura, Y. and Yoshimura, K. (2014) Initial flux of sediment-associated radiocesium to the ocean from the largest river impacted by Fukushima Daiichi Nuclear Power Plant. *Scientific Reports*, **4**, 3714.

Yoshida, N. and Kanda, J. (2012) Tracking the Fukushima radionuclides. *Science*, **336**, 1115–1116.

Journal of the Meteorological Society of Japan, Vol. 93, No. 1, pp. 49−64, 2015
DOI:10.2151/jmsj.2015-002

Horizontal Resolution Dependence of Atmospheric Simulations of the Fukushima Nuclear Accident Using 15-km, 3-km, and 500-m Grid Models

Tsuyoshi T. SEKIYAMA, Masaru KUNII, Mizuo KAJINO, and Toshiki SHIMBORI

Meteorological Research Institute, Tsukuba, Japan

(Manuscript received 16 June 2014, in final form 1 October 2014)

Abstract

We investigated the horizontal resolution dependence of atmospheric radionuclide (Cs-137) simulations of the Fukushima nuclear accident on March 15, 2011. We used Eulerian and Lagrangian transport models with low- (15-km), medium- (3-km), and high- (500-m) resolutions; both models were driven by the same meteorological analysis that was prepared by our data assimilation system (NHM-LETKF) for each horizontal resolution. This preparation was necessary for the resolution-dependent investigation, excluding any interpolation or averaging of meteorological fields. In the results, the 15-km grid analysis could not reproduce Fukushima's mountainous topography in detail, and consequently failed to depict a complex wind structure over mountains and valleys. In reality, the Cs-137 plume emitted from the Fukushima Daiichi Nuclear Power Plant (FDNPP) was mostly blocked by Mt. Azuma and other mountains along the Naka-dori valley after crossing over Abukuma Mountains on March 15, 2011. However, the 15-km grid simulations could not represent the blockage of the Cs-137 plume, which unnaturally spread through the Naka-dori valley. In contrast, the 3-km and 500-m grid simulations produced very similar Cs-137 concentrations and depositions, and successfully produced the plume blockage and deposition along the Naka-dori valley. In conclusion, low-resolution (15-km grid or greater) atmospheric models should be avoided for assessing the Fukushima nuclear accident when a regional analysis is needed. Meanwhile, it is reasonable to use 3-km grid models instead of 500-m grid models due to their similarities and the high computational burden of 500-m grid model simulations.

Keywords model simulation; resolution dependence; data assimilation; Fukushima nuclear accident; cesium-137

1. Introduction

1.1 Atmospheric simulations of the Fukushima nuclear accident

The 2011 Tohoku earthquake occurred off the Pacific coast of Japan on March 11, 2011 and triggered tsunami waves, which caused severe disaster at the Fukushima Daiichi Nuclear Power Plant (FDNPP). The accident became the largest nuclear disaster since Chernobyl, and resulted in the dispersion and deposition of a large amount of radionuclides in the environment of eastern Japan. Since then many numerical simulations have been performed to predict or assess the effects of the nuclear accident using atmospheric chemistry transport models (e.g., Chino et al. 2011; Morino et al. 2011, 2013; Yasunari et al. 2011; Takemura et al. 2011; Schöppner et al. 2011; Sugiyama et al. 2012; Mathieu et al. 2012; Stohl et al. 2012; Katata et al. 2012a, b; Terada et al. 2012; Christoudias and Lelieveld 2013;

Corresponding author: Tsuyoshi Thomas Sekiyama, Atmospheric Environment and Applied Meteorology Research Department, Meteorological Research Institute, 1-1 Nagamine, Tsukuba, Ibaraki 305-0052 Japan
E-mail: tsekiyam@mri-jma.go.jp

Table 1. Spatial resolution of Fukushima radionuclide atmospheric simulation models with a global domain.

model	spatial resolution
Schöppner et al. (2011)	1° × 1° (≈ 90 km × 110 km)
Takemura et al. (2011)	0.56° × 0.56° (≈ 50 km × 60 km)
Yasunari et al. (2011)	1° × 1° (≈ 90 km × 110 km) [global domain]
	0.18° × 0.18° (≈ 16 km × 20 km) [regional domain]
Stohl et al. (2012)	0.5° × 0.5° (≈ 45 km × 55 km)
Mathieu et al. (2012)	0.5° × 0.5° (≈ 45 km × 55 km) [global domain]
	0.125° × 0.125° (≈ 11 km × 14 km) [regional domain]
Christoudias and Lelieveld (2013)	0.5° × 0.5° (≈ 45 km × 55 km)
Arnold et al. (2015)	0.2° × 0.2° (≈ 18 km × 22 km)
	0.5° × 0.5° (≈ 45 km × 55 km)

Table 2. Spatial resolution of Fukushima radionuclide atmospheric simulation models with a regional domain.

model	spatial resolution
Chino et al. (2011)	2 km × 2 km
	3 km × 3 km
Morino et al. (2011)	6 km × 6 km
Katata et al. (2012a, 2012b) and Terada et al. (2012)	9 km × 9 km
	3 km × 3 km
	1 km × 1 km
Sugiyama et al. (2012)	27 km × 27 km
	9 km × 9 km
	3 km × 3 km
	1 km × 1 km
Adachi et al. (2013)	3 km × 3 km
Morino et al. (2013)	3 km × 3 km
Hu et al. (2014)	3 km × 3 km
Saito et al. (2015)	5 km × 5 km

Adachi et al. 2013; Saito et al. 2015; Hu et al. 2014; Arnold et al. 2015). Some models were used to estimate the amount of radionuclides released from the FDNPP, coupled with a reverse analysis. Others were used to estimate the health damage to local residents or to investigate the meteorological causes of inhomogeneous radioactive contamination. Those models can be categorized into two types according to their domains: global and regional models. Global models have a large domain covering not only Japan but also America and Europe; however, their resolutions are not very fine compared with regional models. The horizontal resolutions of global models are approximately 50 km varying from 11 km to 110 km (Table 1). In contrast, regional models have a relatively finer resolution, but their domains often only cover eastern Japan. The horizontal resolutions of regional models are often 3 km, varying from 1 km to 9 km (Table 2). Incidentally, the atmospheric simulation models of the Chernobyl nuclear accident have often had lower resolutions, even when they were used with regional domains (Table 3). The lower model resolutions are most likely attributed to the topographical features of Chernobyl, which is located on very flat terrain. The nearest mountains are more than 500 km away from Chernobyl. It would be unnecessary to make the model resolution very high for continental-scale or very flat area simulations. However, it is unclear what resolution is good enough to regionally represent the advection and deposition of radionuclides in the case of Fukushima because Japan has a complex topography. More than 70% of the Japanese territory is mountainous. Small plains and basins are scattered throughout the remaining area where the population is concentrated. Fukushima is not an exception to the topographical complexity.

Table 3. Spatial resolution of Chernobyl radionuclide atmospheric simulation models.

model	spatial resolution
Bradt et al. (2002)	25 km × 25 km [outer domain] 5 km × 5 km [inner domain]
Davoine et al. (2007)	1.125° × 1.125° (≈ 110 km × 140 km)
Evangeliou et al. (2013)	2.5° × 1.27° (≈ 230 km × 140 km) [global domain] 0.66° × 0.51° (≈ 60 km × 55 km) [Europe domain]

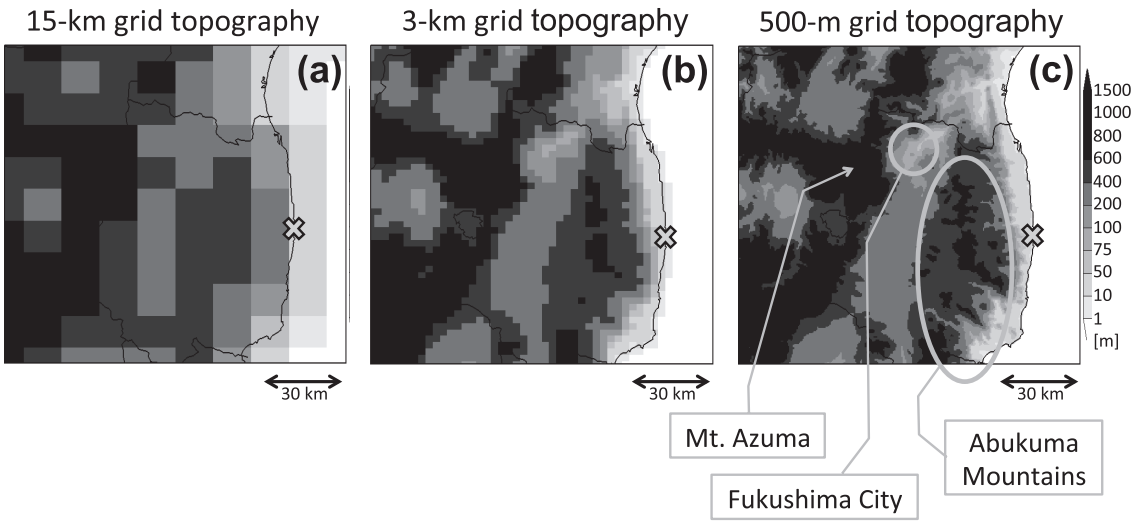

Fig. 1. Fukushima's topography depicted by the (a) 15-km, (b) 3-km, and (c) 500-m grid scales. The cross indicates the location of FDNPP. The Abukuma Mountains have peaks of approximately 1000 m. Fukushima City is located in a narrow basin 70 m above sea level (asl). Mt. Azuma has several peaks of which the highest is 2035 m asl.

1.2 Fukushima's topography

Fukushima is a mountainous region with few plains. FDNPP is located on the coastline of the Pacific Ocean, but the flat area around the power plant is very narrow (Fig. 1c). The Abukuma Mountains, which are as high as 1000 m, are located just behind the power plant; the distance between the FDNPP premises and Abukuma Mountain foothills is only a few kilometers. Fukushima City, the capital of Fukushima Prefecture, is situated beyond the mountain range; it is located in a long narrow basin that is approximately 70 km from FDNPP. Furthermore, 2000-m mountain peaks (Mt. Azuma) are seen just behind the city. These mountains and the basin are well depicted in Fig. 1c with a 500-m horizontal resolution grid. In contrast, it is difficult to recognize those features in Fig. 1a with a 15-km horizontal resolution grid. Fine structures, such as small valleys, are not depicted in Fig. 1b (3-km grid) compared with Fig. 1c (500-m grid), but the rough shapes of the mountains and basins are apparent in the 3-km and 500-m grid maps.

As mentioned above, the 3-km grid is the most popular horizontal resolution in the regional simulation models of the Fukushima nuclear accident (Table 2). However, it is not evident that the 3-km grid resolution can properly reproduce the advection and deposition of radionuclides associated with the FDNPP accident. On the other hand, the global simulation models of the FDNPP accident (Table 1) commonly use much lower resolutions than the 15-km grid scale that cannot depict Fukushima's complex topography in detail (Fig. 1a). Nevertheless, some researchers validated their global simulation results with domestic observations in Japan (e.g., Stohl et al. 2012) and investigated the health damage to local residents (e.g.,

Christoudias and Lelieveld 2013). If their simulations are accurate, then there is no need to use higher resolution models, because the computational burdens exponentially increase with finer model resolutions. However, the validity of using 15-km or lower resolutions for the regional assessment of the FDNPP accident has not been proven.

1.3 Objective

This study investigated whether the 3-km grid (representative of the regional model resolution) and 15-km grid (representative of the global model resolution) models adequately simulate the radioactive pollution of the FDNPP accident compared with a very high-resolution model (500-m grid). These simulations focused on Cs-137 radionuclides only because the available observations were spatially dispersed throughout Fukushima and its neighboring areas. To double-check the resolution dependence, we managed two types of chemistry transport models: the Eulerian and Lagrangian models. Both models were driven by the same meteorological analysis with 15-km, 3-km, and 500-m horizontal resolution grids. Eulerian models indirectly describe air motion by focusing on specific locations through which the air flows over time. Lagrangian models directly describe air motion by following an individual air parcel as it moves. Both models have advantages and disadvantages. For example, Eulerian models explicitly forecast radionuclide concentrations, and can implement chemical and physical processes in detail, but are not good at handling point source emissions. In contrast, Lagrangian models are good at handling point source emissions, but are susceptible to sampling noise when there are few Lagrangian particles.

In addition, we generally encounter difficulties in obtaining meteorological analyses with arbitrary horizontal resolutions. It is impossible for Lagrangian models to arbitrarily obtain a high- (low-) resolution analysis just by using simple interpolation (averaging) of the meteorological fields because the amount of information is not adequately increased (decreased enough) in the meteorological field by such simple calculation. Meanwhile, many Eulerian chemistry transport models are driven by the meteorological analysis calculated by their own dynamical module, wherein the meteorological field is nudged by another analysis with a different resolution. Consequently, the calculated meteorological analysis may be a mixture of the dynamical module simulation and another analysis with a different resolution. Therefore, we conducted the data assimilation to make the arbitrary-resolution analysis independent from other resolution models and analyses. The details of our data assimilation are described in Section 2.1. Then, the chemistry transport models are described in Sections 2.2 and 2.3. We present the results and discussion in Section 3, and the conclusion in Section 4.

2. Methodology

2.1 Preparation of meteorological analyses

Prior to calculating the radionuclide transport, we prepared meteorological analyses, which had three different horizontal resolutions, using a flow-dependent data assimilation system assembled and validated by Kunii (2013). This data assimilation system comprises the Japan Meteorological Agency's nonhydrostatic model (JMA-NHM) and the local ensemble transform Kalman filter (LETKF), which are together called NHM-LETKF. The system calculated all the necessary meteorological variables, which were stored every 10 min, to subsequently drive the radionuclide transport models. In this study, the horizontal resolutions were set to 15 km, 3 km, and 500 m. Here, a one-way nested data assimilation scheme was implemented, wherein the first guess of a lower resolution model is used as a boundary condition for finer-resolution model integration (Kunii 2013). The nested inner model runs independently from the outer coarse model, except for the boundary condition. We defined the 15-km resolution as the typical grid scale of high-resolution global simulations (cf. Table 1). The 3-km resolution was defined as the typical grid scale of regional simulations implemented for the FDNPP accident (cf. Table 2). The 500-m resolution was considered higher than that of any other Fukushima simulation models and was expected to depict Fukushima's complex topography.

The meteorological model JMA-NHM was developed by JMA (Saito et al. 2006, 2007) and has been used for government-operated weather forecasts. Operationally, JMA-NHM is initialized by the JMA non-hydrostatic-model four-dimensional variational data assimilation system (JNoVA, Honda et al. 2005). Most of the regional simulation models for the FDNPP accident use the JNoVA grid-point-value (GPV) data as the initial/boundary conditions or pseudo-observations (Chino et al. 2011; Morino et al. 2011, 2013; Katata et al. 2012a, b; Terada et al. 2012; Adachi et al. 2013; Draxler et al. 2015; Saito et al. 2015). In contrast, we calculated the meteorological analyses by running our own data assimilation system (NHM-LETKF) instead of using the JNoVA GPV. The data assimilation scheme LETKF

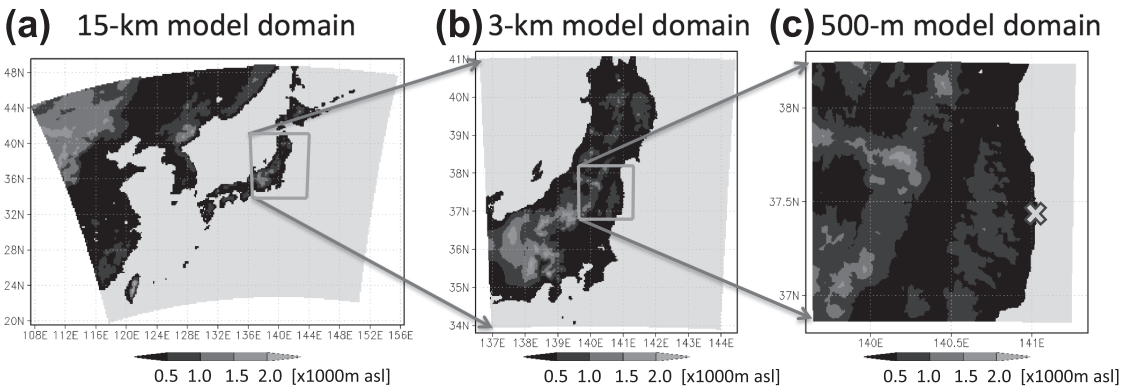

Fig. 2. NHM-LETKF model domains of the (a) 15-km, (b) 3-km, and (c) 500-m grid spacing analyses. The cross in panel (c) indicates the location of FDNPP.

is an ensemble Kalman filter (EnKF) implementation developed by Hunt et al. (2007). The application of EnKFs enables an evaluation of uncertainties of the analysis fields and leads to a probabilistic prediction through ensemble forecasting. LETKF has been applied to various simulations, such as weather forecast modeling (e.g., Miyoshi and Aranami 2006; Miyoshi and Yamane 2007; Miyoshi and Kunii 2012; Kunii and Miyoshi 2012; Kunii et al. 2012; Kunii 2013) and chemistry transport modeling (e.g., Sekiyama et al. 2010, 2011a, b; Kang et al. 2011; Miyazaki et al. 2012; Nakamura et al. 2013).

In this study, the 15-km grid spacing analysis was calculated by the outer NHM-LETKF, whose domain covered East Asia (Fig. 2a), and was initiated at 6:00 UTC March 9, 2011 with 20 ensemble members. This domain comprises 241 × 193 horizontal grid points on the Lambert conformal projection and 50 vertical levels up to approximately 22 km in the terrain-following hybrid vertical coordinates, which include 11 levels below 1 km but above ground level (agl). The horizontal coverage of this configuration is similar to that of the JNoVA system routinely operated by JMA. The initial and boundary conditions of the NHM-LETKF cycle were obtained from the JMA operational global prediction system. We added initial and lateral boundary perturbations derived from the JMA operational one-week ensemble prediction system to each ensemble member in accordance with Saito et al. (2012). The 15-km grid spacing JMA-NHM implemented a modified Kain–Fritsch convective parameterization scheme (Kain and Fritsch 1993) along with the 3-ice-bulk cloud microphysics (Lin et al. 1983). For the turbulence scheme, the improved Mellor–Yamada level 3 closure model (Nakanishi and Niino 2004, 2006) was implemented. This LETKF analyzed all the prognostic variables of JMA-NHM, i.e., wind components (u, v, w), temperature (T), pressure (p), water vapor mixing ratio (q_v), and water/ice microphysics variables. Here, LETKF employed an adaptive inflation scheme, which adaptively estimates the multiplicative inflation factors at each grid point (Miyoshi 2011; Miyoshi and Kunii 2012). The covariance localization parameters were set to 150 km in the horizontal, 0.2 ln p coordinate in the vertical, and 3 h in the time dimension. These localization parameters correspond to the length at which the Gaussian localization function becomes $e^{-0.5}$. The NHM-LETKF cycle was succeeded with a 6-h time interval, wherein the observation data were grouped into 1-h time slots and were four-dimensionally assimilated (Hunt et al. 2004). To assimilate the observation data, we used JMA's operational dataset, which was integrated and quality-controlled for the JNoVA mesoscale weather prediction like Kunii (2013). The JNoVA dataset contains observations acquired by radiosondes, weather observatories, pilot balloons, wind profilers, aircrafts, ships, buoys, and satellites. However, satellite radiances and radar precipitation analyses were not assimilated in this study because observation operators for these observations have not yet been installed in the NHM-LETKF system. Instead, we additionally assimilated surface wind observations acquired by the automated meteorological data acquisition system (AMeDAS) and Tokyo Electric Power

Company (TEPCO) monitoring posts. AMeDAS is a surface observation network managed by JMA. The network currently comprises approximately 1,300 stations throughout the country, which are laid out at average intervals of 17 km. The TEPCO monitoring posts are placed at FDNPP, and the Fukushima Dai-ni Nuclear Power Plant that is located to 12 km south of FDNPP. The monitoring post datasets are freely available to the public at the TEPCO website (http:// www.tepco.co.jp/nu/fukushima-np/index-j.html).

The 3-km grid spacing analysis was calculated by the nested NHM-LETKF, whose domain covered eastern Japan (Fig. 2b), and was initiated at 6:00 UTC March 10, 2011 with 20 ensemble members. This domain comprises 215 × 259 horizontal grid points in the Lambert conformal projection and 60 vertical levels up to approximately 22 km in the terrain-following hybrid vertical coordinate. The lateral boundary conditions were supplied from the outputs of the outer (15-km grid) NHM-LETKF cycle. Here, nearly the same configurations were implemented in both the 3-km grid spacing JMA-NHM and the 15-km simulation, but the convective parameterization scheme was not activated for the former. The covariance localization parameters were set to 50 km in the horizontal, 0.1 ln p coordinate in the vertical, and 3 h in the time dimension. The inner NHM-LETKF cycle was succeeded with a 3-h time interval, and its data assimilation was performed four-dimensionally. We used the same observation data (i.e., JNoVA, AMeDAS, and TEPCO datasets) that were used in the 15-km data assimilation. Furthermore, the 500-m grid spacing analysis was calculated by the second nested NHM-LETKF whose domain mostly covered Fukushima Prefecture (Fig. 2c) with 281 × 301 horizontal grid points in the Lambert conformal projection and 60 vertical levels up to approximately 22 km in the terrain-following hybrid vertical coordinate. In Fig. 2c, the location of the FDNPP is indicated with a cross along the coastline. The lateral boundary conditions were supplied from the outputs of the 3-km NHM-LETKF cycle. The covariance localization parameters were set to 25 km in the horizontal, 0.1 ln p coordinate in the vertical, and 3 h in the time dimension. Basically, the same configurations were implemented for the 500-m grid spacing JMA-NHM and the 3-km simulation. Moreover, the same observation data were assimilated during the second nested NHM-LETKF cycle. The triple-nested data assimilation experiments were conducted with horizontal resolutions of 15 km, 3 km, and 500 m.

To generate the terrain features in the computational domains of these 15-km, 3-km, and 500-m grid JMA-NHMs, we used the global digital elevation data with a horizontal grid spacing of 30 arc s (GTOPO30), which is approximately 900 m in the east–west direction and 700 m in the south–north direction, provided from the U.S. Geological Survey (https://lta.cr.usgs.gov/GTOPO30). For each domain, the GTOPO30 data was smoothed in the approximately 1.5 times coarser resolution of each model (i.e., 800 m for the 500-m grid model, 5 km for the 3-km grid model, and 25 km for the 15-km grid model). In general, this smoothing procedure is indispensable for meteorological model simulation to avoid the computational instability and error-amplification caused by precipitous terrains (= coordinate distortions). Figure 1 shows the terrains after the smoothening.

2.2 Eulerian transport model

We conducted Eulerian simulations using the Regional Air Quality Model 2 (RAQM2) that was originally developed to simulate Asian air quality and aerosol properties (Kajino et al. 2012). RAQM2 implements a Eulerian transport scheme and a triple-moment modal aerosol dynamics module. The aerosol dynamics, such as dry deposition, grid-scale rainout (cloud condensation nuclei and ice nuclei activations, and subsequent cloud microphysical processes), and washout (coagulation between aerosols and settling hydrometeors) processes, as well as advection, diffusion, sub-grid-scale convection/scavenging, and gravitational settling are calculated offline by coupling with meteorological models. In this study, RAQM2 was driven by the meteorological analyses with 15-km, 3-km, or 500-m resolutions prepared by NHM-LETKF. The analyses were taken into RAQM2 every 10 min and linearly interpolated within each 10-min interval. RAQM2 and NHM-LETKF shared the same model domain and horizontal grid resolution, but their vertical resolutions were converted from NHM-LETKF's 50 or 60 layers (expanded from the surface to approximately 22 km asl) to RAQM2's 20 layers (expanded from the surface to approximately 10 km asl). The radionuclide transport version of RAQM2 was developed for the Fukushima nuclear accident simulation (Adachi et al. 2013). This version of RAQM2 implements simplified aerosol dynamics compared with those of Kajino et al. (2012) by assuming aerosol hygroscopicity and perpetual particle size distribution; nucleation, condensation, and coagulation were not considered here. Still, we described the nature of the aerosol dynamics, such as

dry deposition and grid-scale rainout/washout (i.e., wet deposition) processes, based on the prescribed size distribution. Details of the dry and wet deposition processes are described in Sections 2.2.7 and 2.2.8 of Kajino et al. (2012), respectively. In this study, all the radioactive Cs-137 was contained in sulfate aerosol particles (mixed with organic compounds) when it was transported in the atmosphere. The particle size distribution of sulfate aerosols was assumed to be log-normal with a number equivalent geometric mean dry diameter = 0.5 μm, a geometric standard deviation = 1.6, a particle density = 1.83 g cm^{-3}, and a hygroscopicity = 0.4, assuming a sulfate–organic mixture. We used the emission scenario of the Cs-137 release from the FDNPP that was estimated by the Japan Atomic Energy Agency (JAEA) (cf. Chino et al. 2011; Katata et al. 2012a; Terada et al. 2012). Following the time series of the emission scenario, Cs-containing sulfate aerosols were injected into a grid cell above the FDNPP at every time step. The grid cell was assigned by the Cs-137 release height scenario estimated by JAEA that varied temporally from 20 m to 150 m agl.

2.3 Lagrangian transport model

We conducted Lagrangian simulations using the JMA operational regional atmospheric transport model (JMA-RATM) that was originally developed for volcanic ash fall forecasts (Shimbori et al. 2009, 2010). JMA-RATM uses a Lagrangian scheme (Iwasaki et al. 1998; Seino et al. 2004) and implements advection, horizontal and vertical diffusions, gravitational settling, dry deposition, and wet scavenging processes offline. The radionuclide transport version of JMA-RATM was developed by Saito et al. (2015) for the World Meteorological Organization (WMO) at the request of the United Nations Scientific Committee on the Effects of Atomic Radiation (UNSCEAR, Draxler et al. 2015). In this study, JMA-RATM was driven by the NHM-LETKF meteorological analyses with 15-km, 3-km, or 500-m resolutions. The analyses were taken into JMA-RATM every hour, and the vertical advection was calculated using a spatially averaged (9 grid cells) vertical velocity and was assumed to be terrain-following at the lowermost model layer. All the radioactive Cs-137 was assumed to be contained in sulfate aerosol particles when it was transported in the atmosphere.

For the wet deposition of Cs-containing aerosol particles, only a washout process (i.e., below-cloud scavenging) was considered, wherein the scavenging rate was set as $2.98 \times 10^{-5} \times P^{0.75}$ s^{-1} for liquid rain and $2.98 \times 10^{-5} \times P^{0.30}$ s^{-1} for solid snow; P is the surface precipitation intensity [mm h^{-1}]. The wet scavenging was applied under the height of approximately 1500 m asl. The dry deposition was simply computed by the deposition rate of 10^{-5} s^{-1} according to Sportisse (2007) and Draxler and Rolph (2012). For the gravitational settling, the particle size distribution of sulfate aerosols was assumed to be log-normal with a mean diameter of 1.0 μm, a standard deviation of 1.0, and a uniform particle density of 1.0 g cm^{-3}. The number of Lagrangian particles was set to a constant 100,000 per hour. The particles were uniformly emitted at the location of FDNPP from the ground surface to 100 m agl. After the model calculation, the hourly particle concentration and deposition outputs were multiplied by the hourly Cs-137 emission rate of JAEA (cf. Chino et al. 2011; Katata et al. 2012a; Terada et al. 2012) at the time of particles emission. Then, the multiplied values were summed at each grid point.

3. Results and discussion

3.1 Meteorology

In this study, we focused the simulation on March 15, 2011 (UTC) because we needed to investigate the radioactive plumes that outflowed landward. According to Morino et al. (2013), their standard experiment with the JAEA emission scenario indicates that most of the Cs-137 deposition over land (mainly in Fukushima Prefecture) occurred during the period from March 15 to 16 (Japanese Standard Time; JST) and accounts for 72 % of the total deposition over land between March 10, 2011 and April 20, 2011.

The comparison of the meteorological analyses of NHM-LETKF is shown in Figs. 3 and 4. It was either raining or snowing over eastern Japan on March 15, 2011, as depicted by the JMA Radar/rain gauge-Analyzed Precipitation (RAP) data in Fig. 3a. JMA operationally produces the RAP data by calibrating radar echo observations with 1-h accumulated rain gauge precipitation data (AMeDAS) throughout Japan. Figure 3a shows a 24-h accumulation of RAP interpolated onto 1-km grids on March 15, 2011 UTC. In general, the quantitative simulation of precipitation is difficult for models, compared with dynamical variables, such as wind, pressure, and temperature because precipitation involves a chemical phase transition. Nonetheless, the NHM-LETKF analyses (Figs. 3b, c, d) demonstrated good agreement with RAP in regard to synoptic-scale precipitation. Note that the 24-h accumulated precipitation of the 15-km, 3-km, and 500-m grid spacing analyses were very

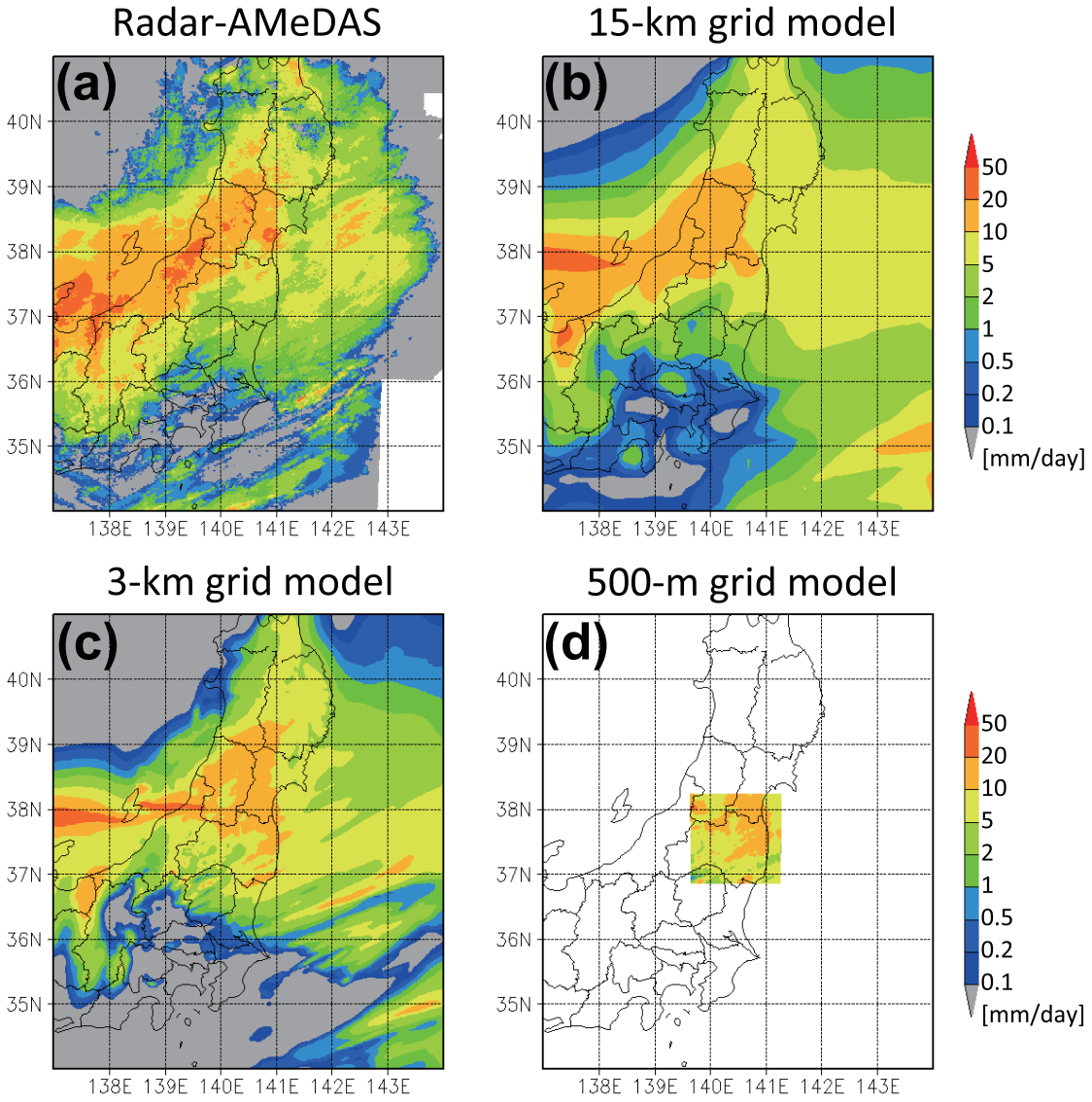

Fig. 3. Precipitation intensity [mm/day] accumulated from 00:00 UTC March 15 to 00:00 UTC March 16, 2011 derived from (a) the JMA RAP radar observations, (b) the outputs of the 15-km grid model JMA-NHM, (c) the outputs of the 3-km grid model JMA-NHM, and (d) the outputs of the 500-m grid model JMA-NHM.

similar. The difference among them was smaller than that between RAP and the simulated precipitation. This similarity suggests that there would not be a large difference in the wet deposition due to the precipitation distribution of each model resolution.

In contrast, there was a large difference among the analyses of the horizontal winds in the planetary boundary layer (PBL), as shown in Fig. 4. The wind direction and speed (10-min mean) in the lowermost layer (from the surface to 40 m agl) at 15:00 UTC March 15, 2011 is depicted. The three scenes of Fig. 4 project the same area, including the northern part of the Abukuma Mountains, FDNPP, and Fukushima City. At the two AMeDAS points that were located in Souma City near the coastline and Fukushima City in the Naka-dori valley, we compared the wind direc-

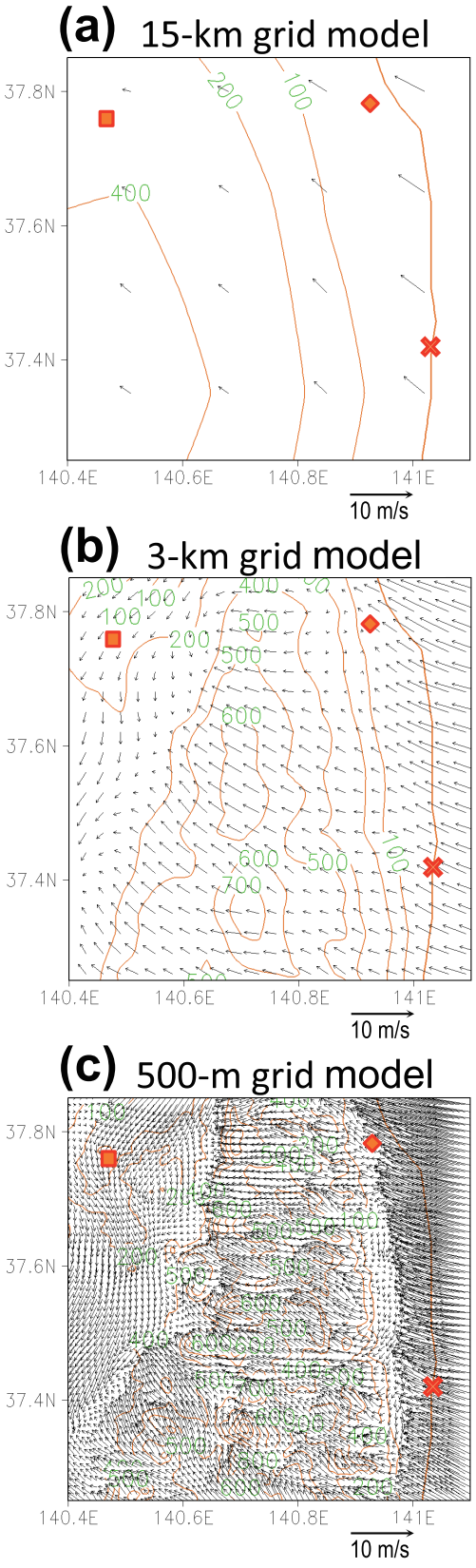

tions and speeds with the corresponding AMeDAS observations (Table 4). The 15-km analysis (Fig. 4a) did not adequately simulate the northerly winds around Fukushima City along the Naka-dori valley because the model could not represent the Abukuma Mountains or the Naka-dori valley. As shown in Table 4, the wind direction of the 15-km grid analysis at Fukushima City was completely different from the corresponding observations that were consistent with the 3-km and 500-m grid analyses. For transport simulations, it was important that the wind direction was southerly or northerly in Fukushima City, because the Naka-dori valley is oriented in the north–south direction. Between the 3-km (Fig. 4b) and 500-m (Fig. 4c) grid analyses, the wind fields were roughly similar, although only the 500-m grid analysis depicted a fine wind structure over the mountains and valleys. When the wind blows in the east–west direction at the Naka-dori valley, the 15-km grid analysis performs reasonably in some situations. Indeed, the predominant wind direction was often westerly in the period between March 14 and 16, 2011 except the afternoon of March 15, in Fukushima City. During that period the 15-km grid analysis was sometimes consistent with the 3-km and 500-m grid analyses; however, the land contamination did not occur when the wind direction was westerly. Furthermore, while there was a large dependence of the PBL wind field on the spatial resolution, there was little difference in the free-tropospheric winds among the 15-km, 3-km, and 500-m grid analyses (not shown). These features are consistent with the previous study (Takemi 2013) that compared local-scale wind fields over Eastern Fukushima in March 2011 between 2-km and 400-m grid models. In the case of the FDNPP accident, the radionuclide release height was estimated to be low (20–150 m agl; Chino et al. 2011; Katata et al. 2012a; Terada et al. 2012); also winter is responsible for the

Fig. 4. Surface wind direction and speed (10-min mean) in the northern area of the Abukuma Mountains, Fukushima, at 15:00 UTC March 15, 2011 as simulated by the (a) 15-km grid model JMA-NHM, (b) 3-km grid model JMA-NHM, and (c) 500-m grid model JMA-NHM. The orange lines depict the contours of altitude. The cross indicates the location of FDNPP. The diamond symbol indicates the location of the AMeDAS Souma observatory, and the square symbol indicates the location of the AMeDAS Fukushima City observatory (cf. Table 4). Note that the wind vectors of the 500-m grid model are drawn for every other grid point.

Table 4. Surface wind direction and speed (10-min mean) of AMeDAS and model simulations at Souma observatory and Fukushima City observatory on 15:00 UTC March 15, 2011.

	AMeDAS	15-km model	3-km model	500-m model
Souma	SW 1.0 m s^{-1}	ESE 3.6 m s^{-1}	SE 1.6 m s^{-1}	SE 1.2 m s^{-1}
Fukushima City	NNE 0.6 m s^{-1}	ESE 1.4 m s^{-1}	NE 1.6 m s^{-1}	N 1.6 m s^{-1}

relatively stable PBL. Considering these factors, the resolution dependence of the PBL wind field is likely to cause a large difference in the advection of the radioactive plumes between the 15-km simulation and the other simulations.

3.2 Surface concentration of Cs-137

According to the TEPCO monitoring post data, the northerly wind in the vicinity of FDNPP gradually shifted clockwise to a southeasterly wind between 6:00 JST (21:00 UTC the day before) and 12:00 JST (3:00 UTC) on March 15, 2011. Then, the southeasterly wind continued for more than 10 h and flowed from FDNPP on the coastline to an inland area. During that time, the radioactive plume is supposed to sweep across Fukushima and the neighboring prefectures. The simulation results of this dispersal is shown in Fig. 5, which illustrates the 24-h averaged Cs-137 concentrations in the lowermost layer (from the surface to 40 m agl) between 00:00 UTC on March 15 and 00:00 UTC on March 16.

Looking at the 3-km (Fig. 5b) and 500-m (Fig. 5c) grid Eulerian simulations, the Cs-137 distributions agreed well. The Cs-137 plume crossed over the Abukuma Mountains, and was mostly blocked by Mt. Azuma and other mountains along the Naka-dori valley. However, the 15-km grid Eulerian simulation (Fig. 5a) did not represent the blockage of the Cs-137 plume, which broadly spread out through the Naka-dori valley as far as Yamagata Prefecture. As expected by the PBL wind errors, the 15-km grid transport simulation behaved unnaturally. Similar characteristics were also observed in the Lagrangian simulation results. The 15-km grid Lagrangian simulation (Fig. 5d) behaved completely differently from the 3-km (Fig. 5e) and 500-m (Fig. 5f) grid Lagrangian simulations. Similar to the Eulerian simulations, the 3-km and 500-m grid Lagrangian simulations agreed well; the blockage of the Cs-137 plume was successfully reproduced along the Naka-dori valley. In addition, the 15-km grid Lagrangian simulation (Fig. 5d) had a very similar Cs-137 distribution to that of the Eulerian simulation with the same grid resolution (Fig. 5a); however, their concentrations were quantitatively different. This similarity was not expected because Eulerian models are generally not good at handling point-source-emissions compared with Lagrangian models.

An analogous diagnosis can be obtained by the calculation of the absolute spatial correlation coefficients among the 15-km, 3-km, and 500-m grid Cs-137 distributions (Table 5). All the correlations were calculated within the area of the 500-m grid model domain using the concentration values illustrated in Fig. 5. The values were used without logarithmic transformation. Both Eulerian and Lagrangian simulations presented high correlations between the 3-km and 500-m grid distributions (0.90–0.85). In contrast, there was a relatively low correlation between the 15-km and 500-m grid simulations (0.64–0.65), and between the 15-km and 3-km grid simulations (0.75–0.78).

3.3 Deposition of Cs-137

The Japanese government has conducted aerial surveys since the nuclear accident to measure cesium deposition amounts on the ground over the entire area of eastern Japan with JAEA (Torii et al. 2012), as shown in Fig. 6. Note that this deposition represents all of the cesium emissions from the FDNPP accident until the autumn of 2011. However, as mentioned above, most of the Cs-137 deposition over land (especially in Fukushima) occurred only on March 15, 2011. Therefore, it is possible to validate the simulation results of March 15, 2011, whether they are plausible or not, by comparing them with the aerial observations of the accumulated deposition. In fact, Fig. 6 clearly illustrates the northwestward-flowing Cs-137 pollution emitted from FDNPP and its blockage by the mountains along the Naka-dori valley. The model results of the one-day accumulated deposition of Cs-137 on March 15, 2011 UTC are shown in Fig. 7.

In both the 15-km grid Eulerian (Fig. 7a) and Lagrangian (Fig. 7d) model results, a highly polluted

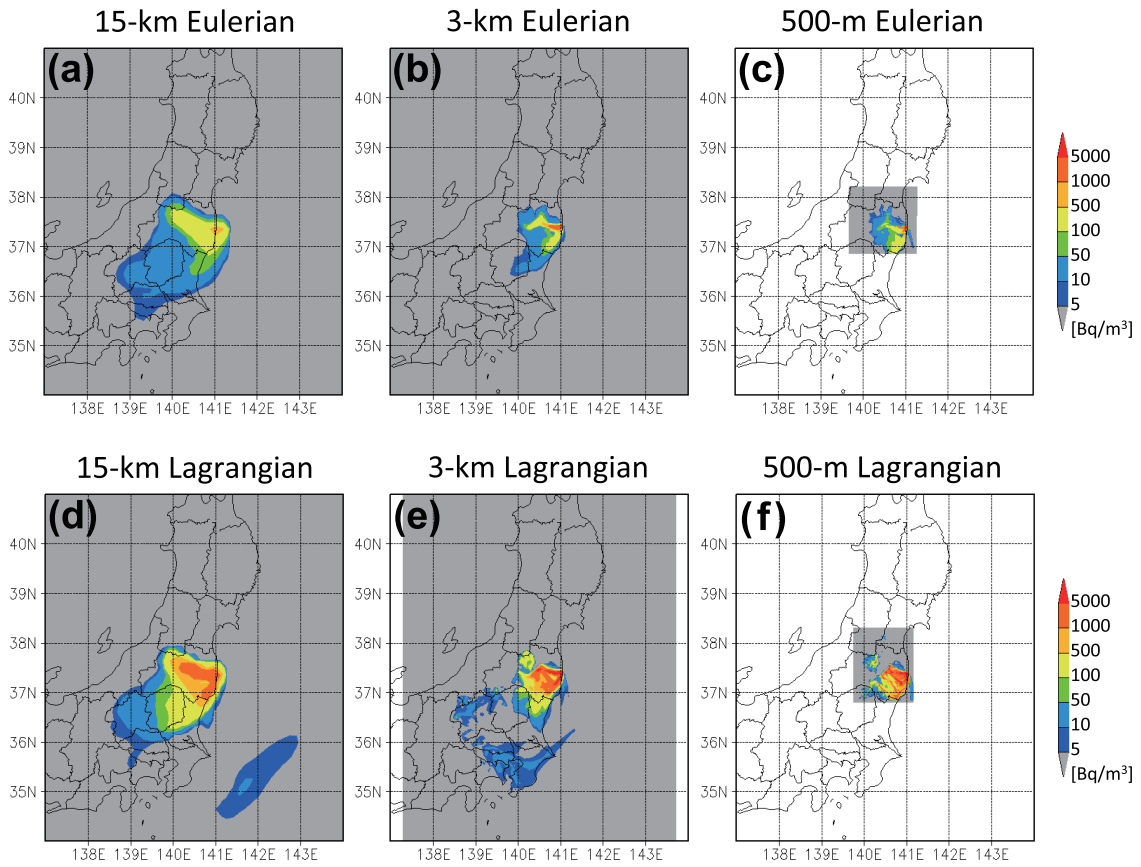

Fig. 5. Surface Cs-137 concentration averaged from 00:00 UTC March 15 to 00:00 UTC March 16, 2011 as simulated by the Eulerian model RAQM2 with the (a) 15-km grid spacing meteorological analysis, (b) 3-km grid spacing meteorological analysis, and (c) 500-m grid spacing analysis. The same as simulated by the RAQM2, but simulated by the Lagrangian model JMA-RATM with the (d) 15-km grid spacing meteorological analysis, (e) 3-km grid spacing meteorological analysis, and (f) 500-m grid spacing analysis.

Table 5. Horizontal distribution correlations of the surface Cs-137 concentrations as simulated by the models.

	15-km grid ↔ 3-km grid	3-km grid ↔ 500-m grid	500-m grid ↔ 15-km grid
Eulerian models	0.75	0.9	0.64
Lagrangian models	0.78	0.85	0.65

area broadly extended beyond Mt. Azuma and the other mountains through the Naka-dori valley as far as Yamagata and Niigata Prefectures. This distribution is similar to that of the surface concentrations shown in Figs. 5a and 5d. In addition, the most polluted area was not located near FDNPP but in the vicinity of the inland border between Fukushima and Yamagata Prefectures. This unrealistic pollution was caused by the wet deposition of the Cs-137 plume that passed over the mountains beyond the Naka-dori valley and intercepted a heavy precipitation area (cf., Fig. 3b). This pollution hotspot does not exist in the aerial observations (Fig. 6), but Arnold et al. (2015) also reported similar inland pollution with their simulation using a 0.2° (≈ 20 km) model resolution. This pollution might be a common characteristic of low-resolution models. In contrast, both the 3-km (Figs. 7b, e) and 500-m (Figs. 7c, f) grid models

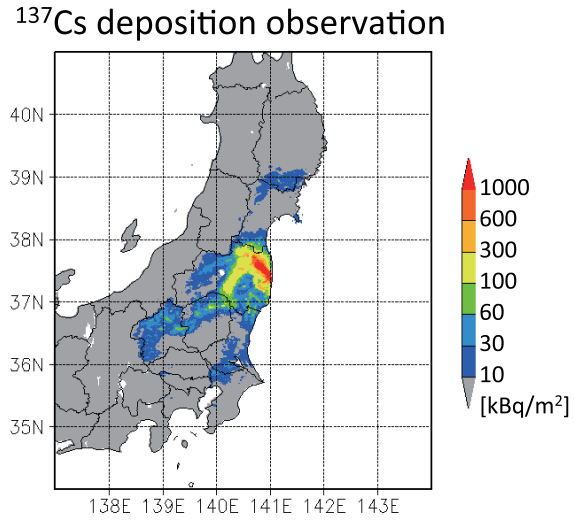

Fig. 6. Measured Cs-137 deposition based on aerial sampling, which was conducted by the Japanese government (Torii et al. 2012). Note that this deposition represents all of the Cs-137 emissions from the FDNPP until the autumn of 2011.

limited the heavily polluted area to mostly within eastern Fukushima near FDNPP and did not produce an unrealistic deposition in comparison with the aerial observations. However, there was a large discrepancy in the distribution and strength of Cs-137 deposition between the Eulerian and Lagrangian simulations. This discrepancy was caused by the difference of dynamical and physical processes in the aerosol models, such as the treatment of rainout and washout, which should be examined in a future study. The correlation coefficients among the simulated Cs-137 deposition distributions presented a good agreement between the 3-km and 500-m grid simulations, and a very poor agreement between the 15-km and 500-m grid simulations (Table 6). The correlations were calculated in the same way as in Table 5. The coefficient of the 3-km and 500-m Eulerian (Lagrangian) model simulations was 0.84 (0.63), while the coefficient was 0.42 (0.27) for the 15-km and 500-m simulations and 0.54 (0.54) for the 15-km and 3-km simulations. This result indicated that a 3-km grid model could be alternated with a 500-m grid model, but it was unacceptable to use a 15-km grid model instead of a 500-m grid model.

4. Conclusion

We investigated the horizontal resolution dependence of atmospheric radionuclide simulations of the Fukushima nuclear accident on March 15, 2011. We used Eulerian and Lagrangian transport models with low- (15-km), medium- (3-km), and high- (500-m) resolutions. Both Eulerian and Lagrangian models were driven by the same meteorological analysis that was independently prepared by an EnKF data assimilation system using the JMA operational weather forecast model. This independent preparation of each resolution analysis was definitely necessary for the resolution-dependence investigation, excluding any interpolation or averaging of meteorological fields.

Regarding the meteorological analyses, there was a large difference in the PBL wind field between the 15-km grid resolution and the other grid resolutions. The 15-km grid analysis could not reproduce Fukushima's mountainous topography in detail. Consequently, it failed to depict a complex wind structure over mountains and valleys. This error in the wind field caused a large difference in the radionuclide transport and deposition simulations. In reality, the Cs-137 plume emitted from FDNPP was mostly blocked by Mt. Azuma and other mountains along the Naka-dori valley after crossing over the Abukuma Mountains. However, the 15-km grid simulations did not represent the blockage of the Cs-137 plume, which unnaturally spread through the Naka-dori valley. In contrast, the 3-km and 500-m grid simulations successfully replicated the Cs-137 plume blockage along the Naka-dori valley. The 3-km and 500-m grid simulations produced very similar Cs-137 surface concentrations and deposition distributions. Notably, the Eulerian and Lagrangian models qualitatively behaved in the same manner, but quantitatively yielded different results, although they were driven by the same meteorological analysis. This was most likely because these two models had completely different aerosol physics (cf. sensitivity studies conducted by Draxler et al. 2015; Morino et al. 2013; Hu et al. 2014) and vertical advection handling at the lowermost model layer.

In conclusion, we suggest that it is illogical to use low-resolution (15-km or more grid) atmospheric models to assess the Fukushima nuclear accident when a regional analysis is needed due to the unrealistic performance of the 15-km grid simulations in the local Fukushima area. Meanwhile, it is reasonable to use 3-km grid models instead of 500-m grid models due to the similarities between the 3-km and 500-m grid simulations and the high computational

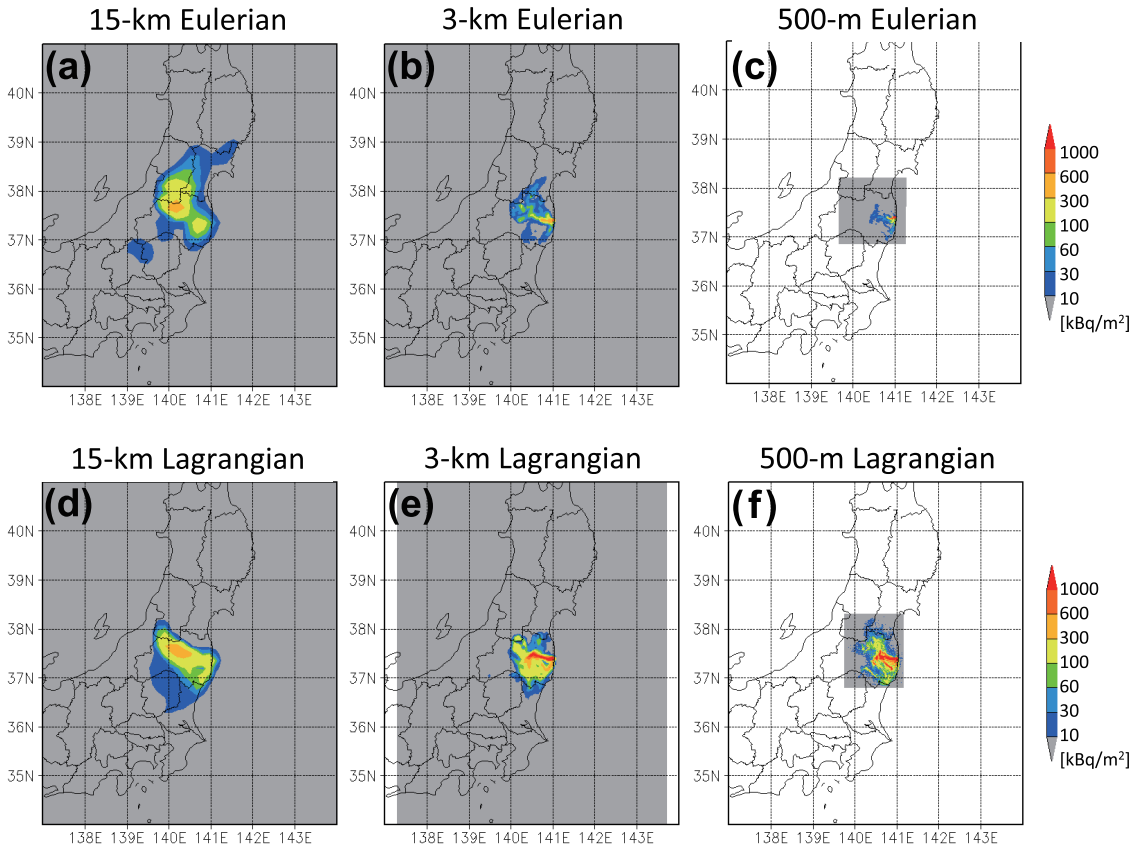

Fig. 7. Total deposition of Cs-137 accumulated from 00:00 UTC March 15 to 00:00 UTC March 16, 2011 as simulated by the Eulerian model RAQM2 with the (a) 15-km grid spacing meteorological analysis, (b) 3-km grid spacing meteorological analysis, and (c) 500-m grid spacing analysis. The same as simulated by the RAQM2, but simulated by the Lagrangian model JMA-RATM with the (d) 15-km grid spacing meteorological analysis, (e) 3-km grid spacing meteorological analysis, and (f) 500-m grid spacing analysis.

Table 6. Horizontal distribution correlations of the Cs-137 depositions as simulated by the models.

	15-km grid ↔ 3-km grid	3-km grid ↔ 500-m grid	500-m grid ↔ 15-km grid
Eulerian models	0.54	0.84	0.42
Lagrangian models	0.54	0.63	0.27

burden of 500-m grid simulations. In general, a 500-m grid simulation requires more than 200 times as many CPU resources as a 3-km grid simulation. Therefore, after ensuring the computational resources to perform a 3-km grid Fukushima simulation, other resources should be allotted for performing ensemble analysis or high-quality data assimilation. However, it is noted that the Fukushima nuclear accident occurred during winter, and a different resolution-dependence would have been found if the accident had occurred in another season.

Acknowledgments

We are grateful to Dr. K. Saito (MRI) and Prof. T. Iwasaki (Tohoku University) for their help and encouragement. We thank Dr. M. Chino (JAEA) for providing the emission inventory data and Dr. T. Torii (JAEA) for providing the aerial survey data.

This study was supported by JSPS KAKENHI Grant Number 24340115 and MEXT KAKENHI Grant Number 24110003.

References

Adachi, K., M. Kajino, Y. Zaizen, and Y. Igarashi, 2013: Emission of spherical cesium-bearing particles from an early stage of the Fukushima nuclear accident. *Sci. Rep.*, **3**, 2554, doi:10.1038/srep02554.

Arnold, D., C. Maurer, G. Wotawa, R. Draxler, K. Saito, and P. Seibert, 2015: Influence of the meteorological input on the atmospheric transport modelling with FLEXPART of radionuclides from the Fukushima Daiichi nuclear accident. *J. Environ. Radioact.*, **139**, 212–225.

Brandt, J., J. H. Christensen, and L. M. Frohn, 2002: Modelling transport and deposition of caesium and iodine from the Chernobyl accident using the DREAM model. *Atmos. Chem. Phys.*, **2**, 397–417.

Chino, M., H. Nakayama, H. Nagai, H. Terada, G. Katata, and H. Yamazawa, 2011: Preliminary estimation of release amounts of ^{131}I and ^{137}Cs accidentally discharged from the Fukushima Daiichi Nuclear Power Plant into the atmosphere. *J. Nucl. Sci. Technol.*, **48**, 1129–1134.

Christoudias, T., and J. Lelieveld, 2013: Modelling the global atmospheric transport and deposition of radionuclides from the Fukushima Dai-ichi nuclear accident. *Atmos. Chem. Phys.*, **13**, 1425–1438.

Davoine, X., and M. Bocquet, 2007: Inverse modelling-based reconstruction of the Chernobyl source term available for long-range transport. *Atmos. Chem. Phys.*, **7**, 1549–1564.

Draxler, R., and G. Rolph, 2012: Evaluation of the Transfer Coefficient Matrix (TCM) approach to model the atmospheric radionuclide air concentrations from Fukushima. *J. Geophys. Res.*, **117**, D05107, doi:10.1029/2011JD017205.

Draxler, R., D. Arnold, M. Chino, S. Galmarini, M. Hort, A. Jones, S. Leadbetter, A. Malo, C. Maurer, G. Rolph, K. Saito, R. Servranckx, T. Shimbori, E. Solazzo, and G. Wotawa, 2015: World Meteorological Organization's model simulations of the radionuclide dispersion and deposition from the Fukushima Daiichi nuclear power plant accident. *J. Environ. Radioact.*, **139**, 172–184.

Evangeliou, N., Y. Balkanski, A. Cozic, and A. P. Møller, 2013: Simulations of the transport and deposition of ^{137}Cs over Europe after the Chernobyl Nuclear Power Plant accident: Influence of varying emission-altitude and model horizontal and vertical resolution. *Atmos. Chem. Phys.*, **13**, 7183–7198.

Honda, Y., M. Nishijima, K. Koizumi, Y. Ohta, K. Tamiya, T. Kawabata, and T. Tsuyuki, 2005: A pre-operational variational data assimilation system for a non-hydrostatic model at the Japan Meteorological Agency: Formulation and preliminary results. *Quart. J. Roy. Meteor. Soc.*, **131**, 3465–3475.

Hu, X., D. Li, H. Huang, S. Shen, and E. Bou-Zeid, 2014: Modeling and sensitivity analysis of transport and deposition of radionuclides from the Fukushima Daiichi accident. *Atmos. Chem. Phys.*, **14**, 11065–11092.

Hunt, B. R., E. J. Kostelich, and I. Szunyogh, 2004: Four-dimensional ensemble Kalman filtering. *Tellus A*, **56**, 273–277.

Hunt, B. R., E. J. Kostelich, and I. Szunyogh, 2007: Efficient data assimilation for spatiotemporal chaos: A local ensemble transform Kalman filter. *Physica D*, **230**, 112–126.

Iwasaki, T., T. Maki, and K. Katayama, 1998: Tracer transport model at Japan Meteorological Agency and its application to the ETEX data. *Atmos. Environ.*, **32**, 4285–4295.

Kain, J., and J. Fritsch, 1993: Convective parameterization for mesoscale models: The Kain–Fritsch scheme. *The Representation of Cumulus Convection in Numerical Models*. *Meteor. Monogr.*, **46**, 165–170.

Kajino, M., Y. Inomata, K. Sato, H. Ueda, Z. Han, J. An, G. Katata, M. Deushi, T. Maki, N. Oshima, J. Kurokawa, T. Ohara, A. Takami, and S. Hatakeyama, 2012: Development of the RAQM2 aerosol chemical transport model and predictions of the Northeast Asian aerosol mass, size, chemistry, and mixing type. *Atmos. Chem. Phys.*, **12**, 11833–11856.

Kang, J. S., E. Kalnay, J. Liu, I. Fung, T. Miyoshi, and K. Ide, 2011: "Variable localization" in an ensemble Kalman filter: Application to the carbon cycle data assimilation. *J. Geophys. Res.*, **116**, D09110, doi:10.1029/2010JD014673.

Katata, G., M. Ota, H. Terada, M. Chino, and H. Nagai, 2012a: Atmospheric discharge and dispersion of radionuclides during the Fukushima Dai-ichi nuclear power plant accident. Part I: Source term estimation and local-scale atmospheric dispersion in early phase of the accident. *J. Environ. Radioact.*, **109**, 103–113.

Katata, G., H. Terada, H. Nagai, and M. Chino, 2012b: Numerical reconstruction of high dose rate zones due to the Fukushima Dai-ichi nuclear power plant accident. *J. Environ. Radioact.*, **111**, 2–12.

Kunii, M., T. Miyoshi, and E. Kalnay, 2012: Estimating the impact of real observations in regional numerical weather prediction using an ensemble Kalman filter. *Mon. Wea. Rev.*, **140**, 1975–1987.

Kunii, M., and T. Miyoshi, 2012: Including uncertainties of sea surface temperature in an ensemble Kalman filter: A case study of Typhoon Sinlaku (2008). *Wea. Forecasting*, **27**, 1586–1597.

Kunii, M., 2013: Mesoscale data assimilation for a local severe rainfall event with the NHM-LETKF system. *Wea. Forecasting*, 1586–1597.

Lin, Y. L., R. D. Farley, and H. D. Orville, 1983: Bulk parameterization of the snow fields in a cloud model. *J. Climate Appl. Meteor.*, **22**, 1065–1092.

Makihara, Y., N. Uekiyo, A. Tabata, and Y. Abe, 1996: Accuracy of Radar-AMeDAS Precipitation. *IEICE Trans. Communications*, **79**, 751–762.

Mathieu, A., I. Korsakissok, D. Quélo, J. Groëll, M. Tombette, D. Didier, E. Quentric, O. Saunier, J.-P. Benoit, and O. Isnard, 2012: Atmospheric dispersion and deposition of radionuclides from the Fukushima Daiichi nuclear power plant accident. *Elements*, **8**, 195–200.

Miyazaki, K., H. J. Eskes, K. Sudo, M. Takigawa, M. van Weele, and K. F. Boersma, 2012: Simultaneous assimilation of satellite NO_2, O_3, CO, and HNO_3 data for the analysis of tropospheric chemical composition and emissions. *Atmos. Chem. Phys.*, **12**, 9545–9579.

Miyoshi, T., and K. Aranami, 2006: Applying a four-dimensional local ensemble transform Kalman filter (4D-LETKF) to the JMA nonhydrostatic model (NHM). *SOLA*, **2**, 128–131.

Miyoshi, T., and S. Yamane, 2007: Local ensemble transform Kalman filtering with an AGCM at a T159/L48 resolution. *Mon. Wea. Rev.*, **135**, 3841–3861.

Miyoshi, T., 2011: The Gaussian approach to adaptive covariance inflation and its implementation with the local ensemble transform Kalman filter. *Mon. Wea. Rev.*, **139**, 1519–1535.

Miyoshi, T., and M. Kunii, 2012: The local ensemble transform Kalman filter with the Weather research and forecast model: Experiments with real observations. *Pure. Appl. Geophys.*, **169**, 321–333.

Morino, Y., T. Ohara, and M. Nishizawa, 2011: Atmospheric behavior, deposition, and budget of radioactive materials from the Fukushima Daiichi nuclear power plant in March 2011. *Geophys. Res. Lett.*, **38**, L00G11, doi:10.1029/2011GL048689.

Morino, Y., T. Ohara, M. Watanabe, S. Hayashi, and M. Nishizawa, 2013: Episode analysis of deposition of radiocesium from the Fukushima Daiichi nuclear power plant accident. *Environ. Sci. Technol.*, **47**, 2314–2322.

Nakamura, T., H. Akiyoshi, M. Deushi, K. Miyazaki, C. Kobayashi, K. Shibata, and T. Iwasaki, 2013: A multi-model comparison of stratospheric ozone data assimilation based on an ensemble Kalman filter approach. *J. Geophys. Res.*, **118**, 3848–3868.

Nakanishi, M., and H. Niino, 2004: An improved Mellor-Yamada level 3 model with condensation physics: its design and verification. *Bound.-Layer Meteor.*, **112**, 1–31.

Nakanishi, M., and H. Niino, 2006: An improved Mellor-Yamada level-3 model: Its numerical stability and application to a regional prediction of advection fog. *Bound.-Layer Meteor.*, **119**, 397–407.

Rojas-Palma, C., H. Madsen, F. Gering, R. Puch, C. Turcanu, P. Astrup, H. Müller, K. Richter, M. Zheleznyak, D. Treebushny, M. Kolomeev, D. Kamaev, and H. Wynn, 2003: Data assimilation in the decision support system RODOS. *Radiat. Prot. Dosim.*, **104**, 31–40.

Saito, K., T. Fujita, Y. Yamada, J. Ishida, Y. Kumagai, K. Aranami, S. Ohmori, R. Nagasawa, S. Kumagai, C. Muroi, T. Kato, H. Eito, and Y. Yamazaki, 2006: The operational JMA nonhydrostatic mesoscale model. *Mon. Wea. Rev.*, **134**, 1266–1298.

Saito, K., J. Ishida, K. Aranami, T. Hara, T. Segawa, M. Narita, and Y. Honda, 2007: Nonhydrostatic atmospheric models operational development at JMA. *J. Meteor. Soc. Japan*, **85B**, 271–304.

Saito, K., H. Seko, M. Kunii, and T. Miyoshi, 2012: Effect of lateral boundary perturbations on the breeding method and the local ensemble transform Kalman filter for mesoscale ensemble prediction. *Tellus A*, **64**, 11594, doi:10.3402/tellusa.v64i0.11594.

Saito, K., T. Shimbori, and R. Draxler, 2015: JMA's regional atmospheric transport model calculations for the WMO technical task team on meteorological analyses for Fukushima Daiichi nuclear power plant accident. *J. Environ. Radioact.*, **139**, 185–199.

Schöppner, M., W. Plastino, P. P. Povinec, G. Wotawa, F. Bella, A. Budano, M. De Vincenzi, and F. Ruggieri, 2011: Estimation of the time-dependent radioactive source-term from the Fukushima nuclear power plant accident using atmospheric transport modelling. *J. Environ. Radioact.*, **114**, 10–14.

Seino, N., H. Sasaki, J. Sato, and M. Chiba, 2004: High-resolution simulation of volcanic sulfur dioxide dispersion over the Miyake Island. *Atmos. Environ*., **38**, 7073–7081.

Sekiyama, T. T., T. Y. Tanaka, A. Shimizu, and T. Miyoshi, 2010: Data assimilation of CALIPSO aerosol observations. *Atmos. Chem. Phys.*, **10**, 39–49.

Sekiyama, T. T., M. Deushi, and T. Miyoshi, 2011a: Operation-oriented ensemble data assimilation of total column ozone. *SOLA*, **7**, 41–44.

Sekiyama, T. T., T. Y. Tanaka, T. Maki, and M. Mikami, 2011b: The effects of snow cover and soil moisture on Asian dust: II. Emission estimation by lidar data assimilation. *SOLA*, **7A**, 40–43.

Shimbori, T., Y. Aikawa, and N. Seino, 2009: Operational implementation of the tephra fall forecast with the JMA mesoscale tracer transport model. *CAS/JSC WGNE Res. Act. Atmos. Ocean. Modell.*, **39**, 5.29–5.30.

Shimbori, T., Y. Aikawa, K. Fukui, A. Hashimoto, N. Seino, and H. Yamasato, 2010: Quantitative tephra fall prediction with the JMA mesoscale tracer transport model for volcanic ash: A case study of the eruption at Asama volcano in 2009. *Pap. Met. Geophys.*, **61**, 13–29 (in Japanese with English abstract).

Sportisse, B., 2007: A review of parameterizations for

modelling dry deposition and scavenging of radionuclides. *Atmos. Environ.*, **41**, 2683–2698.

Stohl, A., P. Seibert, G. Wotawa, D. Arnold, J. F. Burkhart, S. Eckhardt, C. Tapia, A. Vargas, and T. J. Yasunari, 2012: Xenon-133 and caesium-137 releases into the atmosphere from the Fukushima Dai-ichi nuclear power plant: Determination of the source term, atmospheric dispersion, and deposition. *Atmos. Chem. Phys.*, **12**, 2313–2343.

Sugiyama, G., J. Nasstrom, B. Pobanz, K. Foster, M. Simpson, P. Vogt, F. Aluzzi, and S. Homann, 2012: Atmospheric dispersion modeling: Challenges of the Fukushima Daiichi response. *Health Phys.*, **102**, 493–508.

Takemi, T., 2013: High-resolution meteorological simulations of local-scale wind fields over complex terrain: A case study for the eastern area of Fukushima in March 2011. *Theor. Appl. Mech. Jpn.*, **61**, 3–10.

Takemura, T., H. Nakamura, M. Takigawa, H. Kondo, T. Satomura, T. Miyasaka, and T. Nakajima, 2011: A numerical simulation of global transport of atmospheric particles emitted from the Fukushima Daiichi nuclear power plant. *SOLA*, **7**, 101–104.

Terada, H., G. Katata, M. Chino, and H. Nagai, 2012: Atmospheric discharge and dispersion of radionuclides during the Fukushima Dai-ichi nuclear power plant accident. Part II: verification of the source term and analysis of regional-scale atmospheric dispersion. *J. Environ. Radioact.*, **112**, 141–154.

Torii, T., Y. Sanada, T. Sugita, A. Kondo, Y. Shikaze, M. Takahashi, M. Ishida, Y. Nishizawa, and Y. Urabe, 2012: *Investigation of radionuclide distribution using aircraft for surrounding environmental survey from Fukushima Dai-ichi nuclear power plant.* Japan Atomic Energy Agency, 182 pp (in Japanese with English abstract).

Yasunari, T. J., A. Stohl, R. S. Hayano, J. F. Burkhart, S. Eckhardt, and T. Yasunari, 2011: Cesium-137 deposition and contamination of Japanese soils due to the Fukushima nuclear accident. *Proc. Natl. Acad. Sci.*, **108**, 19530–19534.

ONLINE ISSN 2189-8871

TECHNICAL REPORTS OF THE METEOROLOGICAL RESEARCH INSTITUTE No. 76

Contribution of JMA to the WMO Technical Task Team on Meteorological Analyses for Fukushima Daiichi Nuclear Power Plant Accident and Relevant Atmospheric Transport Modeling at MRI

BY

K. Saito, T. Shimbori, R. Draxler, T. Hara, E. Toyoda, Y. Honda, K. Nagata, T. Fujita, M. Sakamoto, T. Kato, M. Kajino, T.T. Sekiyama, T.Y. Tanaka, T. Maki, H. Terada, M. Chino, T. Iwasaki, M.C. Hort, S.J. Leadbetter, G. Wotawa, D. Arnold, C. Maurer, A. Malo, R. Servranckx and P. Chen

気象研究所技術報告
第 76 号

WMO福島第一原発事故に関する気象解析技術タスクチーム活動と気象研究所の大気拡散モデリング

斉藤和雄・新堀敏基・R. Draxler
原旅人・豊田英司・本田有機・永田和彦・藤田司・坂本雅巳
加藤輝之・梶野瑞王・関山剛・田中泰宙・眞木貴史
寺田宏明・茅野政道・岩崎俊樹
M.C. Hort, S.J. Leadbetter, G. Wotawa, D. Arnold, C. Maurer, A. Malo, R. Servranckx, P. Chen

気 象 研 究 所
METEOROLOGICAL RESEARCH INSTITUTE, JAPAN

OCTOBER 2015

The *Technical Reports of the Meteorological Research Institute* has been issued at irregular intervals by the Meteorological Research Institute (MRI) since 1978 as a medium for the publication of technical report including methods, data and results of research, or comprehensive report compiled from published papers. The works described in the *Technical Reports of the MRI* have been performed as part of the research programs of MRI.

気象研究所技術報告　第76号　平成27年10月
TECHNICAL REPORTS OF THE METEOROLOGICAL
RESEARCH INSTITUTE No.76, October 2015
doi:10.11483/mritechrepo.76

Contribution of JMA to the WMO Technical Task Team on Meteorological Analyses for Fukushima Daiichi Nuclear Power Plant Accident and Relevant Atmospheric Transport Modeling at MRI

by

Kazuo Saito and Toshiki Shimbori
Meteorological Research Institute, Japan Meteorological Agency

Roland Draxler
Air Resource Laboratory, National Oceanic and Atmospheric Administration, USA

Tabito Hara, Eizi Toyoda, Yuki Honda, Kazuhiko Nagata, Tsukasa Fujita and Masami Sakamoto
Japan Meteorological Agency

Teruyuki Kato, Mizuo Kajino, Tsuyoshi T. Sekiyama, Taichu Y. Tanaka and Takashi Maki
Meteorological Research Institute, Japan Meteorological Agency

Hiroaki Terada and Masamichi Chino
Japan Atomic Energy Agency

Toshiki Iwasaki
Tohoku University

Matthew C. Hort and Susan J. Leadbetter
Met Office, United Kingdom

Gerhard Wotawa, Delia Arnold and Christian Maurer
Central Institute for Meteorology and Geodynamics, Austria

Alain Malo and Rene Servranckx
Canadian Meteorological Centre

Peter Chen
World Meteorological Organization

Contents

G-3. NHM-Chem: Sensitivity of Cs deposition to the size and hygroscopicity of Cs-bearing aerosols[1]

G-3-1. Abstract

The emission, transport, and deposition of ^{137}Cs released by the Fukushima Daiichi Nuclear Power Plant (FDNPP) accident were simulated with consideration of the microphysical properties (i.e. size and hygroscopicity) of the Cs-bearing aerosols (carrier aerosols of radioactive Cs). The sensitivity of the simulated deposition of ^{137}Cs to the size and hygroscopicity of the carrier aerosols was assessed and compared with the sensitivity to meteorological fields simulated using different dynamics and physics modules. Two types of Cs-bearing aerosols were considered in the simulation, supermicron water-insoluble and submicron water-soluble particles, in accordance with previously published observational evidence (Adachi et al., 2013 and Kaneyasu et al., 2012). Even though the same transport model was used, the simulated depositions were very different when meteorological models with different dynamics and physics modules were used. The sensitivity of ^{137}Cs deposition to the carrier aerosol size and hygroscopicity, in which the proportion of water-insoluble aerosol emission ranged from 10% to 90%, during the early stage ranged from March. 11-12 to Mar. 12-20, was found to be lower but still as important as the sensitivity to meteorological fields simulated using different dynamics and physics modules. To better understand the environmental behavior of the radioactive Cs discharged from the FDNPP, knowledge of the carrier aerosol microphysical properties is as important as the accuracy of the meteorological simulation and the emission scenario.

G-3-2. Introduction

Three months after the FDNPP accident, Chino et al. (2011) estimated the emission amounts of radioactive ^{137}Cs and ^{131}I associated with the accident by using a reverse estimation method in which both the environment monitoring data and an atmospheric dispersion simulation were used (see section D-2). Since then, many modeling studies have been conducted to assess the emission, dispersion, and deposition amounts of radionuclides associated with the accident (Morino et al. 2011; Yasunari et al., 2011; Schöppner et al. 2011; Takemura et al., 2011; Sugiyama et al., 2012; Stohl et al., 2012; Terada et al., 2012; Katata et al., 2012a, 2012b; Morino et al., 2013; Adachi et al., 2013; Hu et al., 2014; Katata et al., 2015; Sekiyama et al., 2015).

Because numerical models use uncertain parameters and rough assumptions, model inter-comparison and intra-comparison (or sensitivity) studies are essential to assess the uncertainties of numerical simulations. In fact, previous model inter-comparison studies have shown that simulation results vary substantially among models (Draxler et al., 2013a; Katata et al., 2015; SCJ, 2014). Although model inter-comparison studies can show how the simulation results of models using different dynamics, physics, and chemistry modules and emission scenarios differ overall, the reasons for the differences cannot be easily identified. In contrast, model intra-comparison (or sensitivity)

[1] M. Kajino

studies can identify the modules or parameters that are responsible for different results, but under limited conditions that the simulations are performed only by a single model.

Morino et al. (2013) investigated the sensitivity of radioactive Cs dispersion and deposition to the wet-scavenging modules and emission scenarios. Like most previous studies, for the meteorological field they used the output of only one meteorology model. In this study, we used several different meteorology models and simulation techniques to evaluate sensitivity of the transport model results to different meteorological simulations as well.

Another important aspect of this study is that we examined the sensitivity of the simulated deposition to the microphysical properties of Cs-carrying aerosols for the first time. Adachi et al. (2013) reported that in the early stage of the accident, the carrier aerosols of radioactive Cs were spherical, water-insoluble particles (hereafter, Cs-balls), and they predicted that the atmospheric behavior of these aerosols would be different from that of the submicron water-soluble particles described by Kaneyasu et al. (2012). Washout (or below-cloud scavenging) of aerosol particles (i.e., of both types described in this paragraph) is not usually efficient because of their small inertia and slow Brownian motion. In contrast, the submicron water-soluble particles are efficiently scavenged via rainout (or in-cloud scavenging) because the Kelvin (curvature) effect is enough small. Washout is probably the dominant scavenging process of water-insoluble aerosols, because very high supersaturation conditions are needed for rainout of water-insoluble aerosols to occur.

The purpose of this study was to assess the sensitivities described above in order to evaluate the uncertainties of the simulated deposition of ^{137}Cs caused by aerosol microphysical properties (i.e., aerosol size and hygroscopicity) and to compare it to the uncertainty caused by the use of different meteorological simulations.

G-3-3. NHM-Chem

NHM-Chem is a chemical transport model, offline- or online-coupled with Japan Meteorological Agency's non-hydrostatic model (JMA-NHM; Saito et al., 2007). NHM is a numerical weather prediction model of JMA. An Eulerian regional chemical transport model, Regional Air Quality Model 2 (RAQM2) (Kajino et al., 2012a), is used to simulate emission, transport, and deposition of trace gases and aerosols. RAQM2 implements a triple-moment modal aerosol microphysics module that assumes a log-normal size distribution of aerosol populations. This model describes the nature of aerosol dynamical processes, such as nucleation, condensation, coagulation, hygroscopic growth, dry deposition, grid-scale rainout (cloud condensation and ice nuclei activation and subsequent mixed-phase cloud microphysical processes) and washout (coagulation between aerosols and settling hydrometeors) processes, and sub-grid-scale convection and scavenging processes. In the study, the offline-coupled NHM-Chem was used in order to use different meteorological models alternatively, such as the Weather Research and Forecasting (WRF) model (Skamarock et al., 2008) to drive RAQM2.

G-3-4. Simulation settings

In this study, meteorology simulations were performed with NHM and WRF with two different cloud microphysics modules, Morrison et al. (2009) and Lim and Hong (2010), referred to as WRF-MORR and WRF-WDM6, respectively. The two WRF simulations were used so that the sensitivity to just the cloud microphysical process (grid-scale) could be assessed, because wet deposition of ^{137}Cs over Japan dominated over dry deposition in this study.

NHM, WRF, and RAQM2 shared the same domain, which consisted of 215 × 259 grid cells with a 3 km horizontal resolution; this model domain is slightly larger than the area shown in Fig. G-3-1. There were 50 vertical layers up to 50 hPa in NHM, 28 layers up to 100 hPa in WRF, and 20 layers up to 10 km in RAQM2. JMA Meso-Regional Objective Analysis data sets (3 hourly, 5 km × 5 km) were used for the initial and boundary conditions of NHM and WRF. The same analysis data sets were used for the spectral nudging in NHM and for the grid nudging in WRF.

The radionuclide transport version of NHM-Chem was developed for simulations of nuclear power plant accidents such as the FDNPP accident (Adachi et al., 2013; Sekiyama et al., 2015). This version of NHM-Chem uses an aerosol dynamics module that is simplified from that described by Kajino et al. (2012a) because aerosol hygroscopicity and the particle size distribution are assumed to be constant during transport. The nature of the aerosol dynamics such as dry deposition and grid-scale rainout/washout processes are thus described on the basis of the prescribed size distribution and hygroscopicity. Details of the dry and wet deposition processes are described by Kajino et al. (2012a; their sections 2.2.7 and 2.2.8). Even aerosols that are completely water-insoluble (i.e., hygroscopicity κ = 0) can act as cloud condensation nuclei under highly supersaturated conditions. Although water-insoluble aerosols can coagulate with cloud droplets within a cloud (this is also rainout process), for simplicity, in this study we did not consider rainout of Cs-balls and only washout in their wet deposition modeling. Sub-grid scale convection and scavenging processes were not considered. The fog deposition process of Katata et al., (2015) was considered.

We used the emission scenario for ^{137}Cs discharged from the FDNPP from Terada et al. (2012), and considered Cs-bearing aerosols to be of two types. Supermicron water-insoluble particles (Cs-balls) had a lognormal size distribution, number equivalent geometric mean dry diameter $D_{g,n,dry}$ = 2.3 μm, geometric standard deviation σ_g = 1.3, particle density ρ_p = 2.0 g/cm^3, and κ = 0 (Adachi et al., 2013), and submicron water-soluble particles (Kaneyasu et al., 2012) had a lognormal size distribution, $D_{g,n,dry}$ = 0.1 μm, σ_g = 1.6, ρ_p = 1.83 g/cm^3, and κ = 0.4.

For the sensitivity studies, taking into consideration the findings of Adachi et al. (2013), we allowed the proportion of early-stage emissions consisting of Cs-balls during the early stage to range from 10% to 90%, and the ending date of the early stage to range from 12 to 20 March 2011.

The analysis period was from 00:00 UTC on 11 March to 00:00 UTC on 1 April, with a spin-up period of 3 days. Thus, the entire simulation period was from 8 March to 1 April 2011.

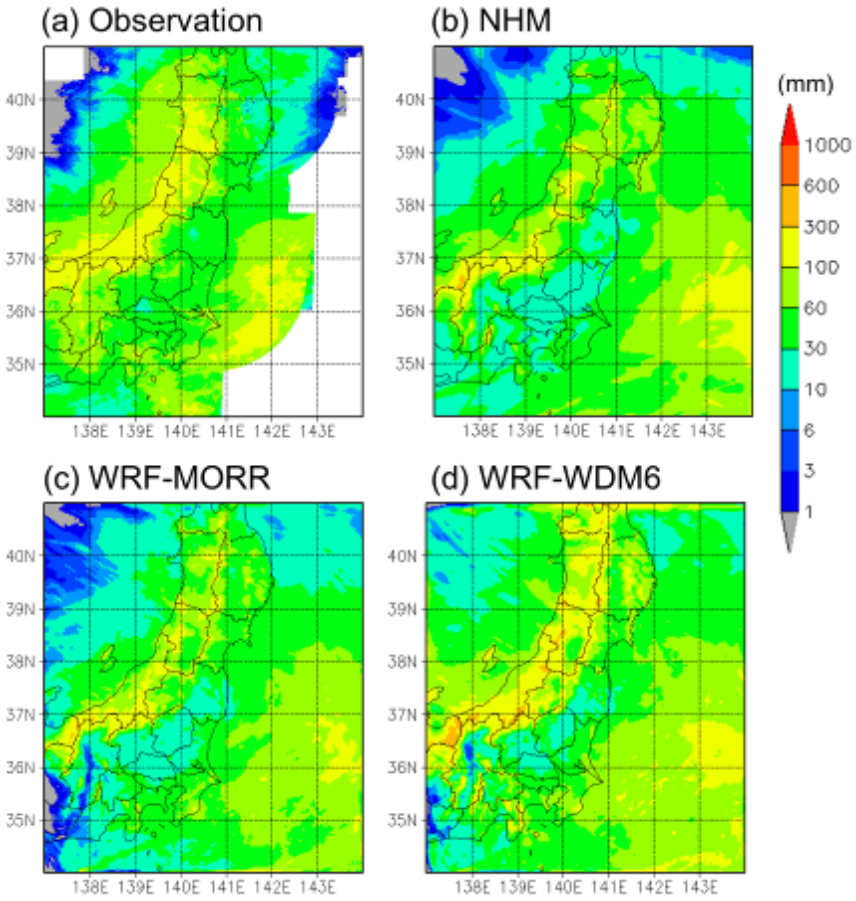

Fig. G-3-1. Cumulative precipitation (mm) from 11 March to 1 April: (a) Radar/rain gauge-analyzed precipitation (RAP) data and precipitation simulated by (b) NHM, (c) WRF-MORR, and (d) WRF-WDM6.

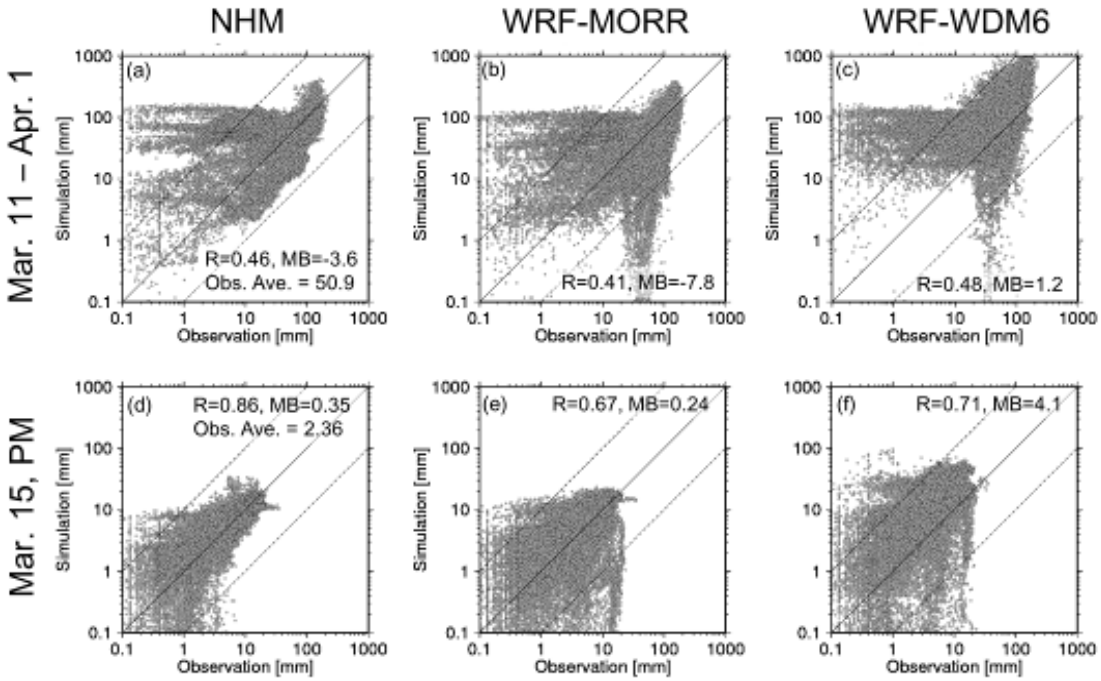

Fig. G-3-2. Scattergrams of simulated and observed (RAP) cumulative precipitation: (a–c) from 11 March to 1 April and (d–f) in the afternoon of 15 March. Simulations were by (a, d) NHM, (b, e) WRF-MORR, and (c, f) WRF-WDM6. The plotted data are for all grids for which both observation and simulation data were available. Although the data are plotted on a log-log scale, the statistics *R*, mean bias (MB), and the observation average (Obs. Ave.) were calculated on a linear-linear basis.

G-3-5. Results and discussion

We compared observed and simulated cumulative precipitation from 11 March to 1 April among the three meteorology models (Figs. G-3-1 and G-3-2). For observed data, we used JMA's radar/rain gauge-analyzed precipitation (RAP) data, which were interpolated to the 3 km resolution grid. We also compared observed and simulated cumulative precipitation on the afternoon of 15 March (Fig. G-3-2, lower panels), when substantial deposition occurred on land (e.g., Morino et al., 2013). All three simulations overestimated precipitation over the ocean by a factor of more than 10 (data points above the 10:1 simulation:observation line in Fig. G-3-2), and the two WRF simulations also underestimated precipitation in the southwestern part of the domain by a factor of more than 10 (data points below the 1:10 simulation:observation line in Fig G-3-2). Our focus was on land regions where the ^{137}Cs deposition was large (>10 kBq/m^2) (see Fig. G-3-3), and we did not expect the large discrepancies between the simulated and observed precipitation over the ocean to substantially affect the modeling of ^{137}Cs deposition in land areas.

The differences due to the different cloud microphysics modules were notable. The simulated precipitation spatial distribution patterns of the two WRFs were similar and different from the NHM pattern, whereas the precipitation amounts in WRF-MORR were fairly close to those in NHM, and those in WRF-WDM6 were much larger than the amounts in the other two simulations (Fig. G-3-2). WRF-WDM6 overestimated precipitation substantially over high-altitude regions (corresponding to locations where the simulated precipitation was >600 mm; Fig. G-3-1d). In the afternoon of 15 March, the overestimation of WRF-WDM6 was substantial; the mean bias (MB) was 4.1 mm and the observation average was 2.36 mm. Judging from the values of the correlation coefficient (R), the performance of NHM was best among the three meteorological simulations (R = 0.86, MB = 0.35 mm). The MB of WRF-MORR was smallest (MB = 0.24 mm), but owing to the square shape of the plotted data, R was 0.67.

Comparison of cumulative ^{137}Cs deposition amounts between aircraft observations (Torii et al., 2012) and simulations by NHM, WRF-MORR, and WRF-WDM6 (Fig. G-3-3), performed under the assumption that 100% of ^{137}Cs was carried by water soluble particles, showed that NHM simulated too much deposition in northern areas (Yamagata, Miyagi, and Iwate prefectures). This deposition was caused by rainout of ice phase precipitation (snow and graupel). For accurate simulation of rainout of ^{137}Cs, the vertical distribution of the ^{137}Cs and the hydrometeor mixing ratio must be accurately predicted. However, because no observations of the vertical profiles of ^{137}Cs are available for the time period of this study, the reason for this overestimation is impossible to identify.

WRF-MORR also simulated too much deposition in Yamagata and Miyagi prefectures, but WRF-WDM6 simulated less deposition in this area. The two WRF simulations reasonably reproduced depositions in the highest deposition areas (>1000 kBq/m^2), but depositions in those areas were underestimated by NHM. The two WRF simulations also reasonably reproduced the higher depositions in the mountainous regions of Tochigi and Gunma prefectures, but they overestimated depositions in the southern area (Tokyo, Kanagawa, Shizuoka, and Chiba prefectures). The NHM

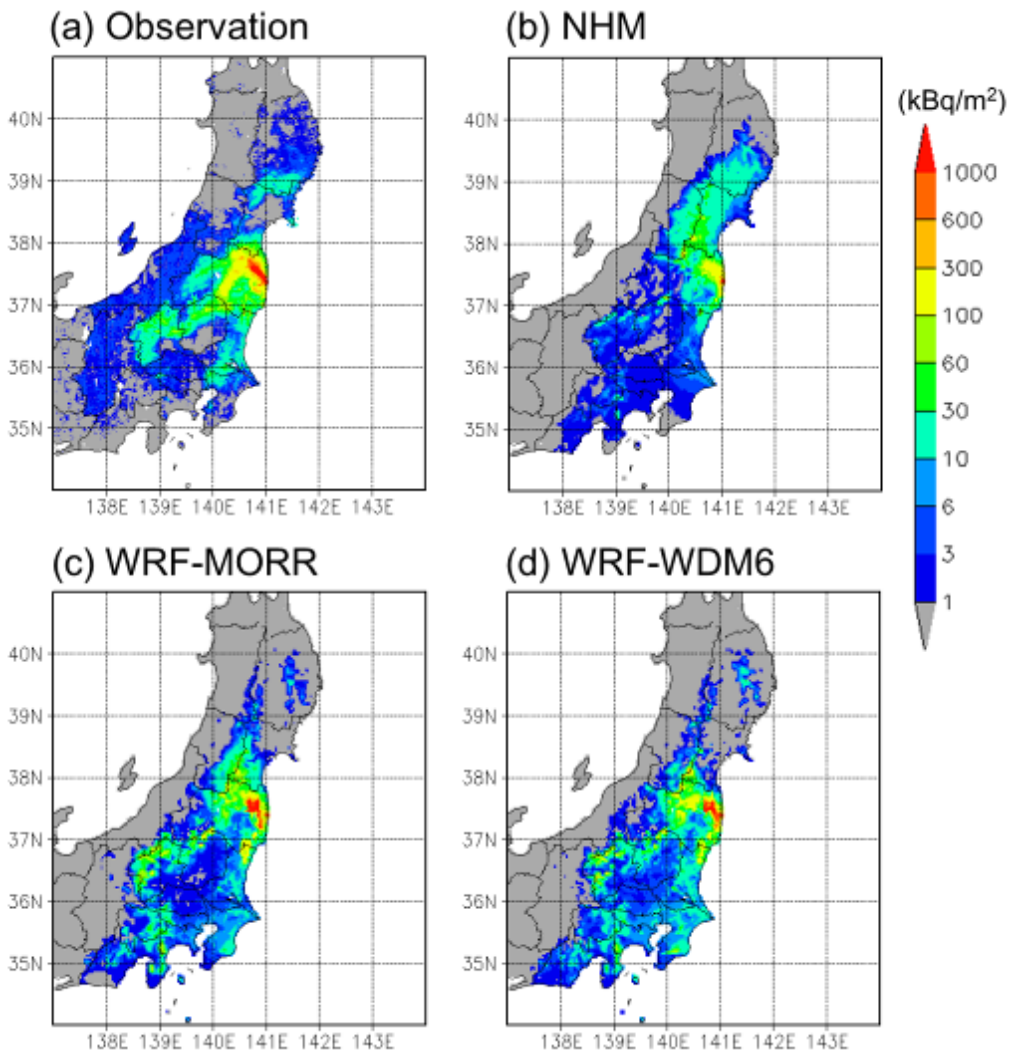

Fig. G-3-3. Cumulative ^{137}Cs deposition amounts (kBq/m^2) in (a) aircraft observations and (b) NHM, (c) WRF-MORR, and (d) WRF-WDM6 simulations. Simulated depositions are shown only for land areas to facilitate visual comparison with the observed deposition.

simulation underestimated deposition in all of these areas (i.e., in Tochigi and Gunma prefectures as well as in Tokyo, Kanagawa, Ibaraki, and Chiba prefectures). It is notable that, even though the transport model was the same, the simulated depositions varied substantially among the different meteorological simulations.

Figure G-3-4 shows depositions of water-soluble and water-insoluble particles simulated by using the three meteorological fields on both land and ocean areas. We compared the simulated depositions with aircraft observation data (Fig. G-3-3a) interpolated to the 3 km resolution grids of the models in Fig. G-3-5. Note that following Morino et al. (2013) and Katata et al. (2015), *R* and MB were calculated only when the observed values were larger than 10 kBq/m^2.

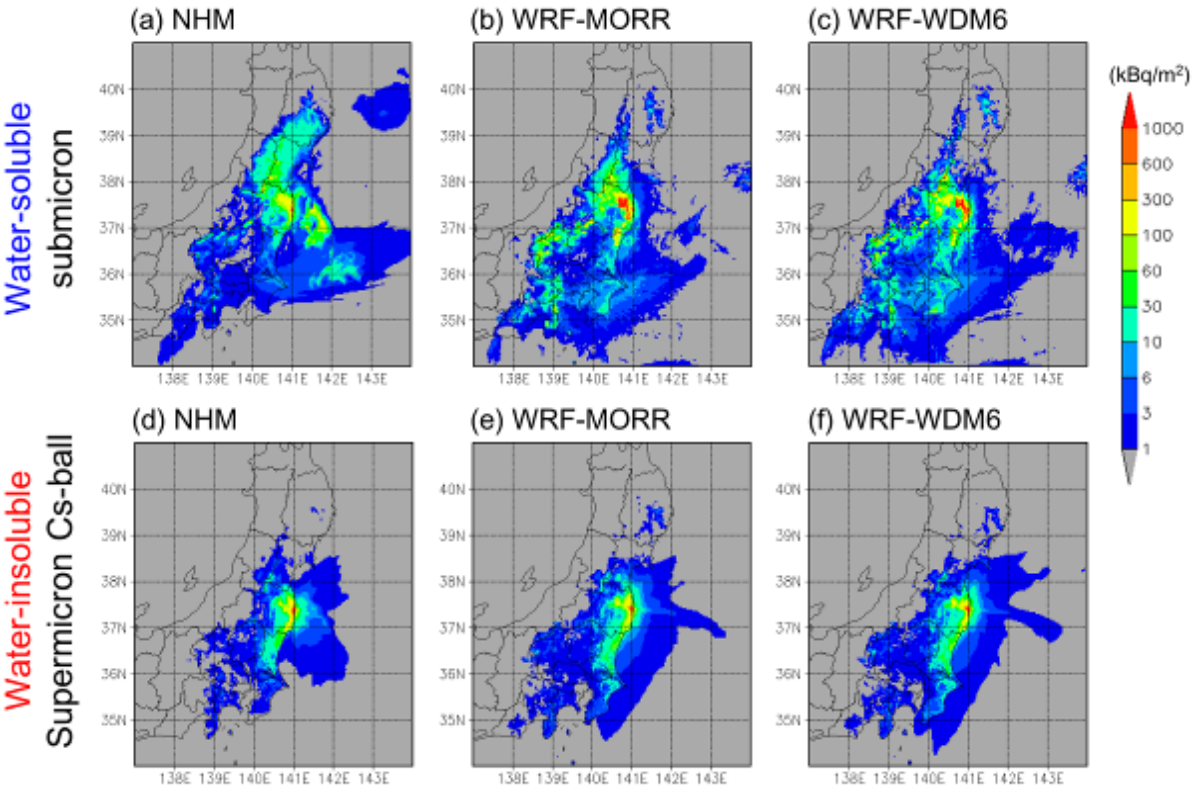

Fig. G-3-4. Cumulative depositions (kBq/m^2) simulated using the meteorological fields of (a, d) NHM, (b, e) WRF-MORR, and (c, f) WRF-WDM6 under the assumption that 100% of Cs was carried by (a–c) water soluble or (d–f) water insoluble particles.

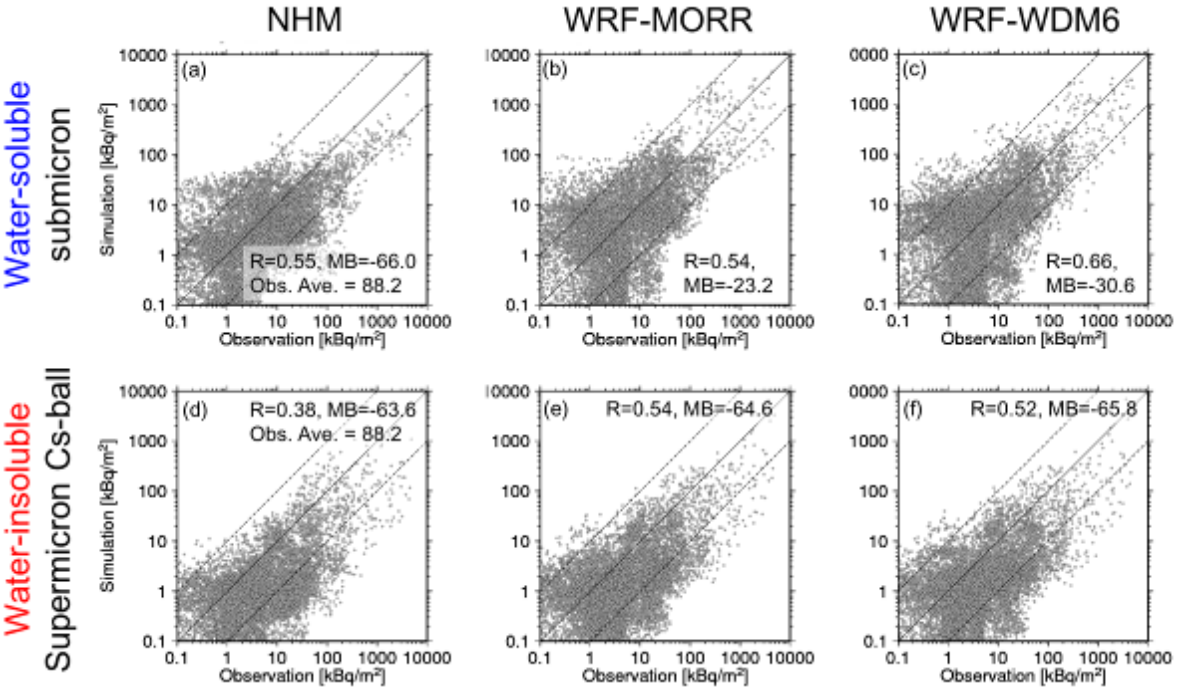

Fig. G-3-5. Scattergrams of cumulative deposition between the (a, d) NHM, (b, e) WRF-MORR, and (c, f) WRF-WDM6 simulations and aircraft observations. The simulations were performed under the assumption that 100% of Cs was carried by (a–c) water soluble or (d–f) water insoluble particles. Although the data are plotted on a log-log scale, the statistics *R* and mean bias (MB) were calculated on a linear-linear basis.

The simulated results were substantially different between Cs-bearing particles assumed to be 100% water soluble or water insoluble, because rainout of the Cs-balls was not considered to occur (compare upper and lower panels in Figs. G-3-4 and G-3-5), whereas the dry deposition velocity of Cs-balls was approximately four times that of the water-soluble submicron aerosols. It is interesting that although the simulation of precipitation by NHM/WRF-WDM6 was good/poor, the simulation of deposition by NHM/WRF-WDM6 was poor/good.

Adachi et al. (2013) detected Cs-balls only in samples collected during the early stage of the accident (14–15 March), but they reported that radioactive Cs was carried by water-soluble aerosols later (20–22 March). Kaneyasu et al. (2012), who analyzed samples collected from 28 April to May 12 and during 12–26 May (i.e., after the later sampling period of Adachi et al., 2013), also reported the radioactive Cs to be carried by water-soluble aerosols. Therefore, the assumption of 100% water-insoluble or water-soluble particles (Figs. G-3-4 and G-3-5) was not realistic; rather, reality must lie somewhere in between. Therefore, under the assumption that Cs-balls, as indicated by Adachi et al. (2013), were emitted only in the early stage of the accident, we used the following settings to test the sensitivity to aerosol microphysical properties:

1. We set the proportion of Cs-ball emissions to values from 10% to 90% during the early stage.
2. We started the early stage on 11 March but varied its ending date between 12 and 20 March 2011 (i.e., before the later sampling of Adachi et al., 2013).

We next compared cumulative depositions simulated using the meteorological fields calculated by NHM and the two WRF simulations between two extreme cases: 10% Cs-ball emission until 12 March and 90% Cs-ball emission until March 20 (Fig. G-3-6). The statistics (MB, root mean square error (RMSE) and *R*) of these comparisons are presented in Table G-3-1, together with the statistics for the three meteorological simulations when emissions were assumed to consist of 100% water-soluble submicron particles.

It is notable that even when the transport model settings and aerosol properties were the same, the fractional bias (MB divided by the observation average) ranged from 0.25 to 0.74, differing by approximately threefold, among the three different meteorological simulations. This difference is marked, because it means, for example, that the emission amount estimated by an inverse model from the deposition amount could vary threefold, depending on the meteorological model used. The ranges of MB, RMSE and *R* in the sensitivity to aerosol properties test results were smaller than their ranges in the sensitivity to meteorology test results (Table G-3-1), but the differences were similarly marked. The fractional bias range differed by approximately twofold between WRF-MORR and WRF-WDM6 (0.35–0.74 and 0.38–0.66, respectively). Therefore, the sensitivity of ^{137}Cs deposition to aerosol microphysical properties was as important as its sensitivity to the meteorological simulation used.

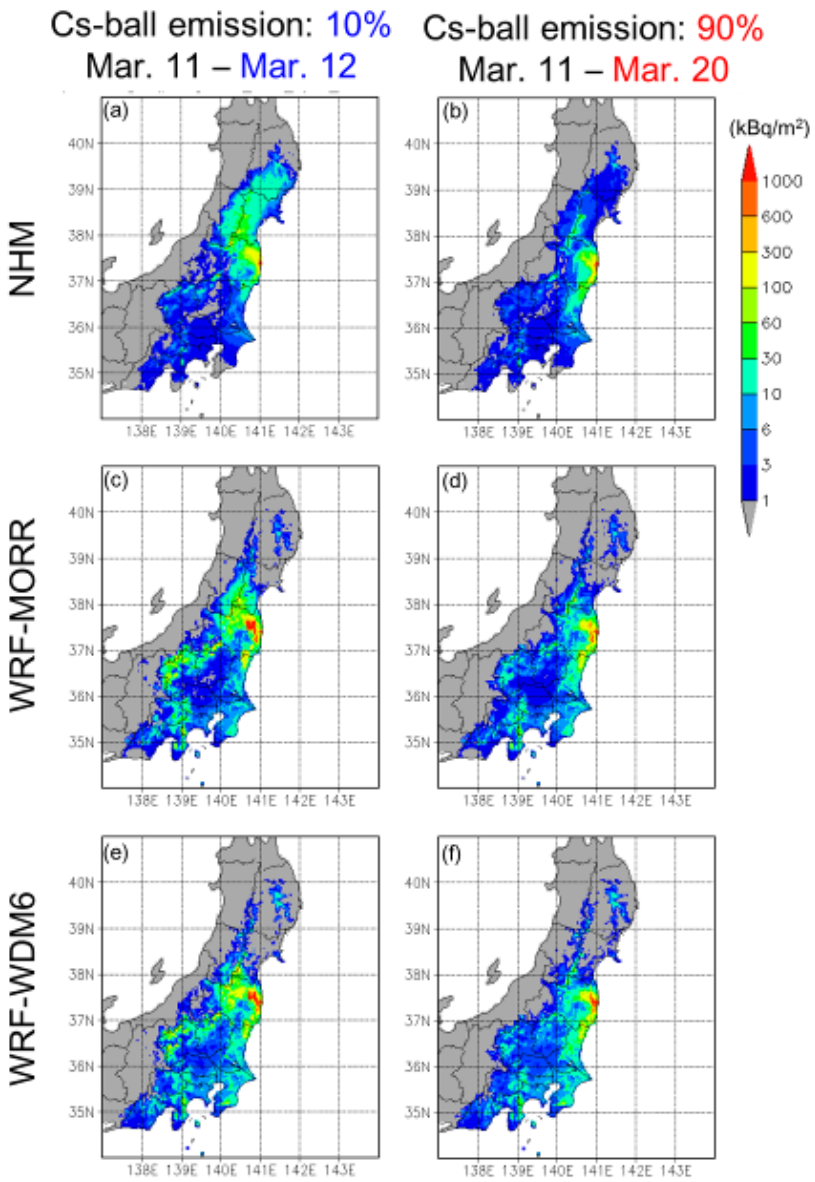

Fig. G-3-6. Simulated cumulative depositions (kBq/m^2) using the meteorological fields calculated by (a, b) NHM, (c, d) WRF-MORR, and (e, f) WRF-WDM6 between the two extreme aerosol microphysical assumptions: (a, c, e) 10% Cs-ball emission from 11 to 12 March and (b, d, f) 90% Cs-ball emission from 11 to 20 March.

Table G-3-1. Ranges of the statistics between observed and simulated cumulative depositions between the two extreme sensitivity tests (10% or 90% Cs-balls and 12 or 20 March as the ending date of the early stage) with each meteorological simulation (first to third row). The bottom row shows the same statistics among the meteorological simulations when no Cs-balls were assumed.

Sensitivity to	MB[1] (min:max) (kBq/m^2)	RMSE[1] (min:max) (kBq/m^2)	R[1] (min:max) (–)	Obs. Ave. (kBq/m^2)	Simulation settings		
					Meteorological simulation	Cs-ball fraction	Ending date of early stage
Aerosol properties	−68.5 : −65.5	274.3 : 295.0	0.39 : 0.55	88.2	NHM	10–90%	Mar.12 – 20
Aerosol properties	−57.2 : −22.8	251.1 : 272.5	0.53 : 0.59	88.2	WRF–MORR	10–90%	Mar.12 – 20
Aerosol properties	−54.6 : −30.2	225.9 : 244.2	0.65 : 0.70	88.2	WRF–WDM6	10–90%	Mar.12 – 20
Meteorology simulations	−66.0 : −23.2	233.0 : 274.9	0.54 : 0.66	88.2	NHM, WRF–MORR, WDM6	0%	–

[1] linear–linear statistics

G-3-6. Summary

We simulated the emission, transport, and deposition of ^{137}Cs released due to the FDNPP accident. The sensitivity of the simulated depositions of radioactive Cs to the size and hygroscopicity of the carrier aerosols was assessed and compared with the sensitivity to the meteorological simulation.

Two types of Cs-bearing aerosols, water-insoluble supermicron particles (Cs-balls) and water-soluble submicron particles were considered in the simulation. The simulated depositions of the two aerosols were significantly different because rainout was not considered to occur with Cs-balls, and the dry deposition velocities of Cs-balls were approximately four times those of the water-soluble particles.

Even when the transport model was used with exactly the same settings, the simulated depositions were very different among the different meteorological simulations: The fractional bias (MB divided by observation average) ranged from 0.25 to 0.74, an approximately threefold difference. The sensitivity of ^{137}Cs deposition to particle size and hygroscopicity (determined by adjusting the proportion of water-insoluble Cs emission between 10% and 90% and the ending date of the early stage between 12 and 20 March 2011) was smaller but just as important as the sensitivity to the meteorological simulation (in which 100% of Cs was assumed to be water soluble, as in previous studies). To better understand the environmental behavior of radioactive Cs discharged from the FDNPP, knowledge of the aerosol microphysical properties is as important as the accuracy of the meteorological simulations and emission scenarios.

In future work, several new wet deposition modules and emission scenarios, together with new meteorological simulations (for example, NHM-LETKF as in Sekiyama et al., 2015), will be added to the current sensitivity analysis study to provide a more robust uncertainty estimation of the numerical simulation techniques. It would also be interesting to estimate the sensitivity to the modeling approach (Lagrangian or Eulerian), because the both approaches have been used in FDNPP accident simulation studies.

気象研究所技術報告は，1978（昭和53）年の初刊以来,気象研究所が必要の都度発行する刊行物であり,気象研究所の研究計画に基づき実施した研究に関する手法、データ、結果等についてのまとめ、または、すでに公表した研究論文類をとりまとめ総合的報告としたものを掲載する。

ONLINE ISSN 2189-8871

気　象　研　究　所　技　術　報　告
第　76　号
平成27年10月　発行

編集兼
発行者　気　象　研　究　所

〒305-0052　茨城県つくば市長峰１－１
TEL(029)853-8535

6. Publication list 1954-2015

論文リスト（英文誌）1954-2015

2015

1. Igarashi, Y., Kajino, M., Zaizen, Y., Adachi, K., and Mikami, M., Atmospheric radioactivity over Tsukuba, Japan: a summary of three years of observations after the FDNPP accident, Progress in Earth and Planetary Science 2:44, 2015. doi: 10.1186/s40645-015-0066-1.
2. Kajino, M., G-3. NHM-Chem: Sensitivity of Cs deposition to the size and hygroscopicity of Cs-bearing aerosols, Technical Reports of the Meteorological Research Institute, 76, 132–142, 2015.
3. Sekiyama, T. T., Kunii, M., Kajino, M., and Shinbori, T., Horizontal Resolution Dependence of Atmospheric Simulations of the Fukushima Nuclear Accident Using 15-km, 3-km, and 500-m Grid Models, J. Meteorol. Soc. Jpn., 93B, 49–64, 2015.

2014

1. Abe, Y., Iizawa, Y., Terada, Y., Adachi, K., Igarashi, Y., and Nakai, I., Detection of uranium and chemical state analysis of individual radioactive microparticles emitted from the Fukushima nuclear accident using multiple synchrotron radiation X-ray analyses, Analytical Chemistry, 86, 8521-8525, 2014.

2013

1. Aoyama, M., Uematsu, M., Tsumune, D., and Hamajima, Y., Surface pathway of radioactive plume of TEPCO Fukushima NPP1 released ^{134}Cs and ^{137}Cs, Biogeosciences, 10, 3067-3078, 2013. doi: 10.5194/bg-10-3067-2013.
2. Tsumune, D., Tsubono, T., Aoyama, M., Uematsu, M., Misumi, K., Maeda, Y., Yoshida, Y., and Hayami, H., One-year, regional-scale simulation of ^{137}Cs radioactivity in the ocean following the Fukushima Daiichi Nuclear Power Plant accident, Biogeosciences, 10, 5601-5617, 2013.
3. Povinec, P.P., Aoyama, M., Biddulph, D., Breier, R., Buesseler, K., Chang, C., Golser, R., Hou, X., Ješkovský, M., and Jull, A., Cesium, iodine and tritium in NW Pacific waters-a comparison of the Fukushima impact with global fallout. Biogeosciences, 10, 5481-5496. 2013.
4. Kumamoto, Y., Murata, A., Kawano, T., and Aoyama, M., Fukushima-derived radiocesium in the northwestern Pacific Ocean in February 2012, Applied Radiation and Isotopes, 81, 335-339, 2013. doi: 10.1016/j.apradiso.2013.03.085.
5. Toyama, C., Muramatsu, Y., Igarashi, Y., and Aoyama, M., Atmospheric fallout of ^{129}I in Japan before the Fukushima accident: Regional and global contributions, 1963-2005, Environmental Science & Technology, 47(15), 8383-8390, 2013. doi: 10.1021/es401596z.
6. Adachi, K., Kajino, M., Zaizen, Y., and Igarashi, Y., Emission of spherical cesium-bearing particles from an early stage of the Fukushima nuclear accident. Scientific Reports, 3, Article number 2554, 2013. doi:10.1038/srep02554.

2012

1. Toyama, C., Muramatsu, Y., Uchida, Y., Igarashi, Y., Aoyama, M., and Matsuzaki, H., Variations of ^{129}I in the atmospheric fallout of Tokyo, Japan 1963-2003, Journal of Environmental Radioactivity, 113, 116-122, 2012. doi: 10.1016/j.jenvrad.2012.04.014.
2. Inomata, Y., Aoyama, M., Tsumune, D., Motoi, T., and Nakano, H., Optimum interpolation analysis of basin-scale ^{137}Cs transport in surface seawater in the North Pacific Ocean, Journal of Environmental Monitoring, 14, 3146-3155, 2012. doi: 10.1039/C2EM30707C.
3. Aoyama, M., Tsumune, D., Uematsu, M., Kondo, F., and Hamajima, Y., Temporal variation of ^{134}Cs and ^{137}Cs activities in surface water at stations along the coastline near the Fukushima Dai-ichi Nuclear Power Plant accident site, Japan. Geochem. J, 46, 321-325, 2012.
4. Aoyama, M., Tsumune, D., and Hamajima, Y., Distribution of ^{137}Cs and ^{134}Cs in the North Pacific Ocean: impacts of the TEPCO Fukushima-Daiichi NPP accident, Journal of Radioanalytical and Nuclear Chemistry, 1-5, 2012. doi: 10.1007/s10967-012-2033-2.

5. Honda, M. C., Aono, T., Aoyama, M., Hamajima, Y., Kawakami, H., Kitamura, M., Masumoto, Y., Miyazawa, Y., Takigawa, M., and Saino, T., Dispersion of artificial caesium-134 and-137 in the western North Pacific one month after the Fukushima accident, Geochem. J, 46, e1-e9, 2012.
6. Povinec, P. P., Hirose, K., and Aoyama, M., Radiostrontium in the Western North Pacific: characteristics, behavior, and the Fukushima impact, Environmental Science & Technology, 46, 10356-10363, 2012. doi: 10.1021/es301997c.
7. Tsumune, D., Tsubono, T., Aoyama, M., and Hirose, K., Distribution of oceanic ^{137}Cs from the Fukushima Dai-ichi Nuclear Power Plant simulated numerically by a regional ocean model, Journal of Environmental Radioactivity, 111, 100-108, 2012.

2011

1. Aoyama, M., Fukasawa, M., Hirose, K., Hamajima, Y., Kawano, T., Povinec, P.P., and Sanchez-Cabeza, J. A., Cross Equator transport of ^{137}Cs from North Pacific Ocean to South Pacific Ocean, BEAGLE2003 cruises, Progress in Oceanography, 89, 7-16, 2011. doi:10.1016/j.pocean.2010.12.003.
2. Buesseler, K., Aoyama, M., and Fukasawa, M., Impacts of the Fukushima nuclear power plants on marine radioactivity. Environmental Science & Technology, 45(23), 9931-9935, 2011. doi: 10.1021/es202816c.
3. Povinec, P. P., Aoyama, M., Fukasawa, M., Hirose, K., Komura, K., Sanchez-Cabeza, J.A., Gastaud, J., Jeskovsky, M., Levy, I., and Sykora, I., ^{137}Cs water profiles in the South Indian Ocean - an evidence for accumulation of pollutants in the subtropical gyre. Progress in Oceanography, 89 , 17-30, 2011. doi:10.1016/j.pocean.2010.12.004.
4. Gastaud, J., Povinec, P.P., Aoyama, M., Hirose, K., Sanchez-Cabeza, J.A., Levy, I., Roos, P., Eriksson, M., Bosc, E. and Rezzoug, S., Transport and scavenging of Pu in surface waters of the Southern Hemisphere Oceans, Progress in Oceanography, 89, 92-100, 2011. doi:10.1016/j.pocean.2010.12.009.
5. Hirose, K., Kim, C.S., Yim, S.A., Aoyama, M., Fukasawa, M., Komura, K., Povinec, P.P., and Sanchez-Cabeza, J.A., Vertical profiles of plutonium in the central South Pacific, Progress in Oceanography, 89, 101-107, 2011. doi:10.1016/j.pocean.2010.12.010.
6. Tsumune, D., Aoyama, M., Hirose, K., Bryan, F., Lindsay, K. and Danabasoglu, G., Transport of ^{137}Cs to the Southern Hemisphere in an Ocean General Circulation Model, Progress in Oceanography, 89, 38-48, 2011. doi:10.1016/j.pocean.2010.12.006.
7. Sanchez-Cabeza, J.A., Levy, I., Gastaud, J., Eriksson, M., Osvath, I., Aoyama, M., Povinec, P.P. and Komura, K., Transport of North Pacific ^{137}Cs labeled waters to the south-eastern Atlantic Ocean. Progress in Oceanography, 89, 31-37, 2011. doi:10.1016/j.pocean.2010.12.005.
8. Levy, I., Povinec, P.P., Aoyama, M., Hirose, K., Sanchez-Cabeza, J.A., Comanducci, J-F., Gastaud, J., Eriksson, M., Hamajima, Y., Kim, C.S., Komura, K., Osvath, I., Roos, P. and Yim, S.A., Marine anthropogenic radiotracers in the Southern Hemisphere: new sampling and analytical strategies, Progress in Oceanography, 89, 120-133, 2011. doi:10.1016/j.pocean.2010.12.012.

2010

1. Inomata,Y., Igarashi, Y., Yoshioka, K., Tanaka, T. Y., and M, Chiba., Temporal variation of ^{222}Rn at the summit of Mt. Fuji associated with the Asian continental outflow, Atmospheric Environment, 44,3856-3865, 2010.
2. Nakano, H., Motoi, T., Hirose, K., and Aoyama, M., Analysis of ^{137}Cs concentration in the Pacific using a Lagrangian approach. Journal of Geophysical Research, 115, C06015, 2010. doi:10.1029/2009JC005640.
3. Hirose, K., Igarashi, Y., Aoyama, M., and Inomata, Y., Depositional behaviors of plutonium and thorium isotopes at Tsukuba and Mt. Haruna in Japan indicate the sources of atmospheric dust. Journal of Environmental Radioactivity, 101,106-112, 2010.

4. Zhang, Y., Zeng, J., Yamada, M., Wu, F., Igarashi, Y., and Hirose, K., Characterization of Pu concentration and its isotopic composition in a reference fallout material. Science of the Total Environment, 408(5), 1139-1144, 2010.

2009

1. Aoyama, M., Hamajima, Y., Fukasawa, M., Kawano, T., and Watanabe, S., Ultra low level deep water ^{137}Cs activity in the South Pacific Ocean, Journal of Radioanalytical and Nuclear Chemistry, 2009. doi:10.1007/s10967-009-0253-x.
2. Hirose, K., Aoyama, M., and Povinec, P.P., $^{239, 240}$Pu /^{137}Cs ratios in the water column of the North Pacific: a proxy of biogeochemical processes, Journal of Environmental Radioactivity, 100, 258-262, 2009.
3. Igarashi, Y., Inomata, Y., Aoyama, M., Hirose, K., Takahashi, H., Shinoda, Y., Sugimoto, N., Shimizu, A., and Chiba, M., Possible change in Asian dust source suggested by atmospheric anthropogenic radionuclides during the 2000s, Atmospheric Environment, 43, 2971-2980, 2009.
4. Inomata, Y., Aoyama, M., and Hirose, K., Analysis of 50-y record of surface ^{137}Cs concentrations in the global ocean using the HAM-global database, Journal of Environmental Monitoring, 11(1), 116-125, 2009. doi: 10.1039/b811421h.
5. Hirose, K., Igarashi, Y., Aoyama, M., and Inomata, Y., Depositional behaviors of plutonium and thorium isotopes at Tsukuba and Mt.Haruna in Japan indicate the sources of atmospheric dust, Journal of Environmental Radioactivity, 101(2), 106-112, 2009. doi:10.1016/j.jenvrad.2009.09.003.
6. Igarashi Y., Kikawada, Y., Oda, K., Yamauchi, R., Nomura, M., Honda, T., Oi, T., and Hirose, K., Anomalous Uranium Isotope Ratio in Atmospheric Deposits in Japan, Journal of Nuclear Science and Technology, 46(12), 1094-1098. 2009.

2008

1. Aoyama, M., Hirose, K., Nemoto, K., Takatsuki, Y., and Tsumune, D., Water masses labeled with global fallout ^{137}Cs formed by subduction in the North Pacific, Geophysical Research Letters, 35, L01604, 2008. doi:10.1029/2007GL031964.
2. Hirose, K., Igarashi, Y., and Aoyama, M., Analysis of the 50-year records of the atmospheric deposition of long-loved radionuclides in Japan, Applied Radiation and Isotopes, 66, 1675-1678, 2008.
3. Hirose, K., Aoyama, M., Igarashi, Y., and Komura, K., Improvement of ^{137}Cs analysis in small volume seawater samples using the Ogoya underground facility, Journal of Radioanalytical and Nuclear Chemistry, 276,3,795-798, 2008.
4. Aoyama, M., Hirose, K., Nemoto, K., Takatsuki, Y., and Tsumune, D., Water masses labeled with global fallout ^{137}Cs formed by subduction in the North Pacific, Geophysical Research Letters, 35, L01604, 2008. doi:10.1029/2007GL031964.

2007

1. Hirose, K., Aoyama, M., and Kim, C.S., Plutonium in Seawater of the Pacific Ocean, Journal of Radioanalytical and Nuclear Chemistry, 274 No. 3, 635-638, 2007.
2. Hirose, K., Igarashi, Y., and Aoyama, M., 50 years records of atmospheric deposition of long-lived anthropogenic radionuclides in Japan, International Conference on Environmental Radioactivity: From Measurements and Assessments to Regulation, IAEA-CN-145, 95-96, 2007.
3. Hirose, K., Igarashi, Y., and Aoyama, M., Recent trends of plutonium fallout observed in Japan: Comparison with natural lithogenic radionuclides, thorium isotopes, Journal of Radioanalytical and Nuclear Chemistry, 273 No.1, 115-118, 2007.
4. Hirose, K., Aoyama, M., Fukasawa, M., Kim, C. S., Komura, K., Povinec, P. P., and Sanchez-Cabeza, J. A., Plutonium and ^{137}Cs in surface water of the South Pacific Ocean, Science of the Total Environment, 381, 243-255, 2007.

2006

1. Yamamoto, M., Sakaguchi, A., Sasaki, K., Hirose, K., Igarashi, Y., and Kim, C.K., Seasonal and spatial variation of atmospheric ^{210}Pb and ^{7}Be deposition: features of the Japan Sea side of Japan, Journal of Environmental Radioactivity, 86, 110-131, 2006.
2. Hirose, K., Aoyama, M., Kim, C.S., Kim, C.K., and Povinec, P.P., Plutonium isotopes in seawater of the North Pacific: effects of close-in fallout, INTERNATIONAL CONFERENCE ON ISOTOPES AND ENVIRONMENTAL STUDIES. Eds. P. Povinec, J.A. Sanchez-Cabeza. Vol. 8 of Radioactivity in the Environment, Elsevier, London, 2006.
3. Aoyama, M., Hirose, K., and Igarashi, Y., Re-construction and updating our understanding on the global weapons tests ^{137}Cs fallout, Journal of Environmental Monitoring, 8, 431-438, 2006.
4. Aoyama, M., Fukasawa, M., Hirose, K., Mantoura, R.F.C., Povinec, P.P., Kim, C.S., and Komura, K., Southern Hemisphere Ocean Tracer Study (SHOTS): An overview and preliminary results, INTERNATIONAL CONFERENCE ON ISOTOPES AND ENVIRONMENTAL STUDIES. Eds. P. Povinec, J.A. Sanchez-Cabeza, Vol. 8 of Radioactivity in the Environment, Elsevier, London, 2006.
5. Inoue, H.Y., Matsueda, H., Igarashi, Y., Sawa, Y., Wada, A., Nemoto, K., Sartorius, H., and Schlosser, C., Seasonal and long-term variations in atmospheric CO_2 and ^{85}Kr in Tsukuba, Central Japan, Journal of the Meteorological Society of Japan, 84/6, 959-968, 2006.

2005

1. Hirose, K., Aoyama, M., Igarashi, Y., and Komura, K., Extremely low background measurements of ^{137}Cs in seawater samples using an underground facility (Ogoya), Journal of Radioanalytical and Nuclear Chemistry, 263, 349-353, 2005.
2. Povinec, P.P., Aarkrog, A., Buesseler, K.O., Delfanti, R., Hirose, K., Hong, G.H., Ito, T., Livingston, H.D., Nies, H., Noshkin, V.E., Shima, S., and Togawa, O., ^{90}Sr, ^{137}Cs and ^{239,240}Pu concentration surface water time series in the Pacific and Indian Oceans- WOMARS results, Journal of Environmental Radioactivity, 81, 63-87, 2005.
3. Igarashi, Y., Aoyama, M., Hirose, K., Povinec, P.P., and Yabuki, S., What anthropogenic radionuclides (^{90}Sr and ^{137}Cs) in atmospheric deposition, surface soils and Aeoliandusts suggest for dust transport over JAPAN, Water, Air, and Soil Pollution: Focus, 5, 51-69, 2005.

2004

1. Hirose, K., Kim, C.K., Kim, C.S., Chang, B.W., Igarashi, Y., and Aoyama, M., Wet and dry depositions of plutonium in Daejeon, Korea, The Science of the Total Environment, 332, 243-252, 2004.
2. Povinec, P.P., Hirose, K., Honda, T., Ito, T., MarianScott, E., and Togawa, O., Spatial distribution of ^{3}H, ^{90}Sr, ^{137}Cs and ^{239,240}Pu in surface waters of the Pacific and Indian Oceans - GLOMARD database, Journal of Environmental Radioactivity, 76, 113-137, 2004.
3. Aoyama, M., and Hirose, K., Artificial Radionuclides database in the Pacific Ocean: Ham database, TheScientificWorldJOURNAL, 4, 200-215, 2004.
4. Hirota, M., Nemoto, K., Wada, A., Igarashi, Y., Aoyama, M., Matsueda, H., Hirose, K., Sartorius, H., Schlosser, C., Schmid, S., Weiss, W., and Fujii, K., Spatial and Temporal Variations of Atmospheric ^{85}Kr Observed During 1995-2001 in Japan: Estimation of Atmospheric ^{85}Kr inventory in the Northern Hemisphere, Journal of Radiation Research, 45, 405-413, 2004.
5. Hirose, K., Chemical Speciation of Thorium in Marine Biogenic Particulate matter, The Scientific World JOURNAL 4, 67-76, 2004.

2003

1. Hirose, K., and Aoyama, M., Analysis of ^{137}Cs and ^{239,240}Pu concentrations in surface waters of the Pacific Ocean, Deep-Sea Research II, 50, 2675-2700, 2003.
2. Hirose, K., Aoyama, and Povinec, P.P., Concentration of particulate plutonium in surface and deep-water, samples collected during the IAEA'97 expedition, Deep-Sea Research II, 50, 2639-2647, 2003.

3. Povinec, P.P., Livingston, H.D., Shima, S., Aoyama, M., Gastaud, J., Goroncy, I., Hirose, K., Huynh-Ngoc, L., Ikeuchi, Y., Ito, T., Rosa, J.L., Kwong, L.L.W., Lee, S.H., Moriya, H., Mulsow, S., Oregioni, B., Pettersson, H., and Togawa, O., IAEA'97 expedition to the NW Pacific Ocean-Results of oceanographic and radionuclide investigations of the water column, Deep-Sea Research II, 50,2607-2637, 2003.
4. Ito, T., Povinec, P.P., Togawa, O., and Hirose, K., Temporal and Spatial variation of anthropogenic radionuclides in seawater of the Japan Sea, Deep-Sea Research II, 50, 2701-2711, 2003.
5. Tsumune, D., Aoyama, M., and Hirose, K., Behavior of ^{137}Cs and concentrations in the North Pacific in an ocean general circulation model, Journal of Geophysical Research, 108, C8, 3262, 2003.
6. Hirose, K., and Aoyama, M., Present Background Levels of Surface ^{137}Cs and $^{239, 240}$Pu Concentrations in the Pacific, Journal of Environmental Radioactivity, 69(1-2), 53-60, 2003.
7. Tsumune, D., M. Aoyama, and K. Hirose, Numerical simulation of ^{137}Cs and $^{239, 240}$Pu concentrations by an ocean general circulation model, Journal of Environmental Radioactivity, 69(1-2), 61-84, 2003.
8. Aoyama, M., and Hirose, K., Temporal variation of ^{137}Cs water column inventory in the North Pacific since the 1960s, Journal of Environmental Radioactivity, 69(1-2),107-117, 2003.
9. Hirose, K., Igarashi, Y., Aoyama, M., Kim, C.K., Kim, C.S., Chang, B.W., Recent trends of plutonium fallout observed in Japan: plutonium as a proxy for desertification, J. Environ. Monit, 5, 302-307, 2003.
10. Igarashi, Y., Aoyama, M., Hirose, K., Miyao, T., Nemoto, K., Tomita, M., and Fujikawa, T., Resuspension: Decadal Monitoring Time Series of the Anthropogenic Radioactivity Deposition in Japan, Journal of Radiation Research, 44, 319-328, 2003.
11. Kim, C.K., Kim, C.S., Chang, B.U., Choi, S.W., Chung, C.S., Hong, G.H., Hirose, K., and Igarashi, Y., Plutonium isotopes in seas around the Korean Peninsula, The Science of the Total Environment, 318, 197-209, 2003.
12. Kim, C.K., Kim, C.S., Chang, B.U., Choi, S.W., Chung, C.S., Hong, G.H., Hirose, K., and Pettersson, H.B.L., ^{240}Pu /^{239}Pu atom ratios in the bottom sediments of the NW Pacific Ocean, Journal of Radioanalytical and Nuclear Chemistry, 258(2), 265-268, 2003.
13. Lee, H.N., Tanaka, T., Chiba, M., and Igarashi, Y., Long range transport of Asian dust from dust storms and its impact on Japan, Water, Air, and Soil Pollution, 3, 231-243, 2003
14. Hirose, K., Implication of POC/^{234}Th ratios in oceanic particulate matter: an approach to particle aggregation, Papers of Meteorology and Geophysics, 53, 4, 109-118, 2003.

2002

1. Hirose, K., Miyao, T., Aoyama, M., and Igarashi, Y., Plutonium isotopes in the Sea of Japan, Journal of Radioanalytical and Nuclear Chemistry, 252, 293-299, 2002.
2. Hirose, K., and Aoyama, M., Chemical speciation of plutonium in seawater, Analytical and Bioanalytical Chemistry, 372, 418-420, 2002.
3. Hong, G.H., Kim, Y.I., Lee, S.H., Cooper, L.W., Choe, S.M., Tkalin, A.V., Lee, T., Kim, S.H., Chung, C.S., and Hirose, K., $^{239+240}$Pu and ^{137}Cs concentrations for zooplankton and nekton in the Northwest Pacific and Antarctic Oceans 1993-1996, Marine Pollution Bulletin, 44, 660-665, 2002.

2001

1. Igarashi, Y., Aoyama, M., Nemoto, K., Hirose, K., Miyao, T., Fushimi, K., Suzuki, M., Yasui, S., Asai, Y., Aoki, I., Fujii, K., Yamamoto, S., Sartorius, H., and Weiss, W., ^{85}Kr measurement system for continuous monitoring at Meteorological Research Institute, Japan, Journal of Environmental Monitoring, 3, 688-696, 2001.
2. Igarashi, Y., Aoyama, M., Hirose, K., Miyao, T., and Yabuki, S., Is it Possible to use ^{90}Sr and ^{137}Cs as tracers for the aeolian transport?, Water. Air. And Soil Pollution, 130, 349-354, 2001
3. Hirose, K., Igarashi, Y., Aoyama, M., and Miyao, T., Long-term trends of plutonium fallout observed in Japan, In Plutonium in the Environment, 251-266, 2001.

4. Aoyama, M., Hirose, K., Miyao, T., Igarashi, Y., and Povinec, P.P., ^{137}Cs activity in surface water in the western North Pacific, J. Radioanal. Nucl. Chem., 248, 3, 789-793, 2001.
5. Aoyama, M., Hirose, K., Miyao, T., Igarashi, Y., and Povinec, P.P., Temporal variation of ^{137}Cs inventory in the western North Pacific, J Radioanal Nucl Chem, 248, 3, 785-787, 2001
6. Hirose, K., Aoyama, M., Miyao, T., and Igarashi, Y., Plutonium in seawaters on the western North Pacific, J Radioanal Nucl Chem, 248, 3, 771-776, 2001.
7. Tsumune. D., Aoyama, M., Hirose, K., Maruyama, K., and Nakashiki, N., Caluculation of Artificial Radionuclides in the Ocean by an Ocean General Circulation Model, J Radioanal Nucl Chem, 248, 3, 777-783, 2001.

2000

1. Shiraishi, K., Kimura, S., Yonehara, H., Takada, J., Ishikawa, M., Igarashi, Y., Aoyama, M., Komura, K., and Nakazima, T., Survey of external dose around the JCO facility using sugar samples and ESR method, Adv. ESR Appl, 16, 9-14, 2000.
2. Komura, K, Yamamoto, M., Muroyama, T., Murata, Y., Nakanishi, T., Hoshi, M., Takada, J., Ishikawa, M., Kitagawa, K., Suga, S., Endo, A., Tozaki, N., Mitsugashira, T., Hara, M., Hashimoto, T., Takano, M., Yanagawa, Y., Tsuboi, T., Ichimasa, M., Ichimasa, Y., Imura, H., Sasajima, E., Seki, R., Saito, Y., Kondo, M., Kojima, S., Muramatsu, Y., Yoshida, S., Shibata, S., Yonehara, H., Watanabe, Y., Kimura, S., Shiraishi, K., Bannai, T., Sahoo, S.K., Igarashi, Y., Aoyama, M., Hirose, K., Uehiro, M., Doi, T., and Matsuzawa, T., The JCO criticality accident at Tokai-mura, Japan: an overview of the sampling campaign and preliminary results, J. Environ. Radioactivity, 50, 3-14, 2000.
3. Igarashi, Y., Miyao, T., Aoyama, M., Hirose, K., Sartorius, H., and Weiss, W., Radioactive noble gases in the surface air monitored at MRI, Tsukuba, before and after the JCO accident, J. Environ. Radioactivity, 50, 107-118, 2000.
4. Miyao, T., Hirose, K., Aoyama, M., and Igarashi, Y., Trace of the recent deep water formation in the Japan Sea deduced from historical ^{137}Cs data, Geophys. Res. Lett., 27, 22, 3731-3734, 2000.
5. Aoyama, M., Hirose, K., Miyao, T., and Igarashi, Y., Low level ^{137}Cs measurements in deep seawater samples, Appl. Radiat. Isot, 53, 159-162, 2000.
6. Igarashi, Y., Sarutorius, H., Miyao, T., Weiss, W., Fushimi, K., Aoyama, M., Hirose, K., and Inoue, H.Y., ^{85}Kr and ^{133}Xe monitoring at MRI, Tsukuba and its importance, J. Environ. Radioactivity, 48, 191-202, 2000.

1999

1. Hirose, K., Amano, H., Baxter, M.S., Chaykovskaya, E., Chumichev, V.B., Hong, G.H., Isogai, K., Kim, C.K., Kim, S.H., Miyao, T., Morimoto. T, Nikitin, A., Oda, K., Pettersson, H.B.L., Povinec, P.P., Seto, Y., Tkalin, A., Togawa, O., and Veletova, N.K., Anthropogenic radionuclides in seawater in the East Sea/Japan Sea: Results of the first-stage Japanese-Korean-Russian expedition, J. Environ. Radioactivity, 43, 1-13, 1999.
2. Igarashi, Y., Aoyama, M., Miyao, T., Hirose, K., Komura, K., and Yamamoto, M., Air concentration of radiocaesium in Tsukuba, Japan following the release from the Tokai waste treatment plant: comparisons of observations with predictions, Applied Radiation and Isotopes, 50, 1063-1073, 1999.
3. Igarashi, Y., Aoyama, M., Miyao, T., Hirose, K., and Tomita, M., Anomalous ^{90}Sr deposition during the fall, 1995 at MRI, Tsukuba, Japan, J. Radioanal. Nucl. Chem, 239(3), 539-542, 1999.
4. Ikeuchi, Y., Amano, H., Aoyama, M., Berezhnov, V.I., Chaykovskaya, E., Chumichev, V.B., Chung, C.S., Gastaud, J., Hirose, K., Hong, G.H., Kim, C.K., Kim, S.H., Miyao, T., Morimoto, T., Nikitin, A., Oda, K., Pettersson, H.B.L., Povinec, P.P., Tkalin, A., Togawa, O., and Veletova, N.K., Anthropogenic radionuclides in seawater of the Far Eastern Seas, Sci. Total Environ., 237/238, 203-212, 1999.

5. Pettersson, H.B.L., Amano, H., Berezhnov, V.I., Chaykovskaya, E., Chumichev, V.B., Chung, C.S., Gastaud, J., Hirose, K., Hong, G.H., Kim, C. K., Lee, S.H., Morimoto, T., Nikitin, A., Oda, K., Povinec, P.P., Suzuki, E., Tkalin, A., Togawa, O., Veletova, N.K., Volkov, Y., and Yoshida, K., Anthropogenic radionuclides in sediments in the NW Pacific Ocean and its marginal seas:results of the 1994-1995 Japanese-Korean-Russian expeditions, Sci. Total Environ, 237/238, 213-224, 1999.

1998

1. Igarashi, Y., Hirose, K., and Otsuji-Hatori, M., Beryllium-7 Deposition and Its Relation to Sulfate Deposition, J. Atmos. Chem, 29, 217-231, 1998.
2. Miyao, T., Hirose, K., Aoyama, M., and Igarashi, Y., Temporal variation of ^{137}Cs and $^{239, 240}$Pu in the sea of Japan, J. Environ. Radioactivity, 40, 239-250, 1998.

1997

1. Hirose, K., Complexation-scavenging of plutonium in the ocean, Radioprotection - Colloq, 32, C2-225 - C2-230, 1997.

1996

1. Igarashi, Y., Otsuji-Hattori, M., and Hirose, K., Recent deposition of ^{90}Sr and ^{137}Cs observed in Tsukuba, J. Environ. Radioactivity, 31, 157-169, 1996.
2. Otsuji-Hatori. M., Igarashi, Y., and Hirose, K., Preparation of a Reference Fall out Material for Activity Measurements, J. Environ Radioactivity, 31, 2, 143-155, 1966.

1995

1. Aoyama, M., and Hirose, K., The temporal and spatial variation of ^{137}Cs concentration in the western North Pacific and its marginal seas during the period from 1979 to 1988, J. Environ. Radioactivity, 29, 57-74, 1995.
2. Hirose, K., Geochemical studies on the Chernobyl radioactivity in environmental samples, J. Radioanal. Nucl. Chem., Articles, 197, 315-335, 1995.

1994

1. Hirose, K., Takatani, S., and Aoyama, M., Deposition of ^{90}Sr and plutonium isotopes derived from the Chernobyl accident in Japan, J. Radioanal. Nucl. Chem., Articles, 182, 349-358, 1994.

1993

1. Hirose, K., and Sugimura, Y., Chemical speciation of particulate ^{238}U, $^{239, 240}$Pu and Th isotopes in seawater, Sci. Total Environ., 130/131, 517-524, 1993.
2. Hirose, K., Takatani, S., and Aoyama, M., Wet deposition of radionuclides derived from the Chernobyl accident, J. Atmos. Chem., 17, 61-71, 1993.
3. Shiraishi, K., Igarashi, Y., Yamamoto, M., and Nakajima, T., Concentrations of thorium and uranium in freshwater samples collected in the former USSR, J. Radioanal. Nucl. Chem., 185,157-165, 1993.

1992

1. Aoyama, M., Hirose, K., and Takatani, S., Particle size dependent dry deposition velocity of the Chernobyl radioactivity, In Precipitation Scavenging and Atmosphere - Surface Exchange.volume 3, The 22e Summers Volume: Application and Appraisals. Coordinated by S.E. Schwartz and W.G.N. Slinn. Hemisphere Publishing Corporation, Washington, 1581-1593, 1992.
2. Hirose, K., Sugimura, Y., and Aoyama, M., Plutonium and ^{137}Cs in the western North Pacific: estimation of residence time of plutonium in surface water, Appl. Radiat. Isot, 43, 349-359, 1992.

1991

1. Aoyama, M., Hirose, K., and Sugimura, Y., The temporal variation of stratospheric fallout derived from the Chernobyl accident, J. Environ. Radioactivity, 13, 103-115, 1991.
2. Hirose, K., and Sugimura, Y., Chemical speciation of particulate uranium in seawater, J. Radioanal. Nucl. Chem., Articles, 149, 83-96, 1991.

1990

1. Hirose, K., and Sugimura, Y., Plutonium isotopes in the surface air in Japan: effect of Chernobyl accident, J. Radioanal. Nucl. Chem., Articles, 138, 127-138, 1990.
2. Hirose, K., Aoyama, M., and Sugimura, Y., Plutonium and cesium isotopes in river waters in Japan, J. Radioanal. Nucl. Chem., Articles, 141, 191-202, 1990.
3. Hirose, K., Aoyama, M., and Sugimura, Y., Short and long term effects of Chernobyl radioactivity on deposition and air concentrations in Japan, IAEA-SM 306/129, 141-149, 1990.

1988

1. Aoyama, M., Evidence of stratospheric fallout of caesium isotopes from Chernobyl accident, Geophys. Res. Lett., 15, 327-330, 1988.
2. Miyake, Y., Saruhashi, K., Sugimura, Y., Kanazawa, T., and Hirose, K., Contents of ^{137}Cs, plutonium and americium isotopes in the southern ocean waters, Pap. Met. Geophys, 39, 95-113, 1988.

1987

1. Aoyama, M., Hirose, K., and Sugimura, Y., Deposition of gamma-emitting nuclides in Japan after the reactor-IV accident at Chernobyl, J. Radioanal. Nucl. Chem., Articles, 116, 291-306, 1987.
2. Hirose, K., Aoyama, M., Katsuragi, Y., and Sugimura, Y., Annual deposition of Sr-90, Cs-137 and Pu-239, 240 from the 1961-1980 nuclear explosions: a simple model, J. Meteor. Soc. Japan, 65, 259-277, 1987.

1986

1. Aoyama, M., Hirose, K., Suzuki, Y., and Sugimura, Y., High level radioactive nuclides in Japan in May, Nature, 321, 819-820, 1986.
2. Hirose, K., Sugimura, Y., and Katsuragi, Y., ^{90}Sr and $^{239+240}$Pu in the surface air in Japan: their concentrations and size distributions, Pap. Met. Geophys, 37, 255-269, 1986.
3. Katsuragi, Y., and Aoyama, M., Seasonal variation of Sr-90 fallout in Japan through the end of 1983, Pap. Met. Geophys., 37, 15-36, 1986.
4. Suzuki, Y., Inoue, H., Katsuragi, Y., and Sugimura, Y., The distribution of 85Krin the air over the North and South Pacific Ocean Mem., Natl. Inst. Polar Res., Spec. Issue, 40, 462-466, 1986.

1985

1. Hirose, K., and Sugimura, Y., A new method of plutonium speciation in seawater, J. Radioanal. Nucl. Chem, Articles, 92, 363-369, 1985.

1984

1. Hirose, K., and Sugimura, Y., Plutonium in the surface air in Japan, Health Phys., 46, 1281-1285, 1984.
2. Inoue, H., Katsuragi, Y., and Shigehara, K., Tritiated water vapor in the surface air at Tokyo, Pap. Met. Geophys, 35, 11-20, 1984.

1983

1. Katsuragi, Y., A study of ^{90}Sr fallout in Japan, Pap. Met. Geophys., 33, 277-291, 1983.
2. Katsuragi, Y., Kawamura, K., and Inoue, H., Tritium fallout in Tokyo, Pap. Met. Geophys, 34, 21-30, 1983.

1982

1. Inoue, H., and Katsuragi, Y., A study of tritium fallout in Japan, Pap. Met. Geophys, 32, 21-28, 1982.
2. Katsuragi, Y., Hirose, K., and Sugimura, Y., A study of plutonium fallout in Japan, Pap. Met. Geophys, 33, 85-93, 1982.

1981

1. Hirose, K., and Sugimura, Y., Concentration of Uranium and the activity ratio of ^{234}U /^{238}U in surface air-effect of atmospheric burn-up of cosmos-954, Pap. Met. Geophys., 32, 317-322, 1981.
2. Hirose, K., and Sugimura, Y., Plutonium content of river water in Japan, Pap. Met. Geophys, 32, 301-305, 1981.
3. Sugimura, Y., and M. Mayeda, An improved method of analysis of uranium in sea water using chelating resin, Pap. Met. Geophys, 32, 167-171, 1981.

1980

1. Sugimura, Y., The uranium content and the activity ratio ^{234}U /^{238}U in sea water in the Pacific ocean, Isotope Marine Chemistry, 211-246, 1980.

1979

1. Sugiura, Y., Saruhashi, K., and Miyake, Y., Evaluation on the disposal of radioactive wastes into the North Pacific. - the effect of steady flow and up - welling, Proc. The 3rd NEA Seminar on Marine Radioecology, 1979.

1978

1. Miyake, Y., Nuclear weapons and radioactive pollution of the earth's environment, In, Proc. Internal Symp. On the damage and after-effects of the atomic bombing of Hiroshima and Nagasaki July 21-Aug., 9, 1977, Tokyo, 164-188, 1978.

1976

1. Miyake, Y., and Saruhashi, K., A critical study on the IAEA definition of high level radioactive waste unsuitable for dumping at sea, Pap. Met. Geophys. 27, 75-80, 1976.
2. Miyake, Y., and Saruhashi, K., Disposal of radioactive waste into deep seas, J. Radiat. Res., 17, 42-43, 1976.
3. Miyake, Y., and Sugimura, Y., The plutonium content in the Pacific Ocean waters, Proc. of Symp. on Transuranium Nuclides in the Environment, San Francisco, 17-21 Nov. 1975, USERDA and IAEA, IAEA-SM-199/22, 91-105,1976.
4. Sugimura, Y., Symposium II plutonium in environment, II-1.Distribution and behavior of plutonium in the global environments, J. Radiat. Res., 17, 4-5, 1976.
5. Sugiura, Y., Saruhashi, K., and Miyake, Y., Evaluation on the disposal of radioactive wastes into the North Pacific, Pap. Met. Geophys, 27, 81-87, 1976.

1975

1. Miyake, Y., Shimada, T., Kawamura, K., Sugimura, Y., Shigehara, K., and Saruhashi, K., Distribution of tritium in the Pacific ocean, Rec. Oceanogr. Works Japan, 13, 17, 1975.
2. Miyake, Y., Katsuragi, Y., and Sugimura, Y., Plutonium fallout in Tokyo, Pap. Met. Geophys, 26, 1-8, 1975.
3. Miyake, Y., Sugimura, Y., and Hirao, Y., Uranium, thorium and potassium contents in granitic and basaltic rocks in Japan, In, The Natural Radiation Environment II, II, Proc. 2nd Intnl. Symp. On Natural Radiation Environment, Aug. 7-11, 1972, Houston, Texas, USA, ed. J. A. S. Adams, W. M. Lowder, T. F. Gesell, 535-558,1975.
4. Saruhashi, K., I-1 The global radioactive contamination due to nuclear weapon testings, J. Radiat. Res., 16, 47, 1975.
5. Saruhashi, K., Katsuragi, Y., Kanazawa, T., Sugimura, Y., and Miyake, Y., ^{90}Sr and ^{137}Cs in the Pacific waters, Rec. Oceanogr. Works Japan, 13, 1-15, 1975.

1973

1. Miyake, Y., and Saruhashi, K., The radio-carbon model of the ocean, Pap. Met. Geophys, 24, 263-271, 1973.
2. Miyake, Y., Saruhashi, K., and Sugimura, Y., The isotopic ratio ^{234}U /^{238}U in sea water and its bearings on the isotopic ratio in river waters, Oceanogr. Works Japan, 12, 23-25, 1973.
3. Miyake, Y., Sugimura, Y., and Saruhashi, K., Content of plutonium in river water in Japan, Pap. Met. Geophys, 24, 75-78, 1973.
4. Miyake, Y., Sugimura, Y., and Yasujima, T., Thorium isotope content in river water in Japan, Pap. Met. Geophys, 24, 67-73, 1973.

1972

1. Miyake, Y., Sugimura, Y., and Uchida, T., A new method of spectrophotometric determination of uranium in sea water and uranium content with ^{234}U /^{238}U ratio in the Pacific water, Rec. Oceanogr. Works Japan, 11, 53-63, 1972.

1970

1. Miyake, Y., Katsuragi, Y., and Sugimura, Y., A study on plutonium fallout, J. Geophys. Res., 75, 2329-2330, 1970.
2. Miyake, Y., Sugimura, Y., and Mayeda, M., The uranium content and the activity ratio ^{234}U /^{238}U in marine organisms and sea water in the western North Pacific, J. Oceanogr. Soc. Japan, 26, 123-129, 1970.

1969

1. Miyake, Y., Radioactive contamination of the ocean, Bull. Jpn. Soc. Fisheries Oceanogr., Nov., 1969, 1969.

1968

1. Miyake, Y., and Sugimura, Y., Plutonium content in the western North Pacific waters, Pap. Met. Geophys, 19, 481-485, 1968.
2. Miyake, Y., Katsuragi, Y., and Sugimura, Y., Deposition of plutonium in Tokyo through the end of 1966, Pap. Met. Geophys, 19, 267-276, 1968.

1967

1. Miyake, Y., and Kanazawa, T., Atmospheric ozone and radioactive fallout, Pap. Met. Geophys., 18, 311-326, 1967.
2. Miyake, Y., Radioactive contamination of the ocean, J. Radiat. Res., 8, 1, 1967.
3. Miyake, Y., Sea, radioactivity in, International Dictionary of Geophysics, 1-7, 1967.

1966

1. Miyake, Y., and Saruhashi, K., On the radio-carbon age of the ocean waters, Pap. Met. Geophys., 17, 218-223, 1966.
2. Miyake, Y., and Sugimura, Y., Ratio ^{234}U /^{238}U and the uranium concentration in seawater in the western North Pacific, J. Geophys. Res., 71, 3083-3087, 1966.

1965

1. Kuroda, P. K., Miyake, Y., and Nemoto, J., Strontium isotopes Global circulation after the Chinese nuclear explosion of 14 May 1965, Science, 150, 1289-1290, 1965.
2. Miyake, Y., Saruhashi, K., Katsuragi K., and Kanazawa, T., Radioactivity of dust and rain - the ratio of Cs-137 and Sr-90 in the radioactive fallout, Proc. Internl. Conf. On Cloud Physics,Tokyo, IAMAP, 395-399, 1965.
3. Park, K., George, M.J., Miyake, Y., Saruhashi, K., Katsuragi, Y., and Kanazawa, T., Strontium-90 and caesium-137 in Columbia river plume, July 1964, Nature, 208, 1084-1085, 1965.

1964

1. Miyake, Y., and Sugimura, Y., Uranium and radium in the western North Pacific waters, Studies on Oceanography, Prof. K. Hidaka Sixtieth Birthday Commemorative Volume, Univ. of Tokyo Press, Tokyo, 274-278, 1964.
2. Miyake, Y., and Ohtsuka, Y., Beryllium-7 in rain water, Pap. Met. Geophys, 15, 89-92, 1964.
3. Miyake, Y., A sequential procedure for the radiochemical analysis of marine material, Annex to safety series 11."Method of surveying and monitoring marine radioactivity, IAEA, Vienna, 26, 1964.
4. Miyake, Y., Atomic weapons and the pollution of the sea, The East, 3, 64-68, 1964.
5. Miyake, Y., Saruhashi, K., Katsuragi, Y., Kanazawa, T., and Sugimura, Y., Uranium, radium, thorium, Ionium, strontium 90 and cesium 137 in coastal waters of Japan, In, Recent Researches in the Fields of Hydrosphere, Atmosphere and Nuclear Geochemistry, published by Editorial Committee of Sugawara Festival Volume, Maruzen Co. Ltd., 127-141, 1964.
6. Miyake, Y., Sugimura, Y., and Tsubota, H., Content of uranium, radium, and thorium in river waters in Japan, In, The Natural Radiation Environment, ed. By J. A. S. Adams and W. M. Lowder, Univ. of Chicago Press, Chicago, Rice Univ. Semicentennial Series, 219-225, 1964.
7. Sugimura, Y., Torii, T., and Murata, S., Uranium distribution in drake passage waters, Nature, 204, 464-465, 1964.

1963

1. Folsom, T.R., and Saruhashi, K., A comparison of analytical techniques used for determination of fallout cesium in sea water for oceanographic purpose, J. Radiat. Res., 4, 39-53, 1963.
2. Miyake, Y., and Tsubota, H., Estimation of the direct contribution of meteoric water to river waters by means of fall-out radio-cesium and radiostrontium, "Radioisotopes in Hydrology" Proc. IAEA Symp., Tokyo. IAEA, Vienna, 425-431, 1963.
3. Miyake, Y., Artificial radioactivity in the Pacific ocean, IUGG Monograph, 20 Radioactive traces in oceanography, 1963.
4. Miyake, Y., Saruhashi, K., Katsuragi, K., and Kanazawa, T., Deposition of Cs-137 and Sr-90 in Tokyo through the end of July 1963, Pap. Met. Geophys, 13, 180-181, 1963.
5. Miyake, Y., Saruhashi, K., Katsuragi, Y., Kanazawa, T., and Tsunogai, S., Deposition of ^{90}Sr and ^{137}Cs in Tokyo through the end of July 1963, Pap. Met. Geophys, 14, 58-65, 1963.
6. Miyake, Y., Sugiura, Y., and Tsubota, H., II. Contents of uranium, radium, and thorium in river waters in Japan, The Natural Radiation Environment, RICE Univ. semicentennial Pub, 1963.

1962

1. Miyake, Y., Saruhashi, K., Katsuragi, Y., and Kanazawa, T., Seasonal variation of radioactive fallout, J. Geophys. Res., 67, 189-193, 1962.
2. Miyake, Y., Saruhashi, K., Katsuragi, Y., and Kanazawa, T., Penetration of ^{90}Sr and ^{137}Cs in deep layers of the Pacific and vertical diffusion rate of deep water, J. Radiat. Res., 3, 141-147, 1962.
3. Miyake, Y., Saruhashi, K., Katsuragi, Y., and Kanazawa, T., The peak in radioactive fallout in the temperate zone of the northern hemisphere, J. Radiat. Res., 3,148-152, 1962.
4. Sugimura, Y., and Sugimura, T., Uranium in recent Japanese sediments, Nature, 194, 568-569, 1962.

1961

1. Miyake, Y., Saruhashi, K., Katsuragi, Y., and Kanazawa, T., Cesium 137 and strontium 90 in sea water, J. Radiat. Res., 2 25-28, 1961.
2. Miyake, Y., Saruhashi, K., Katsuragi, Y., and Kanazawa, T., Cesium 137 and strontium 90 in sea water, Pap. Met. Geophys., 12, 85-88, 1961.

1960

1. Miyake, Y., and Saruhashi, K., Vertical and horizontal mixing rates of radioactive material in the ocean, Disposal of Radioactive wastes IAEA Vienna, 167-173, 1960.
2. Miyake, Y., and Katsuragi, Y., Strontium 90 in western North Pacific surface waters, Pap. Met. Geophys., 11, 188-190, 1960.

3. Miyake, Y., Saruhashi, K., Katsuragi, Y., and Kanazawa, T., Radioactive fallout in Japan and its bearings on meteorological conditions, Pap. Met. Geophys., 11, 151-158, 1960.

1959

1. Miyake, Y., Saruhashi, K., and Katsuragi, Y., The Sr-90 fallout and the air motion, Pap. Met. Geophys., 9, 172-176, 1959.
2. Miyake, Y., Special committee on oceanic research, Working Group on Radioactivity in the Ocean, 1959.

1958

1. Miyake, Y., and Saruhashi, K., Distribution of man-made radio-activity in the North Pacific through summer 1955, J. Mar. Res., 17, 383-389, 1958.
2. Miyake, Y., and Sugiura, Y., The method of measurement of radioactivity in sea water, Pap. Met. Geophys., 9, 48-50, 1958.
3. Miyake, Y., Hazards to human health of radioactive dust, Radio Japan, 2, 3-5, 1958.
4. Miyake, Y., The distribution of artificial radioactivity in the equatorial region in the Pacific in the summer of 1956, The Proc. 9th Pacific Science Congress, 16, 227, 1958.

1957

1. Miyake, Y., and Saruhashi, K., The world-wide strontium 90 deposition during the period from 1951 to the fall of 1955, Pap. Met. Geophys., 8, 241-243, 1957.
2. Miyake, Y., The biological effects of nuclear tests - warning by Japanese scientists, Radio Japan, 1, 3-5, 1957.
3. Miyake, Y., XI. Methods for the measurement of radioactivity in sea water, Annuals of International Geophysical Year, 5, 1957.
4. Miyake, Y., XII. Radioactivity as a tracer of air motions in the atmosphere, Symp. On radioactivity, IGY, Utrecht, 360, 1957.
5. Miyake, Y., Sugiura, Y., Saruhashi, K., and Kanazawa, T., The estimation of the amount of Sr-90 deposition and the external infinite gamma does in Japan due to man-made radioactivity, Pap. Met. Geophys., 8, 222-231, 1957.

1956

1. Miyake, Y., On the distribution of radioactivity in the North Pacific ocean in 1954-1955, Internl. Conf. For Peaceful Uses of Atomic Energy in Geneva, August 1955, 13, pp.381-384, 1956.
2. Miyake, Y., Radioactivity in rain water and air, Proc. Internl. Conf. For Peaceful Uses of Atomic Energy in Geneva, August 1955, 13, 345-349, 1956.
3. Sugiura, Y., and Kanazawa, T., On the radioactive fallout collected in Tokyo on 26th November, 1955, Pap. Met. Geophys., 7, 128-135, 1956.

1955

1. Miyake, Y., and Sugiura, Y., Radiochemical analysis of radio-nuclides in sea water collected near BIKINI atoll, Pap. Met. Geophys., 6, 90-92, 1955.
2. Miyake, Y., Effects of atomic explosions on the atmosphere and sea, The research in the effects and influences of the nuclear bomb text explosions, 1-6, 1955.
3. Miyake, Y., Kigoshi, K., and Saruhashi, K., Radiochemical analysis of fission products contained in the soil collected at Tokyo, May, 1954, Pap. Met. Geophys., 6, 1, 93-94, 1955.
4. Miyake, Y., The artificial radioactivity in rain water observed in Japan, 1954-1955, Research in the Effects and Influences of the Nuclear Bomb Test Explosions Science, 151-159, 1955.
5. Miyake, Y., The artificial radioactivity in rain water observed in Japan, from autumn 1954 to spring 1955, Pap. Met. Geophys., 6, 26-32, 1955.
6. Miyake, Y., Sugiura, Y., and Kameda, K., On the artificial radioactivity in the sea near Japan, Pap. Met. Geophys., 6, 90-92, 1955.
7. Miyake, Y., Sugiura, Y., and Kameda, K., On the distribution of radioactivity in the sea around Bikini atoll in June, 1954, Pap. Met. Geophys., 5, 253-262, 1955.

8. Miyake, Y., Sugiura, Y., and Kameda, K., Research in the effects and influence of the nuclear bomb test explosions, Soc. For Promotion of Science, 415-417, 1955.

1954

1. Miyake, Y., Kigoshi, K., Sugiura, Y., and Saruhashi, K., A study on the productivity in coastal waters by means of the radio-carbon, Pap. Met. Geophys., 5, 89-94, 1954.
2. Miyake, Y., The artificial radioactivity in rain water observed in Japan from May to August, 1954, Pap. Met. Geophys, 5, 173-177, 1954.

7. Publication list (in Japanese) 1954-2015

論文リスト（和文誌）1954-2015

2015

1. 足立光司, 電子顕微鏡がとらえた放射性粒子, 地球化学, 49,185–193, 2015.
2. 木村徹, 五十嵐康人,「大気降下物試料の放射能分析の品質管理」, Proceedings of the 16th Workshop Environmental Radioactivity. KEK Proceedings 2015-4 , 23-27, 2015.

2014

1. 青山道夫, 東電福島原発事故後の海洋での放射能汚染の推移 （With English Abstract）. YAKUGAKU ZASSHI, Journal of the Pharmaceutical Society of Japan. 2014.

2013

1. 青山道夫, 極低レベル放射能測定：少量表層海水および極深層海水試料への応用.放射線, 39(1), 17-20, 2013.

2012

1. 青山道夫, 福島第一原子力発電所から放出された放射性セシウム同位体の北太平洋における総量と分布, 日本原子力学会誌, 54, 780-783, 2012.
2. 青山道夫, 五十嵐康人, 1957 年から始まる気象研究所における環境放射能研究の歴史, 放射線, 38(3), 123-128, 2012.
3. 青山道夫, 海洋に放出された放射性物質の長期地球規模での挙動, 検証！福島第一原発事故-放射性物質の実際と科学者たちの活動の記録（化学 4 月号別冊）. 4, 33-38, 2012.
4. 青山道夫, 五十嵐康人, 広瀬勝己, 月間降下物測定 660 ヶ月が教えること-^{90}Sr, ^{137}Cs および Pu 降下量 1957 年 4 月～2012 年 3 月-. 科学, 82(4), 0442-0457, 2012.

2011

1. 青山道夫, 福島原子力発電所事故による海洋汚染. 理大科学フォーラム, 11(通 巻 329 号), 42-45, 2011.
2. 津旨大輔, 坪野考樹, 青山道夫, 廣瀬勝巳, 福島第一原子力発電所から漏洩した ^{137}Cs の海洋拡散シミュレーション(With English Abstract). 電力中央研究所報告書, V11002, PP.18, 2011.

2009

1. 五十嵐康人, 放射性同位体分析, In 岩坂泰信, 西川雅高, 山田丸, 洪天祥（編）, 黄砂, 古今書院, pp81-87, 東京, 2009.
2. Igarashi, Y., Anthropogenic Radioactivity in Aerosol -A Review Focusing on Studies during the 2000s-, 保健物理, 44(3), 2009.
3. 猪股弥生, 五十嵐康人, 千葉長, 青山道夫, 廣瀬勝己, 再現期間を用いた降水時における高ガンマ線線量率の異常値判定. Radioisotopes, 58, 37-42, 2009.

2007

1. 三浦誓也, 貝森優希, 工藤英嗣, 野呂幸男, 時枝隆之, 廣瀬勝己, 青森県における大気中クリプトン-85 濃度調査, 青森県原子力センター所報, 1, 43-44, 2007.
2. 廣瀬勝己, 青山道夫, Kim、S.A. Kim, 太平洋の海水中のプルトニウムの挙動について, 日本放射化学会誌 別冊, 8 supplement, 103, 2007.

2006

1. 青山道夫, 大気と海洋深層における核実験起源フォールアウトの超低レベル放射能測定, ADIOISOTOPES, 55, 429-438, 2006.
2. 小村和久, 青山道夫, 秋山正和, 氏平祐輔, 大田裕二, 大塚良仁, 大西勝基, 櫻井敬久, 篠原伸夫, Ge 検出器の使用状況に関するアンケート報告, RADIOISOTOPES, 55, 699-707,2006.

2004

1. 廣瀬勝己, 化学トレーサーを利用した海洋変動の研究, 測候時報第 71 巻特別号, 71, S81-S86, 2004.
2. 五十嵐康人, 廣瀬勝己, 放射性降下物標準試料の調製を通じた ^{90}Sr, ^{137}Cs,プルトニウムなどの人工放射性核種分析の相互比較と参照値の決定, 放射化分析, No. 17, 39-42, 2004.

2002

1. 五十嵐康人, ^{90}Sr と ^{137}Cs を用いたダスト輸送過程と再飛散, エアロゾル研究, 12, 17(4), 252, 2002.

1986

1. 鈴木款, 井上久幸, 杉村行勇, 大気中の放射性クリプトンの分布, 地球化学, 20, 106-108, 1986.

1978

1. 葛城幸雄, 人工放射性物質, 天気, 25, 第 11 号, 20-23, 1978.
2. 猿橋勝子, 海洋中の放射性物質を指標とした物質の移動・拡散, 水汚染の機構と解析－環境科学持論－, 日本地球化学編, 東京, 産業図書, 271-287, 1978.
3. 三宅泰雄, 猿橋勝子, 杉村行勇, 葛城幸雄, 金沢照子, 核兵器と地球環境の放射能汚染, 被爆の実相と被爆者の実情 －1977 年 NGO 被爆問題シンポジウム報告書, ISDA－ JNPC 編集, 朝日イブニングニュース社発行, 182-212, 1978.

1976

1. 葛城幸雄, 日本における放射性降下物, 天気, 23, No. 7, 333-345, 1976.
2. 杉村行雄, 環境のなかのプルトニウム, 自然, 3 月号, 1976.

1975

1. 三宅泰雄, 島田利夫, 川村清, 重原好次, 地上大気のトリチウム含量と気象との関係, 日本地球化学会 “環境問題特別号”, 131-135, 1975.

1974

1. 三宅泰雄, 葛城幸雄, 最近の ^{90}Sr 降下物の起源, 天気, 21, 639-644, 1974.

1971

1. 葛城幸雄, 人工放射能による大気汚染, 気象研究ノート, 107, 258-282, 1971

1970

1. 三宅泰雄, 葛城幸雄, 最近の日本における放射性塵の降下, 天気, 17, 593-598, 1970.

1965

1. 葛城幸雄, 日本における Cs-137 および Sr-90 降下について(I), 天気, 12, 323-328, 1965.
2. 葛城幸雄, 日本における Cs-137 および Sr-90 降下について(II) "成層圏における人工放射性物質の滞留時間の推定", 天気, 12, 377-384, 1965.

1964

1. 三宅泰雄, 葛城幸雄, 金沢照子, 放射性降下物の現状と将来, 科学, 34, 142-148, 1964.

1963

1. 三宅泰雄, フォールアウトの気象学の側面, 天気, 9, No. 1, 1962.

1962

1. 三宅泰雄, フォールアウトの気象学的側面, 天気, 9, 1-6, 1962.
2. 三宅泰雄, 猿橋勝子, 放射能による水の汚染, 水利科学, 23, 1-14, 1962.

1958

1. 三宅泰雄, 猿橋勝子, 放射化学と海洋, 科学, 28, 510-513, 1958.

1956

1. 三宅泰雄, 杉浦吉雄, 葛城幸雄, 1955 年 4 月旭川地方に降った放射性の落下塵,気象集誌, 第 2 号, 34, 226-230, 1956.

1955

1. 三宅泰雄, 放射能雨の性格, 測候時報, 22, 196-202, 1955.
2. 三宅泰雄, 日本に降った人工放射性雨・雪[II]9 月～12 月, 天文と気象, 21, 1-8, 1955.
3. 三宅泰雄, 杉浦吉雄, 亀田和久, 日本近海の海水放射能について, 昭和 29 年度海洋資源開発調査報告（黒潮班）, 81-82, 1955.
4. 三宅泰雄, 放射能雨の性格, 測候時報, 22, No. 7, 196-202, 1955.

1954

1. 三宅泰雄, 日本に降った人工放射性雨(1954 年 5-7 月), 天文と気象, 20, 1-8, 1954.
2. 三宅泰雄, 杉浦吉雄,亀田和久, ビキニ海域における人工放射能の分布とその海洋学的考察" ビキニ灰とそれによる傷害 第三", 科学, 24, 601-605, 1954.
3. 三宅泰雄, 有住直介, 磯野謙治, 田島英三, ビキニの灰とそれによる傷害（つづき）日本に降った放射能雨, 科学, 24, No. 8, 405-409, 1954.

年代・雑誌名不明

1. 三宅泰雄, 放射能とその作用, 遺伝,（1975？）
2. 三宅泰雄, 第 II 編 環境の放射能汚染と化学分析,（1970？）
3. 三宅泰雄, 猿橋勝子, 杉村行勇, 海洋における放射性核種, 海洋化学講座, 第 6 巻, 海洋無機化学, 第 4 章, 109-170,（1969？）
4. 三宅泰雄, 田島英三, 日米放射能会議, 8-18,（1954？）

8. History of the studies at the Meteorological Research Institute

表：研究の歴史

研究の歴史

放射能調査研究費以前および、放射能調査研究費での研究

西暦	年度	予算項目	予算項目							
				課題名	課題名	課題名	課題名	課題名	課題名	課題名
1954	昭和29年									
1955	S30	北太平洋観測（日・米・加）								
1956	S31	北太平洋赤道海域観測（日・米・仏）								
1957	S32	国際地球観測年事業費								
1958	S33	国際地球観測年事業費	放射能調査研究費	放射化学分析(落下塵・降水・海水中の放射性物質の研究)		深海水の循環に関する研究（以下深海水）				
1959	S34		放射能調査研究費	放射化学分析		深海水				
1960	S35	国際原子力機関委託研究	放射能調査研究費	放射化学分析		深海水				
1961	S36	国際原子力機関委託研究	放射能調査研究費	放射化学分析		深海水				
1962	S37	国際インド洋観測（日・米・ソ・英・仏）	放射能調査研究費	放射化学分析		深海水				
1963	S38	国際インド洋観測（日・米・ソ・英・仏）	放射能調査研究費	放射化学分析		深海水				
1964	S39	オレゴン州立大学との共同研究	放射能調査研究費	放射化学分析		深海水				
1965	S40		放射能調査研究費	放射化学分析	海洋中の放射性廃棄物のモニタリングの測定法に関する研究（以下海洋廃棄物モニタリング）	深海水		海水中における放射廃棄物の化学的挙動の研究(以下廃棄物化学的挙動）		
1966	S41		放射能調査研究費	放射化学分析	海洋廃棄物モニタリング	深海水		廃棄物化学的挙動		
1967	S42		放射能調査研究費	放射化学分析	海洋廃棄物モニタリング	深海水		廃棄物化学的挙動		
1968	S43		放射能調査研究費	放射化学分析	海洋廃棄物モニタリング	深海水		廃棄物化学的挙動		
1969	S44		放射能調査研究費	放射化学分析		深海水		廃棄物化学的挙動		
1970	S45		放射能調査研究費	放射化学分析		深海水		廃棄物化学的挙動		
1971	S46		放射能調査研究費	放射化学分析		深海水		廃棄物化学的挙動		

放射能調査研究費以前および、放射能調査研究費での研究

西暦	年度	予算項目	予算項目							
				課題名	課題名	課題名	課題名	課題名	課題名	課題名
1972	S47		放射能調査研究費	放射化学分析				放射性固体廃棄物の海洋処分に伴う鉛直拡散に関する研究(以下廃棄物鉛直拡散)		
1973	S48		放射能調査研究費	放射化学分析				廃棄物鉛直拡散		
1974	S49		放射能調査研究費	放射化学分析				廃棄物鉛直拡散	大気中におけるKr-85およびH-3挙動と蓄積に関する調査研究(以下Kr-85／H-3)	
1975	S50		放射能調査研究費	放射化学分析				廃棄物鉛直拡散	Kr-85／H-3	
1976	S51		放射能調査研究費	放射化学分析				廃棄物鉛直拡散	Kr-85／H-3	
1977	S52		放射能調査研究費	放射化学分析				数種の放射性核種の同時測定による深海拡散の研究(以下深海拡散)	原子力施設に由来する放射性気体の広域分布に関する調査研究(以下放射性気体)	
1978	S53		放射能調査研究費	放射化学分析				深海拡散	放射性気体	環境における超ウラン元素の分布と挙動に関する研究(以下超ウラン元素)
1979	S54		放射能調査研究費	放射化学分析				深海拡散	放射性気体	超ウラン元素
1980	S55		放射能調査研究費	放射化学分析				深海拡散	放射性気体	超ウラン元素
1981	S56		放射能調査研究費	放射化学分析				深海拡散	放射性気体	超ウラン元素
1982	S57		放射能調査研究費	放射化学分析				深海拡散	放射性気体	超ウラン元素
1983	S58		放射能調査研究費	放射化学分析				深海拡散	放射性気体	超ウラン元素
1984	S59		放射能調査研究費	放射化学分析				深海拡散	放射性気体	超ウラン元素
1985	S60		放射能調査研究費	放射化学分析				深海拡散	放射性気体	超ウラン元素
1986	S61		放射能調査研究費	放射化学分析				深海拡散	放射性気体	超ウラン元素
1987	S62		放射能調査研究費	放射化学分析				深海拡散	放射性気体	超ウラン元素
1988	S63		放射能調査研究費	放射化学分析				深海拡散	放射性気体	超ウラン元素
1989	H1		放射能調査研究費	放射化学分析				深海拡散	放射性気体	超ウラン元素
1990	H2		放射能調査研究費	放射化学分析				深海拡散	放射性気体	超ウラン元素
1991	H3		放射能調査研究費	放射化学分析				深海拡散	放射性気体	超ウラン元素
1992	H4		放射能調査研究費	放射化学分析	海洋における放射性核種の挙動に関する調査研究(以下海洋放射性核種)				放射性気体	超ウラン元素
1993	H5		放射能調査研究費	放射化学分析	海洋放射性核種				放射性気体	超ウラン元素
1994	H6		放射能調査研究費	放射化学分析	海洋放射性核種				放射性気体	超ウラン元素
1995	H7		放射能調査研究費	放射化学分析	海洋放射性核種				放射性気体	超ウラン元素

放射能調査研究費以前および、放射能調査研究費での研究

西暦	年度	予算項目	予算項目							
				課題名	課題名	課題名	課題名	課題名	課題名	課題名
1996	H8		放射能調査研究費	大気圏の放射性核種の動態に関する研究（以下大気圏放射性核種）	海洋環境における放射性核種の挙動に関する研究（以下海洋環境放射性核種）					
1997	H9		放射能調査研究費	大気圏放射性核種	海洋環境放射性核種					
1998	H10		放射能調査研究費	大気圏放射性核種	海洋環境放射性核種					
1999	H11		放射能調査研究費	大気圏放射性核種	海洋環境放射性核種					
2000	H12		放射能調査研究費	大気圏放射性核種	海洋環境放射性核種					
2001	H13		放射能調査研究費	大気圏の放射性核種の長期的動態に関する研究(以下大気圏放射性核種）	海洋環境における放射性核種の長期挙動に関する研究(以下海洋環境放射性核種）				大気中の放射性気体の実態把握に関する研究　（以下放射性気体）	
2002	H14		放射能調査研究費	大気圏放射性核種	海洋環境放射性核種				放射性気体	
2003	H15		放射能調査研究費	大気圏放射性核種	海洋環境放射性核種				放射性気体	
2004	H16		放射能調査研究費	大気圏放射性核種	海洋環境放射性核種				放射性気体	
2005	H17		放射能調査研究費	大気圏放射性核種	海洋環境放射性核種				放射性気体	
2006	H18		放射能調査研究費	放射性降下物の長期変動と再浮遊に関する研究（以下放射性降下物）	海洋環境における放射性核種の長期挙動に関する研究(以下海洋環境放射性核種）					
2007	H19		放射能調査研究費	放射性降下物	海洋環境放射性核種					
2008	H20		放射能調査研究費	放射性降下物	海洋環境放射性核種					
2009	H21		放射能調査研究費	放射性降下物	海洋環境放射性核種					
2010	H22		放射能調査研究費	放射性降下物	海洋環境放射性核種					

放射能調査研究費以前および、放射能調査研究費での研究

西暦	年度	予算項目	予算項目							
				課題名	課題名	課題名	課題名	課題名	課題名	課題名
2011	H23(8月から)		放射能調査研究費	「大気を通じた人工放射性核種の陸圏・水圏への沈着およびその後の移行過程の解明研究（以下陸圏水圏人工放射性核種）」						
2012	H24		放射能調査研究費	陸圏水圏人工放射性核種						
2013	H25		放射能調査研究費	陸圏水圏人工放射性核種						
2014	H26		放射能調査研究費	陸圏水圏人工放射性核種						
2015	H27(4月から)		放射能調査研究費	「人工放射性核種のバックグラウンド大気監視と数値解析に関する研究（以下BG放射性核種）」						

表紙の図説明

2015 年 8 月までの ^{90}Sr および ^{137}Cs 月間降下量

福島第一原発事故後の大気の放射能汚染の実態把握を継続しています。2011 年 3 月の事故以降に確定できた^{90}Srおよび^{137}Cs月間降下量を対数軸で誤差と併せてプロットしています。^{134}Cs は事故直後には ^{137}Cs とほぼ等量降下していますから、放射性セシウム全体ではこのプロットのほぼ倍量となります。ただし、^{90}Sr、^{137}Cs はどちらもおよそ 30 年の半減期で減衰しますが、^{134}Cs はおよそ 2 年で半減します。図示した誤差は計測の統計誤差で、1 シグマです。測定誤差は本来全ての測定値につき表示すべきですが、グラフが見づらくなるため、従来はあえて表示してきませんでした。また、数十年前のデータについては誤差データが伝えられていません。

福島第一原発事故以前に採取され、分析や前処理途上だった試料については、事故の汚染によって実験室環境および測定室環境、測定機器のバックグラウンドなどが大幅に上昇したため、蒸発濃縮工程においても試料の汚染（コンタミネーションと言います）の問題が発生します。そのため、観測値を求めること自体が困難になっていましたが、試料を汚染の水準の低い関西にて分析しこの問題の回避に努めました。しかし、本文中にあるように、細心の注意と努力にもかかわらず、2010 年の後半および 2011 年初のデータは欠測となってしまいました。

徐々に実験環境の除染や測定機器の入れ替えなどを実施して事故以前のきれいな実験環境を追求し、データを求めるように努めています。また、IAEA が実施した分析相互比較に参画するなどし、その精度の維持管理に努めていますので、現状のデータの信頼性は担保できていると考えています。

A caption of the cover art

Monthly depositions of ^{90}Sr and ^{137}Cs before August 2015.

We have been monitoring the deposition amounts for the purpose of understanding the actual condition of radioactive pollution after the accident of Fukushima Daiichi Nuclear Power Plant (FDNPP). The monthly deposition amounts of both ^{90}Sr and ^{137}Cs, which were successfully fixed values after the accident in March 2011, are shown in logarithmic axis with error widths. Since the deposition amounts of ^{134}Cs were nearly equal to those of ^{137}Cs, the total amounts of radioactive cesium were approximately two times of the values in this figure. We would like to note that the half-lives of ^{90}Sr and ^{137}Cs are approximately 30 years, however, ^{134}Cs decays to half in about 2 years. The error widths are one sigma in statistical error of measurements. Although the error widths of all measurement values were better to be shown, error values used to be not shown on purpose to avoid busy figure in the former versions. In addition, error data before several decades are not handed down.

For the analysis of samples collected before the accident of FDNPP and not measured then, significant increase of background values were severe problem, because environments including laboratories and instruments were polluted, and it was also problem that samples could have been polluted in the operations of concentration or other preprocesses (contamination problem). We overcame the difficulty by carrying the analysis out in western Japan (Kansai area) where the pollution level was low, however, the data during the latter part of 2010 and the former part of 2011 were lacked in spite of our efforts as described in the main text.

We are making efforts to recover clean working environment as before the accident, by cleaning of the environments, exchanging instruments, etc. for the purpose of acquire the correct data. In addition, we maintain the precision of the data, for example, by participating inter-comparison programs performed by IAEA, so that, the credibility of the data are assured (please refer to the section: quality control of radioactive analysis of atmospheric deposition samples).

注：本報告書は一般配布を目的として
2016　年 8　月 1 日に作成された。